2,6-Diarylphenylsilylium Ions:
Synthesis and Study of a New Class of Silyl Cations

Dissertation

zur

Erlangung der naturwissenschaftlichen Doktorwürde

(Dr. sc. nat.)

vorgelegt

der

Universität Zürich

von

Simon Duttwyler

von Ehrendingen AG

Promotionskomitee:

Prof. Dr. Jay S. Siegel (Vorsitz)

Prof. Dr. Kim K. Baldridge

Prof. Dr. Peter Hamm

Prof. Dr. Thomas Müller

Prof. Dr. Jean-Pierre Sauvage

Zürich, 2010

ABSTRACT OF THE DISSERTATION

2,6-Diarylphenylsilylium Ions:

Synthesis and Study of a New Class of Silyl Cations

by

Simon Duttwyler

University of Zurich, 2010

Prof. Dr. Jay S. Siegel, Chair

Silylium ions are group 14 analogs of carbocations of the general structure R_3Si^+. Their most striking feature is their extreme electrophilicity. The generation of long-lived silyl cationic species has therefore necessitated the development of novel synthetic approaches and weakly nucleophilic reaction conditions. It was only in 2002 that the crystal structure of a triarylsilylium ion dispelled any doubt about the existence of tricoordinate silyl cations in the condensed phase. In the recent years, several research groups have succeeded in applying silylium ion chemistry to the preparation of other reactive intermediates and in the field of Lewis acid catalysis.

In this thesis, the synthesis and study of 2,6-diarylphenylsilylium ions is described. The terphenyl skeleton was expected to provide steric enshrouding of the positively charged cavity as well as an overall thermodynamic stabilization by internal π coordination. In addition, variation of the number of electron-donating methyl groups on the flanking rings should allow for a tunable silyl Lewis acidity. The cations were successfully generated by hydride abstraction from their hydrosilane precursors and showed a reactivity comparable to that of arene-coordinated trialkylsilylium ions. NMR spectroscopy revealed an attenuation of silyl cationic character upon increasing π basicity of the flanking rings.

Calculations suggested that the favored conformation of (2,6-diarylphenyl)dimethylsilylium ions is of C_1 symmetry, with the silicon center primarily interacting with one of the *ortho* carbon atoms of a lateral ring. Crystal structures and a detailed analysis of the NMR data of the cations were in full agreement with the computations and indicated a preference for C_1 geometry in the solid state and in solution. The same result was found for the terphenyldiisopropylsilyl congeners, which exhibited enhanced steric bulk about the silicon center. A quantitative correlation between ^{29}Si NMR shift and electron density of the flanking rings was derived from a Hammett analysis.

Hydride transfer from silanes of different steric enshrouding to the trityl cation was shown to occur directly from silicon to the central carbon atom of Ph_3C^+. Several compounds were tested as alternative hydride abstraction reagents. The two diarylmethylium ions (*p*-tolyl)$_2$CH$^+$ and (mesityl)(*p*-tolyl)CH$^+$ turned out to be promising candidates.

In an attempt to prepare one of the terphenylsilylium ions with a carborane as the counterion, crystals of an unusual bicyclic, silyl-substituted allyl cation were isolated. Based on a postulated protonation–hydrosilylation cascade, directed synthesis of the allyl cation was accomplished. Its mechanism of formation was investigated using deuterium-labeled starting materials. The results were fully consistent with the mechanistic hypothesis.

The silylium-like species $[Et_3Si(X)]^+$ (X = fluorobenzene or triethylsilane) and one of the terphenylsilylium ions in combination with carborane counterions were shown to abstract fluoride from fluorobenzene. C–F activation by the former cation afforded phenylated carboranes; reaction with the terphenylsilylium ion gave the respective fluorosilane and the fluorosilane phenylated in a *meta* position of a flanking ring. Based on the unprecedented finding that silyl Lewis acids can activate fluoroarenes, a Friedel–Crafts arylation protocol was developed.

ZUSAMMENFASSUNG

2,6-Diarylphenylsilyliumionen:

Synthese und Untersuchung einer neuen Klasse von Silylkationen

von

Simon Duttwyler

Universität Zürich, 2010

Prof. Dr. Jay S. Siegel, Chair

Silyliumionen sind höhere Analoge von Carbokationen der Struktur R_3Si^+. Was sie vor allem auszeichnet, ist ihre enorme Elektrophilie. Die Erzeugung langlebiger Silylkationen hat deshalb die Entwicklung neuartiger synthetischer Wege und schwach nucleophile Reaktionsbedingungen bedingt. Erst 2002 wurden mit der Kristallstruktur eines Triarylsilyliumions letzte Zweifel an der Existenz dreifach koordinierter Siliziumkationen ausgeräumt. In den vergangenen Jahren haben verschiedene Forschungsgruppen Silyliumionen erfolgreich zur Erzeugung reaktiver Zwischenstufen und in der Lewissäure-Katalyse angewandt.

In dieser Arbeit werden die Synthese und Untersuchung von 2,6-Diarylphenylsilyliumionen beschrieben. Vom Terphenyl-Gerüst wurden eine sterische Abschirmung der positiv geladenen Silylgruppe sowie eine thermodynamische Stabilisierung des Kations durch interne π-Koordination erhofft. Zusätzlich sollte eine Veränderung der Anzahl elektronendonierender Methylgruppen an den seitlichen Ringen eine Steuerung der Lewis-Acidität erlauben. Die Kationen wurden durch Hydrid-Abstraktion von ihren Hydrosilan-Vorläufern erzeugt und zeigten eine Reaktivität vergleichbar mit derjenigen von Aren-koordinierten Trialkylsilyliumionen. NMR-Messungen machten eine Abschwächung des Silizium-kationischen Charakters mit steigender π-Basizität deutlich.

Berechnungen zufolge nehmen (2,6-Diarylphenyl)dimethylsilyliumionen eine Konformation mit C_1-Symmetrie an, in der das Siliziumatom bevorzugt mit einem *ortho*-Kohlenstoffatom eines seitlichen Ringes wechselwirkt. Kristallstrukturen und eine detaillierte Analyse von NMR-Daten ergaben eine sehr gute Übereinstimmung mit den Berechnungen und legten C_1-Symmetrie im festen Zustand und in Lösung nahe. Dasselbe Resultat wurde im Falle der Terphenyldiisopropylkationen gefunden, die eine noch stärkere Abschirmung des Siliziumzentrums aufweisen. Ein quantitativer Zusammenhange zwischen ^{29}Si-Verschiebungen und der Elektronendichte der seitlichen Ringe wurde aus einer Hammett-Analyse abgeleitet.

Der Hydridtransfer von Silanen unterschiedlicher sterischer Abschirmung zum Tritylkation erfolgte direkt vom Silizium zum zentralen Kohlenstoffatom von Ph_3C^+. Mehrere Verbindungen wurden auf ihre Eignung als Hydridakzeptoren hin getestet. Die beiden Diarylmethyliumionen (*p*-tolyl)$_2$CH$^+$ und (mesityl)(*p*-tolyl)CH$^+$ erwiesen sich dabei als vielversprechende Kandidaten.

In einem Versuch, ein Terphenylsilyliumion mit einem Carborananion zu erzeugen, wurden Kristalle eines ungewöhnlichen bicyclischen, Silizium-substituierten Allylkations isoliert. Auf der Grundlage einer postulierten Protonierungs–Hydrosilylierungs-Kaskade wurde die gezielte Synthese des Allylkations erreicht. Der entsprechende Mechanismus wurde mittels deuterierter Edukte untersucht. Die Resultate waren in voller Übereinstimmung mit der mechanistischen Hypothese.

Die Silylium-artigen Kationen [Et$_3$Si(X)]$^+$ (X = Fluorbenzol oder Triethylsilan) und eines der Terphenylsilyliumionen, gepaart mit einem Carborananion, abstrahierten Fluorid von Fluorbenzol. C–F-Aktivierung ergab mit dem ersten Kation Phenylcarborene; im anderen Fall wurden Terphenyldimethylfluorsilane erhalten. Auf der Grundlage der Beobachtung, dass Silyl-Lewissäuren eine Aktivierung von Fluorarenen bewirken können, wurde eine Friedel–Crafts-Arylierungsvorschrift entwickelt.

Acknowledgement

PROF. JAY S. SIEGEL

for allowing me to work in his group, for his constant support, and for acquanting me with intriguing facets of stereochemistry and physical organic chemistry.

PROF. KIM K. BALDRIDGE

for her outstanding calculations, for a great collaboration, and for helpful discussions.

PROF. CHRISTOPHER A. REED

for allowing me to work in his group and a great collaboration.

SIMON JURT, NADJA BROSS AND DR. THOMAS FOX

for solving all NMR issues this work brought in its wake.

PD ANTHONY LINDEN AND SASCHA BLUMENTRITT

for the elucidation of crystal structures.

PD LAURENT BIGLER AND URS STALDER

for the measurement of mass spectra.

PAOLA ROMANATO

for a long teamwork that could not have been better.

OLIVER ALLEMANN

for joining the group and continuing challenging silyl cation projects.

FITORE KASUMAJ, ROMAN MAAG, MARTIN SEYFRIED,
DERIK FRANTZ, SILVIA ROCHA, AND PAOLA ROMANATO

for their friendship through all the years.

ALL SIEGEL, FINNEY, AND BALDRIDGE GROUP MEMBERS

for the unique working environment.

This thesis is dedicated to my family.

Contents

List of Figures

List of Tables

List of Schemes

Chapter 1

Background

1.1 Summary

A key observation in silicon chemistry is that low-coordinate species are much rarer than in the chemistry of carbon. This applies to neutral compounds, *i.e.*, analogs of alkenes, alkynes, and arenes, as well as to silylium ions, the cousins of carbenium ions. Silyl cationic intermediates exhibit an extreme electrophilicity, which can be rationalized in terms of diminished electronic stabilization, σ bond polarization, and the high affinity of silicon to electronegative main group elements. The extraordinary reactivity of R_3Si^+ systems has necessitated the development of weakly nucleophilic reaction conditions, in particular the design of inert counteranions. In 2002, the combination of bulky substituents at silicon, a clever leaving group approach, and the choice of an anion suitable for crystallization culminated in the structural characterization of the trimesitylsilylium ion, a silyl cation devoid of intermolecular coordination. In the years to follow, fundamental research and the development of synthetically useful silyl Lewis acids have proceeded in parallel, leading to a number of fascinating compounds and a clearer understanding of the scope and limitations of silylium ion chemistry.

1.2 Silicon versus Carbon

Why is CO_2 a gas but SiO_2 is a rock? Silicon and carbon, although close relatives in the periodic table, behave differently in many regards. The most striking phenomenon is that carbon readily adopts a tri- or dicoordinate bonding geometry in addition to its tetrahedral state, while silicon prefers coordination numbers of four or higher and forms unsaturated compounds only if forced to (Figure 1.1). Three factors lead to the markedly different chemistry of the two elements: siz, electronegativity, and bond strengths to main group elements.

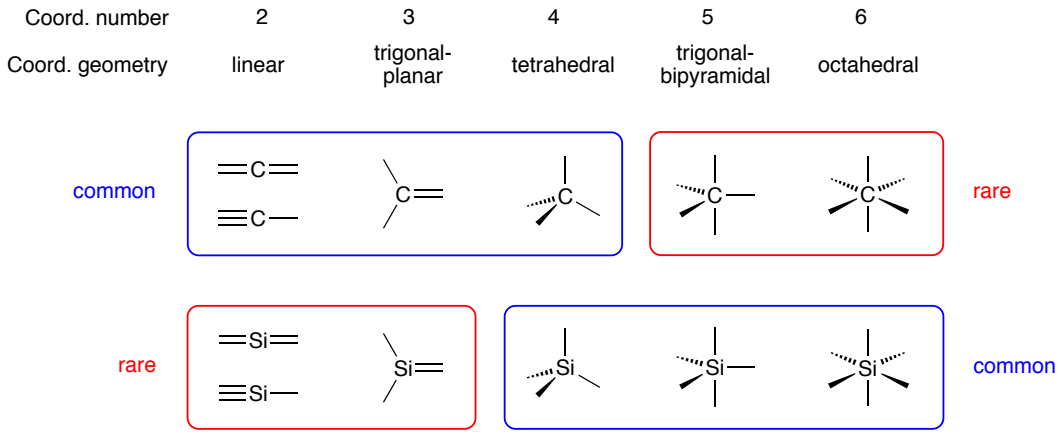

Figure 1.1. Coordination modes of carbon and silicon.

Silicon forms longer bonds than carbon because it uses $3s$ and $3p$ valence orbitals that are bigger than $2s$ and $2p$ orbitals. The covalence radii of Si, 1.17 Å, and C, 0.77 Å, lead to mean Si–Si, Si–C and C–C distances of 2.34 Å, 1.94 Å and 1.54 Å, thus typical Si–Si and Si–C bonds are *ca*. 52% and 26% longer than a C–C bond. In compounds of second-row elements, relatively short interatomic distances and a good overlap between the $2p$ orbitals result in strong double bonds, *e.g*. 728 kJ mol^{-1} for C=C in ethene versus 377 kJ mol^{-1} for C–C in ethane, or 748 kJ mol^{-1} for C=O in formaldehyde versus 385 kJ mol^{-1} for C–C in methanol.[1] For silicon, increased bond lengths and the diffuse electron distribution of the $3p$ orbitals lead to a diminished π overlap. Therefore, unsaturation becomes energetically

less favorable than the the formation of two σ bonds. Typical Si=Si rotational barriers, which serve as an indicator of the π bond strength, lie in the range of 105–130 kJ mol^{-1}.[2]

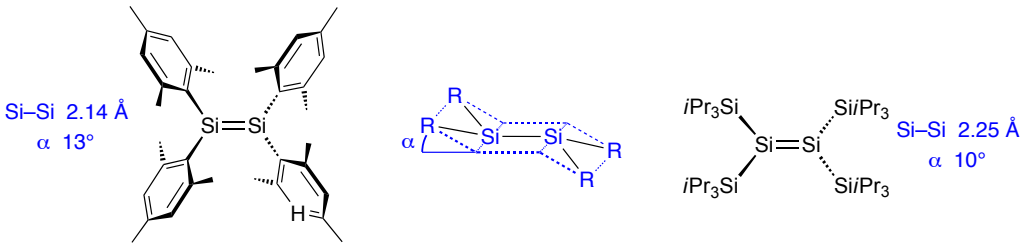

1 **2**

The preparation of silicon analogs of alkenes, alkynes, allenes, and benzene has challenged chemists over the past 90 years.[3] Long-lived species with an Si=Si unit were first prepared and structurally characterized in the 1980s. Aryl- and silyl-substituted members of this family comprise disilenes **1** and **2**.[4–6] The observed Si–Si distances of 2.14 Å and 2.26 Å and slight trans-bent distortions were interpreted as the manifestation of "soft" double bonds pertaining to a shallow energy surface. Compounds **3** and **4** are young representatives of the classes of silabenzenes and silaallenes.[7, 8] Similarly to **1** and **2**, enhanced kinetic inertness was achieved with bulky substituents at silicon.

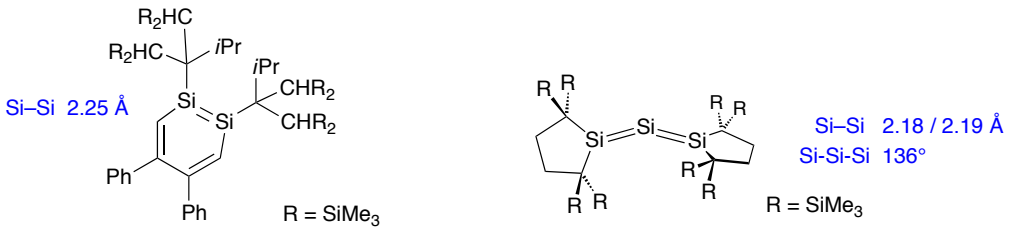

3 **4**

In contrast to benzene, hexasilabenzene Si_6H_6 has been predicted to adopt a puckered D_{3d} geometry **5b** and not the flat D_{6h} form **5a**, and its prismane-like constitutional isomer **5c** is apparently even more stable.[9–11] The preparation of a benzene-like Si_6R_6 species together with its crystal structure has only very recently been reported.[12] Si_6Tip_6 (**6**) is a chair-like sila-isomer of benzene with considerable electron delocalization over four of the ring atoms.

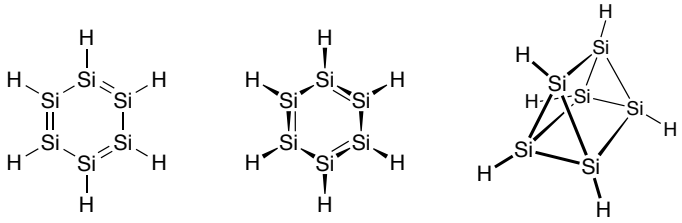

5a **5b** **5c**

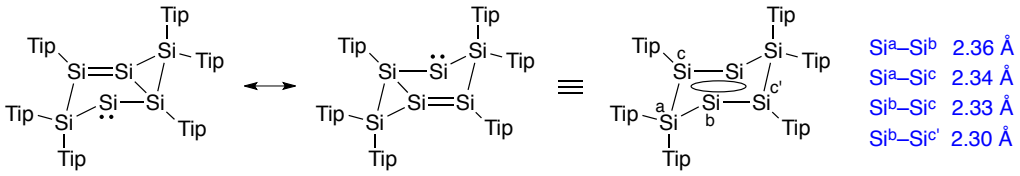

6

Disilynes bearing bulky aryl or silyl substituents were first reported in 2004 and 2008.[13, 14] The solid-state structures of **7** and **8** exhibited an additional minor shortening of the Si–Si distances, as compared to disilenes, and a pronounced trans-bent geometry. These features were in line with a theoretical analysis of heavier group 14 alkyne analogs that had appeared shortly before the first crystal structure of a disilyne was published.[15] According to the discussed bonding models, lone pair-like electron density starts accumulating on the heavy atoms on going from Si to Pb, at the expense of electron density in orbitals with bonding character. From the study of disilenes and disilynes, it can be concluded that formal Si–Si double and triple bonds are *ca*. 6 % and 13 % shorter than a typical single bond. In alkenes and alkynes, the bond shortening is twice as pronounced. This finding has brought to the fore that 3*p*–3*p* interactions are limited in unsaturated silicon compounds.

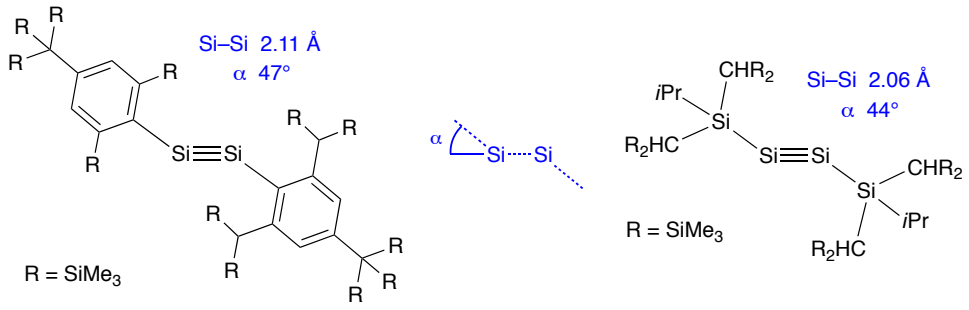

7 **8**

The Pauling electronegativities of carbon and silicon are 2.5 and 1.8, respectively. The lower electronegativity of silicon results in polarized bonds $Si^{\delta+}$–$X^{\delta-}$ by an inductive effect (X = main group element). This polarization leads to highly increased bond dissociation energies (BDE) when X = O, N or halogen due to a strong electrostatic component in addition to the covalent bond component (Table 1.1). In fact, the BDE of Si–F bonds in fluorosilanes are matched by no other combination of two elements.[16] On the other hand, BDE for Si–H and and Si–C bonds are lower than or comparable to the corresponding values for C–H and C–C. In these cases, reduced orbital overlap in the silanes is not counterbalanced by the effect of electronegativity differences.

Table 1.1. Bond dissociation energies (kJ mol^{-1}) of H_3C–X, H_3Si–X, Me_3C–X and Me_3Si–X molecules. Values of the two most recent compilations are given.[1, 16]

X	H_3C–X	H_3Si–X	Me_3C–X	Me_3Si–X
H	439	384	404	396
CH_3	377	375	366	352
OH	385	–[b]	401	556
NH_2[a]	356	–[b]	359	418
F	481	636	–[b]	661
Cl	350	456	355	490
Br	302	377	304	427
I	241	297	233	343

[a] NHMe for Me_3Si; [b] no recent value available.

As a result of relatively long interatomic distances and bond polarization, R_4Si compounds show the tendency to form $R_4SiR'_n$ adducts (n = 1–4) with coordination numbers of up to eight.[17] In such cases, the partially positively charged silicon center in $R_4Si^{\delta+}$ acts as a Lewis acid that is coordinated by additional ligands, often nitrogen-, oxygen- or fluorine-based Lewis bases. Compounds **9**–**11** were characterized by X-ray crystallography and exhibited close Si–N contacts in the order of 1.9–2.0 Å.[17–19]

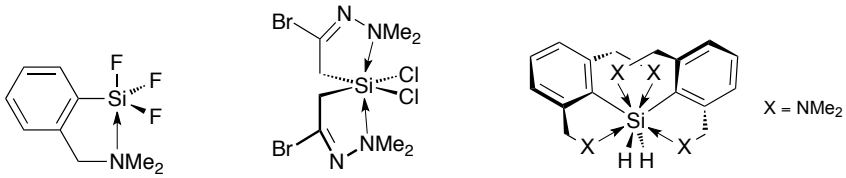

9 **10** **11**

^{29}Si NMR spectroscopy is an important tool for the study of silanes and reactive silicon-based species such as silylenes and silyl cations. Interestingly, the magnitude of the chemical shift is primarily determined by the coordination mode of the central silicon atom, higher coordination numbers generally causing an upfield shift (Figure 1.2). Thus free silylenes exhibit relatively high shifts of roughly 80–300 ppm relative to $SiMe_4$, while penta- and hexacoordinate species are observed at negative values, independent of the overall charge. Within a family of compounds, electron richness or deficiency correlates with the shielding of the ^{29}Si nucleus so that *e.g.* in silyl cation-like species diminished interaction with the counteranion or solvent molecules causes a more positive shift. The current records for the highest and lowest ^{29}Si NMR resonances are held by a saturated cyclic silylene and decamethylsilicocene, which appear at +567 ppm and −577 ppm.[20, 21]

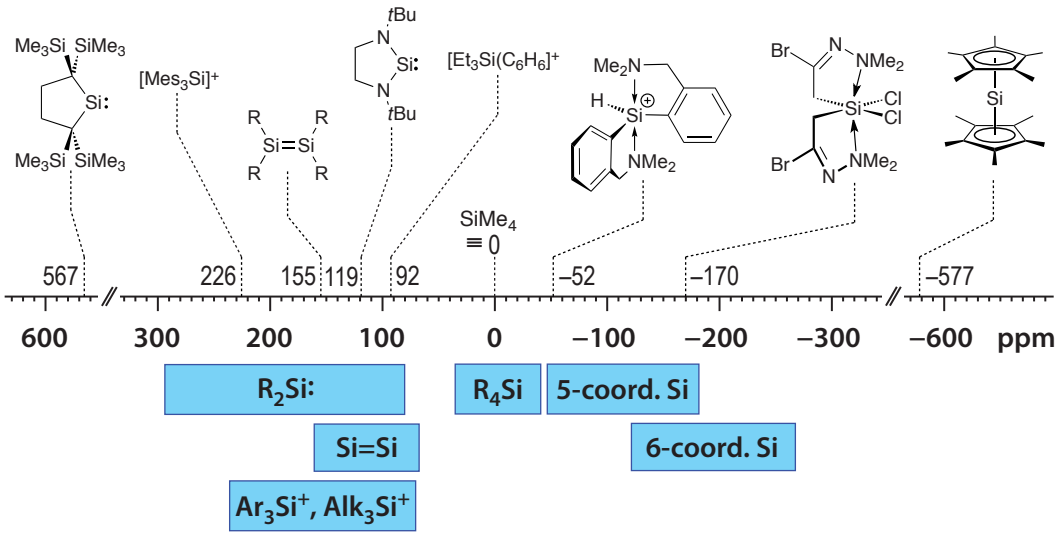

Figure 1.2. ^{29}Si NMR shifts of important classes of silicon compounds. The silylene on the left and decamethylsilicocene hold the current records for the highest and lowest NMR shifts, respectively.[20, 21]

Returning to the question posed at the beginning of this section: Why is carbon dioxide gas composed of individual CO_2 molecules but SiO_2 is a high-melting solid built up by a three-dimensional Si–O network? Carbon readily forms double bonds, and bearing two singly bonded oxygen substituents is often an energetically less favorable situation than the formation of a C=O carbonyl unit. Thus CO_2 is a stable compound, but $O{=}C(OH)_2$ and $C(OH)_4$ are not. In contrast, silicon prefers to have four oxygen ligands in a tetrahedral arrangement to the situation O=Si=O because the formation of Si–O π bonds is not associated with a substantial decrease in energy. So has a long-lived molecule with an Si=O unit ever been made? A close approach to a silanone has been presented only very recently. Treatment of the NHC-stabilized silylene **12** (NHC = *N*-heterocyclic carbene) with N_2O afforded the tetracoordinate silane **13**, which was isolated in 94 % yield (Scheme 1.1).[22] It exhibited a ^{29}Si NMR shift of -74.2 ppm (**12**: -12 ppm) and an Si–O distance of 1.54 Å, which is 7 % shorter than a typical Si–O bond; the distance Si–C_{NHC} was 1.93 Å. While it is tempting to draw the Lewis structure of **13** with an Si=O double bond, the molecule has a considerable zwitterionic character NHC^+–Si–O^- comparable to the tetrahedral intermediate resulting from the attack of a carbonyl compound by a nucleophile.

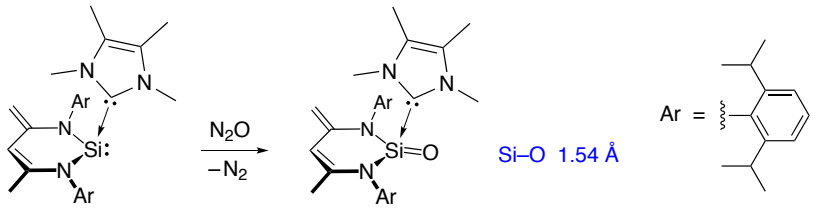

12 **13**

Scheme 1.1. Formation of a silanone-like species.

1.3 Silylium Ions

Silylium ions R_3Si^+ are the silicon analogs of carbenium ions R_3C^+.* Their most striking feature is their extreme electrophilicity, which is the reason that chemists attempted in vain to isolate tricoordinate silicon cations for over 50 years of research.[24, 25] Only in the 1990s the development of new synthetic strategies and suitable counterions made it possible to generate long-lived silylium-like species. A seminal piece of work during this period was the isolation and structural characterization of the first triarylsilylium ions. Concurrently to the quest for the free trialkylsilylium ion, systems with reduced degrees of silyl cationic character and potential synthetic utility have been reported in the past ten years.

1.3.1 General Properties of Silylium Ions

The differences between silicon and carbon pointed out above, size, electronegativity and bond strengths, have important ramifications for the chemistry of silylium ions. All three of them lead to an enhanced reactivity as compared to carbenium ions.

Size differences affect the electronic stabilization of R_3Si^+ and R_3C^+ systems. Carbocations are often stabilized by interactions of filled orbitals of the substituents with the central empty $2p$ orbital. If a second-row element is directly bonded to the formal C^+, effective donation of electron density can occur because of a favorable size and relative energy of orbitals between R and C^+. In trialkylcarbenium ions, electronic stabilization has been rationalized in terms of a π_{alkyl}–$2p$ interaction (Figure 1.3). Evidence for such an orbital overlap are experimentally determined bond shortenings. In the crystal structure of the *tert*-butyl cation, the C–C^+ distances lie in the range of 1.43–1.46 Å, indicating partial double bond character.[26, 27] In the case of R_3Si^+, the Si–R distances are longer than in R_3C^+, and overlap of the empty, relatively big $3p$ orbital with ligand orbitals is diminished. Both factors cause a reduced electronic stabilization in silyl cations. Si–C_{alkyl} bond shortenings in silyium-like ions are usually not observed or in the order of $\leq 3\,\%$.[28]

*According to IUPAC conventions, a silyl cation is any positively charged silicon species in which Si possesses a formal charge, analogous to the term carbocation.[23] Tricoordinate ions R_3Si^+ are called silylium ions, and the expression silanium ion refers to pentacoordinate species R_5Si^+.

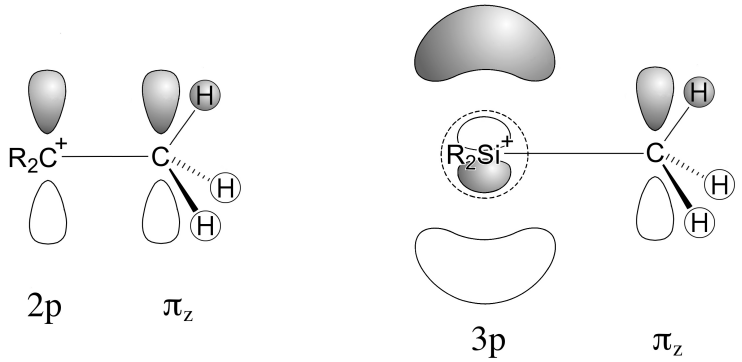

Figure 1.3. Electronic stabilization of alkylcarbenium ions (left) and of alkylsilylium ions (right). The dashed circle represents a spherical node of the Si 3*p* orbital.

The low electronegativity of silicon is of significance because it leads to a partially positively charged Si center in R_3Si^+ through the σ framework in addition to the electron deficiency caused by the vacant $3p$ orbital. In silylium ions, the combination of bond polarization and reduced Si–R orbital overlap creates an extraordinarily high Lewis acidity which manifests itself in the tendency of alkyl-substituted systems to interact even with the most weakly coordinating anions and solvents of low basicity such as benzene.[29, 30]

Strong Si–X (X = F, O, Cl, N) bonds represent a fundamental challenge in silylium ion chemistry: A species R_3Si^+ is in principle capable of interacting or reacting with any nucleophile carrying one of the electronegative elements. Indeed, solvents and anions commonly considered as inert, such as dichloromethane or PF_6^-, often coordinate to silicon or are decomposed by halide transfer. Early attempts to generate silylium ions were therefore plagued by the unprecedented affinity of these species to electronegative elements and the unavailability of suitable counteranions.

1.3.2 Assessment of Silylium Ion Character

Similarly to a free carbenium ion R_3C^+, an ideal silylium ion R_3Si^+ adopts a trigonal-planar geometry and is essentially not interacting with its counterion or solvent molecules (Figure 1.4 a). In the condensed phase, these requirements are practically never fulfilled,

and varying degrees of $X\cdots Si^{+}$ interactions are observed, where X is a source of electron density occupying a fourth coordination site around the silicon center (Figures 1.4 b and c). When are such ions still silylium ions and in which cases have they become covalent species or silyl-substituted solvent cations? Compounds should be named after their predominant mesomeric structure, so it is necessary to have a means of determining the amount of positive charge on a silicon atom.

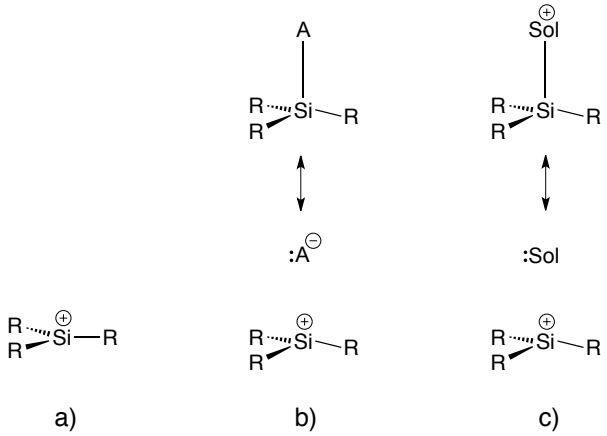

Figure 1.4. An ideal silylium ion (a) and anion- or solvent-coordinated silyl cationic systems (b, c).

Atomic charges are not observables, therefore indirect methods have to be applied to assess silylium ion character. Today, such analyses are primarily carried out on the basis of crystal structure investigations and ^{29}Si NMR spectroscopy.[31]

A perfectly tricoordinate silyl cation possesses a sum of angles around Si of $\Sigma\angle$(C-Si-C) = 360° (Figure 1.5). X-ray diffraction studies allow precise structure determinations in the solid state and reveal potential interactions of the Si center with anion or solvent molecules or intramolecular sources of electron density, such as heteroatoms or π systems. To date, the trimesitylsilylium ion represents the only structurally characterized trigonal-planar R_3Si^{+} species with R = hydrocarbon substituent.[32]

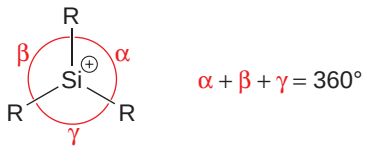

Figure 1.5. Sum of angles around Si in an ideal silylium ion.

Within a group of structurally comparable silyl cations, build-up of positive charge causes a downfield ^{29}Si NMR shift. For the free Me_3Si^+ ion, chemical shifts of 356–413 ppm relative to $SiMe_4$ have been predicted,[33–35] but it has been found both empirically and by calculations that the ^{29}Si resonances are highly sensitive to changes in electron density caused by approaching anions and neutral groups or molecules.[31, 35] The trimesitylsilylium and the tridurylsilylium ions may serve as references: they resonate at 226 ppm and 227 ppm, respectively, and represent model compounds in which a decrease in the chemical shift by tetracoordination is unlikely but a certain shielding by π_{aryl}–$3p$ interactions comes into play.[32, 33, 36–38]

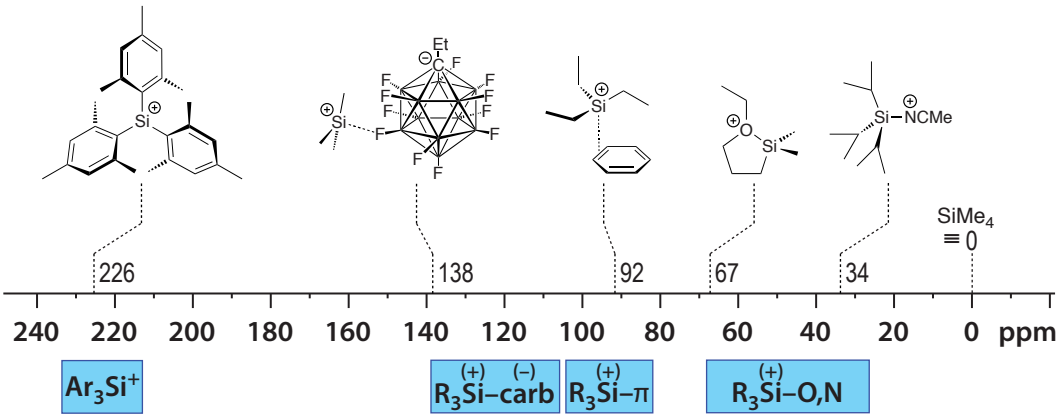

Figure 1.6. ^{29}Si NMR shifts of silyl cationic systems; carb = carborane counterion, π = coordinating π system, O,N = ether or nitrile ligand.

Most silyl cationic species exhibit ^{29}Si resonances far lower than 200 ppm; typical values are 120–90 ppm as a result of anion–Si^+ or arene–Si^+ interactions (Figure 1.6). Stronger donors, such as ethers or nitriles, cause resonances in the range of 70–30 ppm.

There is a continuum from rare cases of true silylium ions that fulfill the above-mentioned criteria to systems $[R_3Si\cdots X]^+$, where positive charge is distributed between the R_3Si moiety and an additional Lewis base.

1.3.3 Synthesis of Silylium Ions

Silyl cations are usually generated by a hydride transfer from the hydrosilane precursor of the cation to a carbocation (Scheme 1.2 a). This strategy is closely related to the Bartlett–Condon–Schneider reaction in carbocation chemistry and relies on the higher bond strength of C–H vs Si–H.[39–41] As the hydride acceptor, the trityl cation (Ph_3C^+) has been used most often. It can be prepared in combination with a variety of counterions, has a relatively low reactivity towards organic compounds and solvents and yields inert triphenylmethane as the only by-product, which can easily be removed by washing the reaction mixture with hexane.

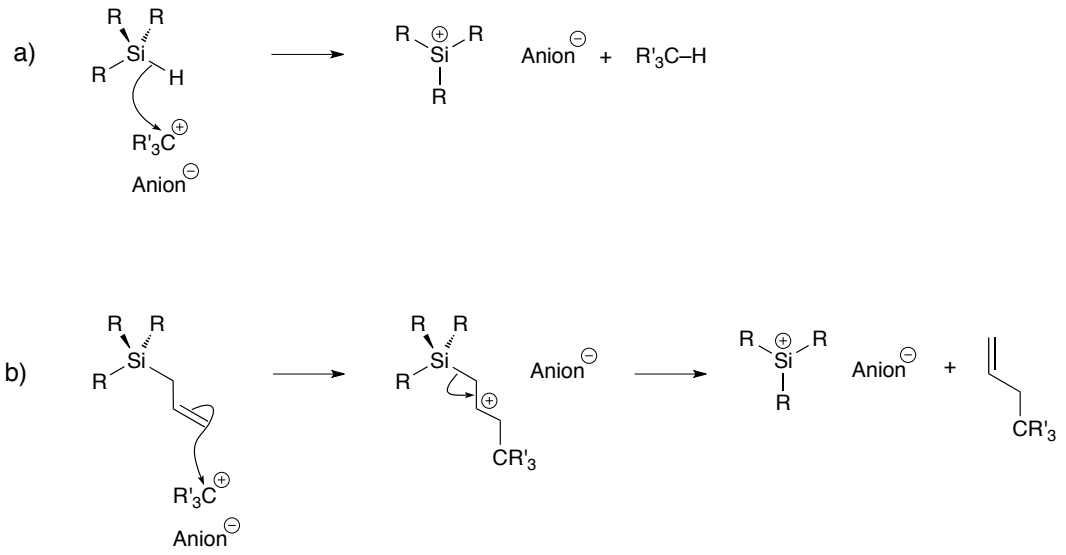

Scheme 1.2. Generation of silylium ions by a) hydride abstraction and b) the allyl leaving group approach.

Alternatively, especially if the target silylium ion carries bulky substituents, the allyl leaving group approach can be applied (Scheme 1.2 b). It also takes advantage of dif-

ferences in bond strengths (C–C > Si–C) and was key to the successful preparation of triarylsilylium ions.[32, 36–38]

Metathesis of halogenated precursors using silver salts, a common strategy to produce carbocations, is usually not successful in the case of halosilanes for thermodynamic reasons. The equilibrium of, *e.g.*, iPr$_3$SiBr + [Ag][CHB$_{11}$H$_5$Br$_6$] $\rightleftharpoons$ iPr$_3$SiBr–CHB$_{11}$H$_5$Br$_6$ + AgBr lies on the *left*, so that mixing of the bromosilane with silver carborane leads to no reaction, whereas addition of the silyl carborane to AgBr in toluene effects dissolution of AgBr.[31]

A crucial point in the preparation of long-lived silylium ions is the choice of the proper counteranion. Because of the extreme halophilicity of R_3Si^+ species, highly inert anions have to be used to prevent strong coordination or decomposition. Anions such as triflate ($CF_3SO_3^-$) or group 15 hexafluorophosphates (PF_6^-, SbF_6^-, AsF_6^-) afford covalent compounds R_3Si–OSO_2CF_3 or fluorosilanes R_3Si–F when paired with silylium ions.

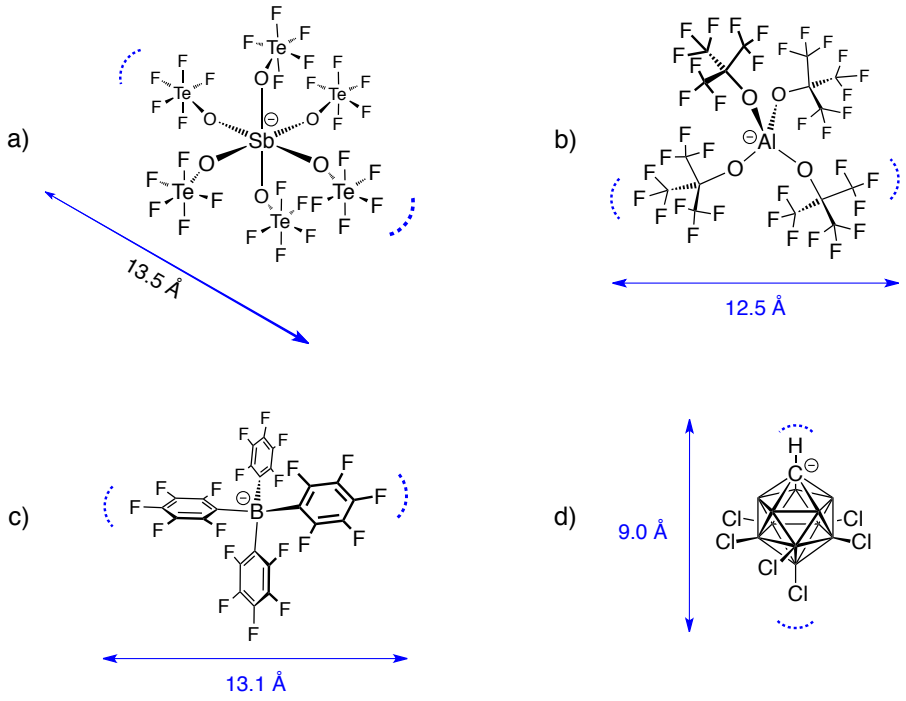

Figure 1.7. Representatives of currently used classes of weakly coordinating anions: a) group 15 teflates, b) alkoxyaluminates, c) tetraarylborates and d) halogenated carboranes. Approximate sizes are given including the van der Waals radii of the respective atoms.

Several classes of weakly coordinating anions for the preparation of reactive group 14 cations have been developed over the past twenty years, among them perfluorinated group 15 teflates, alkoxyaluminates, tetraarylborates and halogenated carboranes (Figure 1.7 a–d).[42] They owe their low basicity to the delocalization of negative charge over a large volume and the low polarizability of the individual halogen atoms on their surface. Of these four classes of anions, only polyfluorinated tetraarylborates and the carboranes are inert enough to resist halide abstraction or other degradation pathways.

The widely used perfluorinated $B(C_6F_5)_4^-$ has the advantage that it can be prepared in one step from bromopentafluorobenzene and trichloroborane on a multi-gram scale. It coordinates extremely weakly to silicon, and its salts generally have a high solubility in organic solvents. However, crystallization of silylium ions is often hampered by the formation of oily products. Moreover, it decomposes to give $B(C_6F_5)_3$ and C_6HF_5 in reaction mixtures of high Brønsted acidity.[43]

Halogenated derivatives of $CB_{11}H_{12}^-$ are the most inert anions known and exhibit an extremely low basicity towards Brønsted and silyl Lewis acids (Figure 1.8 a).[31, 44–46] Moreover, solubilities and crystallizing properties of their salts can be tuned by varying the cage substituents. Disadvantages of working with carborane anions are laborious syntheses and the costs for starting materials.

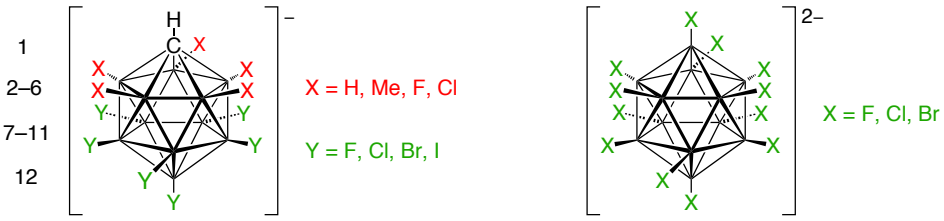

Figure 1.8. Numbering scheme and most common substitution patterns of (a) halogenated carborane $CHB_{11}X_5Y_6^-$ anions and (b) dodecaborane $B_{12}X_{12}^{2-}$ dianions.

Recent reports on perhalogenated dodecaborates $B_{12}X_{12}^{2-}$ have shown that these dianions exhibit a basicity comparable to those of halogenated carboranes (Figure 1.8 b).[47–49] Although salts of $B_{12}X_{12}^{2-}$ possess limitied solubilites due to increased lattice energies,

their straightforward and relatively cheap preparation starting from $NaBH_4$ makes them promising candidates for a new generation of weakly coordinating anions.[50]

Only a small group of solvents is compatible with the high reactivity of silylium ions. For their preparation and characterization in solution, non-halogenated or halogenated arenes and liquid sulfur dioxide are suitable, and for precipitation and crystal growth, saturated hydrocarbons are used. However, trialkylsilylium ions are so Lewis-acidic that to date, every cation prepared in the condensed phase interacted with an external or intramolecular source of electron density to give a tetracoordinate silylium-like species.

1.4 Landmarks in Silylium Ion Chemistry

The development of weakly nucleophilic reaction conditions in the 1990s represented a significant progress in the chemistry of reactive silicon species and paved the way for the generation of cations with unprecedented silylium ion character. Landmarks that followed shortly were the isolation and structural characterization of arene- and carborane-coordinated cations and the preparation of free triarylsilylium ions. In the years to follow, further focal points emerged: the synthesis of delocalized systems and the application of silyl cations as Lewis acid catalysts.

1.4.1 Arene- and Carborane-Coordinated Silylium Ions

In 1993, Lambert and coworkers reported on the generation of trialkylsilylium ions in aromatic solvents using the $B(C_6F_5)_4^-$ anion and presented the crystal structure of the solvate $[Et_3Si(toluene)]^+$ (**14**$^+$) in $[Et_3Si(toluene)][B(C_6F_5)_4]$·toluene.[30, 51, 52] This study sparked

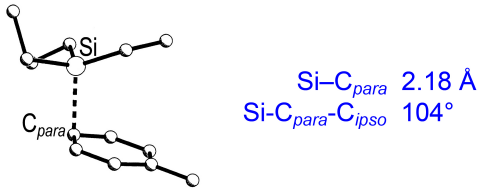

Figure 1.9. X-ray crystal structure of **14**$^+$ in [**14**][$B(C_6F_5)_4$]·toluene (H atoms omitted).[30]

off a heated debate about the nature of arene-coordinated silyl cations.[53–57] In **14**$^+$, the toluene molecule was in a C_{para}–Si distance of 2.18 Å to the Et_3Si moiety, and the position of the Si atom relative to the ring indicated a geometry between those of pure η^1-π and σ complexes (Figure 1.9). So was the observed species a silylium ion (**14a**$^+$) or a Wheland intermediate (**14b**$^+$)?

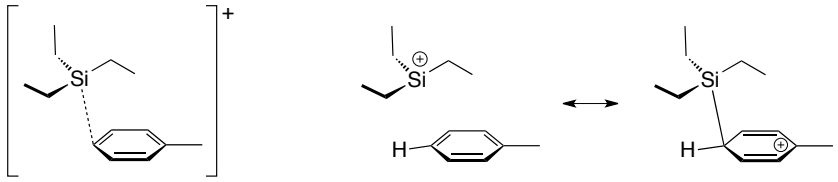

14$^+$ **14a**$^+$ **14b**$^+$

The sum of angles around silicon Σ∠(C-Si-C), 341°, and the solid state ^{29}Si NMR shift, 94 ppm, were not consistent with the model of a free silylium ion. On the other hand, the toluene ring possessed an almost undistorted planar geometry with C–C distances of 1.37–1.40 Å, and in the solid state ^{13}C NMR spectrum, coordinating and free toluene could not be distinguished. These findings indicated little positive charge on the aromatic ring and rejected a pure σ model. Furthermore, a fast arene ligand exchange on the NMR time scale was observed when the material was dissolved in a mixture of aromatic solvents. As a whole, **14**$^+$ was best described as a toluene molecule occupying a fourth coordination site around an Et_3Si fragment with some, albeit not full, silylium ion character. The type of arene–Si bonding lied between those of classical σ and π complexes.

At the time of the publication of **14**$^+$, the development of halogenated carboranes enabled Reed and coworkers to prepare solvent-free silylium carboranes.[28, 35, 58] Among the structurally characterized compounds, iPr$_3$Si–CHB$_{11}$H$_5$Cl$_6$ (**15**) represented the closest approach to a trialkylsilylium ion.[35]

In the crystal, the anion interacted with the iPr$_3$Si fragment via one of the lower-belt chlorine atoms. The Si–Cl distance, 2.32, was 0.30 Å or 15 % longer than a covalent Si–Cl bond, and the distance B–Cl$_{coord}$ was 1.88 Å, 5 % longer than the average of the other five B–Cl bonds. The sum of angles around Si was 352°, with the Si atom at a distance of 0.31 Å from the plane defined by its directly attached C atoms. The solid state ^{29}Si NMR

resonance of **15** was observed at 115 ppm, significantly downfield from that of $\mathbf{14}^{+}$, but still far from the values projected for a free trialkylsilylium ion. Even though **15** was clearly not a salt in the solid state, it dissociated into ions $[i\mathrm{Pr_3Si(solv)}]^{+}$ $\mathrm{CHB_{11}H_5Cl_6}^{-}$ in solution and reacted with nucleophiles exclusively at silicon and not by B–Cl cleavage; it behaved *as if* it was a silyl cation. Therefore the term *silylium-like* was coined for such species.

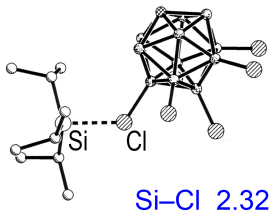

Figure 1.10. Crystal structure of **15** (H atoms omitted).[35]

A number of anion-coordinated trialkylsilylium ions have been prepared and structurally characterized in the past four years (Table 1.2).[29, 47, 48, 59, 60] All of them exhibit Si–halogen contacts with Pauling bond orders of 0.33–0.48. A comparison of the crystallographic and solid state NMR data shows that the highest degree of ionicity is reached with fluorinated anions. In these cases, the Si–F distance is 20 % longer than a covalent Si–F bond (bond order ca. 0.35), and the coordination geometry of the carbon substituents around Si is almost trigonal-planar with a sum of bond angles of 354°. Also, the solid state ^{29}Si NMR shift of $\mathrm{Me_3Si–CEtB_{11}F_{11}}$ appears at the benchmark value of 138 ppm. Chlorinated and brominated anions have higher and comparable coordination strengths, leading to increased pyramidalization at Si and δ^{29}Si of 106–126 ppm. Interestingly, the doubly charged $\mathrm{B_{12}Cl_{12}}^{2-}$ behaves similarly to the chlorinated monoanions. The iodinated carborane $i\mathrm{Pr_3Si–CHB_{11}H_5I_6}$ possesses the highest basicity in the series, giving rise to a higher halonium character and an NMR shift of 97 ppm in $i\mathrm{Pr_3Si–CHB_{11}H_5I_6}$. This is probably a result of the more facile polarizability of the iodine substituents.

Table 1.2. Structural and solid-state ^{29}Si NMR data of anion-coordinated R_3Si^+ compounds.[61] All cations are coordinated by a halogen atom of the counterion. BO = Pauling bond order, $\Sigma\angle$ = sum of C-Si-C angles, NMR shifts for solvent-free solid samples.

Compound	Si–Hal (Å)	BO[a]	$\Sigma\angle$ (°)	δ(^{29}Si) (ppm)
$Me_3Si–CHB_{11}F_{11}$	1.90	0.33	354.4	–
$Me_3Si–CEtB_{11}F_{11}$	1.88	0.36	354.4	138
$(Me_3Si)_2–B_{12}Cl_{12}$	–	–	–	118
$Et_3Si–CHB_{11}H_5Br_6$[b]	2.43, 2.44	0.41, 0.39	345.0, 349.0	106, 112
$Et_3Si–CHB_{11}H_5Cl_6$[b]	2.28, 2.30	0.42, 0.39	345.8, 348.1	–
$Et_3Si–CHB_{11}Cl_{11}$	2.33	36	349.5	–
$(Et_3Si)_2–B_{12}Cl_{12}$	2.32	0.37	347.8	126
iPr$_3$Si–$CHB_{11}H_5I_6$	2.66	0.48	346.8	97
iPr$_3$Si–$CHB_{11}H_5Br_6$	2.48	0.34	351.0	110
iPr$_3$Si–$CHB_{11}H_5Cl_6$	2.32	0.37	351.8	115
$(i$Pr$_3$Si$)_2–B_{12}Cl_{12}$	2.32, 2.36	0.37, 0.32	349.2, 350.3	117
tBu$_3$Si–$CHB_{11}H_5Br_6$	2.47	0.36	348.7	–

[a] Based on Pauling's original equation $n = \exp[(r_0 - r_x)/0.3]$ and 1.57 / 2.02 / 2.16 / 2.44 Å for Si–Hal, Hal = F–I. [b] Two molecules in the asymmetric unit.

^{29}Si NMR resonances of $Et_3Si–Y$ compounds (Y^- = weakly coordinating anion) in aromatic solvents fall in the range of 80–110 ppm (Table 1.3). Certain numbers are seemingly contradictory, such as those of entries 1, 5 and 7. In terms of anion basicity, $B(C_6F_5)_4^-$ can be assumed to be less coordinating than the chlorinated and brominated carboranes or dodecaboranes. This assumption is based on the observed anion–Si^+ coordination trend within the family of halogenated carboranes (F < Cl $\approx$ Br < I) and the lower Brønsted basicity of $B(C_6F_5)_4^-$ as compared to that of the carboranes.[62] But why should the pair $Et_3Si^+/B(C_6F_5)_4^-$ then give rise to a more shielded ^{29}Si nucleus than $Et_3Si^+/CHB_{11}Me_5Br_6^-$ and $Et_3Si^+/B_{12}Cl_{12}^{2-}$?

Table 1.3. ^{29}Si NMR shifts of Et_3Si–Y compounds (Y^- = weakly coordinating anion in aromatic solvents (ppm vs $SiMe_4$).[63]

Cation	Anion	Solvent	$\delta(^{29}Si)$
Et_3Si^+	$B(C_6F_5)_4^-$	C_6D_6	94
Et_3Si^+	$B(C_6F_5)_4^-$	toluene-d_8	82
Et_3Si^+	$B(C_6F_5)_4^-$	C_6D_6/toluene 3:1	87
$[Et_3Si(toluene)]^+$	$B(C_6F_5)_4^-$	solid state	94
Et_3Si^+	$CHB_{11}Me_5Br_6^-$	C_6D_6	103
Et_3Si^+	$CHB_{11}H_5Cl_6^-$	C_6D_6/PhCl 1:1	105
$(Et_3Si^+)_2$	$B_{12}Cl_{12}^{2-}$	C_6D_6	111

A model that can account for the observed solution-phase NMR resonances was proposed by Reed.[53] When trialkylsilylium-like species are dissolved in arenes, time-averaged signals are observed for both the cationic fragment and the anion, *i.e.* one set of signals each for Et_3Si^+ and for the tetraarylborate or carborane, with free and bound anions being indistinguishable. This finding is consistent with an equilibrium of arene- and anion-coordinated Et_3Si^+ that is fast on the NMR time scale (Scheme 1.3). The detected ^{29}Si resonance is the weighted average of the two species, $\delta_{obs} = \delta_1\chi_1 + \delta_2\chi_2$ (χ_i = mole fractions), and the position of the equilibrium is mainly determined by the strength of the anion–Si interaction and the solvation energy of the anion. A chemical shift of around 90 ppm can be taken as a reference value for δ_1 based on the solid-state resonance of $\mathbf{14}^+$, and a range of roughly 110–120 ppm can be assumed for δ_2 for chloro- and bromocarboranes given the data in Table 1.2.

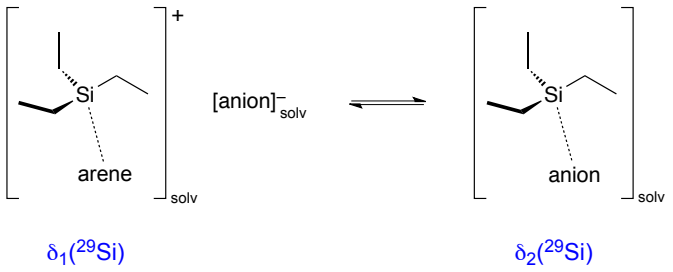

Scheme 1.3. Equilibrium between solvent- and anion-coordinated Et_3Si^+.

In the case of $B(C_6F_5)_4^-$, the equilibrium $[Et_3Si(arene)]^+_{solv}$ $[anion]^-_{solv} \rightleftharpoons [Et_3Si–anion]_{solv}$ lies more on the left than with carborane counteranions because of the relative anion basicities and also because of different solvation energies. Salts of the tetraarylborate generally have a higher solubility in aromatic solvents than carborane salts, probably due to the higher volume/charge ratio and the pentafluorophenyl rings in $B(C_6F_5)_4^-$ (like dissolves like). As a result, the observed ^{29}Si chemical shifts resemble those of δ_1 in the case of $B(C_6F_5)_4^-$ and but are higher in the case of the carboranes because of a significant contribution of the term $\delta_2\chi_2$, *i.e.*, lower values are obtained with the less coordinating anion. This phenomenon can also be interpreted as a solvent leveling effect. The triethylsilylium ion is so electron-deficient that it will always interact with the strongest Lewis base in the medium, analogously to the proton in the condensed phase. As soon as the counterion is less basic than the arene and its solvation does not require too much energy, $[Et_3Si(arene)]^+$ becomes the dominant species.

Scheme 1.4. Formation of 1,2-dichlorobenzene solvate **16**$^+$ and hydride-bridged cation **17**$^+$.

How enormous the hunger of formal Si^+ for electron density is became evident with the isolation of dichlorobenzene- and silane-coordinated trialkylsilylium ions.[59] When iPr_3Si^+ was prepared with the $CHB_{11}Cl_{11}^-$ counterion in 1,2-dichlorobenzene, addition of pentane afforded crystals of the salt $[iPr_3Si(C_6H_4Cl_2)][CHB_{11}Cl_{11}]$ ([**16**][$CHB_{11}Cl_{11}$]) (Scheme 1.4). The solvent molecule was found to interact with Si via one of the chlorine atoms, with a Si–Cl distance of 2.33 Å (Figure 1.11 a). Under the same conditions, but with Me_3SiH as the silane starting material, crystals of $[(Me_3Si)_2H][CHB_{11}Cl_{11}]$ were obtained, containing the silane-coordinated cation $[Me_3Si–H–SiMe_3]^+$ (**17**$^+$) (Figure 1.11 b). X-ray crystallography, computations and NMR as well as IR studies indicated an essentially symmetrical hydride bridge. The isolation and structural characterization of **16**$^+$ and **17**$^+$ impressively underlined that under weakly nucleophilic conditions, R_3Si^+ systems interact

even with n or σ electron density of neutral haloarenes and silanes. Systems containing the motif [Si–H–Si]$^+$ as a result of *intra*molecular bridging have also been reported, and in these cases the three-center bonding seems to be favored over solvent coordination even in relatively Lewis-basic solvents such as benzene, toluene, dichloromethane.[64–68]

Figure 1.11. Crystal structures of a) **16**$^+$ and b) **17**$^+$; H atoms omitted for clarity, except for the bridging H in b).[59]

1.4.2 Free Triarylsilylium Ions

In the years 1997–2001, Lambert and coworkers reported on the synthesis of (aryl)$_3$M$^+$ cations (M = heavier group 14 element, aryl = 2,6-disubstituted arene).[36–38] The bulky substituents were anticipated to afford propeller-shaped cations with minimized M$^+$–solvent and M$^+$–anion interactions.

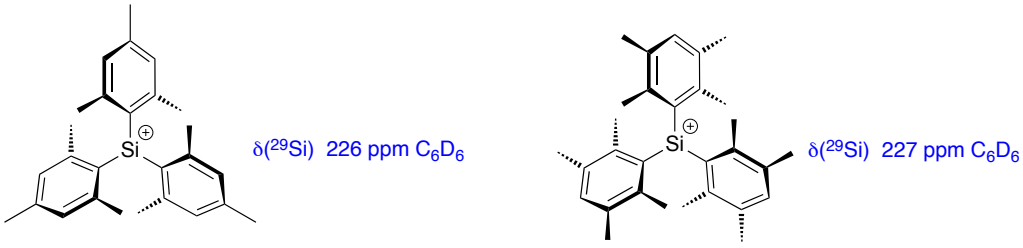

Indeed, [(mesityl)$_3$Si][B(C$_6$F$_5$)$_4$] and [(duryl)$_3$Si][B(C$_6$F$_5$)$_4$] ([**18**][B(C$_6$F$_5$)$_4$], [**19**][B(C$_6$F$_5$)$_4$]), prepared via the via the allyl leaving group approach, possessed unprecedented ^{29}Si chemical shifts of 226 and 227 ppm, indicating significantly higher silylium

ion character than trialkylsilylium-like systems. The deshielding in $\mathbf{18}^+$ was independent of the aromatic solvent (C_6D_6, C_6D_6/toluene-d_8 3:1, C_6D_6/*p*-xylene-d_{10} 1:1) and matched well with the prediction of 230 ppm for this cation in the gas phase.[33]

The crystal structure of $\mathbf{18}^+$ was elucidated in 2002 in a seminal collaboration of Lambert's and Reed's groups.[32] The cation was generated from its allyl-substituted precursor and $Et_3Si–CHB_{11}Me_5Br_6$ (Scheme 1.5). While $B(C_6F_5)_4^-$ as the counterion had yielded an oily product, the use of $CHB_{11}Me_5Br_6^-$ afforded crystals of the composition $[\mathbf{18}][CHB_{11}Me_5Br_6]\cdot C_6H_6$ suitable for X-ray diffraction. In the crystal, $\mathbf{18}^+$ possessed a trigonal-planar geometry around silicon, with $\Sigma\angle$(C-Si-C) = 360° and the expected propeller-like arrangement of the mesityl rings. The average twist angle of the ring planes with respect to the plane defined by the three C_{ipso} atoms amounted to 49°, so that an effective steric shielding of Si^+ by the *ortho* methyl groups and a diminished π_{aryl}–$3p_{Si}$ overlap resulted. The ^{29}Si NMR shift in the solid state was 227 ppm, almost identical to those in solution. This finding indicated that $\mathbf{18}^+$ existed as a free silylium ion also in aromatic solvents.

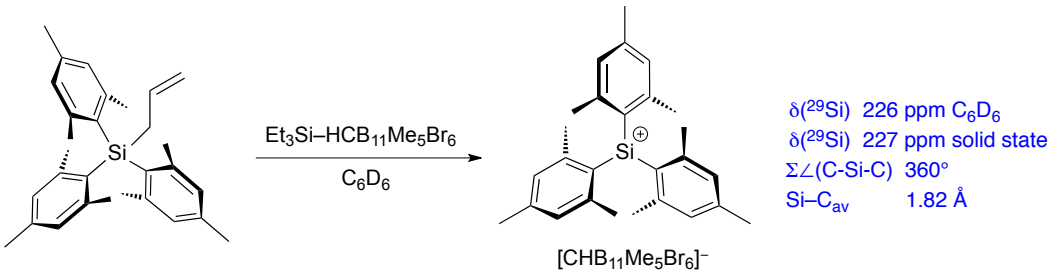

Scheme 1.5. Synthesis of [**18**][$CHB_{11}Me_5Br_6$].

The preparation and structural characterization of $\mathbf{18}^+$ marked the end of the quest for a free silylium ion. It also represented a general milestone in the chemistry of heavier group 14 elements, underscoring that long-lived tricoordinate cations with the positive charge mainly located on the central atom could be generated in the condensed phase.

1.4.3 Delocalized Systems

Over the past years, the group of Sekiguchi has prepared a series of cations with the positive charged being spread over several silicon or germanium atoms.[69–72] These ions represent relatives of cyclopropenium, homocyclopropenium, and cyclic allylic cations, and their synthesis is the result of an effort to extend the carbocation–silyl cation analogy.

Trisilacyclopropenium ion **20**$^+$ was generated from its trisilacyclopropene precursor by silyl group abstraction using the trityl salt [Ph_3C][$BAr^F{}_4$] (Ar^F = 2,3,5,6-tetrafluoro-4-($SiMe_2tBu$)phenyl) and characterized by NMR spectroscopy as well X-ray crystallography (Scheme 1.6). The ^{29}Si NMR signals ($Si^{a,b}$ 285 ppm, Si^c 288 ppm in C_6D_6) were in agreement with strongly, virtually equally deshielded silicon centers. However, they were practically the same as those in toluene and chlorobenzene solution; the same resonances were obtained with two other polyfluorinated tetraarylborate counterions. NMR spectroscopy thus indicated that **20**$^+$ had a lower electrophilicity than trialkylsilylium ions and existed as a weakly coordinated silylium ion in solution. In the crystal, the cation exhibited essentially identical Si_{ring}–Si_{ring} distances of 2.22 and 2.21 Å, which were also consistent with a high degree of charge delocalization

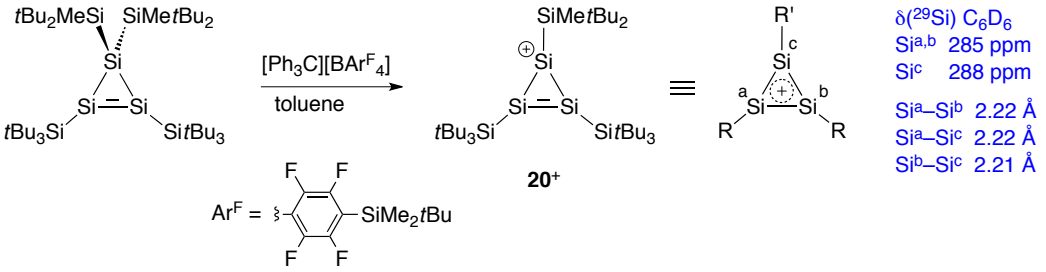

Scheme 1.6. Synthesis of **20**$^+$.

1.4.4 Applications of Silyl Cation Chemistry

While the affinity of silicon to electronegative elements hampered early attempts to prepare silyl cations, it was exploited soon after reliable procedures for the synthesis of arene- and carborane-coordinated R_3Si^+ systems had been published. Leaving group abstraction by

silylium-like species has in the meantime become an important tool in the chemistry of reactive main group and transition metal cations.

Reed and coworkers obtained exceptionally strong Brønsted acids and methylating reagents by the reaction of triethylsilyl carboranes with hydrogen chloride and methyl triflate (Scheme 1.7). Carborane acids $H^{\delta+}$–carborane$^{\delta-}$ are currently the strongest isolable acids, capable of quantitatively protonating alkenes, arenes and fullerene.[46, 73–77] The electrophilicity of methyl carboranes exceeds that of methyl triflate and related reagents and has allowed for the synthesis of rather exotic compounds such as the hexamethylhydrazinediium dication.[77–79]

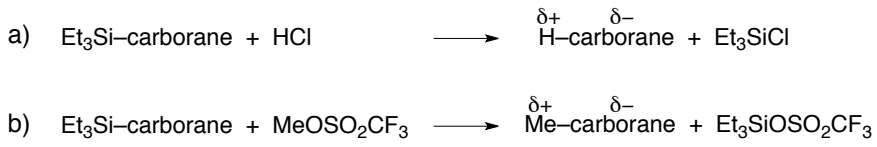

Scheme 1.7. Preparation of a) carborane acids and b) methyl carborane reagents.

In organometallic chemistry, $[Et_3Si(X)][B(C_6F_5)_4]$ (X = toluene or Et_3SiH) has become a workhorse for the chloride abstraction from transition metal complexes. Such reactions have afforded electronically and coordinatively unsaturated intermediates of high Lewis acidity.[80–82] Based on this approach, the group of Heinekey has prepared a series of cationic dihydrogen complexes of rhenium, osmium and iridium (Scheme 1.8).[83–87]

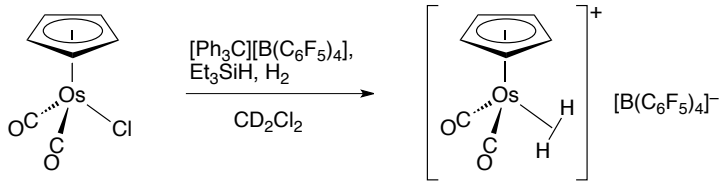

Scheme 1.8. Chloride abstraction from an organometallic complex by *in situ*-generated Et_3Si^+ affording a cationic dihydrogen complex.[87]

As strong Lewis acids, silyl cations also have the potential to act as catalysts in reactions that are promoted by electron-deficient metal(loid) species. The development of weakly nucleophilic conditions has turned out to be a fruitful ground, if not a crucial pre-

requisite, for such transformations; catalysts with pronounced cationic character tend to have a significantly higher activating effect than reagents such as silyl triflates.

An early report on a silylnitrilium catalyst was provided by Helmchen and Jørgensen in 1998.[88] The invetigated Diels–Alder reaction proceeded under mild conditions in the presence of the optically active binaphthyl cation $\mathbf{21}^+$ (Scheme 1.9). Only the *endo* product was obtained, however, the enantiomeric excess was low. Nevertheless, this study demonstrated that cationic silyl Lewis acids were capable of effectively activating carbonyl groups. Moreover, it was an important finding that the excess of oxygen donor atoms with respect to $\mathbf{21}^+$ did not suppress its activity as a catalyst.

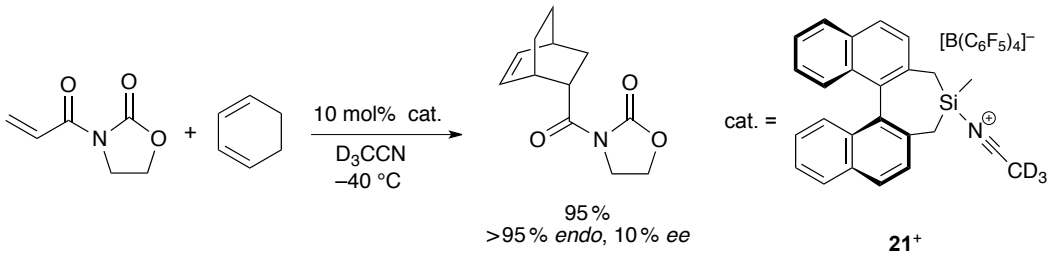

Scheme 1.9. Silylnitrilium ion-mediated Diels–Alder reaction.

The strategy to use silylium-like species as Lewis acid catalysts in Diels–Alder and Mukaiyama aldol reactions was persued by the groups of Sawamura and Oestreich in the years 2005 and 2009.[89, 90] They found that $\mathbf{14}^+$ and the ferrocene-based cation $\mathbf{22}^+$ in combination with the $B(C_6F_5)_4^-$ anion exhibited a significantly higher activity than silyl triflimides or triflates, with $\mathbf{22}^+$ being the most active Lewis acid in the reaction between cyclohexadiene and methyl acrylate (Scheme 1.10). Like in the transformation mediated by $\mathbf{21}^+$, the activity of the catalysts was preserved despite their low concentration relative to the oxygen-containing substrate and product.

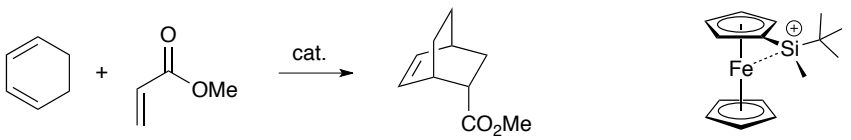

22$^+$

cat.	**22**$^+$ $[B(C_6F_5)_4]^-$	**14**$^+$ $[B(C_6F_5)_4]^-$	Et_3SiNTf_2 (Tf = SO_2CF_3)	Me_3SiOTf
Conditions	5 % cat., CH_2Cl_2, –78 °C, 3 h	1 % cat., PhMe, 0 °C, 1 h	1 % cat., PhMe, 0 °C, 1 h	10 % cat., PhMe, 0 °C, 1 h
Yield	95 %	97 %	13 %	0 %
endo/*exo*	> 99 %	98 %	n.d.	–

Scheme 1.10. Diels–Alder reaction catalyzed by silyl Lewis acids of different reactivity.

Lewis acid catalysis is also of great importance in cationic polymerization. The utility of silyl cations in this field has been demonstrated in two recent publications. In Reed's group it was discovered that silyl carboranes such as $Et_3Si–CHB_{11}H_5Br_6$ catalyze the ring-opening polymerization of the cyclic phosphazene trimer $(NPCl_2)_3$ to give linear $(N{=}PCl_2)_n$ (Scheme 1.11).[91] The product is an important precursor of a variety of tunable nitrogen- and oxygen-containing polymers of the composition $(N{=}PX_2)_n$ (X = NR_2, OR). The silylium-catalyzed reaction proceeded at room temperature, whereas significantly higher temperatures are required in the absence of Lewis acids (melt, 250 °C) or in the presence of BCl_3 (*ca.* 200 °C).[92]

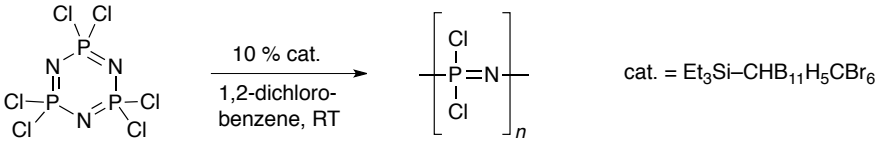

Scheme 1.11. Silyl carborane-promoted polymerization of $(NPCl_2)_3$.

Group 4 metallocene complexes are among the most active catalysts for the polymerization of alkenes. Usually neutral metallocene precursors are converted to electron-deficient cationic species that offer an empty coordination site and allow for the coordination–

insertion mechanism with unsaturated substrates. Anticipating that a pronounced electrophilicity of the metal center would facilitate the initial alkene–metal bonding, Chen and Zhang developed a new class of titanium- and zirconium-based dicationic silylium-metallocenium complexes.[93] Indeed, a rate-enhancing effect by double activation of the

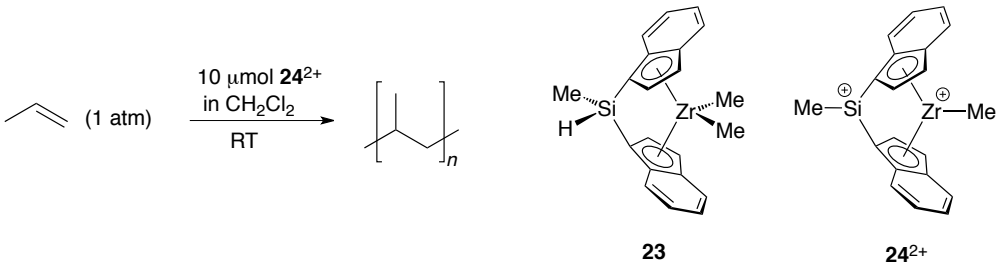

Scheme 1.12. Propene polymerization catalyzed by a dicationic silylium-zirconocenium complex.

precatalysts was observed. Treatment of, *e.g.*, complex **23** with two equivalents of $[Ph_3C][B(C_6F_5)_4]$ afforded dication $\mathbf{24}^{2+}$, and this system showed a 40 % higher activity in the polymerization of propene than the zirconocenium monocation.

More than any other main group reactive intermediate, silyl cations are predestined to effect C–F activation by fluoride abstraction from organic precursors. This activation, which formally affords a carbocation, can be coupled to a subsequent reaction with a hydrosilane, leading to the reduced starting material and a fluorosilane. Because of the opposite relative bond strengths C–F < Si–F and C–H > Si–H, the overall metathesis R_3C–F + R'_3Si–H → R_3C–H + R'_3Si–F is thermodynamically favored.

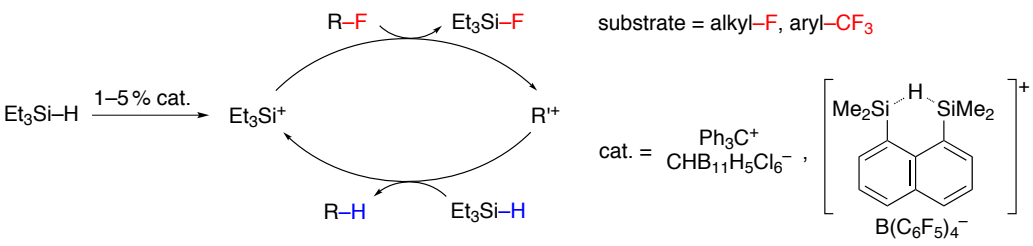

Scheme 1.13. Hydrodefluorination using Et_3SiH and a cationic initiator.

The groups of Mueller and Ozerov have designed systems that bring about hydrodefluorination of saturated and benzylic substrates using Et_3SiH and 1–5 % of a cationic initiator (Scheme 1.13).[60, 65, 94, 95] These reactions could be run at room temperature in aromatic solvents or in neat substrate. As in the case of other silylium-mediated transformations, low nucleophilicity of the counteranion was crucial. While catalysts paired with weakly coordinating anions gave high turnover numbers, reagents such as Et_3SiOTf showed no activity at all.

The advances in silyl cation chemistry over the past 20 years must be regarded as a success story. Compounds whose existence was doubted before the seminal contributions by Lambert and Reed can be generated with relatively little effort today. Reliable synthetic routes and optimized reaction conditions have provided the methodology to generate and study silylium-like species of different color and for different purposes. It will nevertheless be a challenge to synthesize compounds of controlled stability and reactivity in order to further explore the possibilities and limitations of silyl cation chemistry.

Chapter 2

Synthesis of a New Class of Silylium Ions

2.1 Summary

A series of (2,6-diarylphenyl)dimethylsilylium ions was synthesized. On the basis of computations, the diarylphenyl skeleton was expected to provide steric enshrouding of the positively charged cavity as well as an overall thermodynamic stabilization by π_{aryl}–$3p_{\text{Si}}$ interactions. Cations $\mathbf{27}^{+}$ with different flanking rings (xylyl, mesityl, duryl, pentamethylphenyl) were prepared under weakly nucleophilic conditions and examined by NMR spectroscopy. Their ^{29}Si NMR shifts ranged from 80–59 ppm and gave evidence for the tunability of silyl cationic character by controlling the degree of internal π electron donation. The idea behind cation $\mathbf{32}^{+}$ was the synthesis of a silyl Lewis acid that could be used in stereoselectively conducted reactions. This species was prepared successfully, however, *anti–syn* isomerization over one day at room temperature indicated an unexpected configurational lability.

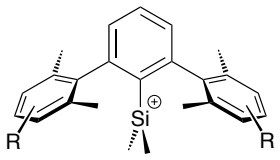

27^{+}

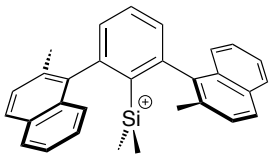

32^{+}

2.2 Introduction

The isolation of toluene solvate $\mathbf{14}^+$ and silyl carboranes such as **15** demonstrated the extraordinary Lewis acidity of tricoordinate silyl cations. A decrease in silylium ion character by adduct formation with weak donors such as arene π systems and covalently bound halogens became apparent from the crystal structures and ^{29}Si NMR shifts. Nonetheless, these systems have been shown to act as powerful silyl Lewis acids, a finding that justifies the term silylium-*like* and has motivated chemists to develop cations with intentional pacification of the silicon center.

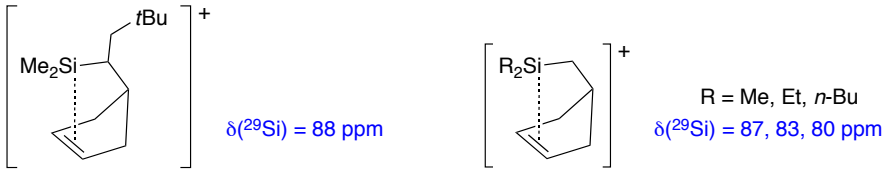

25$^+$ **26**$^+$

Cation stabilization by intramolecular π coordination was first reported by Müller and coworkers, who prepared silanorbornyl systems $\mathbf{25}^+$ and $\mathbf{26}^+$ in 1997 and 2003, respectively.[96, 97] The ^{29}Si resonances in the range of 80–88 ppm as well as further NMR and computational studies were in agreement with a symmetrical alkene–Si interaction, comparable in strength to that of arene-coordinated trialkylsilylium ions.

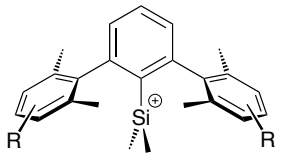

27$^+$

The desire to prepare long-lived silyl cations of controlled Lewis acidity provided the impetus for the current study. We chose $\mathbf{27}^+$ as our target class of cations. The premise was that the 2,6-diarylphenyl scaffold would exert an overall stabilizing effect by π_{aryl}–$3p_{\text{Si}}$ interactions and offer a steric protection of the silicon center. Donation of π_{aryl} electron density from the lateral rings to the empty $3p_{\text{Si}}$ orbital was expected to lead to a reduced amount of positive charge on the silicon center and a decreased silyl Lewis acidity (Figure

2.1 a). The *ortho*,*ortho*-disubstituted rings, entailing restricted rotation about the biaryl bonds, should prevent anion and solvent molecules from interacting with the positively charged cavity (Figure 2.1 b, $\alpha, \beta \approx 90°$).[98, 99]

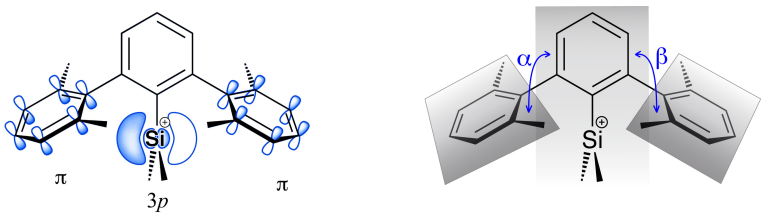

Figure 2.1. Target ions **27**$^+$ with a) schematic representation of the $3p_{Si}$ and π_{aryl} orbitals and b) highlighted dihedral angles of the lateral rings with respect to the central ring.

A key feature of the target system was the anticipated tunability of the silyl Lewis acidity. The degree of π donation should be influenced by varying the number of electron-releasing methyl groups on the flanking rings. A similar effect was observed by Siegel and coworkers in a study of 2,6-diarylbenzoic acids **28**. The pK_a values of **28** varied with the electronic influence of the substituents X and Y (*e.g.*, 6.61, X = OCH_3, Y = H; 5.78, X = $C(O)CH_3$, Y = H), results that were attributed to a dominant polar–π effect.[100]

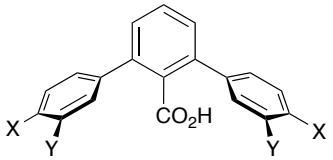

28

X = H, Me, OMe, Hal, C(O)Me
Y = H, OMe, C(O)Me

2.3 Calculations

The highest symmetry that cations **27**$^+$ can adopt is C_{2v}, but one can easily imagine distorted geometries, *e.g.*, with the silicon center being closer to one of the flanking rings or with dihedral angles α, β differing from 90 °, for which the symmetries C_s, C_2 or C_1 result (Figure 2.2).

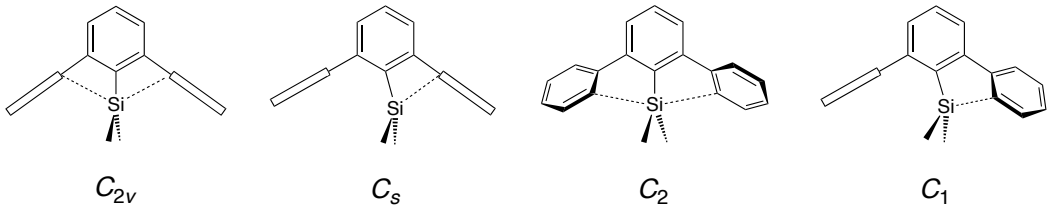

Figure 2.2. Schematic representation of the C_{2v}, C_s, C_2 and C_1 conformations of **27**$^+$ (substituents on flanking rings omitted for clarity).

Hybrid density functional computations including full geometry optimizations at the B3LYP/DZ-(2df,pd) level of theory were performed on the four cations **27a–d**$^+$.[101] For all cations, the C_1 conformer is predicted to be the most stable geometry, and the C_2, C_s and C_{2v} forms are higher in energy by 13–52 kJ mol^{-1} (Table 2.1). For the C_1 geometry, the calculations suggest a specific arene–Si$^+$ interaction with a relatively short C$_{ortho}$–Si distance of *ca.* 2.1 Å.

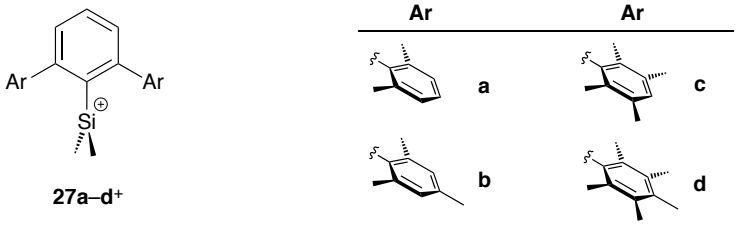

Table 2.1. Calculated relative energies (kJ mol^{-1}) and ^{29}Si NMR shifts (ppm vs SiMe$_4$) of cations **27**$^+$. Relative energies calculated at the B3LYP/DZ(2df,pd) level of theory, chemical shifts at the B3LYP/DZ+(2df,pd)//B3LYP/DZ(2df,pd) level of theory.

	C_1		C_2		C_s		C_{2v}	
	E_{rel}	$\delta(^{29}Si)$	E_{rel}	$\delta(^{29}Si)$	E_{rel}	$\delta(^{29}Si)$	E_{rel}	$\delta(^{29}Si)$
27a$^+$	0	81.21	14.14	200.35	26.23	150.12	40.63	258.59
27b$^+$	0	80.35	17.03	196.65	29.92	128.86	43.97	250.18
27c$^+$	0	62.70	13.22	179.54	31.42	140.54	49.25	250.29
27d$^+$	0	57.88	14.56	177.68	32.72	120.77	51.63	242.55

The calculated ^{29}Si NMR shifts are lowest for the C_1 conformer (58–81 ppm), whereas those for the C_2, C_s and C_{2v} structures are significantly higher, ranging from 150 to 259

ppm. Enhanced electron-donor character of the lateral rings is reflected in the decreasing values on going from **27a**$^+$ to **27d**$^+$.

Given the computated relative energies and ^{29}Si NMR shifts, one could anticipate a dynamic behavior of the cations in solution at ambient temperature. In such an equilibrium, the four degenerate C_1 conformations are equally populated, and the $SiMe_2$ fragment oscillates between the two flanking rings as well as between the two C_{ortho} positions of each ring.

2.4 Synthesis of the Cation Precursors

Hydride transfer from neutral precursors to the trityl cation was the synthetic strategy envisaged to generate cations **27**$^+$ (Scheme 2.1). Therefore silanes **29** were chosen as initial target molecules. Their synthesis involved in a first step Hart coupling of 1,3-dichloro-2-iodobenzene with arylmagnesium bromides to give iodoterphenyls **30** (Scheme 2.2).[102, 103] These reactions proceeded in typical yields of 70 % in the case of **30a–c**, however, reduced yields resulted for **30d**. In this case, roughly equal amounts of the desired product and the 1,2-diaryl-3-iodo compound were obtained.

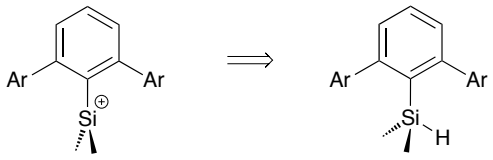

27$^+$ **29**

Scheme 2.1. Target ions **27**$^+$ and neutral silane precursors **29**.

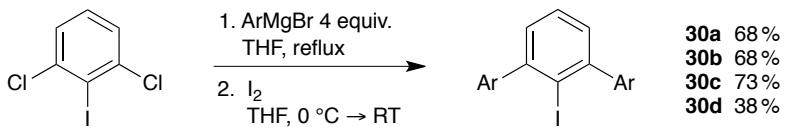

30

30a 68 %
30b 68 %
30c 73 %
30d 38 %

Scheme 2.2. Synthesis of iodoterphenyls **30** by Hart coupling.

Lithiation of the iodoterphenyls and subsequent reaction with chlorodimethylsilane afforded silanes **29** (Scheme 2.3). The procedure initially employed gave yields in the range of 60–90 %, but also 10–30 % of the protonated, and sometimes traces of butylated terphenyls formed (2.3 a). The by-products probably stemmed from the reaction of lithiated **30** with iodobutane from the I–Li exchange. Their formation could be suppressed by the addition of one equivalent of lithium diisopropylamide (LDA) to the solution of **30** prior to the I–Li exchange (2.3 b). As soon as iodobutane formed, it was converted to butene and LiI by LDA; diisopropylamine from this elimination was in turn deprotonated by an additional equivalent of butyllithium to give LDA and butane. By the combined LDA/BuLi strategy, silanes **29** were reliably obtained in high to quantitative yields.

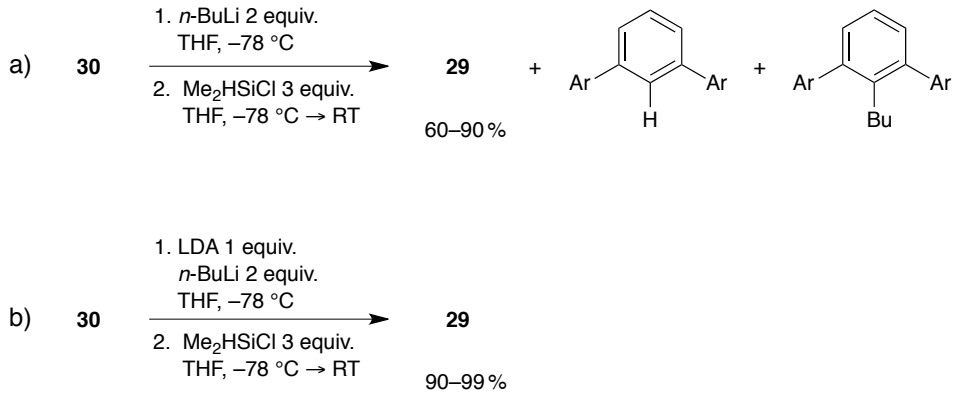

Scheme 2.3. Synthesis of silanes **29** by lithiation–silylation of iodoterphenyls **30**; a) original procedure affording the protonated and butylated by-products, b) improved procedure with additional lithium diisopropylamide in the lithiation step.

Silanes **29** are colorless compounds that can be exposed to air for months without showing any sign of oxidation (**29a** is an oil, **29b**–**d** are crystalline solids). In their ^{1}H NMR spectra, characteristic Si–H and Si–CH_3 signals appear around 4 ppm and 0 ppm, respectively (Figure 2.3). In C_6D_6, the ^{29}Si resonances of **29a**–**d** are -23.0, -23.0, -23.2 and -23.2 ppm, revealing no significant polar-π effect from the lateral rings (Figure 2.4).

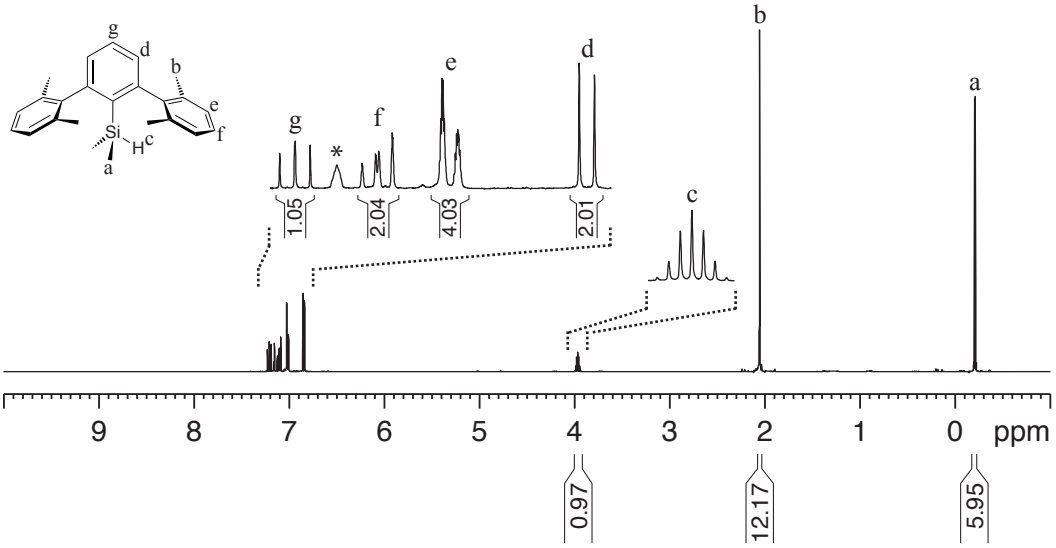

Figure 2.3. ^{1}H NMR spectrum of **29a**. Conditions: 400 MHz, 300 K, 35 mg in 0.6 mL C_6D_6; the signal marked with an asterisk stems from C_6HD_5 = 7.16 ppm.

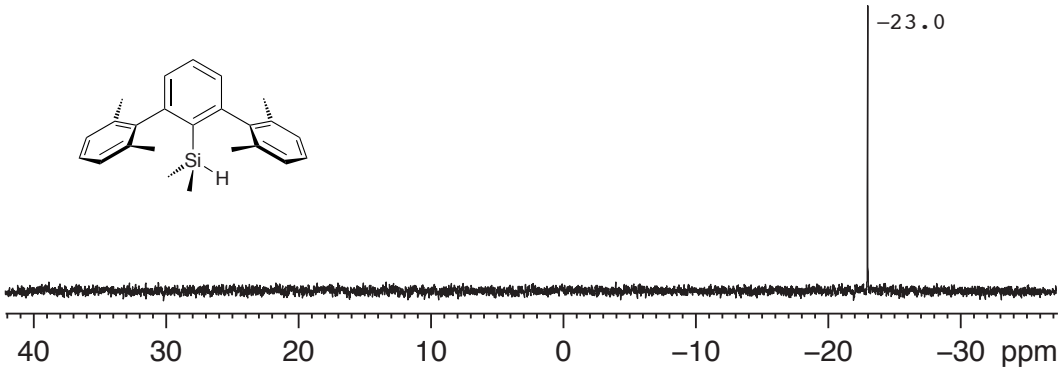

Figure 2.4. ^{29}Si{^{1}H} NMR spectrum of **29a**. Conditions: 80 MHz, 300 K, 35 mg in 0.6 mL C_6D_6, referenced against external $SiMe_4$.

2.5 Synthesis of the Silyl Cations

Trityl salts of weakly coordinating anions $[Ph_3C][Y]$ ($Y^- = B(C_6F_5)_4^-$, carborane$^-$) proved to be efficient hydride abstraction reagents to convert the hydrosilanes to cations **27**$^+$ (Scheme 2.4). When the reactions were followed by ^{1}H NMR spectroscopy, disappearence of the starting materials and formation of the cations and Ph_3CH was observed within hours (**27a**) to one day (**27b**–**d**) at ambient temperature. Based on ^{1}H NMR integrals of such solutions, target ions **27**$^+$ were formed cleanly in 90 % to quantitative yields.

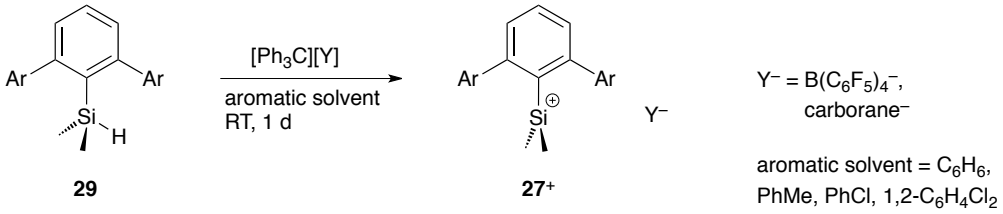

29 **27**$^+$

Scheme 2.4. Generation of cations **27**$^+$ by hydride abstraction from silane precursors **29**.

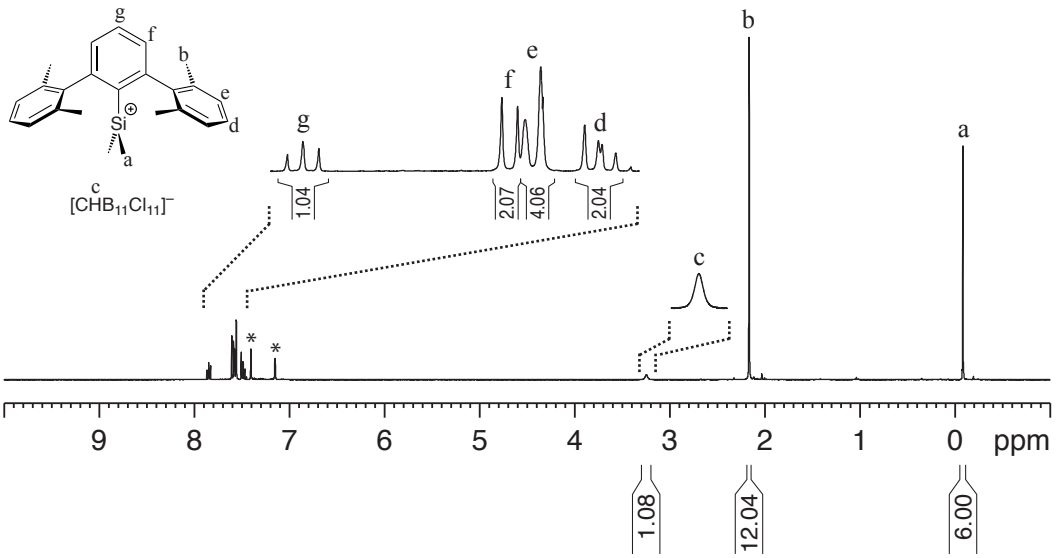

Figure 2.5. ^{1}H NMR spectrum of [**27a**][$CHB_{11}Cl_{11}$]. Conditions: 400 MHz, 300 K, 22 mg in 0.6 mL 1,2-$C_6D_4Cl_2$, referenced against external $SiMe_4$; the signals marked with an asterisk stem from 1,2-$C_6HD_3Cl_2$.

Isolation of the salts [**27**][Y] was possible by precipitation with pentane or hexane. With the counterion $B(C_6F_5)_4^-$, sometimes highly viscuous oils instead of solids were obtained even after several cycles of redissolution–precipitation–solvent evaporation. In this regard the carboranes lived up to their reputation as well-behaved anions and almost always afforded the desired product as yellow powders of high purity (Figure 2.5); isolated yields ranged from 80–95 %. Under an inert atmosphere, cations $\mathbf{27}^+$ did not show any sign of decomposition over months at room temperature, neiter in the solid state nor in solution.

The ^{29}Si NMR shifts of $\mathbf{27a}$–$\mathbf{d}^+$ in C_6D_6 were observed at 80–59 ppm (Figure 2.6, Table 2.2). The enhanced shielding on going from xylyl to pentamethylphenyl lateral rings reflects the anticipated increase in electron donation by more electron-rich π systems. The magnitude of the shifts matches well with those predicted for the C_1 isomers and, in the case of $\mathbf{27a}^+$, is comparable to that of Et_3Si^+ in toluene-d_8 solution (82 ppm).[30] While the observed values are far from shifts of tricoordinate triarylsilylium ions or those projected for free trialkylsilylium ions, the differences in chemical shift between hydrosilanes **29** and their corresponding cations $\mathbf{27}^+$ ($\Delta\delta$ = 82–103 ppm) are consistent with a pronounced build-up of positive charge on the silicon center.

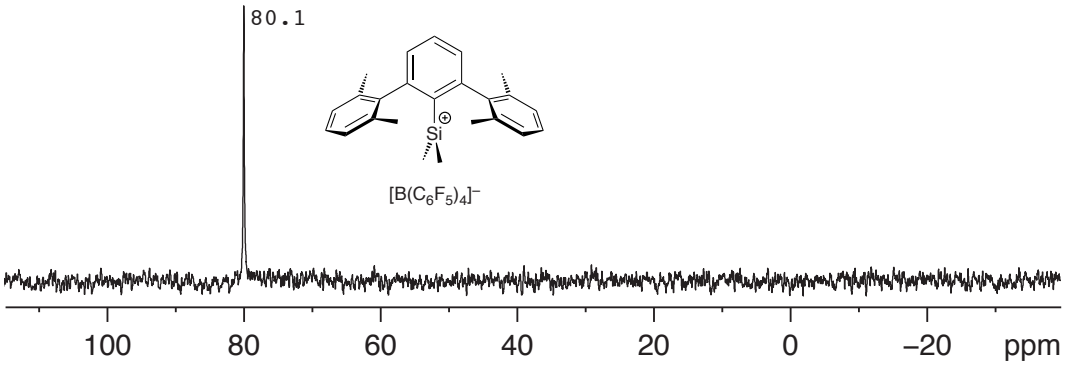

Figure 2.6. ^{29}Si{^{1}H} NMR spectrum of [**27a**][$B(C_6F_5)_4$]. Conditions: 60 MHz, 300 K, oily layer of reaction mixture, *ca.* 240 mg in 0.6 mL C_6D_6, referenced against external $SiMe_4$.

Table 2.2. ^{29}Si NMR shifts of silanes **29** and the respective cations **27**$^+$ (C_6D_6, ppm vs external $SiMe_4$, $B(C_6F_5)_4^-$ anion).

Silane	δ(**^{29}Si**)	Cation	δ(**^{29}Si**)[a]	$\Delta\delta$
29a	–23.0	**27a**$^+$	80.1 (81.2)	+103.1
29b	–23.0	**27b**$^+$	79.1 (80.4)	+102.1
29c	–23.2	**27c**$^+$	60.6 (62.7)	+83.8
29d	–23.2	**27d**$^+$	58.6 (57.9)	+81.8

[a] Values in parentheses are calculated for the C_1 conformer in the gas phase, B3LYP/DZ+(2df,pd)//B3LYP/DZ(2df,pd).

2.6 General Reactivity

Based on the ^{29}Si NMR shifts that indicated effective π_{aryl}–$3p_{\text{Si}}$ interactions and the steric shielding of the $SiMe_2$ moiety, one could have expected a reduced electrophilicity of cations **27**$^+$. However, their reactivity was in no way inferior to the silyl Lewis acidity of arene-coordinated trialkylsilylium ions.

In attempts to generate **27**$^+$ with trityl salts of less inert anions such as BF_4^-, PF_6^-, SbF_6^- and $[B(3,5\text{-}C_6H_3(CF_3)_2)_4]^-$, hydride transfer was immediately followed by anion decomposition to give fluorosilanes **27**–F. Similarly, dissolution of [**27**][$B(C_6F_5)_4$] in chlorinated aliphatic solvents like dichloromethane and 1,2-dichloroethane lead to dark brown reaction mixtures whose NMR spectra showed disappearence of the silyl cations. This finding was in line with chloride abstraction concomitant with solvent decomposition by highly reactive carbocations or chloronium ions.

Addition of CsF, H_2O or $NaBH_4$ to solutions of **27**$^+$ in aromatic solvents afforded fluorosilanes **27**–F, hydrosilanes **27**–H = **29** and silanols **27**–OH. The formation of these products was not very surprising, but it gave evidence for the exclusive attack of silicon by nucleophiles of different hardness and provided a means of converting the cations into derivatives that could be analyzed by GC–MS.

Table 2.3. ^{29}Si NMR shifts of donor adducts of the cations **27**$^+$ ($B(C_6F_5)_4^-$ anion, solvent mixture 1,2-$C_6H_4Cl_2$/C_6D_6 1:1, ppm vs external $SiMe_4$).

Adduct	δ(^{29}Si)
[**27a**(CD_3CN)]$^+$	16.4
[**27b**(CD_3CN)]$^+$	16.4
[**27c**(CD_3CN)]$^+$	15.9
[**27d**(CD_3CN)]$^+$	15.9
[**27a**(PPh_3)]$^+$	11.8 ($^1J_{Si,P}$ = 25 Hz)

Treatment of **27**$^+$ with acetonitrile-d_3 lead to donor adducts [**27**(CD_3CN)]$^+$ with decreased silyl cationic character (Scheme 2.5). These complexes could be prepared either by carrying out the hydride abstraction in the presence of CD_3CN or by addition of one or more equivalents of CD_3CN to solutions of **27**$^+$ in an aromatic solvent. ^{29}Si NMR resonances were observed at 16.4 ppm ([**27a**,**b**(CD_3CN)]$^+$) and 15.9 ppm ([**27c**,**d**(CD_3CN)]$^+$) (Table 2.3). The almost identical values in the typical range of heteroatom-coordinated silyl cations suggested that species with predominant acetonitrilium ion character had formed and that the craving of silicon for π electron density was drastically attenuated. In the ^{1}H (signal of residual CD_2HCN) and ^{13}C NMR spectra, free and bound ligand could not be distinguished. This fast equilibrium on the NMR time scale indicated a barrier of <60 kJ mol^{-1} for CD_3CN exchange according to the Gutowsky–Holm approximation.[104]

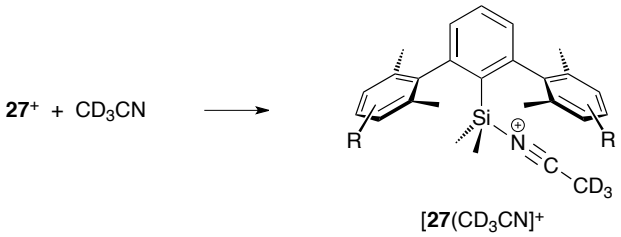

Scheme 2.5. Formation of acetonitrile adducts [**27**(CD_3CN)]$^+$.

The sterically more demanding nucleophile PPh_3 reacted with **27a**$^+$ to give the corresponding phosphonium ion [**27a**(PPh_3)]$^+$ quantitatively according to ^{1}H, ^{13}C, ^{29}Si and ^{31}P NMR spectroscopy (Scheme 2.6 a). Its ^{29}Si signal at 11.8 ppm and the $^1J_{Si,P}$ coupling

of 25 Hz clearly indicated the formation of a tetracoordinate silicon species. Furthermore, with a slight excess of PPh_3, free and bound phosphine gave separate NMR signals over the temperature range 300–340 K, implying a barrier to ligand exchange of >68 kJ mol^{-1} and a stronger coordination than in the case of acetonitrile.

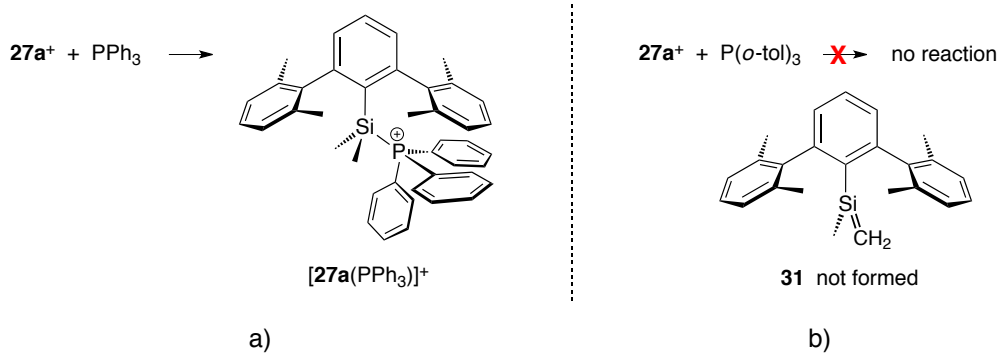

Scheme 2.6. a) Formation of phosphonium ion [**27a**$(PPh_3)]^+$ and b) attempted preparation of the P(*o*-tol)$_3$ analog.

A limit in terms of adduct formation was reached with the phosphine P(*o*-tol)$_3$ (Scheme 2.6 b). Addition of this nucleophile to a solution of $\mathbf{27a}^+$ gave rise to NMR resonances of unchanged starting materials. Apparently, steric crowding about both the silicon and phosphorus atoms prevented a Lewis acid–base reaction. Formation of the terphenylsil*ene* **31** or potential consecutive products were not observed, either. This was an important finding in that it suggested a low Brønsted acidity of the CH_3 groups at silicon despite the electron deficiency of the $SiMe_2$ moiety. In stark contrast, alkyl-substituted carbocations that are not stabilized by adjacent π systems or heteroatoms are extremely acidic. The *tert*-butyl cation, *e.g.*, has been estimated to be about as Brønsted-acidic as protonated benzene;[73] it can equally be regarded as halide-depleted Me_3C–X or as protonated isobutene.

2.7 Coordination by Anions and Aromatic Solvents

Cations $\mathbf{27a–d}^+$ possessed ^{29}Si NMR shifts that indicated internal stabilization of the formal Si^+, based both on a comparison with literature values and the computational results.

But was the silicon center exclusively interacting with the flanking rings? Based on measurements with one anion in one solvent, intermolecular coordination could not be excluded; a small equilibrium fraction of **27**–anion or [**27**(arene)]$^+$ would not exert a pronounced effect on the time-averaged NMR signals. Moreover, the adduct formation of **27a**$^+$ with PPh_3 demonstrated that even relatively bulky nucleophiles were capable of entering the terphenyl cavity.

To address the question of cation–anion interactions, the series [**27a**][Y] with Y^- = $B(C_6F_5)_4{}^-$, $CHB_{11}Cl_{11}{}^-$, $CHB_{11}H_5Cl_6{}^-$ and $CHB_{11}H_5Br_6{}^-$ was prepared, and NMR spectra of the four compounds were recorded under similar conditions. ^{29}Si resonances were observed at 81.3–79.3 ppm on going from $B(C_6F_5)_4{}^-$ to $CHB_{11}H_5Br_6{}^-$, the most basic anion (Table 2.4, entries 1–4); the shift differences were small but fully reproducible. The ^{1}H NMR signals of the Si–CH_3 groups appeared in the range of -0.70 to -0.47 ppm. When silanes **29** are converted to cations **27**$^+$, the Si–CH_3 protons become more shielded, probably because they experience a stronger ring current effect from the lateral rings in the supposed equilibrium of C_1 conformations. Thus both sets of values indicated that increasing anion basicity was associated with a slight decrease in silyl cationic character. Whether this attenuation resulted from a direct anion–Si interaction or a less specific ion pairing could not be decided with certainty.

The chemical shifts of the $SiMe_2$ moiety in [**27a**][$B(C_6F_5)_4$] in 1,2-dichlorobenzene

Table 2.4. ^{29}Si and ^{1}H NMR shifts of the $SiMe_2$ unit in **27a**$^+$ (all samples 15–18 μmol in 0.6 mL solvent, 300 K, C_6D_6 capillary for shimming and locking, ppm vs external $SiMe_4$; spectra recorded on the same instrument within one day).

Anion	Solvent	$\delta(^{29}Si)$	$\delta(^1H)$
$B(C_6F_5)_4{}^-$	1,2-$C_6H_4Cl_2$	81.3	–0.70
$CHB_{11}Cl_{11}{}^-$	1,2-$C_6H_4Cl_2$	80.6	–0.71
$CHB_{11}H_5Cl_6{}^-$	1,2-$C_6H_4Cl_2$	81.0	–0.57
$CHB_{11}H_5Br_6{}^-$	1,2-$C_6H_4Cl_2$	79.3	–0.47
$B(C_6F_5)_4{}^-$	1,2-$C_6H_4Cl_2$/C_6H_6 2:1	80.5	–0.73
$B(C_6F_5)_4{}^-$	1,2-$C_6H_4Cl_2$/toluene 2:1	80.3	–0.66

and mixtures of dichlorobenzene with benzene or toluene ranged from 81.3–80.3 ppm for ^{29}Si and were almost identical for the protons (Table 2.4, entries 1, 5 and 6). Although the slight shielding of the silicon center in the presence of benzene and toluene could be interpreted as an enhanced $\pi_{solvent}$–Si coordination, it could in principle also be caused by a change in the dielectric constant of the medium, *i.e.*, a change in a bulk solvent property.

Clearer evidence for a solvent–Si interaction came from experiments of **27d**$^+$ in mixed non-deuterated/deuterated arenes. Dissolution of [**27d**][$CHB_{11}Cl_{11}$] in a 1:1 mixture of 1,2-dichlorobenzene and C_6D_6 lead to substanstial H–D exchange within days at room temperature (Scheme 2.7, Figure 2.7). This observation was attributed to an acidification of the reaction mixture by initial solvent coordination to the silicon center. Reactions involving the lateral rings seemed unlikely because all positions are blocked by methyl groups.

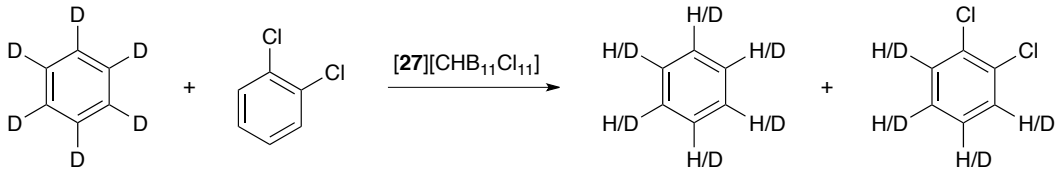

Scheme 2.7. H–D exchange between C_6D_6 and 1,2-$C_6H_4Cl_2$ mediated by silyl cation **27d**$^+$.

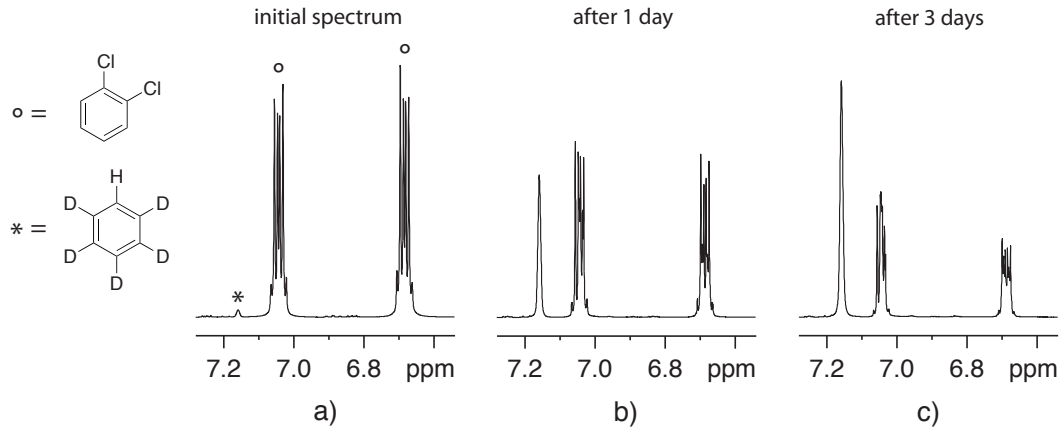

Figure 2.7. Solvent region of the ^{1}H NMR spectrum of [**27d**][$CHB_{11}Cl_{11}$] in C_6D_6–1,2-$C_6H_4Cl_2$ 1:1. a) 10 min after sample preparation, b) after 1 day, c) after 3 days. Conditions: 400 MHz, 300 K, 9 mg in a mixture of C_6D_6 (0.3 mL) and 1,2-$C_6H_4Cl_2$ (0.3 mL).

In the proposed mechanism, π coordination by a solvent molecule is followed by the formation of a Wheland intermediate (Scheme 2.8). This highly acidic species is capable of protonating or deuterating a second solvent molecule, affording arylated **27**–Ar and a new σ complex. From there on, H–D scrambling results from a cascade of subsequent protonation and deuteration steps. Because the equilibrium $\mathbf{27}^+$ + 2 arene $\rightleftharpoons$ **27**–Ar + [arene–H]$^+$ lies on the left, only minor amounts of **27**–Ar are present at any given time so that such species are not observed in the NMR spectra and their effect on the ^{29}Si resoncance is small.

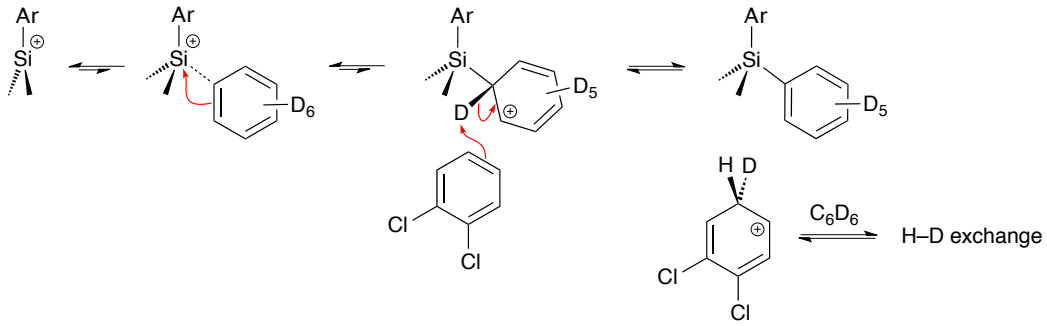

Scheme 2.8. Putative mechanism of solvent acidification by **27d**$^+$ leading to H–D exchange.

2.8 Synthesis of a C_2-Symmetrical System

Embedding a formal $[SiMe_2]^+$ fragment into a terphenyl scaffold had afforded a class of silylium ions with desirable properties: long-term stability, high reactivity and tunability of silyl cationic character. Given the promising results from the studies on $\mathbf{27}^+$, the synthesis of a system with defined stereochemistry was envisaged.

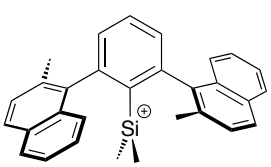

32$^+$

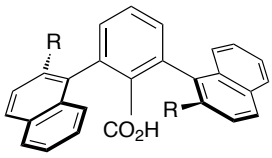

R = OMe, Me

33

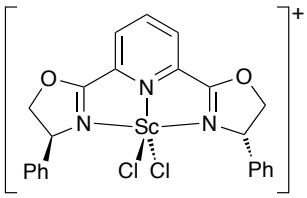

34$^+$

C_2-Symmetrical cation $\mathbf{32}^+$ was chosen as the target. The 2,6-disubstitution pattern of the central ring almost called for a structure with this stereochemistry: substituting the 2 and 6 positions with two identical chiral groups or attaching two unsymmetrical rings in an *anti* fashion would both lead to a chiral, C_2-symmetrical molecule. Carboxylic acids closely related to $\mathbf{32}^+$ were reported by Siegel and coworkers in 1995. Compounds **33** exhibited effective enshrouding of the acid moiety as evidenced by crystal structures, epimerization studies and polar-π effects on the pK_a values.[105] Cation $\mathbf{32}^+$ was expected to exhibit a π stabilization and reactivity comparable to those of $\mathbf{27}^+$. In its racemic or enantiomerically enriched form, it had the potential to work as a silyl cationic catalyst in dia- or enantioselectively conducted reactions, respectively. The utility of Lewis-acidic C_2-symmetrical complexes such as $\mathbf{34}^+$ in Aldol, Michael, and ene reactions was demonstrated by the groups of Evans and Vederas.[106–110]

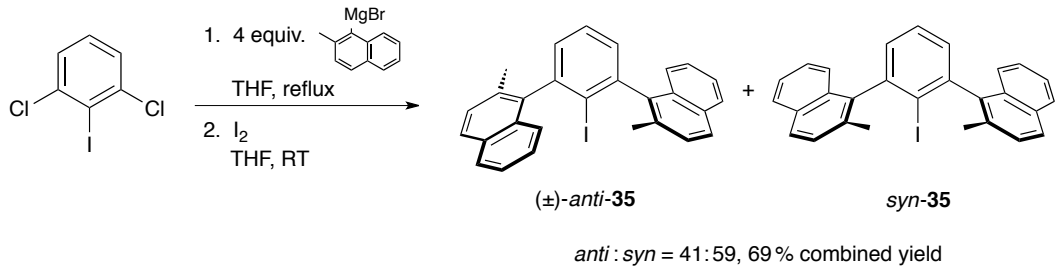

Scheme 2.9. Synthesis of the *anti* and *syn* iodo compounds **35**.

The synthetic strategy to prepare $\mathbf{32}^+$ was the same as for cations $\mathbf{27}^+$: Preparation of the 2,6-diaryl-1-iodobenzene, conversion to the silane, and finally generation of the cation by hydride abstraction. Iodo compound **35** was obtained by Hart coupling as a 41 : 59 mixture of (±)-*anti*-**35** and *syn*-**35** (Scheme 2.9). Enrichment to ratios of 95 : 5 and 15 : 85 was accomplished by recrystallization from nitromethane–toluene.

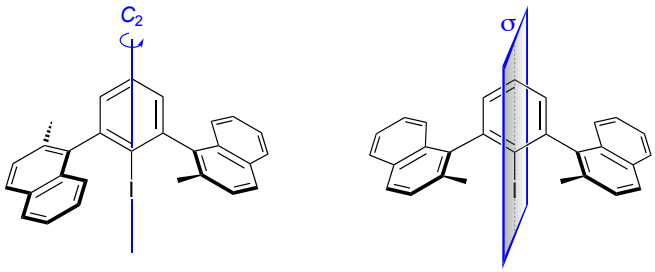

Figure 2.8. Homotopicity and enantiotopicity of the naphthyl rings in *anti*- and *syn*-**35**.

The identity of the isomers could not be established on the basis of their ^{1}H and ^{13}C NMR spectra at this stage of the synthesis. Both gave rise to the same number of signals and similar shifts due to the homotopicity and enantiotopicity of the naphthyl rings in (±)-*anti*-**35** and *syn*-**35**, respectively (Figure 2.8). A distinction of the two compounds became possible after their conversion to the silanes. Iodo compounds **35** possess high configurational inertness: No equilibration of enriched material took place in 1,2-dichlorobenzene over three days at 190 °C, indicating a barrier to biaryl rotation of >170 kJ mol^{-1}.

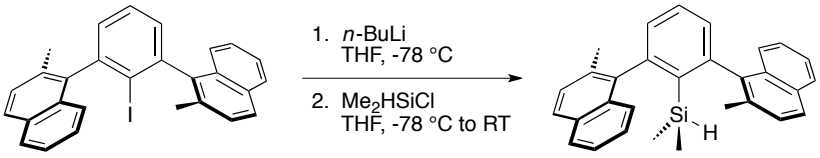

anti : *syn* = 95 : 5

69 %, *anti* : *syn* = 97 : 3
after recrystallization

Scheme 2.10. Synthesis of *anti*-dinaphthylsilane **36**.

Lithiation and subsequent silylation of *anti*-**35** gave hydrosilane **36** in an *anti* : *syn* ratio of 97 : 3 after recrystallization from isopropanol (Scheme 2.10). The isomers could now be dinstinguished on the basis of their ^{1}H and ^{13}C NMR spectra. The silyl CH_3 groups in *anti*-**36** are diastereotopic on any time scale of observation and afford different signals in the NMR spectra (Figure 2.9).

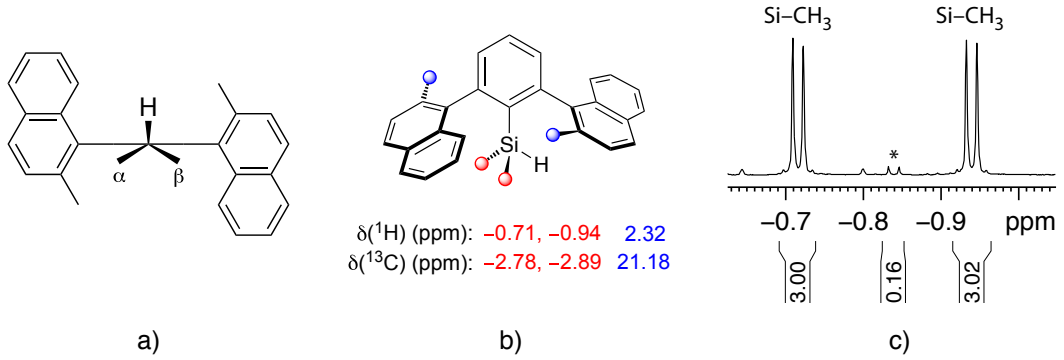

Figure 2.9. Diastereotopicity of the silyl CH_3 groups in *anti*-**36**. a) Lewis structure, view along the Si–C_{aryl} axis, b) ^{1}H and ^{13}C NMR shifts of the silyl CH_3 and aryl CH_3 groups, c) ^{1}H NMR signals of the silyl CH_3 groups. NMR conditions: 300 MHz, 300 K, 9 mg in 0.6 mL $CDCl_3$ (residual $CHCl_3$ = 7.25 ppm, *C*DCl_3 = 77.0 ppm); the signal marked with an asterisk stems from *syn*-**36**.

Enriched *syn*-**36** was prepared similarly to the *anti* isomer in a *syn* : *anti* ratio of 88 : 12. In this compound the silyl CH_3 groups are enantiotopic when the Si–H vector is perpendicular to the plane of the central ring, and fast rotation of the silyl group about the Si–C_{aryl} axis on the NMR time scale leads to one Si–CH_3 signal (Figure 2.10).

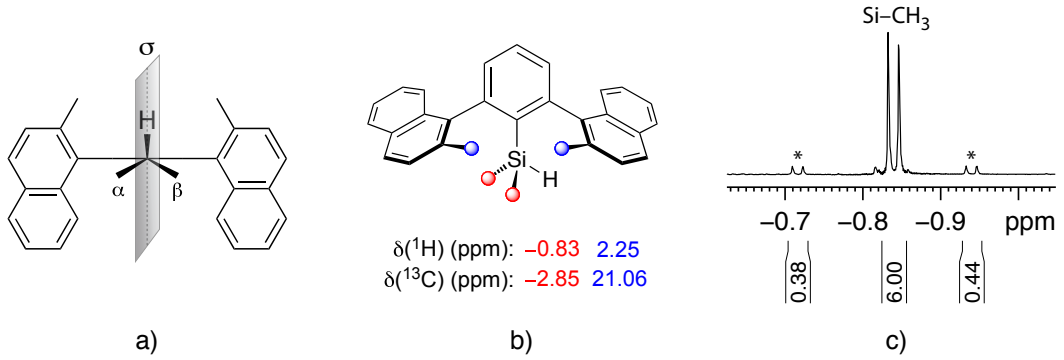

Figure 2.10. Enantiotopicity of the silyl CH_3 groups in *syn*-**36**. a) Lewis structure, view along the Si–C_{aryl} axis, b) ^{1}H and ^{13}C NMR shifts of the silyl CH_3 and aryl CH_3 groups, c) ^{1}H NMR signal of the silyl CH_3 groups. NMR conditions: 300 MHz, 300 K, 7 mg in 0.6 mL $CDCl_3$ (residual $CHCl_3$ = 7.25 ppm, *C*DCl_3 = 77.0 ppm); the signals marked with an asterisk stem from *anti*-**36**.

In the solid state, *anti*-**36** adopts a geometry with approximate C_2 symmetry of the 2,6-C_6H_3(naphthyl)$_2$ moiety and one of the Si–C_{Me} bonds being almost perpendicular with

respect to the plane of the central ring (Figure 2.11). The dihedral angles defined by the

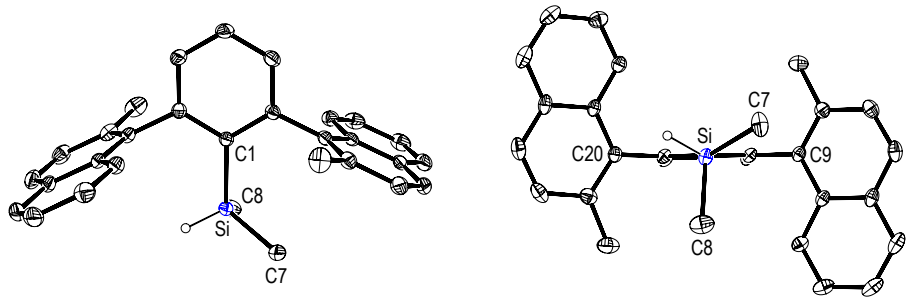

Figure 2.11. X-ray crystal structure of *anti*-**36** (30 % displacement ellipsoids, H atoms except for Si–H omitted for clarity.

least-squares planes through the naphthyl systems and the plane through the central ring are 87.48(7)° and 86.08(7)° for the lateral rings containing C9 and C20, respectively. The central silyl group exhibited Si–C distances of Si–C1 1.906(1) Å, Si–C7 1.862(2) Å and Si–C8 1.863(2) Å.

Hydride abstraction from *anti*-**36** by the trityl cation gave, quite surprisingly, a reaction mixture with two sets of signals in the NMR spectra. The ^{29}Si signals appeared at 46.5 and 46.3 ppm and suggested that two species with similar silyl cationic character had formed. When the hydride abstraction was carried out starting from *syn*-**36** or a mixture of isomers, the same NMR spectra were obtained after one day. Apparently, cation formation was followed by an equilibration of *anti*- and *syn*-**32**$^{+}$ (Scheme 2.11). The isomer ratio indicated a small energy difference of 2 kJ mol^{-1} between the cations. Once they were formed and equilibrium was reached, they showed now sign of decomposition in solution over months at room temperature.

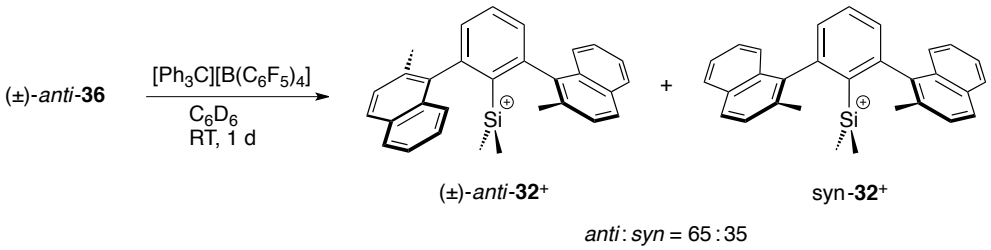

Scheme 2.11. Attempted preparation of *anti*-**32**$^+$.

The ratio of the isomers was determined after assignment of the high-field ^{1}H NMR peaks to the two cations. The silyl CH_3 groups in *syn*-**32**$^+$ are diastereotopic and give rise to two distinct signals at 290 K and below (-0.87 and -1.49 ppm in C_6D_6), whereas the corresponding CH_3 groups of *anti*-**32**$^+$ are homotopic and resonate at -1.22 ppm. NMR spectra recorded over the temperature range 270–340 K indicated that rotation of the silyl group about the Si–C_{aryl} axis in *syn*-**32**$^+$ is associated with a barrier of 57 kJ mol^{-1}.

Isomerization between the *syn* and *anti* form occurrs at a much faster rate with **32**$^+$ than in the case of **35** and **36**. This finding can be attributed to a preferred unsymmetrical π coordination in **32**$^+$, which seems likely given the relatively low ^{29}Si NMR shifts. When silicon is interacting with one of the π systems, the cation adopts a C_1 geometry with Si-C_{ipso}-C_{para} < 180° (C atoms of central ring). In this conformation, repulsive interactions between the silyl group and the non-coordinating naphthyl moiety are reduced, and rotation about the biaryl bond is facilitated in comparison to the neutral compounds **35** and **36** (Figure 2.12).

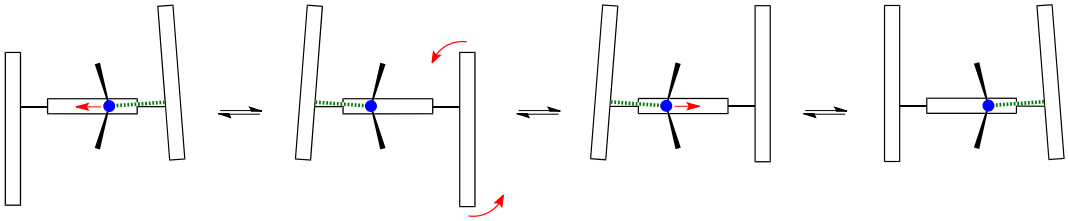

Scheme 2.12. Putative mechanism of the *anti* → *syn* isomerization in **32**$^+$. Blue, Si; green, π coordination; red, movement of Si or naphthyl moiety.

Preliminary studies showed that the acetonitrile adduct [*anti*-**32**(CD_3CN)]$^+$ is less prone to epimerization. When hydride abstraction from *anti*-**36** was carried out in the presence of a slight excess CD_3CN, NMR data were consistent with the formation of the *anti*-acetonitrilium complex, and no change in the spectra was observed over two days at room temperature. Enhanced configurational inertness due to tetracoordination of the silicon center and diminished π–Si interactions would also support the putative mechanism of isomerization depicted in Scheme 2.12.

With the generation of [*anti*-**32**(CD_3CN)]$^+$, synthesis of enantiomerically enriched cationic systems seems close at hand. Treatment of the racemic acetonitrilium ion with an optically active alcohol is expected to give silyl ethers *anti*-**32**–OR* (Scheme 2.13). Separation of the diastereoisomers and reduction of the separated compounds should afford enantiomerically enriched hydrosilanes *anti*-**36**. These in turn can be converted to enriched and presumably configurationally inert [*anti*-**32**(CD_3CN)]$^+$. Silylacetonitrilium ions still act as Lewis acids towards oxygen-containing substrates,[88] which makes further research into the utility of the naphthyl compounds worth persuing.

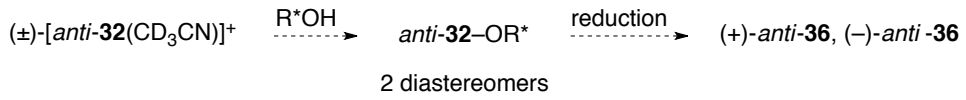

Scheme 2.13. Potential synthesis of resolved **36** via formation of diastereoisomeric silyl ethers.

2.9 Experimental Part

2.9.1 Literature

1,3-dichloro-2-iodobenzene was prepared from lithiated 1,3-dichlorobenzene and iodine according to a literature procedure.[103]

Trityl salts of $B(C_6F_5)_4^-$ and carborane anions were prepared according to literature procedures.[46, 94]

2.9.2 Nomenclature and Atom Numbering

The iodoterphenyl compounds were named according to the IUPAC nomenclature recommandations for terphenyls. The general atom numbering is shown in Figure 2.12 a.

Hydrosilane precursors and the corresponding cations were named as silanes and silylium ions, respectively. The used atom numbering is shown in Figure 2.12b.

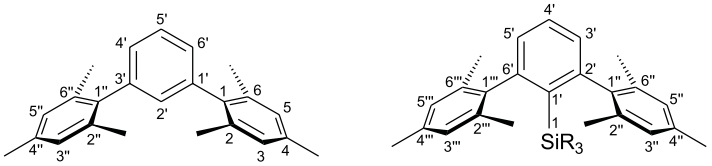

Figure 2.12. Atom numbering of (a) terphenyls and (b) silanes.

2.9.3 Reaction Conditions and Reagents

For reactions, solvents of pro analysi grade were used. Hexane, pentane, THF, benzene-d_6, and toluene-d_8 were distilled from sodium/benzophenone. Halogenated aromatic solvents were distilled from CaH_2. For work-up and purification, distilled solvents of technical grade were used. Table 2.5 lists grades and suppliers of the chemicals used for reactions.

All reactions were carried out under N_2. A dry N_2 atmosphere was used for experiments

in the glovebox ($O_2 < 1$ ppm, $H_2O < 1$ ppm). Glassware for moisture-sensitive reactions was dried at 150 °C for at least 24 hrs and allowed to cool in vacuo.

Table 2.5. Qualities and suppliers of chemicals used for syntheses

Compound	*Quality*	*Supplier*
Benzene-d_6	99.5 % D	CIL
2-Bromomesitylene	99 %	Aldrich
2-Bromomesitylene	99 %	Aldrich
2-Bromo-1,3-dimethylbenzene	99 %	Alfa Aesar
3-Bromo-1,2,4,5-tetramethylbenzene	99 %	Alfa Aesar
1-Bromo-2,3,4,5,6-pentamethylbenzene	99 %	Alfa Aesar
n-Butyllithium ca. 1.6 M in hexane		Aldrich
Toluene-d_8	99.6 % D	CIL

2.9.4 Characterization

Melting points were determined using a heating microscope from Christoffel Labor- and Betriebstechnik and are uncorrected.

Infrared spectra were recorded on a Perkin-Elmer Spectrum One FT-IR spectrophotometer. Compounds were measured as KBr pellets (solids) or as films between NaCl plates (oils). Absorption bands are given in wave numbers (cm^{-1}), and the intesities are characterized as follows: *s* = strong (0–33 % transmission), *m* = medium (34–66 % transission), *w* = weak (67–100 % transmission).

NMR spectra were recorded on Bruker AV-300 (^{1}H), ARX-300 (^{1}H, ^{13}C, ^{29}Si), AV-400 (^{1}H, ^{13}C, ^{11}B, ^{29}Si, ^{31}P), AV-500 (^{1}H, ^{13}C, ^{29}Si) and DRX-600 (^{1}H, ^{13}C, ^{29}Si) instruments.

The signals were referenced against internal $SiMe_4$ ($\delta(Si(CH_3)_4) \equiv 0$ ppm for ^{1}H,

^{13}C, and ^{29}Si) if not otherwise indicated, or solvent peaks (^{1}H: residual $CHCl_3$ 7.25 ppm, residual $CHDCl_2$ 5.32 ppm, residual C_6HD_5 7.16 ppm; ^{13}C: $CDCl_3$ 77.0 ppm, CD_2Cl_2 54.0 ppm, C_6D_6 128.0 ppm). Calibration against external standards (sensitive samples, ^{11}B and ^{19}F) was done using 5 mm tubes containing 10 % (v/v) $SiMe_4$ in C_6D_6, 5 % (v/v) CCl_3F in C_6D_6 or a $BF_3{\cdot}Et_2O$ capillary in acetone-d_6, δ(^{1}H, ^{11}B, ^{19}F and ^{29}Si = 0 ppm).

Data are reported as follows: chemical shift in ppm, multiplicity (*s* = singulet, *d* = doublet, *t* = triplet, *q* = quadruplet, *m* = multiplet, *dd* = doublet of doublet, *dt* = doublet of triplet, etc.), coupling constant ^{n}J in Hz, integration, and interpretation. Multiplicities in ^{13}C NMR spectra were determined using DEPT (Distortionless Enhancement by Polarization Transfer) experiments. Atom-by-atom assignments were made on the basis of HSQC and HMBC experiments.

Mass spectra were recorded on a HP 5890 GC–MS instrument (EI, 70 eV) or by the Laboratory for Mass Spectroscopy of the Organich Chemistry Institute of the University of Zurich (HR-MS). Data are reported as follows: m/z, % relative intensity and possible fragment.

Elemental analyses were performed by the Microanalytical Laboratory of the Organisch-chemisches Institut of the University of Zurich and are given as calculated and found elemental constituents in %.

X-ray structure analyses were carried out by the Laboratorium für Computerchemie und Röntgenstrukturanalyse of the Organisch-chemisches Institut of the University of Zurich. A Nonius KappaCCD diffractometer with Mo$K\alpha$ radiation (λ = 0.71037 Å) was used.

2.9.5 General Procedure for the Preparation of the Iodoterphenyls

The iodoterphenyls were synthesized following a procedure by Hart and coworkers:[102, 103]

To a dry three-necked 50 mL reaction flask, equipped with an addition funnel, condenser with N_2 inlet, and stir bar, Mg turnings (10 mmol) and a small I_2 crystal were added. A solution of Ar–Br (10 mmol) in dry THF (10 mL) was added dropwise. After warming

the mixture for 1 min, formation of the Grignard reagent started. The Ar–Br solution was added at such a rate that the mixture kept refluxing. After complete addition, the reaction mixture was refluxed over a period of 4 hrs. A solution of 1,3-dichloro-2-iodobenzene (2.5 mmol) in dry THF (10 mL) was added over 60 min. The mixture was refluxed for 18 hrs. It was allowed to cool to rt, then cooled to 0 °C in an ice bath. I_2 (10 mmol) was added in one portion. After 30 min the ice bath was removed, and the turbid brown mixture was stirred vigorously at rt for 20 hrs.

After the addition of H_2O (20 mL), $NaHSO_3$ was added until the I_2 color no longer persisted. The mixture was extracted with CH_2Cl_2 (3 × 30 mL), the organic layers were washed with H_2O (40 mL), and the aq. washing layer was re-extracted with CH_2Cl_2 (30 mL). The combined organic layers were dried over $MgSO_4$, filtered, and evaporated. The purification was carried out as described for the individual compounds.

2.9.5.1 2'-Iodo-2,6,2",6"-tetramethyl-1,1':3',1"-terphenyl

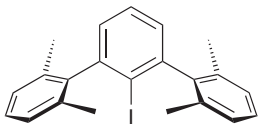

Chemical Formula: $C_{22}H_{21}I$
Molecular Weight: 412.307

The crude product was washed with hexanes and purified by column chromatography (SiO_2, hexanes/CH_2Cl_2 94:6). The iodoterphenyl was obtained as a colorless solid (68 %).

Characterization

M.p.: 138.0–138.5 °C

IR (KBr): 3037*m*, 2968*m*, 2934*m*, 2911*m*, 2852*w*, 2732*w*, 1932*w*, 1858*w*, 1664*w* 1578*m*, 1542*w*, 1478*m*, 1459*s*, 1385*m*, 1295*w*, 1273*w*, 1179*w*, 1163*m*, 1079*m*, 1012*m*, 1001*m*, 900*w*, 803*s*, 770*s*, 734*s*, 695*m*, 684*w*, 563*w*, 549*w*.

^{1}H NMR (300 MHz, 8 mg in 0.6 mL $CDCl_3$): 7.49 (*t*, $^3J = 7.5$, 1 H, H–C(5')), 7.25–7.11 (2 *m*, 6 H, H–C(3, 4, 5, 3", 4", 5")), 7.10 (*d*, $^3J = 7.5$, 2 H, H–C(4', 6')), 2.02 (*s*, 12 H,

CH_3).

$^{13}C\{^1H\}$ NMR (75 MHz, 50 mg in 0.6 mL $CDCl_3$, $\delta(CDCl_3) = 77.0$): 147.2, 144.7, 135.5 (3*s*, 8 quat. C), 128.9, 127.6–127.3 (4*d*, 9 C–H), 106.7 (*s*, C(2')), 20.3 (*q*, CH_3).

MS (EI): 412 (100, $M^{\cdot+}$), 270 (79), 239 (45), 207 (20), 178 (56), 165 (38), 126 (94), 105 (44), 77 (37), 65 (15).

Elemental analysis: Anal. calcd for $C_{22}H_{21}I$: C, 64.09; H, 5.13; found: C, 64.06; H, 4.99.

2.9.5.2 2'-Iodo-2,4,6,2",4",6"-hexamethyl-1,1':3',1"-terphenyl

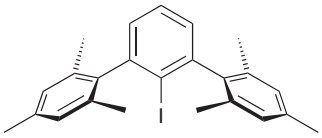

Chemical Formula: $C_{24}H_{25}I$
Molecular Weight: 440.360

The crude product was washed three times with hexane at RT and dried in vacuo. The iodoterphenyl was obtained as fine, off-white needles (68 %).

M.p.: 226–228 °C

IR (KBr): 3043*m*, 3006*s*, 2968*s*, 2941*s*, 2913*s*, 2853*s*, 230*w*, 1945*w*, 1877*w*, 1733*w*, 1612*s*, 1575*s*, 1486*m*, 1450*s*, 1381*s*, 1266*w*, 1179*m*, 1094*m*, 1031*m*, 1013*s*, 1001*s*, 885*w*, 851*s*, 801*s*, 777*m*, 738*s*, 701*m*, 583*m*, 573*m*, 547*m*.

^1H NMR (300 MHz, 9 mg in 0.6 mL $CDCl_3$): 7.45 (*t*, $^3J = 7.5$, 1 H, H–C(5')); 7.07 (*d*, $^3J = 7.5$, 2 H, H–C(4', 6')); 6.95 (*s*, 4 H, H–C(3, 5, 3", 5")); 2.34 (*s*, 6 H, H_3C–C(4, 4")); 1.98 (*s*, 12 H, H_3C–C(2, 6, 2", 6")).

$^{13}C\{^1H\}$ NMR (75 MHz, 50 mg in 0.6 mL $CDCl_3$): 147.2, 142.0, 137.2, 135.3 (4 *s*, 10 quat. C); 128.8, 128.1, 127.8 (3 *d*, 7 C–H); 107.6 (*s*, C(2')); 21.2 (*q*, *C*–C(4, 4")); 20.2 (*q*, *C*–C(2, 6, 2", 6").

MS (EI): 440 (100, $M^{\cdot+}$), 313 (10, $[M - I]^+$), 298 (64, $[M - 2\ CH_3]^+$), 253 (22), 220 (17), 193 (20), 178 (27), 141 (40), 126 (31).

2.9.5.3 2'-Iodo-2,3,5,6,2",3",5",6"-octamethyl-1,1':3',1"-terphenyl

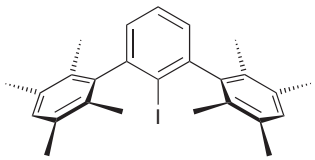

Chemical Formula: $C_{26}H_{29}I$
Molecular Weight: 468.413

The crude product was washed with hexanes and purified by recrystallization from isopropanol. The iodoterphenyl was obtained as a colorless solid (73 %).

Characterization

M.p.: 202.0–202.5 °C

IR (KBr): 3041*m*, 3004*s*, 2960*s*, 2918*s*, 2861*s*, 2730*m*, 1948*w*, 1885*w*, 1822*w*, 1734*w*, 1601*m*, 1571*m*, 1469*s*, 1446*s*, 1411*m*, 1384*s*, 1374*s*, 1325*m*, 1155*m*, 1039*m*, 1012*s*, 893*w*, 867*s*, 843*m*, 790*s*, 735*s*, 685*m*, 662*m*, 654*m*, 606*w*, 582*w*.

^{1}H NMR (300 MHz, 6 mg in 0.6 mL $CDCl_3$, $\delta(CHCl_3)$ = 7.26): 7.46 (*t*, $^3J = 7.5$, 1 H, H–C(5')), 7.06 (*d*, $^3J = 7.5$, 2 H, H–C(4', 6')), 7.04 (*s*, 2 H, H–C(4, 4")), 2.28 (*s*, 12 H, CH_3), 1.89 (*s*, 12 H, CH_3).

^{13}C{^{1}H} NMR (75 MHz, 50 mg in 0.6 mL $CDCl_3$): 148.3, 145.1, 133.5, 131.4 (4 *s*, 12 quat. C), 130.8, 128.6, 127.6 (3 *d*, 5 C–H), 108.1 (*s*, C–I), 20.1, 16.6 (2 *q*, CH_3).

MS (EI): 468 (100, $M^{\cdot+}$), 326 (46), 311 (28), 281 (25), 234 (32), 207 (23), 133 (50), 126 (19), 91 (21).

Elemental analysis: Anal. calcd for $C_{26}H_{29}I$: C, 66.67; H, 6.24; found: C, 66.38; H, 5.97.

2.9.5.4 2'-Iodo-2,3,4,5,6,2",3",4",5",6"-decamethyl-1,1':3',1"-terphenyl

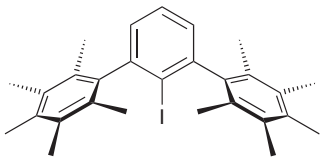

Chemical Formula: $C_{28}H_{33}I$
Molecular Weight: 496.466

The crude product was washed with hexanes and purified by recrystallization from isopropanol/toluene 20:1. The iodoterphenyl was obtained as a colorless solid (38 %).

Characterization

M.p.: 224.5–225.0 °C

IR (KBr): 3037*m*, 2983*s*, 2916*s*, 2724*m*, 1929*w*, 1867*w*, 1807*w*, 1636*w*, 1570*m*, 1448*s*, 1379*s*, 1265*w*, 1154*w*, 1066*s*, 1014*s*, 838*s*, 805*m*, 784*s*, 732*s*, 668*m*, 655*m*, 632*w*, 501*w*.

^{1}H NMR (300 MHz, 5 mg in 0.6 mL $CDCl_3$): 7.42 (*t*, $^3J = 7.4$, 1 H, H–C(5')), 7.04 (*d*, $^3J = 7.4$, 2 H, H–C(4', 6')), 2.31 (*s*, 6 H, H_3C–C(4,4")), 2.26 (*s*, 12 H, CH_3), 1.94 (*s*, 12 H, CH_3).

^{13}C{^{1}H} NMR (75 MHz, 25 mg in 0.6 mL $CDCl_3$): 148.9, 142.9, 134.3, 132.3, 130.9 (5 *s*, 14 quat. C), 128.5, 127.8 (2 *d*, 3 C–H), 109.0 (*s*, C(2')), 17.7, 17.0, 16.6 (3 *q*, CH_3).

MS (EI): 496 (100, $M^{\cdot+}$), 354(27), 309 (25), 248 (36), 207 (18), 162 (46), 91 (25).

Elemental analysis: Anal. calcd for $C_{28}H_{33}I$: C, 67.74; H, 6.70; found: C, 67.86; H, 6.76.

2.9.6 Silanes

General procedure A for the preparation of the terphenylsilanes:

To a dry two-necked 50 mL round-bottom flask, equipped with N_2 inlet, stir bar, and septum, dry THF (25 mL) and the iodoterphenyl (2 mmol) were added. The solution was cooled in an acetone–dry ice bath. *n*-BuLi (1.60 M in hexanes, 4.3 mmol) was added over 1 min. Stirring was continued for an additional 50 min. Chlorodimethylsilane (5 mmol) was

added over 30 s. The mixture was stirred for 30 min, then the cooling bath was removed, and stirring was continued for 60 min at ambient temperature. H_2O (10 mL) and 1 M aq. NaOH (5 mL) were added, and THF was removed under reduced pressure. The mixture was extracted with CH_2Cl_2 (3 × 30 mL), the organic layers were washed with H_2O (40 mL), and the aq. washing layer was re-extracted with CH_2Cl_2 (30 mL). The combined organic layers were dried over $MgSO_4$, filtered, and evaporated. The crude product was purified by filtration through a plug of alumina (deactivated with 5 % H_2O, eluent hexane/CH_2Cl_2 1:1). Additional purification included column chromatography or recrystallization as described in the respective procedures.

General procedure B for the preparation of the terphenylsilanes:

Preparation of a fresh solution of LDA: In a dry two-necked 25 mL round-bottom flask, equipped with an N_2 inlet and a rubber septum, a solution of *i*Pr_2NH (294 mg, 2.91 mmol) in THF (6.3 mL) was prepared. The solution was cooled in an acetone–dry ice bath, and *n*-BuLi (1.42 M in hexane, 2.2 mL, 3.12 mmol) was added over 30 s. The mixture was stirred for 15 min and allowed to warm to RT. The slightly yellow solution of LDA (*c* = 0.342 M) was transferred to a small Schlenk flask and stored in a refrigerator at 5 °C. It was used within a week.

Preparation of the silanes from iodoterphenyls: The iodoterphenyl (0.7 mmol) was dissolved in dry THF (10 mL) in a two-necked 25 mL round-bottom flask that was equipped with an N_2 inlet and a rubber septum. The solution was cooled in an acetone–dry ice bath, and LDA (freshly prepared solution in THF, 0.7 mmol) was added. *n*-BuLi (*ca*. 1.6 M in hexanes, titrated, 1.5 mmol) was added over 1 min. The I–Li exchange was run for 40 min. Me_2HSiCl (3 mmol) was added over 20 s, which usually afforded a clear, colorless solution. The reaction mixture was stirred in the cooling bath for another 30 min and then allowed to warm to RT over 15 min. H_2O (8 mL) was added, and the mixture was stirred vigorously. Two clear and colorless layers were obtained. Aqeous NaOH (1 M, 2 mL) was added to quench HCl from the excess of chlorosilane. The mixture was transferred to a bigger flask, and most of the THF was removed on a rotavap (200 mbar, 40 °C). The crude mixture was extracted with CH_2Cl_2 (3 × 20 mL), and the combined organic layers

were dried over $MgSO_4$, filtered and evaporated to dryness. The crude product was filtered through plug of Al_2O_3 (deactivated with 5% H_2O, 2×2 cm) with hexanes as the eluent. Evaporation of the solvent usually afforded the terphenylsilane already as a pure product by GC–MS and ^{1}H NMR analysis (90–99%). If necessary, additional purification was done by recrystallization.

2.9.6.1 [2,6-Bis(2,6-dimethylphenyl)phenyl]dimethylsilane

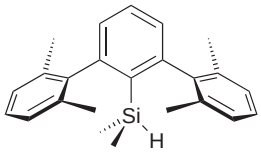

Chemical Formula: $C_{24}H_{28}Si$
Molecular Weight: 344.565

This silane was prepared by procedure A and purified by column chromatography (SiO_2, hexanes) and was obtained as a colorless oil (72%).

Characterization

IR (Film): 3049*m*, 3034*m*, 3018*m*, 2955*s*, 2919*s*, 2858*m*, 2732*w*, 2153*s*, 1928*w*, 1852*w*, 1776*w*, 1654*w*, 1579*m*, 1557*m*, 1460*s*, 1444*s*, 1377*m*, 1246*s*, 1172*m*, 1164*m*, 1121*s*, 1076*m*, 1050*m*, 1031*m*, 986*w*, 899*s*, 838*s*, 808*s*, 768*s*, 745*s*, 735*s*, 708*m*, 697*m*, 655*m*, 627*w*.

^{1}H NMR (300 MHz, 35 mg in 0.6 mL C_6D_6, $\delta(C_6HD_5)$ = 7.16): 7.21 (*t*, $^3J = 7.6$, 1 H, H–C(4')), 7.14–6.99 (2 *m*, 6 H, H–C(3", 4", 5", 3"', 4"', 5"')), 6.85 (*d*, $^3J = 7.6$, 2 H, H–C(3', 5')), 3.97 (*septuplet*, $^3J = 4.1$, 1 H, H–Si), 2.06 (*s*, 12 H, H_3C–C(2", 6", 2"', 6"')), −0.20 (*d*, $^3J = 4.1$, 6 H, H_3C–Si).

^{13}C{^{1}H} NMR (75 MHz, 35 mg in 0.6 mL C_6D_6, $\delta(C_6D_6)$ = 128.0)): 149.4 (*s*, C(2', 6')), 143.4 (*s*, C(1", 1"')), 136.3 (*s*, C(2", 6", 2"', 6"')), 133.9 (*s*, C(1')), 130.3 (*d*, C(4')), 128.3 (*d*, C(3', 5')), 127.6 (*d*, C(4", 4"'), 127.5 (*d*, C(3", 5", 3"', 5"')), 21.2 (*q*, H_3C–C(2", 6", 2"', 6"'), −2.5 (*q*, H_3C–Si).

$^{29}Si\{^{1}H\}$ NMR (120 MHz, 35 mg in 0.6 mL C_6D_6): -23.0.

MS (EI): 344 (24, $M^{\cdot+}$), 329 (100, $[M - CH_3]^+$), 313 (17), 253 (25), 59 (61).

Elemental analysis: Anal. calcd for the silane: C, 83.66; H, 8.19; found: C, 83.84; H, 8.23.

2.9.6.2 [2,6-Bis(2,4,6-trimethylphenyl)phenyl]dimethylsilane

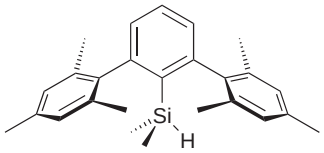

Chemical Formula: $C_{26}H_{32}Si$
Molecular Weight: 372.618

The product was prepared by procedure B and obtained as a colorless solid (96%).

Characterization

M.p.: 120–120.5 °C

IR (KBr): 3048*m*, 2984*m*, 2950*m*, 2915*s*, 2854*m*, 2146*s* (Si–H), 1948*w*, 1882*w*, 1732*w*, 1612*m*, 1569*m*, 1556*m*, 1482*m*, 1444*s*, 1375*m*, 1253*m*, 1244*s*, 1175*m*, 1119*s*, 1085*m*, 1049*m*, 1034*w*, 903*s*, 883*s*, 853*s*, 838*s*, 811*s*, 776*m*, 757*s*, 729*s*, 697*w*, 661*w*, 632*w*, 588*w*, 549*w*.

^{1}H NMR (300 MHz, 45 mg in 0.6 mL C_6D_6, $\delta(C_6HD_5) = 7.16$): 7.26 (*t*, $^{3}J = 7.5$, 1 H, H–C(4')), 6.92 (*d*, $^{3}J = 7.5$, 1 H, H–C(3', 5')), 6.85 (*s*, 4H, H–C(3", 5", 3"', 5"')), 4.03 (septuplet, $^{3}J = 4.1$, 1 H, Si–H), 2.20 (*s*, 6 H, H_3C–C(4", 4"')), 1.08 (*s*, 12 H, H_3C–C(2", 6", 2"', 6"')), -0.15 (*d*, $^{3}J = 4.1$, 6 H, Si–CH_3).

$^{13}C\{^{1}H\}$ NMR (75 MHz, 45 mg in 0.6 mL $CDCl_3$): 149.5 (*s*, C(2', 6'), 140.7 (*s*, C(1", 1"')), 136.7 (*s*, C(4", 4"')), 136.1 (*s*, C(2", 6", 2"', 6"')), 134.5 (*s*, C(1')), 130.3 (*d*, C(4')), 128.4 (*d*, C(3', 5')), 128.3 (*d*, C(3", 5", 3"', 5"')), 21.2 (*q*, C–C(2", 6", 2"', 6"')), 21.2 (*q*, C–C(4", 4"')), -2.3 (*q*, Si–CH_3).

$^{29}Si\{^{1}H\}$ NMR (120 MHz, 45 mg in 0.6 mL C_6D_6): -23.0.

MS (EI): 372 (31, $M^{\cdot+}$), 357 (100, $[M - CH_3]^+$), 178 (7), 59 (58, $[Si(CH_3)_2H]^+$).

Elemental analysis: Anal. calcd for the silane: C, 83.81; H, 8.66; found: C, 84.00; H, 8.42.

2.9.6.3 [2,6-Bis(2,3,5,6-tetramethylphenyl)phenyl]dimethylsilane

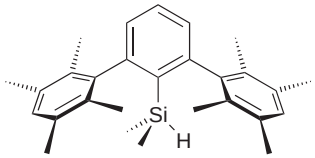

Chemical Formula: $C_{28}H_{36}Si$
Molecular Weight: 400.671

The product was prepared by procedure B and obtained as a colorless solid (97%).

Characterization

M.p.: 163–163.5 °C

IR (Film): 3047*m*, 3002*s*, 2916*s*, 2727*w*, 2154*s*, 1944*w*, 1883*w*, 1825*w*, 1731*w*, 1602*w*, 1579*w*, 1553*m*, 1467*s*, 1442*s*, 1382*s*, 1243*s*, 1190*w*, 1153*w*, 1119*m*, 1035*m*, 1007*m*, 901*s*, 837*s*, 793*s*, 762*m*, 735*s*, 707*m*, 691*m*, 648*m*, 627*m*, 585*m*, 513*w*.

^{1}H NMR (300 MHz, 30 mg in 0.6 mL C_6D_6, $\delta(C_6HD_5)$ = 7.16): 7.30 (*t*, $^3J = 7.5$, 1 H, H–C(4')), 6.98 (*d*, $^3J = 7.5$, 2 H, H–C(3', 5')), 6.94 (*s*, 2 H, H–C(4", 4"')), 3.99 (*septuplet*, $^3J = 4.1$, 1 H, H–Si), 2.17 (*s*, 12 H, H_3C–C(ring)), 2.03 (*s*, 12 H, H_3C–C(ring)), −0.22 (*d*, $^3J = 4.1$, 6 H, H_3C–Si).

^{13}C{^{1}H} NMR (75 MHz, 30 mg in 0.6 mL C_6D_6, $\delta(C_6D_6)$ = 128.0)): 150.7 (*s*, C(2', 6'), 143.5 (*s*, C(1", 1"')), 134.8 (*s*, C(1')), 133.5 (*s*, C(2", 6", 2"', 6"')), 132.1 (*s*, C(3", 5", 3"', 5"')), 130.9 (*d*, C(4", 4"')), 130.1 (*d*, C(4')), 128.2 (*d*, C(3',5')), 20.2, 17.9 (2 *q*, CH_3–C(ring)), −2.5 (*q*, C–Si).

^{29}Si{^{1}H} NMR (120 MHz, 30 mg in 0.6 mL C_6D_6): −23.2.

MS (EI): 400 (21, $M^{\cdot+}$), 385 (100, $[M - CH_3]^+$), 59 (61).

Elemental analysis: Anal. calcd for the silane: C, 83.93; H, 9.06; found: C, 83.91; H, 8.87.

2.9.6.4 [2,6-Bis(2,3,4,5,6-pentamethylphenyl)phenyl]dimethylsilane

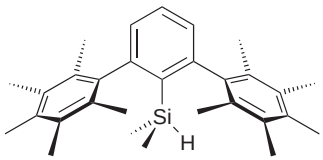

Chemical Formula: $C_{30}H_{40}Si$
Molecular Weight: 428.724

The product was prepared by procedure B obtained and as a colorless solid (92%).

Characterization

M.p.: 214–214.5 °C

IR (Film): 3043*m*, 3028*m*, 2918*s*, 2726*w*, 2181*s*, 1939*w*, 1879*w*, 1820*w*, 1570*w*, 1552*m*, 1444*m*, 1381*m*, 1240*s*, 1190*w*, 1152*w*, 1114*m*, 1066*m*, 1047*m*, 1033*m*, 893*s*, 840*s*, 791*m*, 759*m*, 737*s*, 693*w*, 660*w*, 649*w*, 627*w*.

^{1}H NMR (300 MHz, 7 mg in 0.6 mL $CDCl_3$): 7.41 (*t*, $^3J = 7.6$, 1 H, H–C(4')), 6.96 (*d*, $^3J = 7.6$, 2 H, H–C(3', 5')), 3.47 (*septuplet*, $^3J = 4.1$, 1 H, H–Si), 2.30 (*s*, 6 H, H_3C–C(4", 4"')), 2.24 (*s*, 12 H, H_3C–C(ring)), 1.94 (*s*, 12 H, H_3C–C(ring)), −0.45 (*d*, $^3J = 4.1$, 6 H, H_3C–Si).

^{13}C{^{1}H} NMR (75 MHz, 30 mg in 0.6 mL C_6D_6, $\delta(C_6D_6)$ = 128.0)): 151.5 (*s*, C(2', 6')), 141.3 (*s*, C(1", 1"')), 135.3 (*s*, C(1')), 133.8 (*s*, C(4", 4"')), 132.1 (*s*, C(2", 6", 2"', 6"')), 131.7 (*s*, C(3", 5", 3"', 5"')), 130.0 (*d*, C(4')), 128.4 (*d*, C(3', 5')), 19.1, 16.8, 16.6 (3 *q*, CH_3–C(ring)), -2.4 (*q*, C–Si).

^{29}Si{^{1}H} NMR (120 MHz, 30 mg in 0.6 mL C_6D_6): −23.2.

MS (EI): 418 (22, $M^{\cdot+}$), 413 (100, $[M - CH_3]^+$), 59 (60).

Elemental analysis: Anal. calcd for the silane: C, 84.04; H, 9.40; found: C, 84.01; H, 9.03.

2.9.7 Silylium Ions

General procedure for the preparation of the silylium ions:

Working with the $B(C_6F_5)_4^-$ anion: In a glovebox, a suspension of $[Ph_3C][B(C_6F_5)_4]$ (0.24 mmol) and the silane (0.24 mmol) in dry C_6D_6 (1 mL) was prepared. The oily brown mixture was stirred for 24 hrs at RT. Two layers formed, a dark brown oil at the bottom and a clear yellow upper layer. The brown oil, containing mainly the ionic product, was examined by NMR spectroscopy. Isolation of the product was done by adding pentane or hexane to the oil, removal of the supernatant, and drying the residue in a vacuum. This procedure usually afforded the $B(C_6F_5)_4^-$ salts as foams. Repeated addition of hexane, vigorous stirring or scratching the waxy material with a spatula, and solvent evatoration afforded solid material that could be ground to a powder with a spatula.

Working with carborane anions: In a glovebox, a suspension of $[Ph_3C]$[carborane] (0.05–0.2 mmol) and a slight excess of the silane (1.1–1.3 equivalents) in dry chlorobenzene or 1,2-dichlorbenzene (1–2 mL) was prepared. The mixture was stirred for 24 hrs at RT. Usually a clear yellow to orange solution was obtained. Sometimes a small amount of a precipitate formed; in these cases, the clear supernatant was transferred to a second vial. Precipitation with pentane and hexane, removal of the supernatant, and drying in a vacuum usually afforded a yellow powder. When sticky oils were obtained, addition of pentane or hexane and scratching with a spatula almost always gave powdery product that could be dried in a vacuum. With the carborane anions, NMR characterization was done in chlorobenzene or dichlorobenzene due to reduced solubilities. These solvents are available in deuterated form, but spectra in the non-deuterated solvents (addition of a C_6D_6 capillary for locking and shimming) were in most cases informative enough in terms of checking cation purity.

2.9.7.1 [2,6-Bis(2,6-dimethyl)phenyl]dimethylsilylium Tetrakis(pentafluorophenyl)-borate

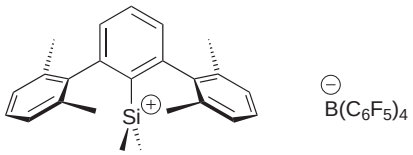

Chemical Formula: $C_{48}H_{27}BF_{20}Si$
Molecular Weight: 1022.593

Prepared according to the general procedure.

Characterization

^{1}H NMR (300 MHz, oily layer, *ca.* 240 mg in 0.6 mL of solution, C_6D_6, $\delta(C_6HD_5)$ = 7.16): 7.31 (*t*, $^{3}J = 7.8$, 1 H, H–C(4')), 7.09 (*d*, $^{3}J = 7.8$, 2 H, H–C(3', 5')), 7.07–7.01 (*m*, 6 H, H–C(3", 4", 5", 3"', 4"', 5"')), 1.69 (*s*, 12 H, H_3C–C(2", 6", 2"', 6"')), −0.64 (*s*, 6 H, H_3C–Si).

^{13}C{^{1}H} NMR (75 MHz, oily layer, *ca.* 240 mg in 0.6 mL of solution, C_6D_6, $\delta(C_6D_6)$ = 128.0): 153.4 (*s*, C(1", 1"')), 150.9–147.2 (*m*, C–F), 146.4 (*s*, C(2', 6')), 145.9 (*s*, C(1')), 139.4 (*d*, C(3", 5", 3"', 5"')), 140.7–136.9 (*m*, C–F), 139.0–135.1 (*m*, C–F), 133.7 (*d*, C(4')) 131.0 (*d*, C(4", 4"')), 130.1 (*s*, C(2", 6", 2"', 6"')), 127.7 (*d*, C(3', 5')), 125 (*m* br., C–B), 20.6 (*q*, C–C(2", 6", 2"', 6"'), −2.8 (*q*, CH_3–Si).

^{29}Si{^{1}H} NMR (60 MHz, oily layer, *ca.* 240 mg in 0.6 mL of solution, C_6D_6): 80.1.

^{19}F NMR (282 MHz, oily layer, *ca.* 240 mg in 0.6 mL of solution, C_6D_6, $\delta(CCl_3F)$ = 0): −131.9 to −132.2 (*m*, 8 F, F–C(2', 6')), −162.7 (*t*, $^{3}J_{F,F} = 21$, 4 F, F–C(4')), −166.4 to −166.8 (*m*, 8 F, F–C(3', 5')).

2.9.7.2 [2,6-Bis(2,4,6-trimethyl)phenyl]dimethylsilylium tetrakis(pentafluorophenyl)-borate

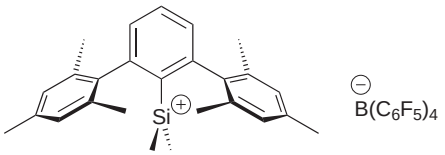

Chemical Formula: $C_{50}H_{31}BF_{20}Si$
Molecular Weight: 1050.646

Prepared according to the general procedure.

Characterization

^{1}H NMR (600 MHz, oily layer, *ca.* 240 mg in 0.6 mL of solution, C_6D_6, $\delta(C_6HD_5)$ = 7.16): 7.34 (*t*, $^{3}J = 7.7$, 1 H, H–C(4')), 7.06 (*d*, $^{3}J = 7.7$, 2 H, H–C(3', 5')), 6.92 (*s*, 4 H, H–C(3", 5", 3"', 5"')), 2.06 (*s*, 6 H, H_3C–C(4", 4"')), 1.73 (*s*, 12 H, H_3C–C(2", 6", 2"', 6"')), −0.55 (*s*, 6 H, H_3C–Si).

^{13}C{^{1}H} NMR (75 MHz, oily layer, *ca.* 240 mg in 0.6 mL of solution, C_6D_6, $\delta(C_6D_6)$ = 128.0): 150.7 (*s*, C(1", 1"')), 150.9–147.2 (*m*, C–F), 146.4 (*s*, C(2', 6')), 145.9 (*s*, C(1')), 141.9 (*s*, C(4", 4"'), 139.9 (*d*, C(3", 5", 3"', 5"')), 140.7–136.8 (*m*, C–F), 139.0–134.9 (*m*, C–F), 133.6 (*d*, C(4')), 130.0 (*s*, C(2", 6", 2"', 6"')), 127.8 (*d*, C(3', 5')), 125 (*m* br., C–B), 20.6 (*q*, C–C(2", 6", 2"', 6"'), 20.3 (*q*, C–C(4", 4"')), −2.8 (*q*, Si–CH_3).

^{29}Si{^{1}H} NMR (oily layer, *ca.* 240 mg in 0.6 mL of solution, 120 MHz, C_6D_6): 79.1.

^{19}F NMR (282 MHz, oily layer, *ca.* 240 mg in 0.6 mL of solution, C_6D_6, $\delta(CCl_3F)$ = 0): −131.9 to −132.2 (*m*, 8 F, F–C(2', 6')), −162.7 (*t*, $^{3}J_{F,F} = 21$, 4 F, F–C(4')), −166.5 to −166.8 (*m*, 8 F, F–C(3', 5')).

MS (EI): From CsF product study, Ter-$SiMe_2F$ was obtained as main product: 390 (30, $M^{\cdot+}$), 375 (18, $[M - CH_3]^+$), 313 (18, $[M - Si(CH_3)_2F]^+$), 77 (100, $[Si(CH_3)_2F]^+$), 63 (19).

MS (EI): Upper reaction layer: The GC showed only one peak, which was the one of triphenylmethane. The nature of the side product was confirmed by a reference GC–MS

with purchased triphenylmethane. 244 (100, $M^{\cdot+}$), 167 (59, $[M - Ph]^+$), 165 (89), 152 (20), 77 (37, $[Ph]^+$), 51 (45).

2.9.7.3 [2,6-Bis(2,3,5,6-tetramethyl)phenyl]dimethylsilylium Tetrakis(pentafluorophenyl)borate

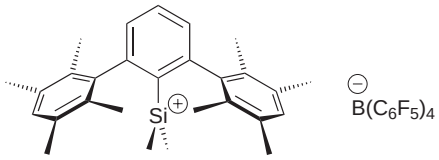

Chemical Formula: $C_{52}H_{35}BF_{20}Si$
Molecular Weight: 1078.699

Prepared according to the general procedure

Characterization

^{1}H NMR (600 MHz, oily layer, *ca.* 240 mg in 0.6 mL of solution, C_6D_6, $\delta(C_6HD_5)$ = 7.16): 7.37 (*t*, $^3J = 7.7$, 1 H, H–C(4')), 7.11 (*d*, $^3J = 7.7$, 2 H, H–C(3', 5')), 6.83 (*s*, 2 H, H–C(4", 4"')), 2.01 (*s*, 12 H, H_3C–C(3", 5", 3"', 5"')), 1.63 (*s*, 12 H, H_3C–C(2", 6", 2"', 6"')), −0.69 (*s*, 6 H, H_3C–Si).

^{13}C{^{1}H} NMR (75 MHz, oily layer, *ca.* 240 mg in 0.6 mL of solution, C_6D_6, $\delta(C_6D_6)$ = 128.0): 155.2 (*s*, C(1", 1"')), 151.6 (*s*, C(3", 5", 3"', 5"')), 150.9–147.2 (*m*, C–F), 147.7 (*s*, C(2', 6')), 146.5 (*s*, C(1')), 140.8–136.9 (*m*, C–F), 139.0–135.0 (*m*, C–F), 133.8 (*d*, C(4", 4"')), 132.9 (*d*, C(4')), 127.8 (*d*, C(3', 5')), 125 (*m* br., C–B), 124.4 (*s*, C(2", 6", 2"', 6"')), 20.7 (*q*, C–C(3", 5", 3"', 5"')), 17.8 (*q*, C–C(2", 6", 2"', 6"')), -5.1 (*q*, C–Si).

^{29}Si{^{1}H} NMR (120 MHz, oily layer, *ca.* 240 mg in 0.6 mL of solution, C_6D_6): 60.6.

^{19}F NMR (282 MHz, oily layer, *ca.* 240 mg in 0.6 mL of solution, C_6D_6, $\delta(CCl_3F)$ = 0): −131.9 to −132.2 (*m*, 8 F, F–C(2', 6')), −162.7 (*t*, $^3J_{F,F} = 21$, 4 F, F–C(4')), −166.5 to −166.8 (*m*, 8 F, F–C(3', 5')).

2.9.7.4 [2,6-Bis(2,3,4,5,6-pentamethyl)phenyl]dimethylsilylium Tetrakis(pentafluorophenyl)borate

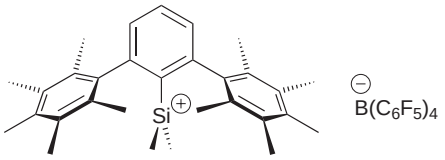

Chemical Formula: $C_{54}H_{39}BF_{20}Si$
Molecular Weight: 1106.752

Prepared according to the general procedure.

Characterization

^{1}H NMR (600 MHz, oily layer, *ca.* 240 mg in 0.6 mL of solution, C_6D_6, $\delta(C_6HD_5)$ = 7.16): 7.37 (*t*, $^{3}J = 7.7$, 1 H, H–C(4')), 7.14 (*d*, $^{3}J = 7.7$, 2 H, H–C(3', 5')), 1.96 (*s*, 12 H, H_3C–C(3", 5", 3"', 5"')), 1.95 (*s*, 6 H, H_3C–C(4", 4"')), 1.70 (*s*, 12 H, H_3C–C(2", 6", 2"', 6"')), −0.69 (*s*, 6 H, H_3C–Si).

^{13}C{^{1}H} NMR (75 MHz, oily layer, *ca.* 240 mg in 0.6 mL of solution, C_6D_6, $\delta(C_6D_6)$ = 128.0): 152.8 (*s*, C(1", 1"')), 151.0–147.3 (*m*, C–F), 150.7 (*s*, C(3", 5", 3"', 5"')), 148.2 (*s*, C(2', 6')), 147.1 (*s*, C(1')), 140.8–137.0 (*m*, C–F), 139.0–135.0 (*m*, C–F), 138.8 (*s*, C(4", 4"'), 132.8 (*d*, C(4')), 127.8 (*d*, C(3', 5')), 125 (*m* br., C–B), 123.8 (*s*, C(2", 6", 2"', 6"')), 18.8 (*q*, C–C(2", 6", 2"', 6"')), 17.6 (*q*, C–C(3", 5", 3"', 5"')), 16.0 (*q*, C–C(4", 4"')), -5.0 (*q*, C–Si).

^{29}Si{^{1}H} NMR (120 MHz, oily layer, *ca.* 240 mg in 0.6 mL of solution, C_6D_6): 58.6.

^{19}F NMR (282 MHz, oily layer, *ca.* 240 mg in 0.6 mL of solution, C_6D_6, $\delta(CCl_3F)$ = 0): −131.9 to −132.2 (*m*, 8 F, F–C(2', 6')), −162.8 (*t*, $^{3}J_{F,F} = 21$, 4 F, F–C(4')), −166.5 to −166.8 (*m*, 8 F, F–C(3', 5')).

2.9.8 Naphthyl System

2.9.8.1 *anti*-1,3-Bis(2-methylnaphthalen-1-yl)-2-iodobenzene

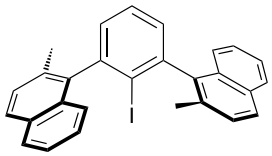

Chemical Formula: $C_{28}H_{21}I$
Molecular Weight: 484.371

Prepared according to the general procedure for iodoterphenyls. The crude product was purified by column chromatography (SiO_2, hexane–CH_2Cl_2 6:1) to give an overall yield of 69 % (*anti*:*syn* 41:59) as a slightly yellow solid. Recrystallization from nitromethane–toluene (14:3, 110 °C, allowed to cool to 5 °C) gave enriched *anti* isomer (15 % with respect to the starting material dichloroiodobenzene, *anti*:*syn* 94.5:5.5) as a slightly yellowish solid.

Characterization

M.p.: 254–256 °C

IR (KBr): 3053*m*, 2915*m*, 2853*w*, 1619*m*, 1595*m*, 1566*m*, 1507*s*, 1452*m*, 1422*m*, 1373*s*, 1335*m*, 1270*w*, 1144*m*, 1089*w*, 1027*m*, 1009*s*, 975*w*, 962*w*, 915*w*, 869*w*, 859*m*, 812*s*, 798*s*, 781*s*, 744*s*, 724*m*, 621*s*, 566*w*, 524*w*.

^{1}H NMR (400 MHz, 7 mg in 0.6 mL $CDCl_3$, $\delta(CHCl_3)$ = 7.25): 7.88–7.82 (*m*, 4 H, naphthyl H), 7.62 (*t*, $^3J = 7.5$, 1 H, H–C(5)), 7.46–7.30 (*m*, 6 H, naphthyl H), 7.28 (*d*, $^3J = 7.5$, 2 H, H–C(4, 6)), 2.30 (*s*, 6 H, naphthyl CH_3).

^{13}C{^{1}H} NMR (100 MHz, 7 mg in 0.6 mL $CDCl_3$, $\delta(CDCl_3)$ = 77.0): 146.0 (*s*), 140.9 (*s*), 133.1 (*s*), 132.1 (*s*), 132.0 (*s*), 129.2 (*d*), 128.7 (*d*), 128.6 (*d*), 127.9 (*d*), 127.8 (*d*), 126.2 (*d*), 125.3 (*d*), 124.9 (*d*), 107.9 (*s*), 20.5 (*q*).

MS (EI): 484 (71, $M^{\cdot+}$), 357 (30), 342 (38), 339 (30), 281 (30), 242 (62), 207 (100).

2.9.8.2 *anti*-[2,6-Bis(2-methylnaphthalen-1-yl)phenyl]dimethylsilane

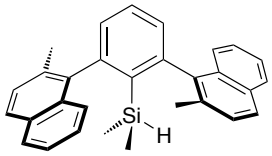

Chemical Formula: $C_{30}H_{28}Si$
Molecular Weight: 416.629

Prepared according to general procedure A and purified by recrystallization from isopropanol. The silane was obtained as a colorless crystalline solid (69 %, *anti*:*syn* 97.0:3.0)

Characterization

M.p.: 186–188 °C

IR (KBr): 3053*m*, 3007*w*, 2977*m*, 2917*m*, 2150*s*, 1618*m*, 1595*m*, 1553*m*, 1507*s*, 1446*m*, 1417*m*, 1376*m*, 1245*s*, 1214*m*, 1126*m*, 1117*m*, 1048*m*, 1026*m*, 901*s*, 839*s*, 813*s*, 784*s*, 748*s*, 732*s*, 669*m*, 623*m*, 569*m*.

^{1}H NMR (400 MHz, 10 mg in 0.6 mL C_6D_6, $\delta(C_6HD_5)$ = 7.16): 7.70–7.60 (*m*, 6 H, naphthyl H), 7.31 (*t*, $^3J = 7.6$, 1 H, H–C(4')), 7.27–7.20 (*m*, 6 H, naphthyl H), 7.08 (*d*, $^3J = 7.6$, 2 H, H–C(3', 5')), 3.66 (*qq*, both $^3J = 4.1$, 1 H, Si–H), 2.31 (*s*, 6 H, naphthyl CH_3), −0.52 (*d*, $^3J = 4.1$ 3 H, Si–CH_3), −0.72 (*d*, $^3J = 4.1$ 3 H, Si–CH_3).

^{13}C{^{1}H} NMR (75 MHz, 10 mg in 0.6 mL C_6D_6, $\delta(C_6D_6)$ = 128.0): 148.0 (*s*), 139.9 (*s*), 137.2 (*s*), 134.3 (*s*), 133.6 (*s*), 132.5 (*s*), 130.1 (*d*), 129.6 (*d*), 128.7 (*d*), 128.2 (*d*), 127.9 (*d*), 126.9 (*d*), 126.1 (*d*), 125.1 (*d*), 21.3 (*q*), −2.4 (*q*), −2.5 (*q*).

^{29}Si{^{1}H} NMR (80 MHz, 10 mg in 0.6 mL C_6D_6): −22.4.

MS (EI): 416 (33, $M^{\cdot+}$), 401 (100, $[M - CH_3]^+$), 385 (20), 340 (19), 259 (17), 215 (28).

Table 2.6. Summary of the X-ray diffraction analysis of **36**.

Crystallized from	*i*-PrOH / toluene
Empirical formula	$C_{30}H_{28}Si$
Formula weight [g mol^{-1}]	416.63
Crystal color, habit	colorless, prism
Crystal dimensions [mm]	0.17 × 0.22 × 0.25
Temperature [K]	160(1)
Crystal system	triclinic
Space group	$P\bar{1}$ (#2)
Z	2
Reflections for cell determination	23052
2θ range for cell determination [°]	4–60
Unit cell parameters a [Å]	7.2778(2)
b [Å]	12.1513(2)
c [Å]	13.8643(4)
α [°]	99.373(2)
β [°]	96.657(1)
γ [°]	102.475(2)
V [Å^3]	1166.54(5)
$F(000)$	444
D_x [g cm^{-3}]	1.186
μ(Mo $K\alpha$) [mm^{-1}]	0.115
Scan type	ϕ and ω
$2\theta_{(max)}$ [°]	60
Transmission factors (min; max)	0.898; 0.982
Total reflections measured	31687
Symmetry independent reflections	6734
R_{int}	0.067
Reflections with $I > 2\sigma(I)$	5205
Reflections used in refinement	6733
Parameters refined	285
Final $R(F)$ [$I > 2\sigma(I)$ reflections]	0.0554
$wR(F^2)$ (all data)	0.1626
Weights: $w = [\sigma^2(F_o^2) + (0.0917P)^2 + 0.3076P]^{-1}$ where $P = (F_o^2 + 2F_c^2)/3$	
Goodness of fit	1.040
Secondary extinction coefficient	0.072(8)
Final Δ_{max}/σ	0.001
$\Delta\rho$ (max; min) [e Å^{-3}]	0.40; –0.62
$\sigma(d_{(C-C)})$ [Å]	0.002 – 0.003

2.9.8.3 Conversion to the Cation

anti-Silane was treated with $[Ph_3C][B(C_6F_5)_4]$ according to the general procedure. Because of the *anti–syn* ^1H isomerization, the ^1H and $^{13}C\{^1H\}$ spectra were complicated in the aromatic region. The isomers were identified based on the signals in the aliphatic region.

anti Cation:

^1H NMR (400 MHz, 10 mg in 0.6 mL C_6D_6, $\delta(C_6HD_5)) = 7.16$): 2.30 (*s*, 6 H, Ar–CH_3), −1.22 (*s*, 6 H, Si–CH_3).

$^{13}C\{^1H\}$ NMR (75 MHz, 10 mg in 0.6 mL C_6D_6, $\delta(C_6D_6) = 128.0$): 21.6 (*q*, Ar–CH_3), −2.5 (*q*, Si–CH_3).

$^{29}Si\{^1H\}$ NMR (80 MHz, 10 mg in 0.6 mL C_6D_6): 46.3.

syn Cation:

^1H NMR (400 MHz, 10 mg in 0.6 mL C_6D_6, $\delta(C_6HD_5)) = 7.16$): 2.00 (*s*, 6 H, Ar–CH_3), −0.87 (*s*, 3 H, Si–CH_3) −1.49 (*s*, 3 H, Si–CH_3).

$^{13}C\{^1H\}$ NMR (75 MHz, 10 mg in 0.6 mL C_6D_6, $\delta(C_6D_6) = 128.0$): 21.2 (*q*, Ar–CH_3), 2.1 (*q*, br, Si–CH_3), −6.3 (*q*, br, Si–CH_3).

$^{29}Si\{^1H\}$ NMR (80 MHz, 10 mg in 0.6 mL C_6D_6): 46.5.

Chapter 3

Conformational Study

3.1 Summary

X-ray crystallographic analysis of **27a**$^+$, **27c**$^+$, and **27d**$^+$ (flanking rings = xylyl, duryl, and pentamethylphenyl, respectively) showed that these cations prefer a C_1 geometry with a C_{ortho}–Si coordination in the solid state. According to an analysis of the ^{13}C NMR signals of the lateral rings, this conformation is also favored in solution. X-ray crystallographic and NMR-spectroscopic data suggested that **27**$^+$ possess mixed silyl cationic and arenium ion character. Cations **40**$^+$ were synthesized in order to probe the effect of larger steric bulk about the silicon center on cation stability. They are stabilized by C_{ortho}–Si interactions to a similar degree as **27**$^+$. The attempted preparation of (2,6-diphenylphenyl)dialkylsilylium ions, which were anticipated to exhibit enhanced silyl Lewis acidity, was not successful and afforded instead cyclized silafluorenes. A Hammett analysis revealed a linear correlation between the ^{29}Si NMR shifts of **27**$^+$ and **40**$^+$ and π_{aryl} basicity as expressed by σ values.

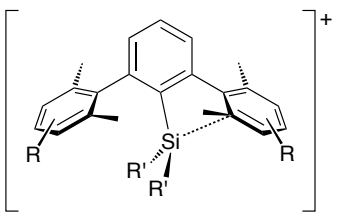

27$^+$ R' = CH_3
40$^+$ R' = *i*Pr

3.2 Introduction

NMR spectroscopy had revealed ^{29}Si NMR shifts of 80–59 ppm for cations **27**$^+$. These values suggested a π-coordinated silicon center and were consistent with the computational results that favored a C_1 geometry for all cations. However, better experimental support for this unsymmetric, specific C_{aryl}–Si interaction interaction was still necessary. Several aspects made a better knowledge about the structure and dynamics of **27**$^+$ worthwhile: a fundamental desire to gain insight into the mode of cation stabilization, a comparison with systems reported in the literature, and the design of future generations of tailor-made 2,6-diarylphenylsilylium ions. X-ray crystallography and NMR spectroscopy represented the main tools for a more thorough study.

3.3 Solid-State Structures

Single crystals suitable for X-ray crystallography were obtained for **27a**$^+$, **27c**$^+$, and **27d**$^+$ in combination with the anions $CHB_{11}H_5Cl_6^-$, $B(C_6F_5)_4^-$, and $CHB_{11}Cl_{11}^-$, respectively. In all structures, the cation is well separated from counterion and solvent (**27c**,**d**$^+$) molecules. Coordination of silicon occurs uniformly through one of the lateral C_{ortho} atoms.

Crystals of the composition [**27a**][$CHB_{11}H_5Cl_6$] were obtained from 1,2-dichlorobenzene–hexane at room temperature; X-ray crystallography revealed the presence of two structurally similar cations in the asymmetric unit (Figure 3.1). Both cations possess the the C_1 conformation predicted by computations and hypothesized from NMR data. In cation 1, the Si–C8 distance is 2.118(3) Å, in cation 2 the corresponding distance is 2.199(3) Å (Table 3.2). These values exceed that of a typical Si–C bond by 0.28 and 0.36 Å or 15 and 20%, respectively. The geometry around silicon is pyramidal with $Si_{\text{out of plane}}$ distances of 0.38 and 0.36 Å ($\Sigma\angle$(C-Si-C) = 347.6(2)°, 348.8(1)°). Experimental and calculated structures are in excellent agreement: predicted parameters are Si–C_{ortho} = 2.169 Å and $\Sigma\angle$(C-Si-C) = 348.6°. From the results of the X-ray crystallographic analysis, the structure of the two cations is best described as a η^1 π coordination of the xylyl ring to the central silyl group.

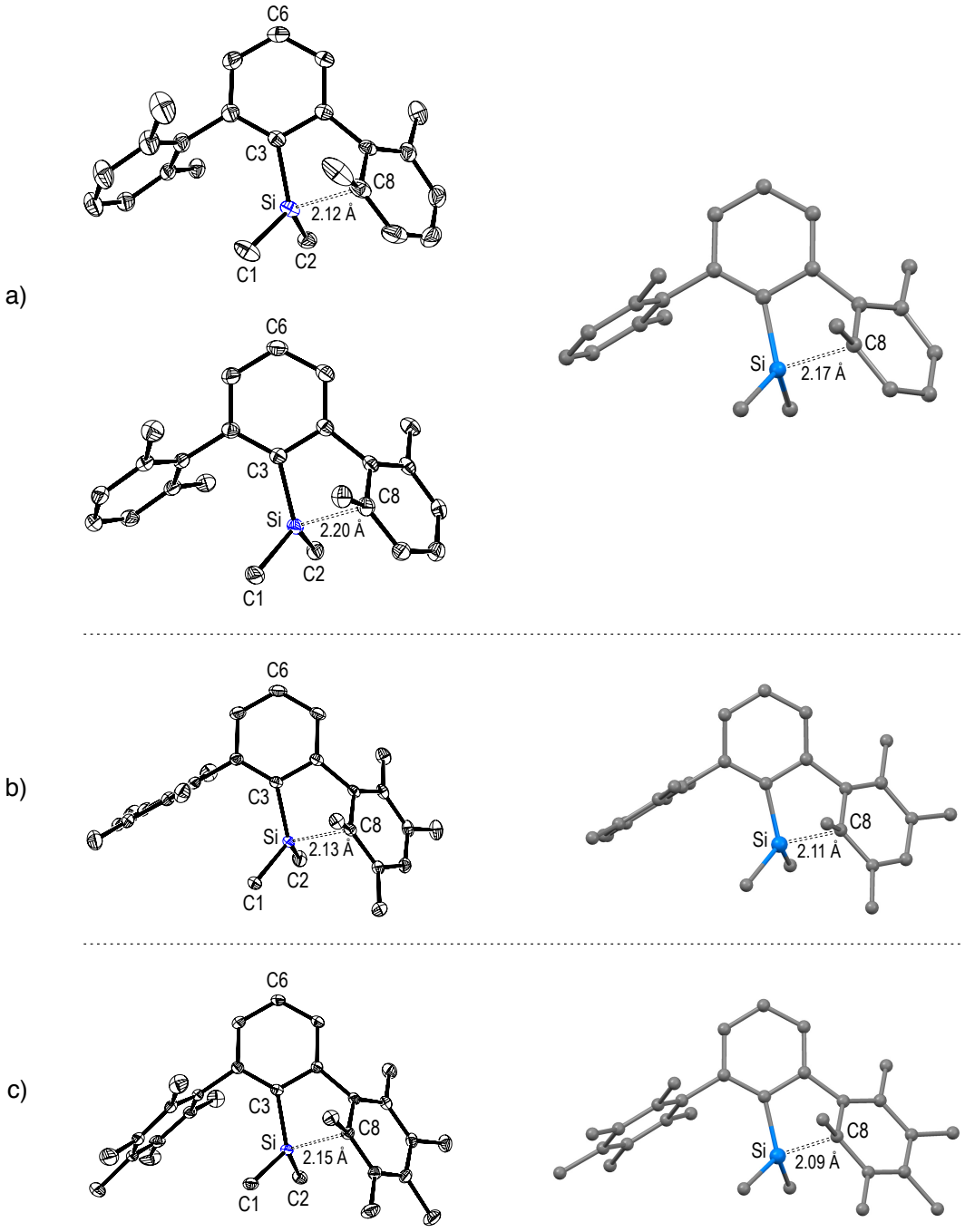

Figure 3.1. X-ray crystal structures (left) and calculated structures (right) of cations **27a**$^+$, **27c**$^+$ and **27d**$^+$ (30% displacement ellipsoids in the ORTEP plots, H atoms omitted for clarity). a) Crystal composition [**27a**][$CHB_{11}H_5Cl_6$], there are two cations in the asymmetric unit; b) crystal composition [**27c**][$B(C_6F_5)_4$] · 0.5 C_6H_5F; c) crystal composition [**27d**][CHB_1Cl_{11}] · 0.5 C_6H_5F.

Table 3.1. Selected distances (Å) and angles (°) in the crystal structures of **27a**$^+$, **27c**$^+$, and **27d**$^+$.

	27a$^+$		**27c**$^+$		**27d**$^+$	
Parameter	Expt[a]	Calcd	Expt	Calcd	Expt	Calcd
Si–C8	2.118(3) / 2.199(3)	2.169	2.126(1)	2.108	2.145(3)	2.092
Si–C1	1.839(3) / 1.836(3)	1.861	1.846(2)	1.864	1.843(3)	1.865
Si–C2	1.842(3) / 1.843(3)	1.863	1.838(2)	1.867	1.835(3)	1.869
Si–C3	1.863(3) / 1.854(3)	1.866	1.853(1)	1.867	1.857(2)	1.867
C6-C3-Si	168.5(2) / 167.0(2)	168.5	167.05(8)	168.2	169.5(1)	168.0
$Si_{\text{out of plane}}$[b]	0.3783(8) / 0.3620(7)	0.367	0.4026(4)	0.405	0.3759(8)	0.410
$\Sigma\angle$(C-Si-C)	347.6(2) / 348.8(1)	348.6	346.11(8)	346.3	346.9(1)	346.0
α[c]	48.2(2) / 55.1(1)	47.5	55.63(8)	47.3	53.2(1)	43.7

[a] There are two cations in the asymmetric unit. [b] Distance between Si and the plane through C1, C2, and C3. [c] Dihedral angle between least-squares planes through coordinating and central ring.

Crystalline samples of [**27c**][$B(C_6F_5)_4$] · 0.5 C_6H_5F and [**27d**][$CHB_{11}Cl_{11}$] · 0.5 C_6H_5F were obtained from fluorobenzene–hexane. Their structural features were similar to those of **27a**$^+$: Si–C_{ortho} distances of 2.126(1) Å/ 2.145(3) Å and $\Sigma\angle$(C-Si-C) of 346.11(8)° / 346.9(1)° are found. Thus in all cases the degree of π coordination, as judged by the Si–C_{ortho} distances, is comparable and resembles that of the toluene solvate **14**$^+$, for which Si–C_{ortho} is 2.12 Å. The fact that both the shortest and the longest distance are found for **27a**$^+$ indicates a shallow potential in the region 2.1–2.2 Å. Packing forces probably also influence the exact geometry of the cation in the solid state. Calculations predict a decrease in Si–C_{ortho} distance on going from **27a**$^+$ to **27d**$^+$.

A more detailed analysis of the X-ray data was carried out in order to address the question of silylium versus arenium ion character. Classical Wheland intermediates such as the toluenium ion or the heptamethylbenzenium ion show a long-short-average pattern in their bond lengths along C_{ipso}-C_{ortho}-C_{meta}-C_{para}, consistent with the principal resonance structures (Figure 3.2 a, b).[74, 111] Moreover, the overall symmetry is roughly C_{2v}, with comparable angles between the C_{ipso}–X vectors and the least-squares plane through the ring.

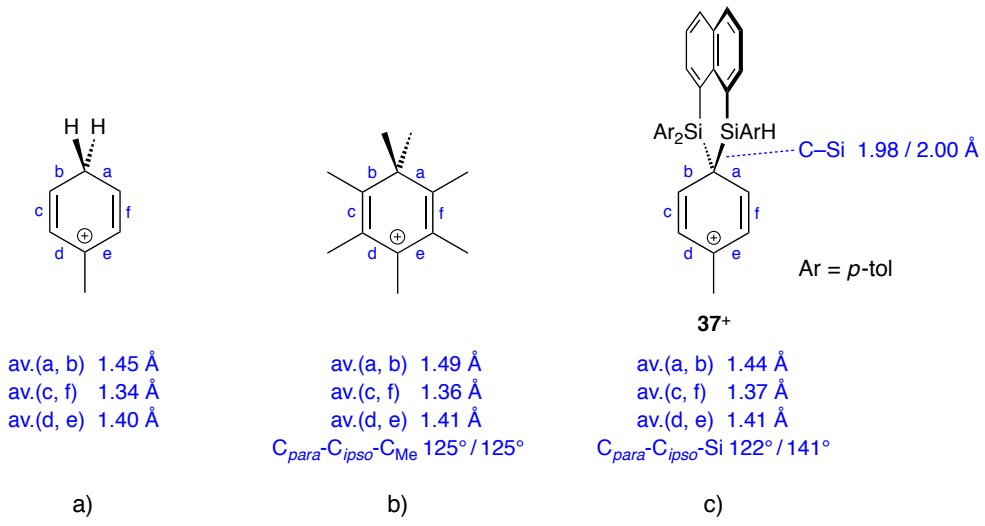

Figure 3.2. Selected distances in the crystal structures of a) the toluenium ion, b) the heptamethylbenzenium ion, and c) disilylated toluenium ion **37**$^+$.[74, 111, 112]

The coordinating rings in cations **27a**$^+$, **27c**$^+$, and **27d**$^+$ show some distortion towards Wheland intermediate character. Interaction of C8 with silicon is associated with a deviation of the angle C11-C8-C13 from 180° (Figure 3.3 a, Table 3.2). Values of 152–158° are observed, indicating incipient tetrahedral coordination about C8. The corresponding angles

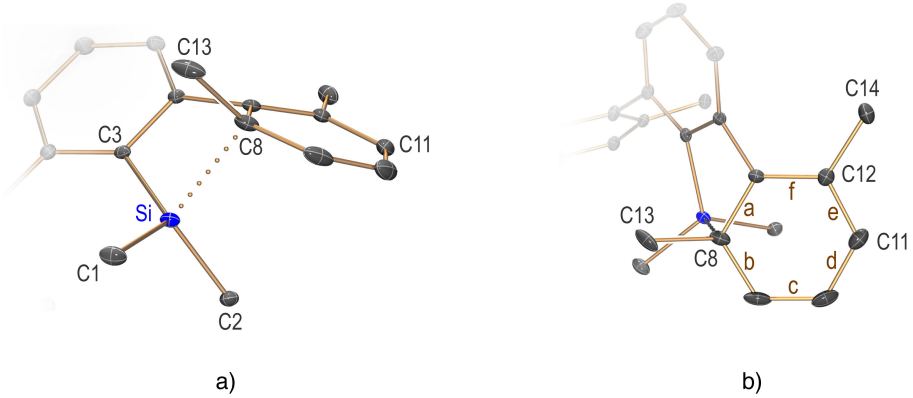

Figure 3.3. Details of cation 1 in the crystal structure of [**27a**][$CHB_{11}H_5Cl_6$]. a) Side view of the coordinating ring; both the silyl group and carbon atom C8 show a deviation from trigonal-planar coordination. b) View onto the coordinating ring.

Table 3.2. Selected distances (Å) and angles (°) in the crystal structures of **27a**$^+$, **27c**$^+$, and **27d**$^+$.

	27a$^+$		**27c**$^+$	**27d**$^+$
Parameter	Cation 1	Cation 2		
C11-C8-Si	107.3(2)	100.6(1)	102.79(6)	105.9(1)
C11-C8-C13	152.2(2)	157.9(2)	153.2(1)	152.2(2)
av.(a, b)	1.441	1.435	1.446	1.441
av.(c, f)	1.379	1.387	1.387	1.393
av.(e, d)	1.381	1.388	1.404	1.416
C8–C13	1.550(5)	1.534(4)	1.536(2)	1.540(3)
C12–C14	1.497(5)	1.499(4)	1.506(2)	1.509(4)

for silicon, C11-C8-Si, fall in the range of 101–107°. Partial arenium ion character is also reflected in the bond lengths. An analysis of the distances within the coordinating rings analogous to that in Figure 3.2 reveals a long-short-intermediate pattern along a/b, c/f, and d/e (Figure 3.3 b, Table 3.2). In addition, the distances C8–C13 are longer than C12–C14, 1.53–1.55 Å vs 1.50–1.51 Å.

The observed angles and distances unmistakably point to a mixed silyl cation/σ complex character of **27**$^+$. On the other hand, the structures of the cations still differ from that of a true silylarenium ion, an example of which was reported in 2007 by Müller and coworkers (Figure 3.2 c).[112] X-ray analysis of silicon-substituted cation **37**$^+$ revealed structural parameters that resemble those of classical Wheland intermediates more closely than **27**$^+$.

It is also useful to compare the structure of **27d**$^+$ with that of related heptasubstituted $[C_6Me_6(E)]^+$ cations (E = electrophile). A continuum of coordination modes is encompassed by the series E = CH_3, Cl, Br, Si, and NO. $[C_6Me_7]^+$ and $[C_6Me_6(NO)]^+$ are prototypical σ and π complexes, while intermediate geometries are observed for E = Cl, Br, and Si (Figure 3.4). The values α and β in the case of **27d**$^+$, 75° and 27°, are indeed only reconcilable with hybrid σ/π character. Assignment to either of the classes of complexes would appear arbitrary.

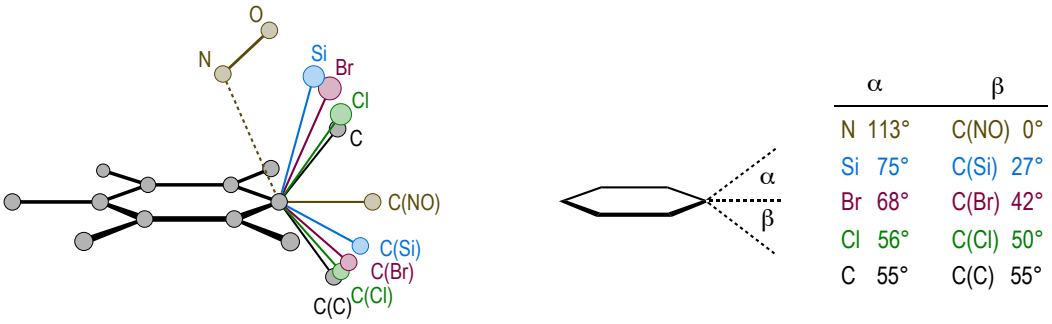

Figure 3.4. Schematic superposition of the X-ray structures of $[C_6Me_6(E)]^+$ complexes. Adapted from Kochi and Hubig,[111] data for E = Si from this work (cation **27d**$^+$). α and β are the angles between the least-squares plane through the benzene ring and the C_{ipso}–E and C_{ipso}–C(E) vectors.

3.4 Conformation of the Cations in Solution

The X-ray crystal structures of **27**$^+$ gave evidence for a specific C_{aryl}–Si coordination in the solid state. An analysis of the NMR signals of the lateral rings was carried out to investigate the conformational preference in solution. The results of this study were also in agreement with a C_{ipso}–Si interaction and C_1 being the favored cation geometry.

Chemical shifts of C_{ipso}–C_{para} of **29** and **27**$^+$ were determined by ^{1}H/^{13}C HSQC and HMBC experiments. Conversion of the silanes to the cations is accompanied by a shielding of C_{ortho} and a deshielding of the other positions (Figure 3.5). The shielding is in the order of 6–9 ppm, while the deshielding of C_{ipso}, C_{meta}, and C_{para} is observed in the ranges 10–12, 12–19, and 3–5 ppm, respectively (Table 3.4).

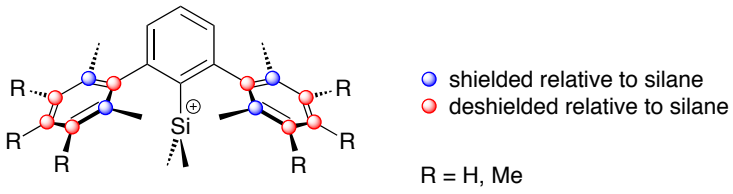

Figure 3.5. Shielding of C_{ortho} and deshielding of the other positions of the lateral rings on going from **29** to **27**$^+$.

Table 3.3. ^{13}C NMR shifts of **29** and **27**$^{+}$; $\Delta\delta = \delta(\mathbf{27}^{+}) - \delta(\mathbf{29}^{+})$. C_6D_6, 300 K, C_6D_6 = 128.0 ppm.

	C_{ipso}	C_{ortho}	C_{meta}	C_{para}
29a	143.4	136.3	127.5	127.6
27a^{+}	153.4	130.1	139.4	131.0
$\Delta\delta$	+10.0	–6.2	+11.9	+3.4
29b	140.7	136.1	128.3	136.7
27b^{+}	150.7	130.0	139.9	141.9
$\Delta\delta$	+10.0	–6.1	+11.6	+5.2
29c	143.5	133.5	132.1	130.9
27c^{+}	155.2	124.4	151.6	133.8
$\Delta\delta$	+11.7	–9.1	+19.5	+2.9
29d	141.3	132.1	131.7	133.8
27d^{+}	152.8	123.8	150.7	138.8
$\Delta\delta$	+11.5	–8.3	+19.0	+5.0

Wheland intermediates display an upfield shift of the ^{13}C signal of the tetracoordinate carbon relative to the free arene, whereas the other carbon atoms are more deshielded.[43, 111] The shift differences between benzene and $C_6H_7^+$ amount to -76, $+56$, $+8$, and $+48$ ppm for C_{ipso}–C_{para}, and similar values were determined in the case of C_6Me_6 vs $C_6Me_7^+$ (Figure 3.6 a, b). ^{13}C and ^{29}Si NMR data of disilylated arenium ions were reported by Mueller in 2002. Cation $\mathbf{38}^{+}$ gave rise to ring resonances at 89, 180, 136, and 167 ppm;

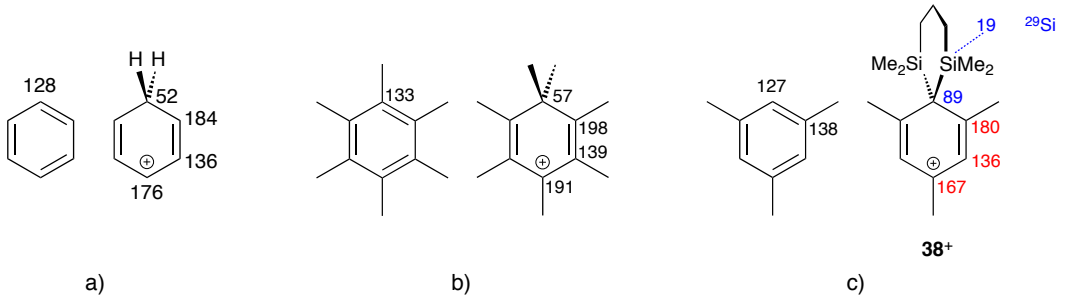

Figure 3.6. ^{13}C and ^{29}Si NMR shifts of a) the benzenium ion, b) the heptamethylbenzenium ion, and c) disilylated mesitylenium ion $\mathbf{38}^{+}$.[43, 111, 113]

the ^{29}Si signal was observed at 19 ppm (Figure 3.6 c).[113] Accordingly, the NMR data of **27**$^+$ suggested an arene–Si coordination primarily involving the C_{ortho} atoms, with some of the positive charge residing on the lateral rings, but weaker than in a full Wheland intermediate. Further support of a C_{ortho}–Si interaction came from ^{1}H/^{13}C and ^{1}H/^{29}Si HMBC spectra. Cross-peaks between C_{ortho} and Si–CH_3 as well as between H_3C–C_{ortho} and the silicon center were probably caused by $^3J_{C,H}$ and $^3J_{Si,H}$ coupling, respectively (Figure 3.7).

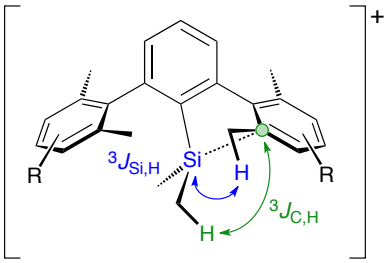

Figure 3.7. $^3J_{C,H}$ and $^3J_{Si,H}$ coupling in **27**$^+$ indicating a C_{ortho}–Si interaction.

A solid-state ^{29}Si{^{1}H} NMR spectrum of **27a**$^+$ contained resonances at 87.3 and 74.2 ppm (Figure 3.8). The two signals were attributed to the presence of two independent cations. The microcrystalline material for this measurement was obtained under the same conditions as the single crystals for the X-ray analysis, *i.e.*, with the carborane counterion

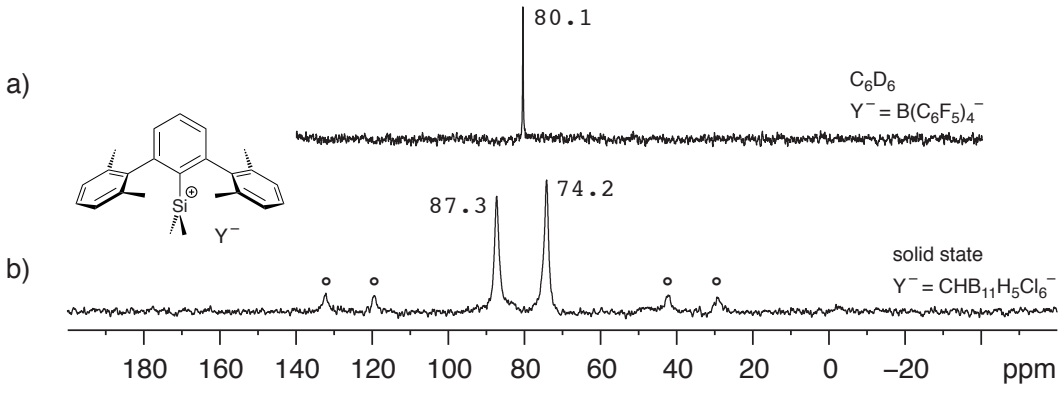

Figure 3.8. a) Solution-phase and b) solid-state ^{29}Si{^{1}H} NMR spectrum of **27a**$^+$. The two signals in the solid-state spectrum are attributed to the presence of two cations in the aysmmetric unit; peaks marked with a circle are spinning side bands.

$CHB_{11}H_5Cl_6^-$ from a 1,2-dichlorobenzene–hexane mixture. Because two cations were found in the asymmetric unit of [**27a**][$CHB_{11}H_5Cl_6$], it was likely that the material used for the solid-state NMR measurement consisted of identical crystals containing the cations in the conformations shown in Figure 3.1 a.* The shifts of 87.3 and 74.2 ppm were close to that of [**27a**][$B(C_6F_5)_4$] in C_6D_6, 80.1 ppm, and suggested that C_1 geometry is also preferred in solution.

The combined computational, X-ray crystallographic, and NMR-spectroscopic data were best in agreement with a conformational preference of $\mathbf{27}^+$ for a C_1 geometry in which donation of π electron density to silicon occurs mainly through C_{ortho} of a flanking ring. According to this model, a rapid equilibrium among the four degenerate C_1 conformers on the NMR time scale leads to dynamic C_{2v} symmetry in solution (Scheme 3.1). Low-temperature NMR experiments carried out with $\mathbf{27b}^+$ in toluene-d_8 from 0 to -30 °C indicated an upper energy barrier limit of 51 kJ mol^{-1} for all processes in the proposed equilibrium. Below -30 °C, increased viscosity of the cation solution lead to severe broadening of the signals.

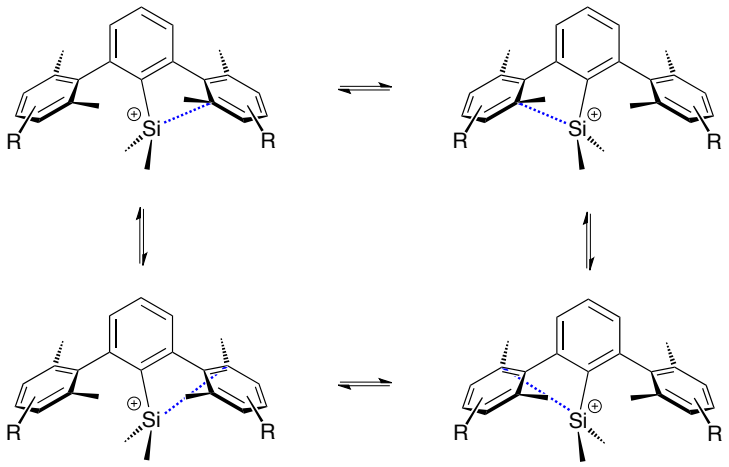

Scheme 3.1. Putative equilibrium among degenerate C_1 conformers of $\mathbf{27}^+$ in solution; C_{ortho}–Si interactions blue.

*Attempts to collect powder diffraction data of the microcrystalline sample for a comparison with the calculated spectrum of the single crystal analysis were thwarted by the moisture sensitivity of the compound; powder films prepared and meticulously sealed in a glove box nevertheless decomposed within minutes when taken out of the box.

3.5 Cations with Isopropyl Groups at Silicon

Variation of the electron richness of the flanking rings exerted a clear influence on the stabilization of cations $\mathbf{27}^+$. The effect of altering the immediate environment about the silicon center was probed by substitution about the silyl methyl groups by isopropyl groups.

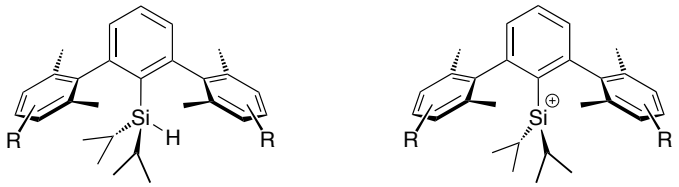

39 **40**$^+$

Diisopropylsilanes **39** were synthesized analogously to dimethylsilanes **29**. The most prominent feature in their ^{1}H NMR spectra were the signals of the isopropyl groups. Diastereotopicity of the two CH_3 groups within each isopropyl group and enantiotopicity of the two isopropyl groups with respect to each other afforded two doublets for the CH_3 groups and one $q \times q \times d$ signal for the C–H protons (Figure 3.9).

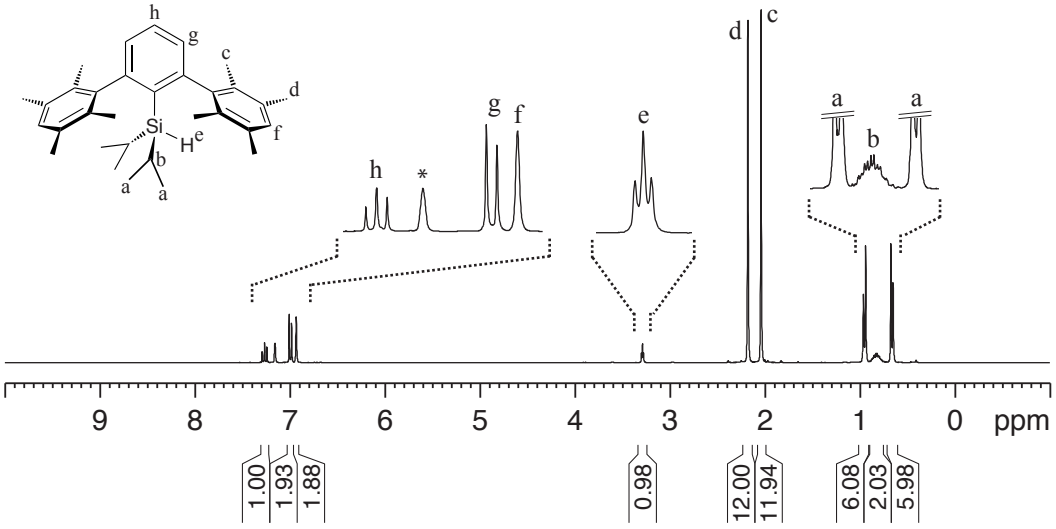

Figure 3.9. ^{1}H NMR spectrum of **39c**. Conditions: 300 MHz, 300 K, 60 mg in 0.6 mL C_6D_6; the signal marked with an asterisk stems from C_6HD_5 = 7.16 ppm.

^{29}Si resonances of **39** appeared at 3.7, 3.6, 4.1, and 4.0 ppm for Ar = xylyl, mesityl, duryl, and pentamethylphenyl (C_6D_6 solution, Ar = flanking ring; Figure 3.10). These values differ from the resonances of **29** by +27 ppm. The deshielding might be attributed to an electronic effect of the isopropyl groups and/or different solvation.[†] However, no further experiments were carried out to investigate this phenomenon.

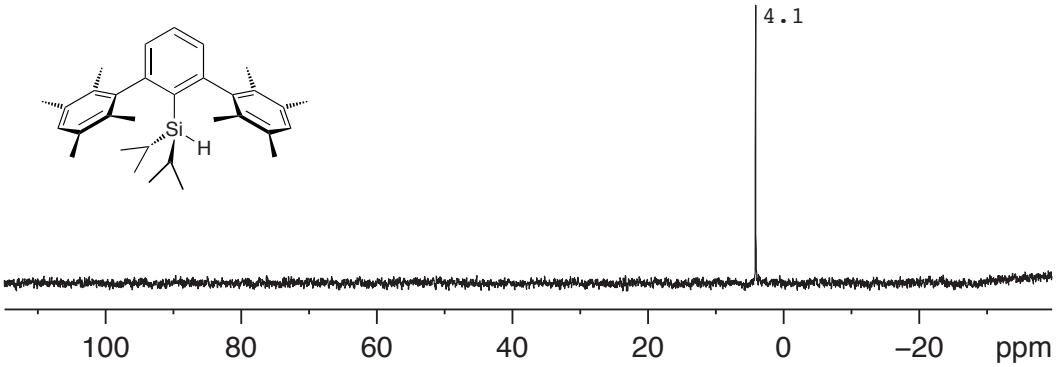

Figure 3.10. ^{29}Si{^{1}H} NMR spectrum of **39c**. Conditions: 60 MHz, 300 K, 60 mg in 0.6 mL C_6D_6, referenced against external $SiMe_4$.

Hydride abstraction from **39** by $[Ph_3C][B(C_6F_5)_4]$ afforded cations **40**$^+$. In these reactions, the steric bulk of the isopropyl groups had a clear rate-retarding effect. Stirring a slight excess of silane with the trityl cation for two weeks at room temperature gave typical conversions of *ca.* 50 % as inferred from NMR spectra and GC–MS analysis after quenching with a nucleophile (Figure 3.11).

Conversion of the hydrosilane precursors to the silyl cations was confirmed by the downfield ^{29}Si resonances that appeared at 95–64 ppm (Figure 3.12, Table 3.4). Although the deshielding with respect to $SiMe_4$was slightly more pronounced in **40**$^+$ than in **27**$^+$, the $\Delta\delta$ values were smaller. Going from the silanes to the cations was accompanied by ^{29}Si shift differences of about 90 (**40a**,**b**$^+$) and 65 ppm (**40c**,**d**$^+$); in the case of **27**$^+$, the corresponding differences were about 105 and 85 ppm.

[†]A deshielding, albeit to a lesser extent, is also seen on going from Et_3SiH to *i*Pr_3SiH ($\delta(^{29}Si)$ 0.4 and 12.3 ppm in C_6D_6, respectively).

In the ^{1}H NMR spectra, the isopropyl groups of **40**$^{+}$ exhibited less complicated signals than their neutral precursors. The presence of one doublet for CH_3 and one septet for the C–H protons indicated enantiotopic methyl groups within each isopropyl group on the NMR time scale of observation and overall C_{2v} symmetry of the cations (Figure 3.11).

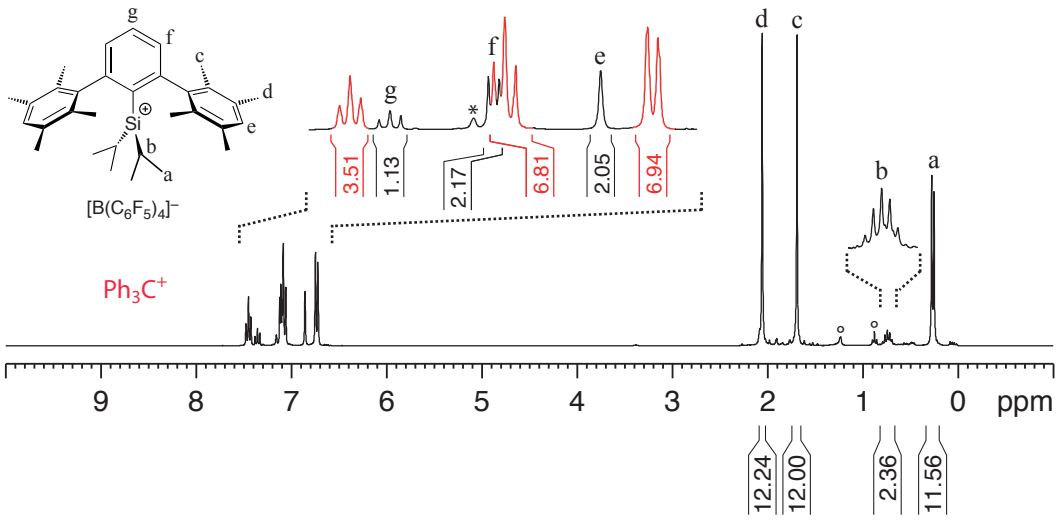

Figure 3.11. ^{1}H NMR spectrum of [**40c**][B(C_6F_5)$_4$]. The reaction mixture was precipitated and dried in a vacuum after 14 days of stirring at RT; the integrals indicate a silyl cation:trityl cation ratio of *ca.* 1:1.1. Conditions: 300 MHz, 300 K, 240 mg (total) in 0.6 mL C_6D_6; the signals marked with a circle stem from hexane, the signal marked with an asterisk stems from C_6HD_5 = 7.16 ppm.

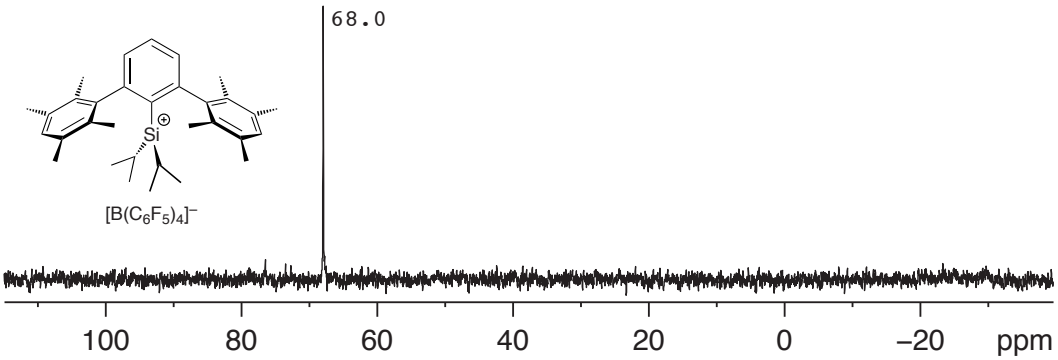

Figure 3.12. ^{29}Si{^{1}H} NMR spectrum of [**40c**][B(C_6F_5)$_4$]. Conditions: 60 MHz, 300 K, 240 mg (total, precipitated reaction mixture that still contained trityl salt) in 0.6 mL C_6D_6, referenced against external $SiMe_4$.

Table 3.4. ^{29}Si and ^{13}C NMR shifts of **39** and **40**$^{+}$; $\Delta\delta = \delta(\mathbf{40}^{+}) - \delta(\mathbf{39}^{+})$. C_6D_6, 300 K, external $SiMe_4$ = 0 ppm for ^{29}Si, C_6D_6 = 128.0 ppm.

	Si	C_{ipso}	C_{ortho}	C_{meta}	C_{para}
39a	3.7	144.1	136.2	127.7	127.6
40a^{+}	95.4	–[a]	–	–	–
$\Delta\delta$	+91.7	–	–	–	–
39b	3.6	141.5	136.2	128.4	136.7
40b^{+}	93.4	150.9	130.4	140.1	141.7
$\Delta\delta$	+89.8	+9.4	–5.8	+11.7	+5.0
39c	4.1	144.3	133.6	132.3	130.8
40c^{+}	68.0	156.7	124.1	152.9	134.3
$\Delta\delta$	+63.9	+ 12.4	–9.5	+20.6	+3.5
39d	4.0	142.1	131.8	132.2	133.7
40d^{+}	67.6	154.1	123.6	151.3	139.0
$\Delta\delta$	+63.6	+12.0	–8.2	+19.1	+5.3

[a] The ^{13}C NMR shifts of this cation could not be determined unambiguously.

An analysis of the ^{13}C NMR signal of the lateral rings revealed a $\Delta\delta$ pattern similar to that in the dimethylsilyl series. Shielding of C_{ortho} by 6–10 ppm and deshielding of C_{ipso}, C_{meta}, and C_{para} by 9–12, 12–21, and 4–5 ppm were observed, respectively (Table 3.4). The magnitude of the differences is essentially identical to those found for **29 / 27**$^{+}$ and suggests a comparable sensitivity of the silicon center to changes in π electron density in both families of cations. Based on the NMR data, the isopropyl groups in **40**$^{+}$ do not diminish C_{ortho}–Si interactions significantly, and in solution the cations probably exist as rapidly equilibrating C_1 conformers.

3.6 Cations Lacking *ortho* Substituents

Steric enshrouding and electronic stabilization had lead to a class of long-lived, yet still reactive silyl cations. What would the consequences of diminished steric protection and π coordination be? To address this question, a study of cations with less substituted flanking

rings was envisaged.

Cations $\mathbf{41}^+$ were chosen as target structures. The lack of *ortho* substituents on the flanking rings should afford a sterically more accessible silyl group and decreased donation of electron electron density from the phenyl π systems. Both factors should were anticipated to enhance the reactivity of the cations.

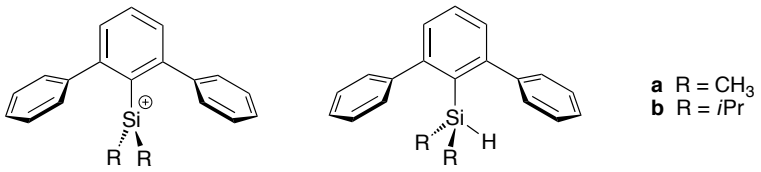

41a,b$^+$ **42a,b**

Precursors **42** were prepared via Hart coupling and subsequent silylation, analogously to the terphenylsilanes **29** and **39**. **42a** and **42b** displayed ^{29}Si NMR shifts of -20.4 and $+6.4$ ppm and otherwise no unusual spectroscopic features.

First attempts to generate **41a** were unfruitful. Treatment of $\mathbf{42a}^+$ with $[Ph_3C][B(C_6F_5)_4]$ in C_6D_6 afforded a black reaction mixture with featureless resonances in the ^{1}H and ^{13}C NMR spectra. No ^{29}Si signal could be detected. Assuming that hydride abstraction would be the first step after mixing the starting materials, cation $\mathbf{42a}^+$ was apparently not a long-lived species under the reaction conditions chosen.

It appeared reasonable that $\mathbf{42a}^+$ would be coordinated intramolecularly, at least to some extent. A fundamental difference between $\mathbf{42a}^+$ and $\mathbf{27}^+$ was that in the latter the C_{ortho} positions were blocked by CH_3 groups, wheras in the former only a hydrogen atom was attached to C_{ortho}. Thus acidification of the *ortho* position upon coordination of the silyl group and eventual loss of a proton represented a possible pathway of consecutive reactions. Decomposition of the newly formed silafluorene could finally have occurred under the acidic conditions.

This hypothesis was tested by carrying out the hydride abstraction in the presence of a sterically hindered Brønsted base. P(*o*-tol)$_3$ does not react with the trityl cation but was expected to act as a proton sponge towards highly acidic Wheland intermediates. Indeed, when silanes **42** were allowed to react under these conditions, silafluorenes **43** were found

as the only silicon-containing products (Scheme 3.2). They were identified by NMR and mass spectroscopy ($\delta(^{29}$Si 0.8 and 12.1 ppm), and the formation of [HP(*o*-tol)$_3$][B(C$_6$F$_5$)$_4$] was confirmed by ^{1}H and ^{31}P NMR spectroscopy.

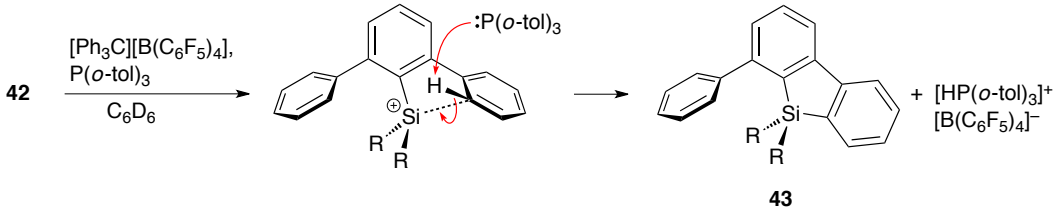

Scheme 3.2. Formation of silafluorenes **43** by hydride abstraction from **42** in the presence of a Brønsted base

The attempted preparation of **41**$^+$ had not afforded long-lived silyl cationic species. However, it was of some value for two reasons. On the one hand, it underscored the acidifying effect that silylium ions can exert on aromatic solvents. This property was already observed with the cation **27d**$^+$ (Section 2.7). On the other hand, it provided this work with a rare example of a Friedel–Crafts silylation. An almost identical silylation procedure was recently published, coincidentally also in the context of the synthesis of silafluorenes.[114]

3.7 Hammett Analysis

Given the data obtained for **27**$^+$ and **40**$^+$, a qualitative influence of the electron richness of the flanking rings on silyl cationic character was evident. A quantitative correlation between π basicity and the ^{29}Si NMR shifts was derived from a Hammett analysis.[100, 115–117]

The analysis is based on the assumption that the C_1 conformation exhibiting C$_{ortho}$–Si coordination represents the thermodynamically favored geometry of the cations.[‡] As a measure for the electron richness of the flanking rings, Hammett substituent constants σ were chosen.[118] Because all cations comprise two or more methyl groups on the lateral rings, the coordination by a xylyl ring is defined as $\Sigma(\sigma) = 0$ (Figure 3.13). In this situation,

[‡]A rapid equilibrium among the four degenerate C_1 forms does not interfere with the Hammett analysis. Despite the likely fluxional behavior, C_1 remains the favored geometry of the cations, and they will spend most of their time in this form.

one *ortho*, one *meta*, and one *para* position relative to the coordinating carbon atom are substituted by hydrogen. When the flanking rings are mesityl groups, one CH_3 substituent *meta* to the coordinating carbon is introduced, and $\Sigma(\sigma) = \sigma_{meta} = -0.069$. By analogy, the sum of Hammett constants is obtained for the two remaining lateral rings, assuming $\sigma_{ortho} \approx \sigma_{para}$ in the absence of severe steric crowding.

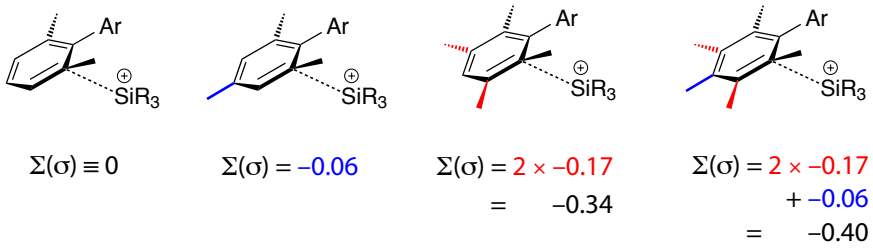

Figure 3.13. Sum of Hammett constants of the lateral rings with respect to the coordinating C_{ortho} atom.

When the ^{29}Si NMR shifts of **27**$^+$ and **40**$^+$ are plotted against $\Sigma(\sigma)$, a reasonable linear relationship between π_{aryl} electron density and shielding of the silicon nucleus is found (Figure 3.14). The ^{29}Si NMR resonances of **27a**,**b**$^+$ and **27c**,**d**$^+$ appear at roughly 80 and

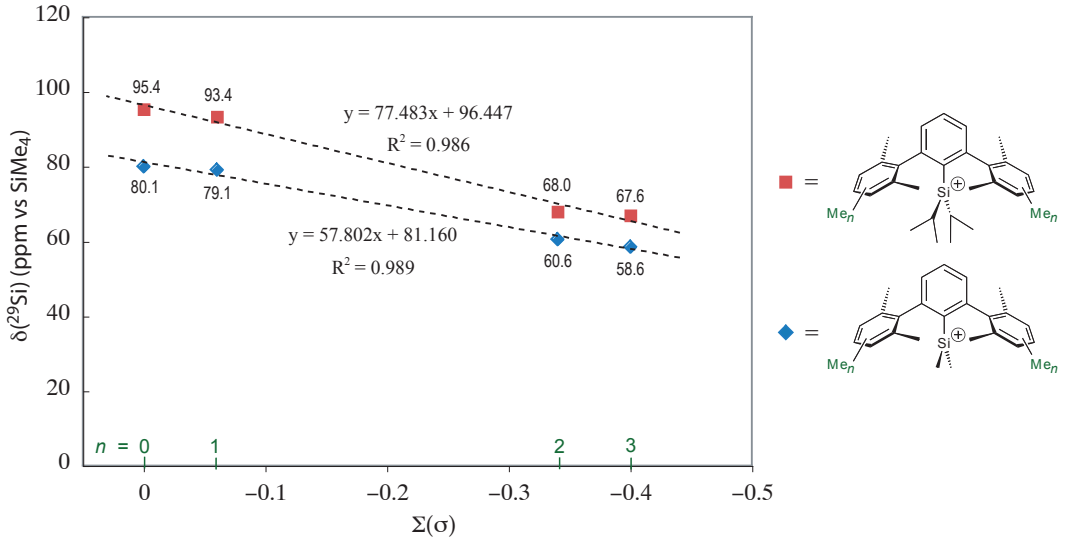

Figure 3.14. Correlation between the ^{29}Si NMR shifts of **27**$^+$ and **40**$^+$ and the sum of Hammett constants of the flanking rings.

60 ppm, respectively; the same holds for **27a**,**b**$^+$ and **27c**,**d**$^+$ (94 and 68 ppm). Apparently, the clustering of shifts is successfully reproduced when C_{ortho} coordination is assumed and position-specific σ values are applied. However, it would not result from a model in which only field effects are considered.

The general utility of such a plot is manifold. First, it offers a means of distinguishing between π stabilization by a direct and specific coordination and pacification by a non-specific increase in electron density, as demonstrated for the cations of the present study. By the same token, an outlier in a series of compounds is likely to exhibit a coordination of silicon that differs from the rest of the series. Moreover, the slope in this kind of plot represents a gauge of how sensitive the central silyl group is towards substituent variation on the flanking rings. Slopes around zero, such as in the case of **29** and **39**, are consistent with a negligible Si–π interaction. Negative values indicate a higher demand of silicon for electron density, which is seen for **27**$^+$ and **40**$^+$. Finally, a $\delta(^{29}\mathrm{Si})$–$\Sigma(\sigma)$ correlation might also serve as a tool for the design of new, tailor-made silyl cationic systems.

3.8 Experimental Part

3.8.1 General

For general reaction conditions and analytical instruments, see Sections 2.9.3 and 2.9.4.

Chlorodiisopropylsilane was purchased from Aldrich and used as received.

3.8.2 Crystal Growth

In general, it was important to carry out crystallization attempts with silyl cation salts of high purity. If the sample contains other compounds, formation of oily precipitates is likely to occur. The presence of residual trityl cation must be avoided because trityl salts crystallize easily, even when there is an excess of silyl cation salt.

Once crystalline material is obtained, it is worthwhile to pick a few crystals of low quality, dissolve them, quench the solution with CsF or H_2O, and take a GC–MS to confirm that the crystals are not trityl salt.

Crystals of the composition [**27a**][$CHB_{11}H_5Cl_6$] were obtained at RT from a dichlorobenzene solution (*ca.* 20 mg of the isolated salt in 0.6 mL) that was layered with hexane in an NMR tube.

Crystals of the composition [**27c**][$B(C_6F_5)_4$] · 0.5 C_6H_5F were obtained at −20 °C from a fluorobenzene solution (*ca.* 30 mg of the isolated salt in 1 mL).

Crystals of the composition [**27d**][$CHB_{11}Cl_{11}$] · 0.5 C_6H_5F were obtained at RT from a fluorobenzene solution (*ca.* 10 mg of the isolated salt in 0.5 mL) that was layered with hexane in a small glass vial.

Table 3.5. Summary of the X-ray diffraction analysis of **27a**$^+$.

Crystallized from	1,2-dichlorobenzene / hexane
Empirical formula	$C_{25}H_{33}B_{11}Cl_6Si$
Formula weight [g mol^{-1}]	693.25
Crystal color, habit	yellow, prism
Crystal dimensions [mm]	0.12 × 0.12 × 0.17
Temperature [K]	160(1)
Crystal system	triclinic
Space group	$P\bar{1}$ (#2)
Z	4
Reflections for cell determination	140037
2θ range for cell determination [°]	4 – 50
Unit cell parameters a [Å]	9.8429(1)
b [Å]	18.7643(2)
c [Å]	19.7438(2)
α [°]	74.8487(7)
β [°]	81.5388(7)
γ [°]	86.2564(7)
V [Å^3]	3480.14(6)
$F(000)$	1416
D_x [g cm^{-3}]	1.323
μ(Mo $K\alpha$) [mm^{-1}]	0.546
Scan type	ω
$2\theta_{(max)}$ [°]	50
Transmission factors (min; max)	0.847; 0.936
Total reflections measured	46883
Symmetry independent reflections	12280
R_{int}	0.058
Reflections with $I > 2\sigma(I)$	9284
Reflections used in refinement	12279
Parameters refined	787
Final $R(F)$ [$I > 2\sigma(I)$ reflections]	0.0434
$wR(F^2)$ (all data)	0.1126
Weights: $w = [\sigma^2(F_o^2) + (0.0486P)^2 + 2.3016P]^{-1}$ where $P = (F_o^2 + 2F_c^2)/3$	
Goodness of fit	1.024
Final Δ_{max}/σ	0.001
$\Delta\rho$ (max; min) [e Å^{-3}]	0.58; –0.55
$\sigma(d_{(C-C)})$ [Å]	0.004 – 0.006

Table 3.6. Summary of the X-ray diffraction analysis of **27c**$^+$.

Crystallized from	C_6D_6 / fluorobenzene / hexane
Empirical formula	$C_{55}H_{37.5}BF_{20.5}Si$
Formula weight [g mol^{-1}]	1126.76
Crystal color, habit	yellow, prism
Crystal dimensions [mm]	0.28 × 0.30 × 0.32
Temperature [K]	160(1)
Crystal system	monoclinic
Space group	$P2_1/c$ (#14)
Z	4
Reflections for cell determination	69557
2θ range for cell determination [°]	4 – 60
Unit cell parameters a [Å]	17.9859(1)
b [Å]	15.1737(2)
c [Å]	18.1876(2)
α [°]	90
β [°]	96.1785(6)
γ [°]	90
V [Å^3]	4934.79(9)
$F(000)$	2284
D_x [g cm^{-3}]	1.516
μ(Mo $K\alpha$) [mm^{-1}]	0.164
Scan type	ϕ and ω
$2\theta_{(max)}$ [°]	60
Transmission factors (min; max)	0.853; 0.963
Total reflections measured	137396
Symmetry independent reflections	14437
R_{int}	0.061
Reflections with $I > 2\sigma(I)$	11007
Reflections used in refinement	14434
Parameters refined	714
Final $R(F)$ [$I > 2\sigma(I)$ reflections]	0.0484
$wR(F^2)$ (all data)	0.1313
Weights: $w = [\sigma^2(F_o^2) + (0.0703P)^2 + 1.4458P]^{-1}$ where $P = (F_o^2 + 2F_c^2)/3$	
Goodness of fit	1.054
Secondary extinction coefficient	0.0153(6)
Final Δ_{max}/σ	0.001
$\Delta\rho$ (max; min) [e Å^{-3}]	0.42; –0.35
$\sigma(d_{(C-C)})$ [Å]	0.00 – 0.00

Table 3.7. Summary of the X-ray diffraction analysis of **27d**$^+$.

Crystallized from	fluorobenzene / pentane
Empirical formula	$C_{34}H_{42.5}B_{11}Cl_{11}F_{0.5}Si$
Formula weight [g mol^{-1}]	997.68
Crystal color, habit	yellow, needle
Crystal dimensions [mm]	0.05 × 0.08 × 0.40
Temperature [K]	160(1)
Crystal system	monoclinic
Space group	$P2_1/c$ (#14)
Z	4
Reflections for cell determination	83953
2θ range for cell determination [°]	4–55
Unit cell parameters a [Å]	9.3563(1)
b [Å]	26.2649(3)
c [Å]	19.5274(2)
α [°]	90
β [°]	101.8077(6)
γ [°]	90
V [Å^3]	4697.17(9)
$F(000)$	2028
D_x [g cm^{-3}]	1.411
μ(Mo $K\alpha$) [mm^{-1}]	0.704
Scan type	ϕ and ω
$2\theta_{(max)}$ [°]	55
Transmission factors (min; max)	0.866; 0.972
Total reflections measured	95624
Symmetry independent reflections	10732
R_{int}	0.067
Reflections with $I > 2\sigma(I)$	7849
Reflections used in refinement	10727
Parameters refined; restraints	550; 42
Final $R(F)$ [$I > 2\sigma(I)$ reflections]	0.0424
$wR(F^2)$ (all data)	0.1068
Weights: $w = [\sigma^2(F_o^2) + (0.0449P)^2 + 4.1538P]^{-1}$ where $P = (F_o^2 + 2F_c^2)/3$	
Goodness of fit	1.020
Final Δ_{max}/σ	0.004
$\Delta\rho$ (max; min) [e Å^{-3}]	0.61; –0.58
$\sigma(d_{(C-C)})$ [Å]	0.003 – 0.005

3.8.3 Synthesis of the Diisopropylsilanes

3.8.3.1 [2,6-Bis(2,6-dimethylphenyl)phenyl]diisopropylsilane

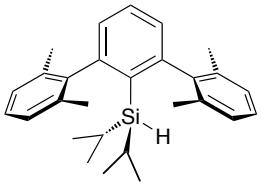

Chemical Formula: $C_{28}H_{36}Si$
Molecular Weight: 400.671

This compound was prepared according to the general procedure A for the synthesis of terphenylsilanes (Section 2.9.6, page 77).

The crude product was purified by recrystallization from ethanol–isopropanol 1:1. The clear hot solution was slowly allowed to cool to RT, which afforded the silane as colorless crystals (89 %).

Characterization

M.p.: 120.5–121.5 °C

IR (KBr): 3037*m*, 3017*m*, 2963*s*, 2935*s*, 2859*s*, 2127*s* 1579*w*, 1555*m*, 1459*s*, 1441*s*, 1374*m*, 1230*w*, 1175*w* 1167*w*, 1120*m*, 1076*m*, 1062*m*, 1046*m*, 1007*s*, 880*s*, 843*s*, 809*s*, 790*s*, 768*s*, 748*s*, 663*m*, 606*m*, 582*w*, 569*w*, 476*m*.

^{1}H NMR (300 MHz, 45 mg in 0.6 mL C_6D_6, C_6HD_5 = 7.16): 7.19 (*t*, $^3J = 7.6$, 1 H, H–C(4')), 7.15–7.07 (*m*, 2 H, H–C(4", 4"')), 7.05–7.01 (*m*, 4 H, H–C(3", 5", 3"', 5"')), 6.87 (*d*, $^3J = 7.6$, 2 H, H–C(3', 5'), 3.37 (*t*, $^3J = 3.1$, 1 H, H–Si), 2.10 (*s*, 12 H, H_3C–C(2", 6", 2"', 6"')), 0.99–0.92 (*m*, 6 H, iPr-CH_3), 0.96–0.80 (*m*, 2 H, iPr-CH), 0.71–0.65 (*m*, 6 H, iPr-CH_3).

^{13}C{^{1}H} NMR (75 MHz, 120 mg in 0.6 mL C_6D_6): 149.4 (*s*, C(2', 6')), 144.1 (*s*, C(1", 1"'); 136.2 (*s*, C(2", 6", 2"', 6"'), 135.9 (*s*, C(1')), 129.7 (*d*, C(4'), 128.6 (*d*, C(3', 5')), 127.7 (*d*, C(3", 5", 3"', 5"')), 127.6 (*d*, C(4", 4"')), 22.6 (*q*, iPr–CH_3), 21.4 (*q*, *C*–C(2", 6", 2"', 6"')), 18.7 (*q*, iPr–CH_3), 11.7 (*d*, iPr–CH).

^{29}Si{^{1}H} NMR (60 MHz, 120 mg in 0.6 mL C_6D_6): 3.7.

MS (EI): 357 ([M − iPr]$^{+}$), 327 (17), 315 (36), 253 (26).

3.8.3.2 [2,6-Bis(2,4,6-trimethylphenyl)phenyl]diisopropylsilane

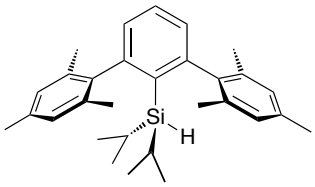

Chemical Formula: $C_{30}H_{40}Si$
Molecular Weight: 428.724

This compound was prepared according to the general procedure A for the synthesis of terphenylsilanes (Section 2.9.6, page 77).

The crude product was purified by recrystallization from isopropanol. The clear hot solution was slowly allowed to cool to 5 °C, which afforded the silane as colorless crystals (71 %). Crystals suitable for X-ray crystallography grew in an isopropanol solution at RT.

Characterization

M.p.: 165–166 °C

IR (KBr): 2939*s*, 2920*s*, 2862*s*, 2129*s*, 1611*m*, 1659*m*, 1557*m*, 1444*m*, 1377*m*, 1180*w*, 1120*m*, 1086*m*, 1048*m*, 1009*m*, 923*w*, 886*m*, 873*m*, 850*s*, 829*s*, 815*s*, 767*m*, 749*m*, 722*m*, 668*m*, 600*m*, 582*m*, 558*w*, 487*m*.

^{1}H NMR (300 MHz, 5 mg in 0.6 mL C_6D_6): 7.23 (*t*, $^{3}J = 7.6$, 1 H, H–C(4')), 6.94 (*d*, $^{3}J = 7.6$, 2 H, H–C(3', 5')), 6.88 (*s*, 4 H, H–C(3", 5", 3"', 5"')), 3.46 (*t*, $^{3}J = 3.1$, 1 H, H–Si), 2.20 (*s*, 6 H, H_3C–C(4", 4"')), 2.13 (*s*, 12 H, H_3C–C(2", 6", 2"', 6"')), 1.03–0.99 (*m*, 6 H, iPr-CH_3), 0.99–0.91 (*m*, 2 H, iPr-CH), 0.72–0.68 (*m*, 6 H, iPr-CH_3).

^{13}C{^{1}H} NMR (75 MHz, 45 mg in 0.6 mL C_6D_6): 149.6 (*s*, C(2', 6')), 141.5 (*s*, C(1", 1"'), 136.7 (*s*, C(4", 4"'), 136.5 (*s*, C(1')), 136.2 (*s*, C(2", 6", 2"', 6"'), 129.6 (*d*, C(4')), 128.9 (*d*, C(3', 5')), 128.4 (*d*, C(3", 5", 3"', 5"')), 22.8 (*q*, iPr–CH_3), 21.4 (*q*, *C*–C(2", 6", 2"', 6"')), 21.1 (*q*, *C*–C(4", 4"')), 18.8 (*q*, iPr–CH_3), 11.8 (*d*, iPr–CH).

^{29}Si{^{1}H} NMR (60 MHz, 45 mg in 0.6 mL C_6D_6): 3.7.

MS (EI): 385 (100, $[M - iPr]^+$), 343 (24), 327 (18).

3.8.3.3 [2,6-Bis(2,3,5,6-tetramethylphenyl)phenyl]diisopropylsilane

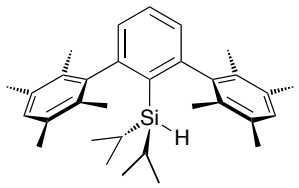

Chemical Formula: $C_{32}H_{44}Si$
Molecular Weight: 456.777

This compound was prepared according to the general procedure A for the synthesis of terphenylsilanes (Section 2.9.6, page 77).

The crude product was purified by recrystallization from isopropanol–ethyl acetate–toluene 10:5:1. The clear hot solution was slowly allowed to cool to 5 °C, which afforded the silane as colorless crystals (87 %).

Characterization

M.p.: 215–216 °C

IR (KBr): 3047*m*, 3003*m*, 2919*s*, 2860*s*, 2140*s*, 1553*m*, 1464*s*, 1439*s*, 1379*s*, 1237*w*, 1116*m*,1059*w*, 1045*m*, 1006*s*, 921*w*, 874*s*, 846*m*, 826*s*, 807*s*, 789*m*, 741*s*, 702*w*, 666*s*, 612*w*, 595*m*, 475*m*.

^{1}H NMR (300 MHz, 60 mg in 0.6 mL C_6D_6, C_6HD_5 = 7.16): 7.27 (*t*, $^{3}J = 7.5$, 1 H, H–C(4')), 7.0 (*d*, $^{3}J = 7.5$, 2 H, H–C(3', 5')), 6.94 (*s*, 2 H, H–C(4", 4"')), 3.29 (*t*, $^{3}J = 3.2$, 1 H, H–Si), 2.18 (*s*, 12 H, H_3C–C(3", 5", 3"', 5"')), 2.04 (*s*, 12 H, H_3C–C(2", 6", 2"', 6"')), 0.97–0.93 (*m*, 6 H, iPr-CH_3), 0.90–0.75 (*m*, 2 H, iPr-CH), 0.70–0.62 (*m*, 6 H, iPr-CH_3).

^{13}C{^{1}H} NMR (75 MHz, 60 mg in 0.6 mL C_6D_6): 150.8 (*s*, C(2', 6')), 144.3 (*s*, C(1", 1"'), 136.9 (*s*, C(1'), 133.6 (*s*, C(2", 6", 2"', 6"')), 132.3 (*s*, C(3", 5", 3"', 5"'), 130.8 (*d*, C(4", 4"'), 129.4 (*d*, C(4')), 128.6 (*d*, C(3', 5')), 22.7 (*q*, iPr–CH_3), 20.3 (*q*, *C*–C(3", 5",

3”’, 5”’)), 18.5 (*q*, iPr–CH_3), 18.4 (*q*, *C*–C(2”, 6”, 2”’, 6”’)), 11.6 (*d*, iPr–CH).

$^{29}Si\{^1H\}$ NMR (60 MHz, 60 mg in 0.6 mL C_6D_6): 4.1.

MS (EI): 413 ($[M - iPr]^+$), 385 (15), 339 (23), 309 (20), 207 (24).

3.8.3.4 [2,6-Bis(2,3,4,5,6-pentamethylphenyl)phenyl]diisopropylsilane

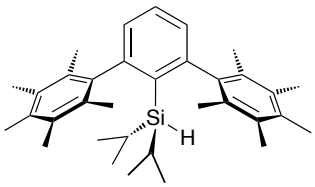

Chemical Formula: $C_{34}H_{48}Si$
Molecular Weight: 484.830

This compound was prepared according to the general procedure A for the synthesis of terphenylsilanes (Section 2.9.6, page 77).

The crude product was purified by recrystallization from isopropanol/toluene 5:2. The clear hot solution was slowly allowed to cool to 5 °C, which afforded the silane as colorless crystals (86%).

Characterization

M.p.: 223–224 °C

IR (KBr): 3054*m*, 2938*s*, 2861*s*, 2139*s*, 1556*s*, 1465*s*, 1443*s*, 1376*s*, 1226*w*, 1115*m*, 1065*m*, 1008*s*, 921*m*, 881*m*, 871*s*, 835*s*, 812*s*, 788*s*, 687*m*, 670*s*, 635*w*, 596*s*, 507*m*, 480*m*, 454*w*.

^1H NMR (500 MHz, 11 mg in 0.6 mL C_6D_6, C_6HD_5 = 7.16): 7.29 (*t*, $^3J = 7.5$, 1 H, H–C(4’)), 7.06 (*t*, $^3J = 7.5$, 2 H, H–C(3’, 5’), 3.38 (*t*, $^3J = 3.4$, 1 H, H–Si), 2.17 (*s*, 12 H, C–C(3”, 5”, 3”’, 5”’)), 2.14 (*s*, 18 H, overlapping H_3C–C(2”, 6”, 2”’, 6”’) and C–C(4”, 4”’)), 0.99 (*d*, $^3J = 7.4$ 6 H, iPr-CH_3), 0.93 (*m*, 2 H, iPr-CH), 0.64 (*d*, $^3J = 7.2$ 6 H, iPr-CH_3).

$^{13}C\{^1H\}$ NMR (125 MHz, 11 mg in 0.6 mL C_6D_6, C_6D_6 = 128.0 ppm): 151.6 (*s*, C(2’,

6')), 142.1 (*s*, C(1", 1"'), 137.2 (*s*, C(1')), 133.7 (*s*, C(4", 4"')), 132.2 (*s*, C(3", 5", 3"', 5"')), 131.8 (*s*, C(2", 6", 2"', 6"'), 129.3 (*d*, C(4'), 128.8 (*d*, C(3', 5')), 22.8 (*q*, iPr–CH_3), 19.6 (*q*, *C*–C(2", 6", 2"', 6"')), 18.5 (*q*, iPr–CH_3), 16.7 (*q*, *C*–C(4", 4"')), 16.6 (*q*, *C*–C(3", 5", 3"', 5"')), 11.6 (*d*, iPr–CH).

$^{29}Si\{^1H\}$ NMR (60 MHz, 11 mg in 0.6 mL C_6D_6): 4.0.

MS (EI): 441 (100, $[M - iPr]^+$), 353 (29), 324 (16), 265 (14), 207 (20).

3.8.4 Terphenyldiisopropylsilylium Ions

General procedure for the preparation of the silylium ions:

In a glovebox, a suspension of $[Ph_3C][B(C_6F_5)_4]$ (0.24 mmol) and the silane (0.24 mmol) in dry C_6D_6 (1 mL) was prepared. The oily brown mixture was stirred for 14 days at RT. Two layers formed, a dark brown oil at the bottom and a clear yellow upper layer. The brown oil, containing mainly the ionic product, was examined by NMR spectroscopy. The spectra indicated the presence of trityl salt even after 14 days of reaction time.

3.8.4.1 [2,6-Bis(2,6-tetramethyl)phenyl]diisopropylsilylium Tetrakis(pentafluorophenyl)borate

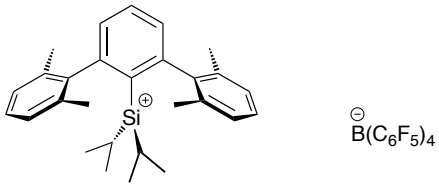

Chemical Formula: $C_{52}H_{35}BF_{20}Si$
Molecular Weight: 1078.699

Prepared according to the general procedure.

For this compound, the $^{29}Si\{^1H\}$ NMR spectrum with a resonance at 95.4 ppm vs external $SiMe_4$ was in agreement with the formation of the desired cation. The ^1H and $^{13}C\{^1H\}$ NMR spectra indicated the formation of at least one more species. Even on the basis of 2D experiments and predictions where resonances would appear based on the data of other cations, the signals could not be assigned unambiguously.

3.8.4.2 [2,6-Bis(2,4,6-tetramethyl)phenyl]diisopropylsilylium Tetrakis(pentafluorophenyl)borate

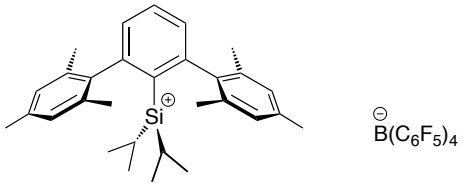

Chemical Formula: $C_{54}H_{39}BF_{20}Si$
Molecular Weight: 1106.752

Prepared according to the general procedure.

Characterization

^{1}H NMR (300 MHz, oily layer, *ca.* 240 mg in 0.6 mL of solution, C_6D_6, $\delta(C_6HD_5)$ = 7.16): 7.34 (*t*, $^{3}J = 7.7$, 1 H, H–C(4')), 7.06 (*d*, $^{3}J = 7.7$, 2 H, H–C(3', 5')), 6.99 (*s*, 4H, H–C(3", 5", 3"', 5"')), 2.09 (*s*, 6 H, H_3C–C(4", 4"')), 1.78 (*s*, 12 H, H_3C–C(2", 6", 2"', 6"')), 0.72 (*septuplet*, $^{3}J = 7.4$, 2 H, *i*Pr–CH), 0.27 (*d*, $^{3}J = 7.4$, 6 H, *i*Pr–CH_3).

^{13}C{^{1}H} NMR (75 MHz, oily layer, *ca.* 240 mg in 0.6 mL of solution, C_6D_6, $\delta(C_6D_6)$ = 128.0): 150.9 (*s*, C(1", 1"')), 150.3–147.9 (*m*, C–F), 146.8 (*s*, C(2', 6'), 144.3 (*s*, C(1')), 141.7 (*d*, C(4", 4"')), 140.1 (*d*, C(3", 5", 3"', 5"')), 140.0–137.7 (*m*, C–F), 138.2–135.8 (*m*, C–F), 132.9 (*d*, C(4')), 130.4 (*s*, C(2", 6", 2"', 6"')), 128.6 (*d*, C(3', 5')), 125 (*m* br., C–B), 20.8 (*q*, C–C(2", 6", 2"', 6"')), 20.4 (*q*, C–C(4", 4"')), 17.7 (*d*, *i*Pr–CH), 17.2 (*q*, *i*Pr–CH_3),.

^{29}Si{^{1}H} NMR (60 MHz, oily layer, *ca.* 240 mg in 0.6 mL of solution, C_6D_6): 93.4.

^{19}F NMR (282 MHz, oily layer, *ca.* 240 mg in 0.6 mL of solution, C_6D_6, $\delta(CCl_3F)$ = 0): -131.9 to -132.2 (*m*, 8 F, F–C(2', 6')), -162.8 (*t*, $^{3}J_{F,F} = 21$, 4 F, F–C(4')), -166.5 to -166.8 (*m*, 8 F, F–C(3', 5')).

3.8.4.3 [2,6-Bis(2,3,5,6-tetramethyl)phenyl]diisopropylsilylium Tetrakis(pentafluorophenyl)borate

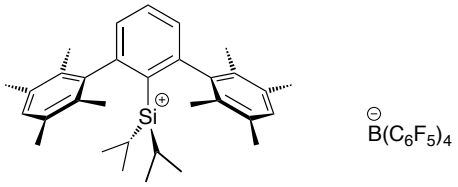

Chemical Formula: $C_{56}H_{43}BF_{20}Si$
Molecular Weight: 1134.805

Prepared according to the general procedure.

Characterization

^{1}H NMR (300 MHz, oily layer, *ca.* 240 mg in 0.6 mL of solution, C_6D_6, $\delta(C_6HD_5)$ = 7.16): 7.36 (*t*, $^{3}J = 7.7$, 1 H, H–C(4')), 7.11 (*d*, $^{3}J = 7.7$, 2 H, H–C(3', 5')), 6.86 (*s*, 2 H, H–C(4", 4"')), 2.06 (*s*, 12 H, H_3C–C(3", 5", 3"', 5"')), 1.69 (*s*, 12 H, H_3C–C(2", 6", 2"', 6"')), 0.74 (*septuplet*, $^{3}J = 7.4$, 2 H, *i*Pr–CH), 0.27 (*d*, $^{3}J = 7.4$, 6 H, *i*Pr–CH_3).

^{13}C{^{1}H} NMR (75 MHz, oily layer, *ca.* 240 mg in 0.6 mL of solution, C_6D_6, $\delta(C_6D_6)$ = 128.0): 156.7 (*s*, C(1", 1"')), 152.9 (*s*, C(3", 5", 3"', 5"')), 150.3–147.9 (*m*, C–F), 148.8 (*s*, C(2', 6')), 144.7 (*s*, C(1')), 140.0–137.7 (*m*, C–F), 138.2–135.8 (*m*, C–F), 134.3 (*d*, C(4", 4"')), 132.0 (*d*, C(4')), 129.2 (*d*, C(3', 5')), 125 (*m* br., C–B), 124.1 (*s*, C(2", 6", 2"', 6"')), 21.2 (*q*, C–C(3", 5", 3"', 5"')), 18.7 (*q*, C–C(2", 6", 2"', 6"')), 17.3 (*q*, *i*Pr–CH_3), 17.1 (*d*, *i*Pr–CH).

^{29}Si{^{1}H} NMR (60 MHz, oily layer, *ca.* 240 mg in 0.6 mL of solution, C_6D_6): 68.0.

^{19}F NMR (282 MHz, oily layer, *ca.* 240 mg in 0.6 mL of solution, C_6D_6, $\delta(CCl_3F)$ = 0): −131.9 to −132.2 (*m*, 8 F, F–C(2', 6')), −162.8 (*t*, $^{3}J_{F,F} = 21$, 4 F, F–C(4')), −166.5 to −166.8 (*m*, 8 F, F–C(3', 5')).

3.8.4.4 [2,6-Bis(2,3,4,5,6-pentamethyl)phenyl]diisopropylsilylium Tetrakis(pentafluorophenyl)borate

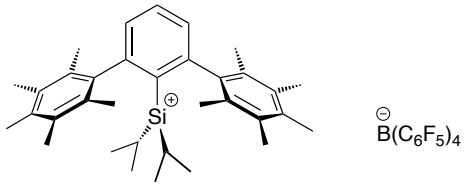

Chemical Formula: $C_{58}H_{47}BF_{20}Si$
Molecular Weight: 1162.858

Prepared according to the general procedure.

Characterization

^{1}H NMR (500 MHz, oily layer, *ca.* 240 mg in 0.6 mL of solution, C_6D_6, $\delta(C_6HD_5)$ = 7.16): 7.35 (*t*, $^{3}J = 7.6$, 1 H, H–C(4')), 7.15 (*d*, $^{3}J = 7.6$, 2 H, H–C(3', 5')), 2.01 (*s*, 12 H, H_3C–C(3", 5", 3"', 5"')), 1.96 (*s*, 6 H, H_3C–C(4", 4"')), 1.75 (*s*, 12 H, H_3C–C(2", 6", 2"', 6"')), 0.72 (*septuplet*, $^{3}J = 7.6$, 2 H, *i*Pr–CH), 0.22 (*d*, $^{3}J = 7.6$, 6 H, *i*Pr–CH_3).

^{13}C{^{1}H} NMR (125 MHz, oily layer, *ca.* 240 mg in 0.6 mL of solution, C_6D_6, $\delta(C_6D_6)$ = 128.0): 154.1 (*s*, C(1", 1"')), 151.3 (*s*, C(3", 5", 3"', 5"')), 151.0–147.3 (*m*, C–F), 148.9 (*s*, C(2', 6')), 145.1 (*s*, C(1')), 140.8–137.0 (*m*, C–F), 139.0 (*s*, C(4", 4"')), 139.0–135.0 (*m*, C–F), 131.9 (*d*, C(4')), 129.1 (*d*, C(3', 5')), 125 (*m* br., C–B), 123.6 (*s*, C(2", 6", 2"', 6"')), 19.7 (*q*, C–C(2", 6", 2"', 6"')), 18.3 (*q*, C–C(3", 5", 3"', 5"')), 17.2 (*q*, *i*Pr–CH_3), 16.8 (*d*, *i*Pr–CH), 16.1 (*q*, C–C(4", 4"')).

^{29}Si{^{1}H} NMR (60 MHz, oily layer, *ca.* 240 mg in 0.6 mL of solution, C_6D_6): 67.6.

^{19}F NMR (282 MHz, oily layer, *ca.* 240 mg in 0.6 mL of solution, C_6D_6, $\delta(CCl_3F)$ = 0): −131.9 to −132.2 (*m*, 8 F, F–C(2', 6')), −162.8 (*t*, $^{3}J_{F,F} = 21$, 4 F, F–C(4')), −166.5 to −166.8 (*m*, 8 F, F–C(3', 5')).

3.8.5 (2,6-Diphenylphenyl)dialkylsilanes

3.8.5.1 [2,6-Diphenylphenyl]dimethylsilane

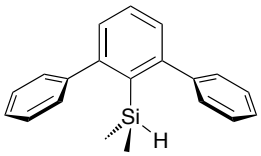

Chemical Formula: $C_{20}H_{20}Si$
Molecular Weight: 288.458

This compound was prepared according to the general procedure A for the synthesis of terphenylsilanes (Section 2.9.6, page 77).

The crude product was purified by filtration through a plug of alumina (deactivated with 5% H_2O) with dichloromethane/hexanes 1:1. After removal of the solvents, a colorless oil was obtained that solidified over one week upon standing at RT (98%).

Characterization

M.p.: 63–64.5 °C

IR (KBr): 3080*w*, 3046*m*, 3029*m*, 2962*m*, 2135*s*, 1598*w*, 1573*w*, 1557*m*, 1492*m*, 1446*m*, 1436*s*, 1248*s*, 1173*m*, 1115*m*, 1074*m*, 1048*m*, 1024*m*, 900*s*, 883*s*, 837*m*, 815*s*, 755*s*, 732*s*, 701*s*, 667*m*, 617*m*, 609*w*, 560*w*, 532*m*.

^{1}H NMR (300 MHz, 44 mg in 0.6 mL C_6D_6): 7.40–7.34 and 7.28–7.10 (overlapping multiplets, 13 H, C_{aryl}–H), 4.09 (*septuplet*, $^3J = 4.0$, 1 H, H–Si), −0.09 (*d*, $^3J = 4.0$, 6 H, Si–CH_3).

^{13}C{^{1}H} NMR (75 MHz, 44 mg in 0.6 mL C_6D_6): 151.4 (*s*), 145.2 (*s*), 135.2 (*s*), 129.8 (*d*), 128.9 (*d*), 128.8 (*d*), 128.2 (*d*), 127.4 (*d*), −0.7 (*q*).

^{29}Si{^{1}H} NMR (80 MHz, 44 mg in 0.6 mL C_6D_6): −20.4.

MS (EI): 288 (76, $M^{\cdot+}$), 271 (100), 255 (31), 195 (55), 136 (31), 77 (24).

3.8.5.2 [2,6-Diphenylphenyl]diisopropylsilane

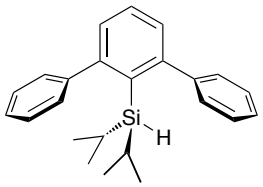

Chemical Formula: $C_{24}H_{28}Si$
Molecular Weight: 344.565

This compound was prepared according to the general procedure A for the synthesis of terphenylsilanes (Section 2.9.6, page 77).

The crude product was purified by filtration through a plug of alumina (deactivated with 5% H_2O) with dichloromethane/hexanes 1:1. After removal of the solvents, the product was obtained as colorless crystals (99%).

Characterization

M.p.: 83–84 °C

IR (KBr): 3053*m*, 2956*s*, 2933*s*, 2884*m*, 2858*s*, 2122*s*, 1598*w*, 1575*m*, 1560*m*, 1494*m*, 1465*m*, 1439*s*, 1383*m*, 1360*w*, 1124*m*, 1071*m*, 1050*m*, 1020*m*, 1015*m*, 1000*s*, 917*w*, 876*s*, 831*s*, 809*s*, 786*s*, 765*s*, 741*s*, 702*s*, 660*s*, 631*s*, 615*m*, 566*w*, 540*m*, 498*w*, 465*m*.

^{1}H NMR (400 MHz, 32 mg in 0.6 mL C_6D_6): 7.40–7.34 and 7.24–7.12 (overlapping multiplets, 13 H, C_{aryl}–H), 3.53 (*t*, $^3J = 5.1$, 1 H, H–Si), 0.96 (*d*, $^3J = 7.4$, 6 H, *i*Pr–CH_3), 0.85 (*d*, $^3J = 7.2$, 6 H, *i*Pr–CH_3), 0.71–0.59 (*m*, 2 H, *i*Pr–CH).

^{13}C{^{1}H} NMR (100 MHz, 32 mg in 0.6 mL C_6D_6): 151.0 (*s*), 145.4 (*s*), 133.9 (*s*), 129.9 (*d*), 129.2 (*d*), 128.5 (*d*), 127.9 (*d*), 127.3 (*d*), 20.9 (*q*), 20.1 (*q*), 13.2 (*d*).

^{29}Si{^{1}H} NMR (80 MHz, 32 mg in 0.6 mL C_6D_6): 6.3.

MS (EI): 301 (100, $[M - i\text{Pr}]^+$), 283 (26), 271 (42), 257 (69), 255 (68).

3.8.6 Silafluorenes

The dimethylsilafluorene was prepared by stirring a mixture of silane (13.2 mg, 45.8 μmol), $[Ph_3C][B(C_6F_5)_4]$ (46.6 mg, 50.5 μmol) and P(*o*-tol)$_3$ (19.8 mg, 65.1 μmol) in a mixture of 1,2-dichlorobenzene and C_6D_6 (0.4 mL of each) at RT for 1 d. ^{1}H, ^{13}C, ^{29}Si and ^{31}P NMR spectroscopy indicated the presence of one new silicon-containing product, Ph_3CH and $[HP(o\text{-tol})_3][B(C_6F_5)_4]$. GC–MS showed peaks and m/z of the silafluorene and Ph_3CH.

The diisopropylsilafluorene was prepared by stirring a mixture of silane (19.9 mg, 57.8 μmol), $[Ph_3C][B(C_6F_5)_4]$ (26.9 mg, 88.4 μmol) and P(*o*-tol)$_3$ (56.6 mg, 61.4 μmol) in 1,2-dichlorobenzene-d_4 (0.8 mL) at RT for 5 d. ^{1}H, ^{13}C, ^{29}Si and ^{31}P NMR spectroscopy indicated the presence of one new silicon-containing product, Ph_3CH and $[HP(o\text{-tol})_3][B(C_6F_5)_4]$. GC–MS showed peaks and m/z of the silafluorene and Ph_3CH.

Chapter 4

Hydride Transfer Reactions

4.1 Summary

The mechanism of hydride tranfer from silanes to the trityl cation (Ph_3C^+) was investigated using Si-deuterated substrates of different steric enshrouding. Deuteride transfer from the silanes to the central carbon atom of the trityl cation was observed exclusively. There was no evidence for a mechanism involving initial reaction with a phenyl ring and subsequent rearrangement to give triphenylmethane. Several cations were tested as potential alternative hydride abstraction reagents. Diarylmethylium ions **50**$^+$ and **51**$^+$ turned out to be promising candidates. Both cations were prepared under weakly nucleophilic conditions. Cation **51**$^+$ converts terphenylsilanes cleanly into the respective silylium ions. Its reactivity is higher than that of the trityl cation by $k_{rel} > 100$.

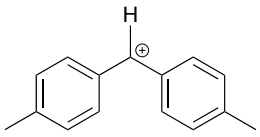

50$^+$

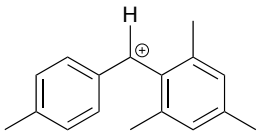

51$^+$

4.2 Introduction

Hydride transfer reactions play a crucial role in the studies presented in the preceding chapters. Hydride abstraction from terphenylsilanes **29** and **39** by the trityl cation was the key step in the preparation of the corresponding silyl cations. It is quite surprising that this reaction takes place at a reasonable rate at room temperature in view of the steric shielding of both the hydrogen atom at silicon and the carbocationic center in Ph_3C^+ (Figure 4.1). A clearer understanding of this step was desirable, on the one hand simply because it was pivotal to the project, but also in the context of the design of alternative hydride abstraction reagents.

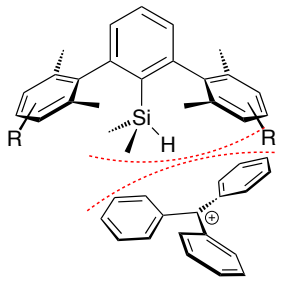

Figure 4.1. Steric crowding in the hydride abstraction from terphenylsilanes by the trityl cation..

4.3 Hydride Transfer from Silanes to the Trityl Cation

The trityl cation owes its stability to the effective delocalization of positive charge. In the principal resonance structures, the formal charge resides on the central carbon atom, C_{ortho}, and C_{para} (Figure 4.2). In principle one can imagine that hydride transfer reactions initially take place at one of the ring carbon atoms and are followed by rearrangement of the cyclo-

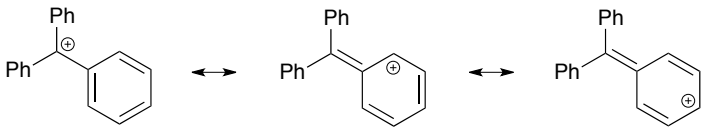

Figure 4.2. Resonance structures of the trityl cation.

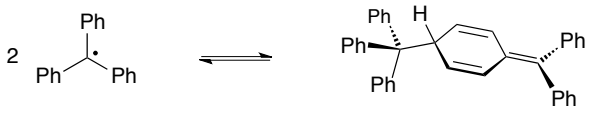

44

Scheme 4.1. Formation of the Gomberg dimer **44** from the trityl radical.

hexadiene to give triphenylmethane. This kind of reactivity would resemble that of the trityl radical, whose dimer is not hexaphenylethane but triene **44**, the Gomberg dimer (Scheme 4.1).[119]

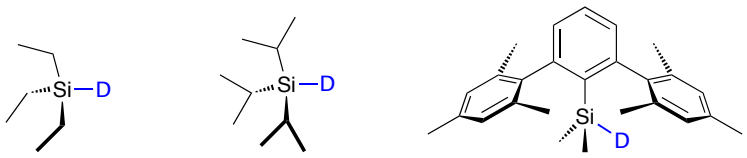

45 **46** **29b**-*d*

The deuterated substrates triethylsilane-*d* (**45**), triisopropylsilane-*d* (**46**), and terphenylsilane **29b**-*d* were expected to shed light on the mechanism of the Si→C hydride transfer. Direct reaction with the central carbon atom would lead to the exclusive formation of Ph_3CD, while any other process would afford one or several isomeric products. At the same time, increasing steric bulk about silicon would reveal a potential change in mechanism.

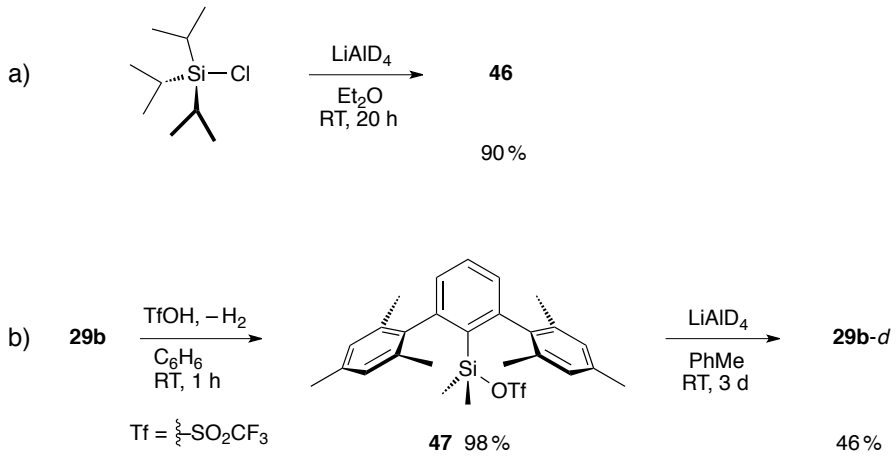

Scheme 4.2. Synthesis of the deuterosilanes **46** and **29b**-*d*.

Compound **45** was commercially available, while the other two substrates were prepared by reduction of chlorotriisopropylsilane and the silyl triflate **47** by $LiAlD_4$ (Scheme 4.2).

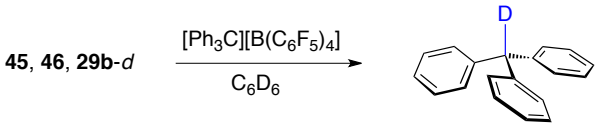

Scheme 4.3. Deuteride transfer to the trityl cation.

Hydride abstraction was carried out by treatment of the deuterated substrate with $[Ph_3C][B(C_6F_5)_4]$ in C_6D_6. The product solutions were directly examined by ^1H, ^2H, and ^{13}C NMR spectroscopy. In all reaction mixtures, Ph_3CD was the exclusive reduced product based on the lack of the central C–H resonance (>99 % formation of Ph_3CD by the integration of other signals). This finding demonstrated that the central carbon atom in Ph_3C^+ marks the hot spot of this cation and acts as the electrophilic center even in reactions with enshrouded substrates. A likely rationale for this behavior is the small amount of positive charge per phenyl group due to the propeller-like arrangement of the rings, which causes reduced π delocalization. This interpretation is in line with an analysis of the observed ^{13}C NMR shifts (Section 4.4).

4.4 Alternative Hydride Abstraction Reagents

Generation of the isopropyl-substituted cations **40** by the trityl cation was slow and did not afford a clean product in the case of **40a**$^+$. Therefore, sterically less hindered reagents that would effect hydride abstraction represented attractive targets.

First experiments were carried out with triethylsilyl carboranes. In view of the internal π stabilization of the terphenylsilyl cations, hydride transfer to Et_3Si^+ was anticipated. Silane **29a** served as the model substrate; reagents that would abstract hydride from it would probably also do so with the other silanes. Moreover, it was synthetically easily accessible.

Treatment of **29a** with $Et_3Si–CHB_{11}H_5Cl_6$ afforded neither **27a**$^+$ nor Et_3SiH (Scheme 4.4 a). Besides unchanged starting materials, small amounts of unidentified compounds were formed according to ^1H NMR spectroscopy. They probably stemmed from reactions involving highly acidic Wheland intermediates (Chapter 5). The reverse reaction, however, took place cleanly. Cation **27a**$^+$ abstracted hydride or deuteride from Et_3SiH or Et_3SiD to give **29a** (Scheme 4.4 b). In this experiment, P(*o*-tol)$_3$ was also added to trap Et_3Si^+ and suppress Brønsted acid chemistry. This result was surprising and indicated that the pacification of C_1-symmetrical **27a**$^+$ by π coordination could only be equated with thermodynamic stabilization *relative to conformations of higher symmetry*, but not necessarily with a stability higher than that of Et_3Si^+.

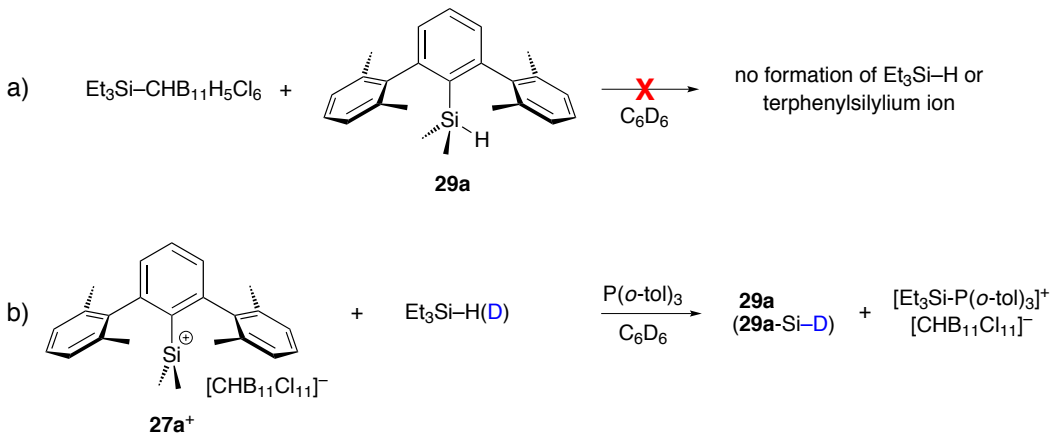

Scheme 4.4. a) Attempted hydride abstraction from **29a** by $Et_3Si–CHB_{11}H_5Cl_6$ and b) observed reverse transfer.

The tropylium ion (**48**$^+$) was the next cation that was tested as a hydride abstraction reagent. [**48**][$B(C_6F_5)_4$] was prepared by treatment of cycloheptatriene with the trityl cation

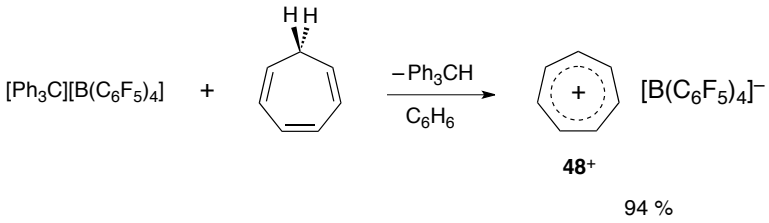

Scheme 4.5. Synthesis of the tropylium salt [**48**][$B(C_6F_5)_4$] from cycloheptatriene.

(Scheme 4.5). Although highly stabilized and therefore potentially less reactive in terms of kinetics, **48**$^+$ was a promising candidate with regard to its sterics.

However, the thermodynamic stabilization turned out to be too big. Mixtures of **48**$^+$ and different silanes remained unchanged over days (Scheme 4.6 a). Conversely, trialkylsilyl carboranes and **27a**$^+$ converted cycloheptatriene to **48**$^+$ by an unprecedented C→Si hydride transfer (4.6 b).

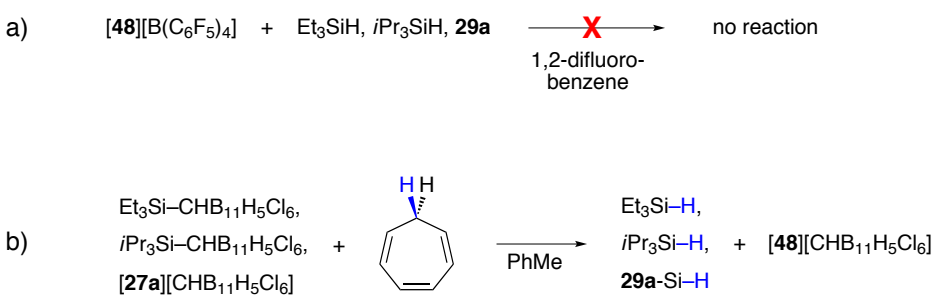

Scheme 4.6. a) Attempted hydride abstraction from silanes by **48**$^+$ and b) C→Si hydride transfer reactions between silylium ions and cycloheptatriene.

Diarylcarbenium ions are sterically less hindered at their central carbon atom than the trityl cation and should therefore be faster hydride abstraction reagents. However, their decreased stability and enhanced reactivity also made their preparation more difficult.

Diphenylethylium ion **49**$^+$ was generated by the protonation of 1,1-diphenylethene by [mesitylene–H][$CHB_{11}H_5Cl_6$] in dichloromethane at −78 °C, as inferred from NMR spectra. However, it was not inert upon warming of the solution to room temperature, possibly because of its high C–H acidity.

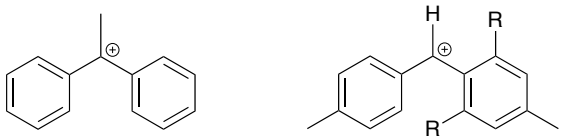

49$^+$ **50**$^+$ R = H
51$^+$ R = CH_3

Diarylmethylium ions **50**$^+$ and **51**$^+$ lack the stabilization by a third substituent at the central carbon atom but are stabilized relative to the parent diphenylmethylium ion by ad-

ditional CH_3 groups on the rings. Moreover, they are much less prone to loss of a proton than cations like **49**$^+$.

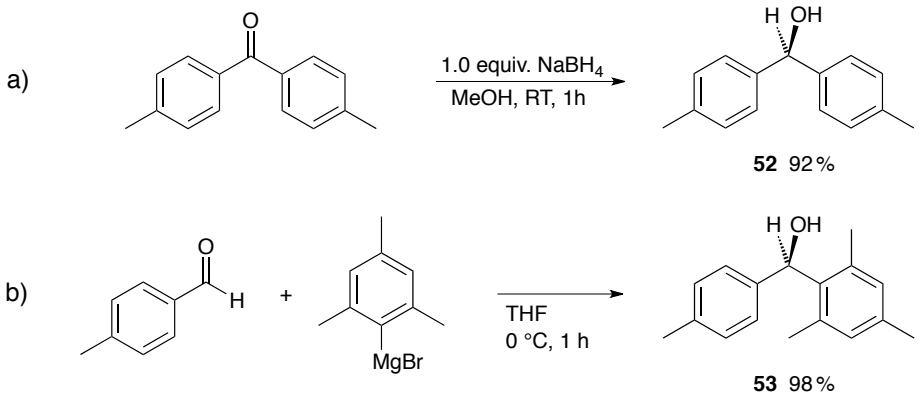

Scheme 4.7. Synthesis of diarylmethyl alcohols **52** and **53**.

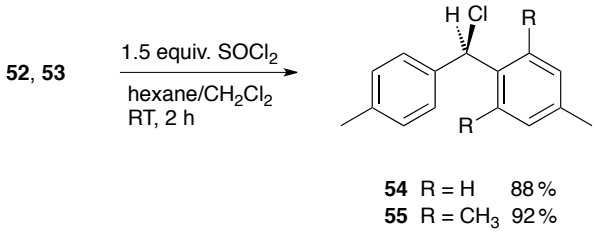

Scheme 4.8. Conversion of the diarylmethyl alcohols to the chloro compounds.

The preparation of **50**$^+$ and **51**$^+$ was accomplished by the synthesis of diarylmethyl alcohols **52** and **53**, which in turn were converted to the corresponding chloro compounds **54** and **55** (Schemes 4.7 and 4.8). Subsequent metathesis with potassium or silver salts of weakly coordinating anions in dichloromethane or chlorobenzene afforded the target cations (Scheme 4.9).

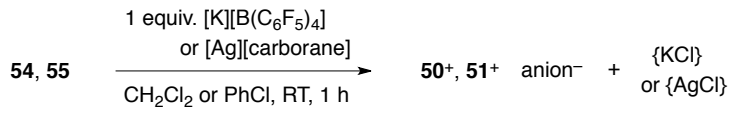

Scheme 4.9. Generation of the diarylmethylium ions by K^+ or Ag^+ salt metathesis.

^{1}H NMR spectroscopy indicated product solutions containing only small amounts of impurities (Figures 4.3 and 4.4). Isolation of the cations, however, was not successful. NMR spectra of precipitated and dried salts showed partial decomposition. Also, addition

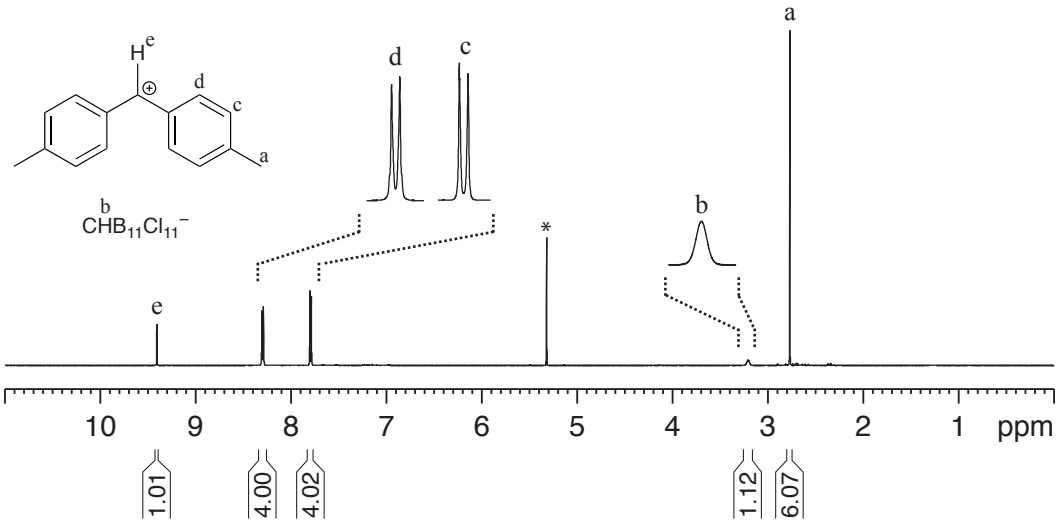

Figure 4.3. ^{1}H NMR spectrum of **50**$^+$. Conditions: 400 MHz, 300 K, 30 mg in 0.6 mL CD_2Cl_2; the signal marked with an asterisk stems from $CHDCl_2$ = 5.32 ppm.

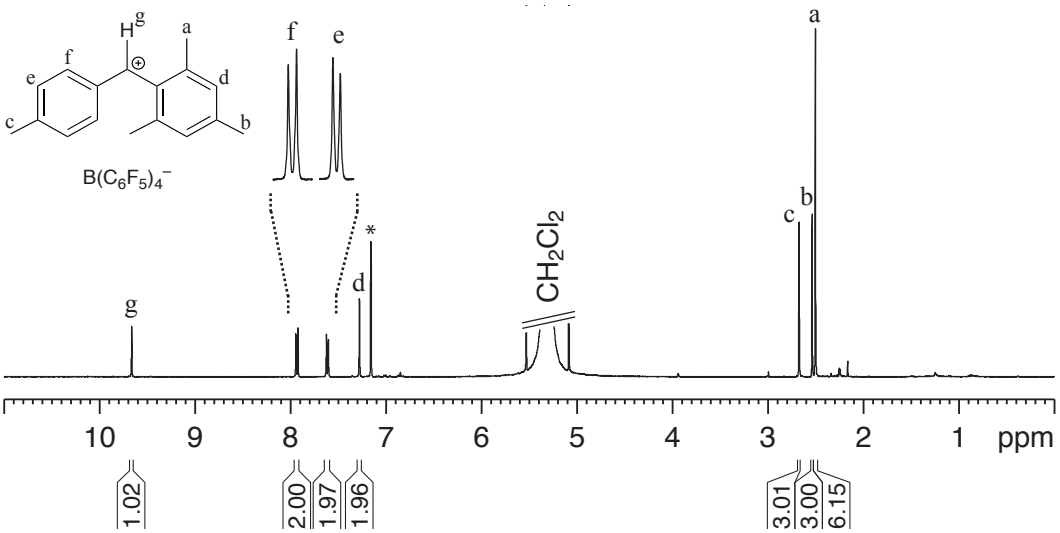

Figure 4.4. ^{1}H NMR spectrum of **51**$^+$. Conditions: 400 MHz, 300 K, 30 mg in 0.4 mL CH_2Cl_2; addition of a 3 mm capillary containing C_6D_6 for locking and shimming, the signal marked with an asterisk stems from C_6HD_5 = 7.16 ppm.

Table 4.1. ^{13}C and ^{1}H NMR shifts of Ph_3C^+, **50**$^+$ and **51**$^+$. CD_2Cl_2 solution, CD_2Cl_2 = 54.0 ppm, $CHDCl_2$ = 5.32 ppm.

	Ph_3C^+		**50**$^+$		**51**$^+$			
Position	^{13}C	^{1}H	^{13}C	^{1}H	$^{13}C^a$		$^{1}H^a$	
C^+	210.2	–	191.2	9.41	189.2		9.67	
C_{ipso}	139.5	–	135.0	–	135.6	136.5	–	–
C_{ortho}	142.4	7.62	144.1	8.30	143.0	153.2	–	–
C_{ortho}–CH_3	–	–	–	–	–	22.4	–	2.50
C_{meta}	130.6	7.84	134.4	7.80	133.2	134.1	7.62	7.28
C_{para}	143.6	8.23	165.9	–	164.4	163.1	–	–
C_{para}–CH_3	–	–	25.0	2.77	24.4	23.8	2.68	2.54

[a] First value corresponds to tolyl ring, second value mesityl ring.

of benzene to freshly prepared cation solutions caused decomposition within one day, probably via electrophilic aromatic substitution. These observations hinted at the high reactivity of **50**$^+$ and **51**$^+$, even though no investigation into the decomposition processes was carried out.

A comparison of the ^{13}C NMR shifts of Ph_3C^+, **50**$^+$, and **51**$^+$ revealed a higher degree of charge delocalization per ring in the diarylmethylium ions than in Ph_3C^+. The C_{para}

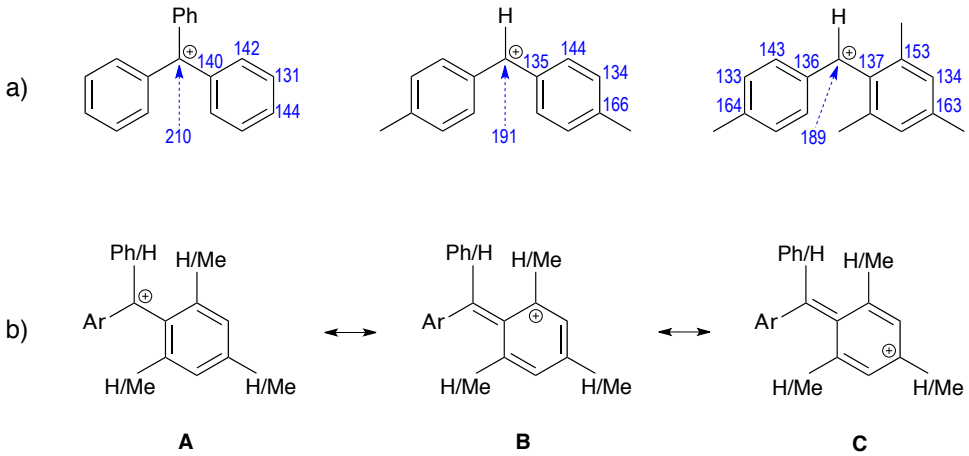

Figure 4.5. a) ^{13}C NMR shifts and b) resonance structures of Ph_3C^+, **50**$^+$ and **51**$^+$.

atoms in the three cations resonated at 144, 166, and 164/163 ppm, respectively (Table 4.1, Figure 4.5). The differences of *ca.* 20 ppm can not fully be explained by the fact that tertiary carbon atoms are compared with quaternary carbon atoms; substitution of hydrogen by a CH_3 group on a benzene ring is usually associated with a deshielding by 5–10 ppm. The observed shifts therefore indicated a higher contribution of resonance structure **C** for $\mathbf{50}^+$ and $\mathbf{51}^+$ than for Ph_3C^+. Diminished charge delocalization in the trityl cation is probably caused by bigger twist angles of the phenyl rings.

Preliminary studies showed that cation $\mathbf{51}^+$ acts as an effective hydride abstraction reagent. Experiments were carried out with silanes **29a**, **29d**, and **39d** in chlorobenzene and monitored by ^{1}H and ^{29}Si NMR spectroscopy. Quantitative conversion of the dimethylsilanes **29a** and **29d** to the silyl cations took place in less than 5 minutes, basically the time it took to prepare the sample and start the NMR measurement on the preshimmed instrument. With the more hindered diisopropylsilane **39d**, complete disappearance of starting material was observed within one hour; using the trityl cation, 50 % conversion had been achieved in 2 weeks. Based on the drastically reduced reaction times, diarylmethylium ion $\mathbf{51}^+$, and presumably also $\mathbf{50}^+$, seems to be of high utility when sterically enshrouded substrates must be activated.

4.5 Experimental Part

4.5.1 General

For general reaction conditions and analytical instruments, see Sections 2.9.3 and 2.9.4.

Triethylsilane-*d* was purchased from Aldrich and used as received.

4.5.2 Deuterated Silanes

4.5.2.1 Triisopropylsilane-*d*

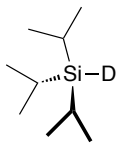

Chemical Formula: $C_9H_{21}DSi$
Molecular Weight: 159.363

In a glovebox, *i*Pr_3SiCl (1.219 g, 6.323 mmol) was dissolved in Et_2O (6 mL) in a 10 mL glass vial. $LiAlD_4$ (302 mg, 7.19 mmol) was added in small portions. The reaction was exothermic. The mixture was stirred at RT for 20 h. The vial was taken to a fume hood, and 1 M HCl was added carefully until the HD evolution ceased. The mixture was extracted with pentane, and the combined organic layers were concentrated using a rotavap (50 mbar, 40 °C). A colorless liquid was obtained which contained only product and traces of pentane according to NMR and GC–MS analysis. The yield was 909 mg (90 %).

^{1}H NMR (500 MHz, 25 mg in 0.6 mL C_6D_6, C_6HD_5 = 7.16): 1.10–1.05 (*m*, 18 H, *i*Pr-CH_3), 1.05–0.97 (*m*, 3 H, *i*Pr-CH).

^{13}C{^{1}H} NMR (75 MHz, 25 mg in 0.6 mL C_6D_6, C_6D_6 = 128.0): 19.5 (*q*), 10.5 (*d*).

^{29}Si{^{1}H} NMR (60 MHz, 25 mg in 0.6 mL C_6D_6, external $SiMe_4$ in C_6D_6 = 0 ppm): 11.8 (*t*, $^1J_{Si,D}$ = 27).

MS (EI): 160 (18, $M^{\cdot+}$), 116 (86, $[M - i\mathrm{Pr}]^+$), 88 (56), 74 (56), 59 (100).

4.5.3 2,6-Bis(2,4,6-trimethylphenyl)phenyldimethylsilyl Triflate

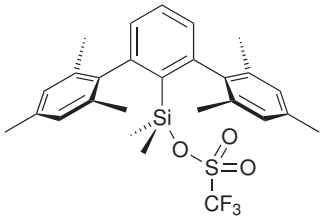

Chemical Formula: $C_{27}H_{31}F_3O_3SSi$
Molecular Weight: 520.679 u

General: The reaction was carried out in the hood under argon. All glassware was dried at 150 °C overnight. Since triflic acid corrodes metal needles, only Pasteur pipets were used for the transfer of liquids.

A solution of triflic acid (91.2 mg, 0.608 mmol) in dry benzene (1 mL) was added to a solution of 2,6-Bis(2,4,6-trimethylphenyl)phenyldimethylsilane (215 mg, 0.577 mmol) in dry benzene (3 mL). The mixture turned orange immediately, and hydrogend gas evolved. The mixture was stirred for 3 hrs at room temperature. Benzene and excess triflic acid were removed under reduced pressure. The remaining solid was dried in a vacuum overnight. The silyl triflate was obtained as a moisture-sensitive off-white powder (293 mg, 0.563 mmol, 98 %). For further reactions and the preparation of IR and NMR samples, the compound was tranferred into a glovebox.

Characterization

M.p.: (sealed capillary) 126.5–128 °C

IR (solution of 6 mg in 0.1 mL benzene, NaCl cell): 2965*w*, 2918*m*, 2859*w*, 1611*w*, 1558*w*, 1446*m*, 1392*s*, 1261*m*, 1244*s*, 1209*s*, 1154*s*, 1125*w*, 1086*w*, 948*s*, 855*s*, 817*s*, 801*s*, 776*w*, 748*w*, 733*w*, 626*s*, 517*w*.

^{1}H NMR (500 MHz, 40 mg in 0.6 mL C_6D_6, C_6HD_5 = 7.15): 7.48 (*t*, $^3J = 7.6$, 1 H, H–C(4')), 7.48 (*s*, 4 H, H–C(3", 5", 3"', 5"')), 7.11 (*d*, $^3J = 7.6$, 2 H, H–C(3', 5')), 2.48 (*s*, 6 H, H_3C–C(4", 4"')), 2.32 (*s*, 12 H, H_3C–C(2", 6", 2"', 6"')), 0.28 (*s*, 6 H, H_3C–Si).

^{13}C{^{1}H} NMR (126 MHz, 40 mg in 0.6 mL C_6D_6, C_6D_6 = 128.0): 150.2 (quat. C), 139.7

(quat. C), 137.7 (quat. C), 136.2 (quat. C), 132.3 (CH), 129.5 (CH), 129.0 (CH), 128.7 (quat. C), 119.0 (q, $^1J_{C,F} = 317$, CF_3), 21.1 (CH_3, CH_3–C(4", 4"'), 20.9 (CH_3, CH_3–C(2", 6", 2"', 6"'), 2.0 (CH_3, Si–C).

$^{19}F\{^1H\}$ NMR (282.4 MHz, 40 mg in 0.6 mL C_6D_6, external CCl_3F in C_6D_6 = 0 ppm): −76.98.

$^{29}Si\{^1H\}$ NMR (59.9 MHz, 40 mg in 0.6 mL C_6D_6, external $SiMe_4$ in C_6D_6 = 0 ppm): 28.3.

4.5.4 2,6-Bis(2,4,6-trimethylphenyl)phenyldeuterodimethylsilane

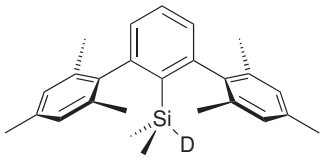

Chemical Formula: $C_{26}H_{31}DSi$
Molecular Weight: 373.624 u

Silyl triflate (161 mg, 0.309 mmol) was dissolved in dry toluene (3 mL). $LiAlD_4$ (18.5 mg, 0.441 mmol) was added, and the mixture was stirred for three days at room temperature. Toluene was removed under reduced pressure. The residue was extracted with hexane (3 × *ca.* 3 mL). The combined hexane layers were washed with water, then brine, and water again. The organic phase was dried with $MgSO_4$, filtered, and evaporated to dryness. Preparative thin-layer chromatography of the crude product (20 × 20 cm, 1 mm SiO_2, eluent cyclohexane–toluene 10:1, band at R_f 0.65) afforded the deuterated silane as a white powder (53 mg, 0.142 mmol, 46 %).

Characterization

M.p.: 117.5–119 °C

IR (KBr): 2975*s*, 2952*s*, 2916*s*, 2855*m*, 2732*w*, 1944*w*, 1877*w*, 1811*w*, 1735*w*, 1611*m*, 1550*s*, 1483*m*, 1444*s*, 1377*m*, 1244*s*, 1174*m*, 1119*s*, 1085*m*, 1049*m*1032*m*, 855*s*, 838*s*, 828*s*, 808*s*, 791*s*, 739*s*, 693*w*, 664*s*, 602*w*, 577*s*, 525*m*, 502*w*.

^{1}H NMR (500 MHz, 22 mg in 0.6 mL C_6D_6, C_6HD_5 = 7.15): 7.24 (*t*, $^{3}J = 7.6$, 1 H, H–C(4')), 6.91 (*d*, $^{3}J = 7.6$, 2 H, H–C(3', 5')), 6.85 (*s*, 4 H, H–C(3", 5", 3"', 5"')), 2.19 (*s*, 6 H, H_3C–C(4", 4"')), 2.08 (*s*, 12 H, H_3C–C(2", 6", 2"', 6"')), −0.16 (*s*, 6 H, H_3C–Si).

^{13}C{^{1}H} NMR (126 MHz, 22 mg in 0.6 mL C_6D_6, C_6D_6 = 128.0)): 149.5 (quat. C), 140.7 (quat. C), 136.7 (quat. C), 136.1 (quat. C), 134.5 (quat. C), 130.3 (CH), 128.4 (CH), 128.4 (CH), 21.2 (CH_3, CH_3–C(2", 6", 2"', 6"')), 21.1 (CH_3, CH_3–C(4", 4"')), −2.5 (CH_3, Si–C).

^{29}Si{^{1}H} NMR (22 mg in 0.6 mL 99.4 MHz, C_6D_6, external $SiMe_4$ in $C_6D_6\bar{0}$ ppm): −23.4 (*t*, $^{1}J_{Si,D}$ = 29.5).

MS (EI): 373 (10, $M^{\cdot+}$), 358 (100, $[M - CH_3]^{+}$), 179 (14), 59 (60).

4.5.5 Carbocations

4.5.5.1 Tropylium Tetrakis(pentafluorophenyl)borate

$[B(C_6F_5)_4]^{-}$

Chemical Formula: $C_{31}H_7BF_{20}$
Molecular Weight: 770.167

Cycloheptatriene (35.9 mg, 390 µmol) was weighed into a small glass vial. Benzene (1 mL) was added quickly to prevent evaporation of the starting material. $[Ph_3C][B(C_6F_5)_4]$ (340 mg, 369 µmol) was added, and the mixture was stirred at RT. After 10 min, a grayish precipitate started forming. The mixture was stirred for another 30 min, then hexane (2 mL) was added, and the vial was put into the glovebox freezer overnight (−20 °C). The supernatant was removed with a Pasteur pipet, and the residue was washed with hexane (3 × 2 mL) and dried in a vacuum overnight at RT. The product was obtained as a slightly grayish powder (268 mg, 348 µmol, 94 %).

^{1}H NMR (300 MHz, non-deuterated 1,2-difluorobenzene, spectrum referenced against external $SiMe_4$ in C_6D_6): 9.1 (*s*).

^{13}C{^{1}H} NMR (75 MHz, non-deuterated 1,2-difluorobenzene, spectrum referenced against external $SiMe_4$ in C_6D_6): 155.4 (*d*).

4.5.5.2 Di(*p*-tolyl)methanol

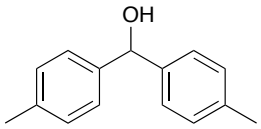

Chemical Formula: $C_{15}H_{16}O$
Molecular Weight: 212.287

4,4'-Dimethylbenzophenone (998 mg, 4.75 mmol) was dissolved in MeOH (30 mL) in a 50 mL round-bottom flask. $NaBH_4$ (178 mg, 4.71 mmol) was added in one portion, and the mixture was stirred at RT. H_2 gas evolved. After 1 h of stirring, the solvent was removed at 280 mbar/40 °C, and H_2O (10 mL) and 1 M HCl (2 mL) were added. The reaction mixture was extracted with CH_2Cl_2, and the organic layers were dried over $MgSO_4$, filtered, and evaporated to dryness. A white solid was obtained, which was clean according to ^{1}H and ^{13}C{^{1}H} NMR spectroscopy and GC–MS. The yield was 985 mg (98 %).

Characterization

^{1}H NMR (300 MHz, $CDCl_3$, $CHCl_3$ = 7.25): 7.27 (*d*, ^3J = 8.0, 4 H, Ar–H), 7.16 (*d*, ^3J = 8.0, 4 H, Ar–H), 5.77 (*s*, 1H, central C–H), 2.35 (*s*, 6 H, CH_3), 2.28 (*s*, 1 H, OH).

^{13}C{^{1}H} NMR (75 MHz, $CDCl_3$, $CDCl_3$ = 77.0): 141.1 (*s*), 137.0 (*s*), 129.1 (*d*), 126.4 (*d*), 75.8 (*d*), 21.0 (*q*).

MS (EI): 212 (39, $M^{\cdot+}$), 197 (35, $[M - CH_3]^+$), 119 (100), 91 (42).

4.5.5.3 Di(*p*-tolyl)chloromethane

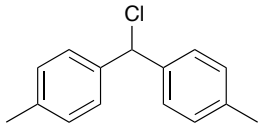

Chemical Formula: $C_{15}H_{15}Cl$
Molecular Weight: 230.733

Di(*p*-tolyl)methanol (322 mg, 1.52 mmol) was dissolved in a mixture of hexane (5 mL) and CH_2Cl_2 (2 mL) in a 2-necked 25 mL round-bottom flask. This solution was prepared

in a glovebox. The flask was transferred to a fumehood, and a condenser, connected to a bubbler (not the vacuum manifold), was attached. The reaction system was kept under N_2 by passing a slight stream of N_2 from the vacuum manifold to the bubbler using a Y splitter in front of the bubbler inlet. $SOCl_2$ (0.2 mL, 2.76 mmol) was added to the flask over 2 min with a plastic syringe. The mixture was stirred at RT. SO_2 started forming, but the mixture did not warm up significantly. Reaction control was done by taking a drop of the reaction mixture and solvolyzing it in MeOH. This mixture was worked up with hexane/H_2O (1 mL/0.5 mL) and checked by GC–MS. After 2 h of stirring, the mixture was concentrated under reduced pressure under N_2. A grayish solid was obtained, which was dried in a vacuum at RT overnight. A colorless solid was obtained. The ^{1}H NMR spectrum and GC–MS analysis after treatment of an aliquot with MeOH contained only product peaks. The yield was 307 mg (88 %). The product was stored in a glovebox.

Characterization

^{1}H NMR (300 MHz, $CDCl_3$, $CHCl_3$ = 7.25): 7.30–7.27 and 7.15–7.12 (two *d*-like signals, but of higher order, 2 × 4 H, Ar–H), 6.09 (*s*, 1 H, central C–H), 2.33 (*s*, 6 H, CH_3).

MS (EI): (GC–MS of the methyl ether: 1 mg of product was allowed to react with 0.2 mL of MeOH, then this solution was extracted with hexane/H_2O (1 mL/0.5 mL) 226 (54, $M^{\cdot+}$), 211 (35, $[M - CH_3]^+$), 195 (100), 165 (34), 135 (43), 119 (38).

4.5.5.4 Mesityl(*p*-tolyl)methanol

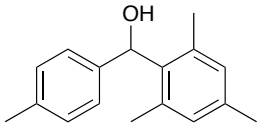

Chemical Formula: $C_{17}H_{20}O$
Molecular Weight: 240.340

A solution of mesitylmagnesium bromide (8.0 mL, 7.4 mmol; 0.92 M in THF, prepared from bromomesitylene and Mg turnings) was added to a 2-necked 50 mL round-bottom flask equipped with a N_2 inlet and a rubber septum. The solution was cooled in an ice/water bath. A solution of *p*-tolualdehyde (800 mg, 6.66 mmol) in dry THF (5 mL) was added over

5 min, and the mixture was stirred at *ca*. 0 °C. First a clear solution was obtained, then after 45 min a colorless precipitate started forming. After 100 min of stirring, H_2O (15 mL) was added to the reactio. The mixture was allowed to warm to RT, and most of the THF was removed under reduced pressure on a rotavap. The mixture was acidified with 1 M HCl (10 mL) and extracted with CH_2Cl_2. The combined organic layers were washed with 0.3 M NaOH in order to remove potential traces of *p*-tolyl-COOH (impurity in the starting material). The organic layers were dried over $MgSO_4$, filtered and evaporated to dryness. A viscous colorless oil was obtained. It was dried at 60 °C/5 mbar on a rotavap. A highly viscous colorless oil was obtained that solidified upon standing at RT after a few weeks. ^{1}H and ^{13}C{^{1}H} NMR spectra contained only product peaks. The yield was 1.561 g (98 %).

Characterization

^{1}H NMR (300 MHz, $CDCl_3$, $CHCl_3$ = 7.25): 7.18–7.15 and 7.13–7.10 (two *d*-like signals, but of higher order, 2 × 2 H, tolyl Ar–H), 6.87 (*s*, 2 H, mesityl Ar–H), 6.30 (broad *s*, 1H, central C–H), 2.34 (*s*, 3 H, CH_3), 2.29 (*s*, 3 H, CH_3), 2.24 (*s*, 6 H, mesityl *ortho*-CH_3), 2.14 (broad *s*, 1 H, OH).

^{13}C{^{1}H} NMR (75 MHz, $CDCl_3$, $CDCl_3$ = 77.0): 140.0 (*s*), 137.2 (*s*), 137.0 (*s*), 136.5 (*s*), 136.0 (*s*), 130.0 (*d*), 128.8 (*d*), 125.4 (*d*), 71.0 (*d*), 21.0 (*q*), 20.8 (*q*), 20.6 (*q*).

MS (EI): 240 (21, $M^{\cdot+}$), 225 (27, $[M - CH_3]^+$), 222 (40), 207 (100), 147 (49), 105 (53).

4.5.5.5 Mesityl(*p*-tolyl)chloromethane

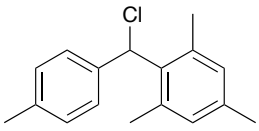

Chemical Formula: $C_{17}H_{19}Cl$
Molecular Weight: 258.786

In a glovebox, mesityl(*p*-tolyl)methanol (330 mg, 1.373 mmol) was dissolved in a mixture of hexane (4 mL) and CH_2Cl_2 (2 mL) in a 2-necked 25 mL round-bottom flask. The flask was sealed with rubber septa and taken to a fume hood. A slight constant stream of

N_2 was passed through the flask by introducing a syringe needle (attached to a tubing of the vacuum manifold) with a slight overpressure of N_2 into the septum of the lateral flask and a second needle leading from the flask to a bubbler. $SOCl_2$ (0.2 mL, 2.8 mmol) was added with a plastic syringe over 1 min. SO_2 started forming, and the reaction mixture was stirred at RT for 2 h. Reaction control was done by taking a drop of the reaction mixture and solvolyzing it in MeOH. This mixture was worked up with hexane/H_2O and checked by GC–MS (1 mL/0.5 mL). The solvent and excess $SOCl_2$were removed under reduced pressure under N_2. The oil that was obtained was dried in a vacuum at RT for 2 h, which afforded an almost colorless (slightly yellowish), viscous oil. ^{1}H NMR indicated clean conversion to the product. The yield was 327 mg (1.26 mmol, 92 %).

Characterization

^{1}H NMR (400 MHz, $CDCl_3$, $CHCl_3$ = 7.25): 7.37 (*d*, $^3J = 8.1$, 2 H, tolyl Ar–H), 6.94 (*d*, $^3J = 8.1$, 2 H, tolyl Ar–H), 6.68 (2 overlapping *s*, 3 H, mesityl Ar–H and central C–H), 2.13 (*s*, 6 H, mesityl *ortho*-CH_3), 2.07 (*s*, 3 H, CH_3), 2.07 (*s*, 3 H, CH_3).

MS (EI): (GC–MS of the methyl ether: 1 mg of product was allowed to react with 0.2 mL of MeOH, then this solution was extracted with hexane/H_2O (1 mL/0.5 mL) x (x, $M^{\cdot+}$), x (x, $[M - CH_3]^+$), xxx.

4.5.5.6 Formation of the Diarylmethylium Ions

The diarylmethylium ions were prepared by mixing equimolar amounts of the chloro compound (*ca.* 50 mg) with [K][$B(C_6F_5)_4$] or [Ag][carborane] in dichloromethane or chlorobenzene (1–2 mL). A deep red solution were obtained within seconds. The reaction was stirred for 1 h at RT, then the inorganic precipitate was allowed to deposit, and the clear supernatant was transferred to another vial. Characterization was done directly from such solutions. NMR data are given in Table 4.1.

Chapter 5

Isolation and Synthesis of a Silyl-Stabilized Allyl Cation

5.1 Summary

Reaction of the terphenylsilane **29b** with strong Brønsted acids afforded allyl cation $\mathbf{62}^{+}$. Single crystals of this cation were isolated in an attempt to prepare the corresponding silyl cation of **29b**. The postulated mechanism of formation involves initial *ipso* protonation of a mesityl ring of **29b**, followed by a Si→C_{ortho} hydride transfer and subsequent C_{meta}–Si bond formation. This hypothesis was tested by treatment of **29b** with the arenium acid [toluene-H]$^{+}$, which gave $\mathbf{62}^{+}$ as the single product. Isotope labeling studies were fully consistent with the proposed mechanism of formation. An analysis of X-ray, NMR and computational data indicated that $\mathbf{62}^{+}$ should be regarded as a silyl-substituted allyl cation rather than a diene-coordinated silyl cation.

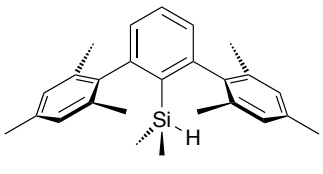

29b

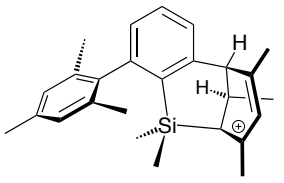

62^{+}

5.2 Introduction

Allyl cations are of fundamental interest to organic chemistry. They constitute an important class of reactive intermediates in organic synthesis, and the research on their structure and stability has challenged physical organic chemists for more than 50 years.[120–122] For the parent allyl cation $[H_2C{=}C{-}CH_2]^+$, gas-phase as well as computational studies suggest a stabilization of about 250 kJ mol^{-1} with respect to the methyl cation CH_3^+, a value between those of secondary and tertiary carbocations.[123, 124] Because of their relatively high stability, a large number of allyl cationic systems could be generated in solution and studied by NMR and UV-Vis spectroscopy as early as in the 1960s, primarily in media of high Brønsted acidity.[120, 125–131] In contrast, single crystals of allyl cations have remained elusive and have usually been obtained as unexpected products in attempts to prepare other reactive intermediates.[132]

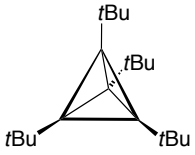

56

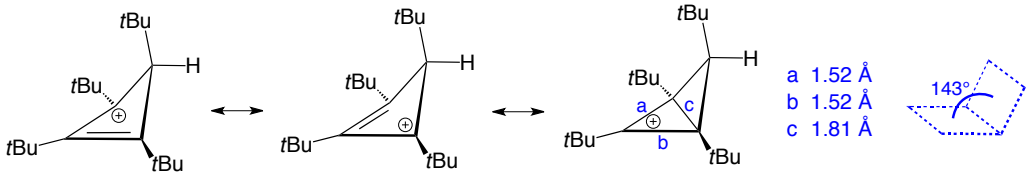

57a$^+$ **57b**$^+$ **57c**$^+$

An early report on the structural characterization of an allyl cationic species not stabilized by adjacent π systems or heteroatoms dates back 25 years. Studying the oxidative ring opening of tetra-*t*-butyltetrahedrane (**56**), Maier and Irngartinger isolated cyclobutenylium ion **57**$^+$ as [**57**][I_3].[133] X-ray diffraction revealed a puckered cation with a dihedral angle of 143° and C–C bond lenghts of 1.52/1.52 Å within the allylic fragment. Moreover, a relatively short distance of 1.81 Å across the formally charged carbon atoms was observed. These features were interpreted as a bonded interaction between C1 and C3 as depicted by

resonance structure **57c**$^+$. Also the ^{13}C NMR spectrum of **57**$^+$ could only be explained by a significant contribution of **57c**$^+$. While in classical allyl cations the terminal carbon atoms are more deshielded than the central position, **57**$^+$ exhibited shifts of 157 ppm for C1/C3 and 196 ppm for C2. This observation was in line with a study on cyclobutenylium ions by Olah and coworkers.[134] From variable-temperature NMR spectra they had concluded that some of the cations adopted a puckered conformation with pronounced C1–C3 interactions. The unsubstituted cyclobutenylium ion exhibited ^{13}C resonances at 142 (C1,3) and 179 ppm (C2) and a barrier to ring flipping of 35 kJ mol^{-1}.

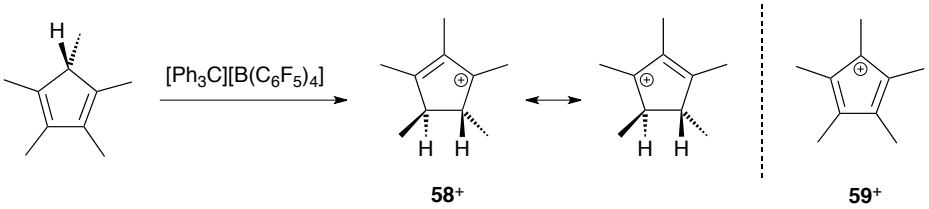

Scheme 5.1. Formation of the pentamethylcyclopentenyl cation **58**$^+$.

In 2002, Lambert prepared the pentamethylcyclopentenyl cation **58**$^+$ by treatment of pentamethylcyclopentadiene with $[Ph_3C][B(C_6F_5)_4]$ (Scheme 5.1).[135] The mechanism of formation of **58**$^+$ has remained unclear, and the original publication won notoriety because NMR and X-ray crystallographic data were first interpreted as those of the cyclopentadienyl cation **59**$^+$.[136–139] Nevertheless, the solid-state structure of **58**$^+$ was an valuable contribution to the field of carbocation chemistry. The essentially C_2-symmetrical cation possessed C1–C2 and C2–C3 bond lengths of 1.39 and 1.40 Å and exhibited trigonal-planar coordination around the three atoms (Figure 5.1). The observed geometry was consistent with equal charge delocalization over the allyl moiety, resulting in C–C distances between those of typical single and double bonds.

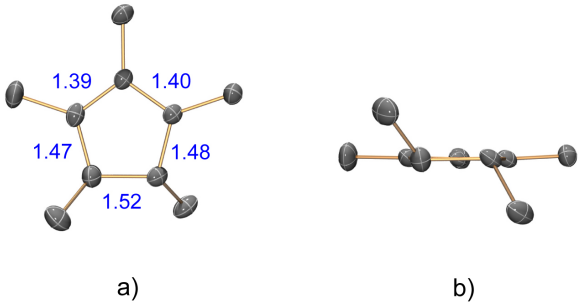

Figure 5.1. X-ray crystal structure of **58**$^+$ in [**58**][B(C_6F_5)$_4$]; H atoms omitted for clariry. a) Top view, b) side view. Blue numbers give ring C–C distances in Å.[135]

More recently, Kitagawa and coworkers reported on the crystal structure of cation **60**$^+$.[140] In the hope of generating a long-lived cyclopentadienyl cation, they treated chlorinated precurser **61** with Ag^+ (Scheme 5.2). However, the rearranged **60**$^+$ was the only carbocation that could be isolated. X-ray and NMR-spectroscopic analysis revealed bond lengths of 1.40/1.40 Å in the allyl moiety, a twist angle of 39° with respect to the phenyl ring as well as ^{13}C NMR shifts of 211, 155 and 241 ppm. Interestingly, two of the C–C distances in the cyclopropane ring were slightly elongated (1.58/1.54 Å) as compared to the parent cyclopropane (1.51 Å), a finding that was attributed to σ–π conjugation.

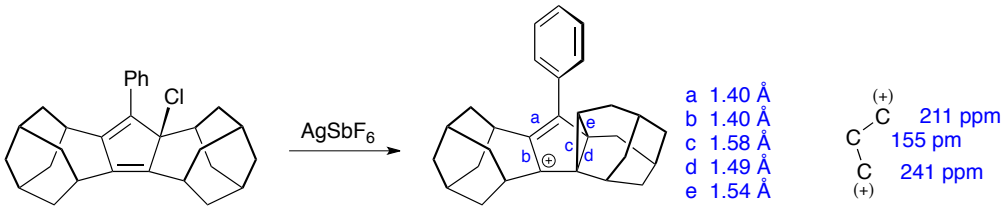

Scheme 5.2. Formation of allyl cation **60**$^+$.

5.3 Isolation of a Silyl-Substituted Allyl Cation

The above survey conveys the impression that crystalline allyl cations tend to arrive as unannounced guests. History seemed to repeat itself when the structure of a rather unusual cation was elucidated in the course of our own research into terphenylsilyl cations.

Treatment of terphenylsilane **29b** with the trityl salt $[Ph_3C][CHB_{11}Me_5Br_6]$ afforded, in addition to the intended silylium carborane [**27b**][$CHB_{11}Me_5Br_6$], a small amount of a second compound, as indicated by NMR spectroscopy. Attempts to crystallize pure [**27b**][$CHB_{11}Me_5Br_6$] from ortho-dichlorobenzene/hexane yielded instead yellow prisms of the minor product [**62**][$CHB_{11}Me_5Br_6$], the identity of which was determined by X-ray crystallography (Scheme 5.3).

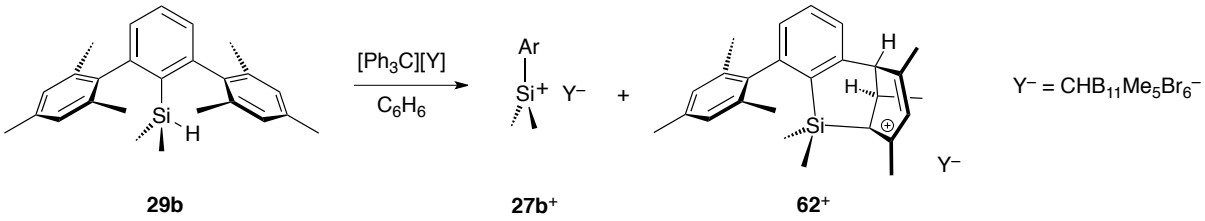

Scheme 5.3. Formation of **62**$^+$.

The crystal structure of [**62**][$CHB_{11}Me_5Br_6$] consists of well-separated cations and anions, and **62**$^+$ can be described as a silabicyclo[3.3.1]nonenyl cation with the formal positive charge distributed over a five-atom unit Si-C18-C19-C20- C21 (Figure 5.2). Selected distances and angles are given in Table 5.1. The unusually short sp^3-sp^2 C18–C19 bond (1.414(5) Å), and unusually long Si–C18 bond (1.966(4) Å), relative to normal lengths, set up a long-short-long-short distortion pattern from C18 to C21. Carbon atoms C16, C18–C21, C23 and C24 all lie in the mean plane through them within 0.025(4), and the sum of angles around C19 and C21 is 360.0(4)° for each atom, indicating trigonal-planar coordination.

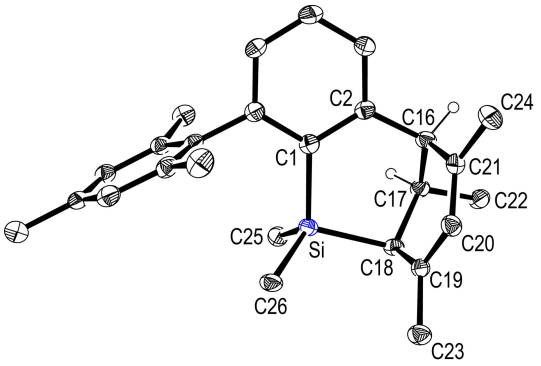

Figure 5.2. X-ray crystal structure of **62**$^+$ in [**62**][$CHB_{11}Me_5Br_6$] (30% displacement ellipsoids, H atoms except for those at C16 and C17 omitted for clarity).

Computations emulated the experimental structure well and provided insight into the orbitals over which the positive charge is distributed.[141] The structure suggested an interaction of the Si–C σ bond with the allyl π system. β-Silyl stabilization of carbenium ions has much precedence and has been exploited synthetically.[142–151]

Table 5.1. Selected distances (Å) and angles (°) for the calculated and the single-crystal X-ray structure of **62**$^+$.

Parameter	Expt.	Cald.	Parameter	Expt.	Calcd.
C18–C19	1.414(5)	1.414	C19–C23	1.486(5)	1.487
C19–C20	1.426(5)	1.421	C21–C24	1.489(6)	1.486
C20–C21	1.359(6)	1.362	C21–C16	1.506(6)	1.487
Si–C18	1.966(4)	2.028	C19-C20-C21	120.4(4)	121.1
Si–C1	1.892(4)	1.880	C18-C19-C20	120.9(4)	120.9
Si–C25	1.869(4)	1.865	C23-C19-C20	117.3(4)	118.1
CSi–C26	1.868(4)	1.861	C20-C21-C16	121.8(4)	121.1
C16–C17	1.526(5)	1.534	C20-C21-C24	120.6(4)	121.6
C17–C18	1.545(5)	1.533	C1-Si-C18	104.4(2)	102.2
C17–C22	1.526(5)	1.530	Si-C18-C19	107.8(3)	103.3

5.4 Mechanistic Hypothesis and Directed Synthesis of the Allyl Cation

One hypothesis to account for the formation of **62**$^+$ involves a protonation–hydrosilylation mechanism (Scheme 5.4). If a mesityl ring of **29b**, the most basic component in the mixture, reacts with a proton source at the *ipso* position, Wheland intermediate **63**$^+$ would form. The acid source could be $C_6H_7^+$ formed from **27b**$^+$ and solvent; the terphenylsilyl cations investigated in this thesis have been shown to acidify aromatic solvents by arene–Si$^+$ interactions (Chapter 2). A subsequent intramolecular hydride transfer from silicon to an *ortho* carbon atom of **63**$^+$ affords silylium ion **64**$^+$. This formal silylium ion–diene system finally collapses to give cation **62**$^+$. The proposed reaction sequence offers an explanation for the observed connectivity and relative stereochemistry in the product; external protonation with concomitant intramolecular hydride transfer leads to the observed configuration with *exo*-H at C16 and *endo*-H at C17.

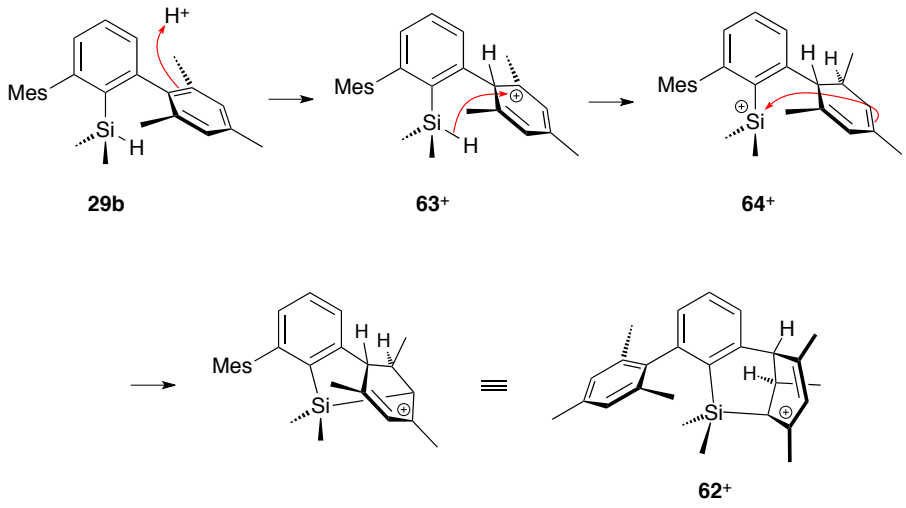

Scheme 5.4. Proposed mechanism of formation of **62**$^+$.

A test of this mechanistic hypothesis comes from intentional treatment of **29b** with strong Brønsted acids. In contrast to the hypothesis, addition of 1 equivalent of triflic acid (TfOH) in benzene—one of the strongest oxyacids[152]—did not give [**62**][OTf], but afforded silyl triflate **47** in quantitative yield. Apparently, the negatively polarized Si–H hydrogen

atom acts as a Brønsted base towards triflic acid, and trapping of the transient silylium ion by the coordinating triflate anion occurs at a much faster rate than ring protonation–hydrosilylation.

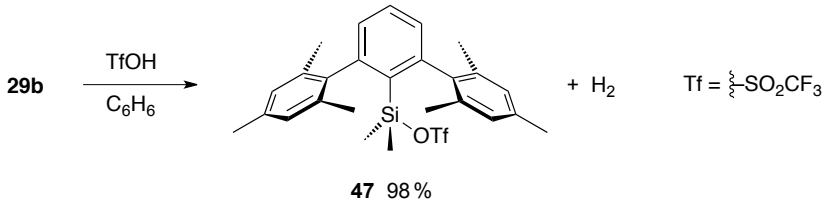

Scheme 5.5. Formation of silyl triflate **47** from hydrosilane **29b** and triflic acid.

An acid more closely related to that suggested in the mechanistic hypothesis would be an arenium carborane [arene–H][$CHB_{11}X_5Y_6$] (X = H, Me, halogen, Y = halogen), a class of isolable, redox-inert protic acids that are even stronger than triflic acid and that are paired with less coordinating anions. Benzenium and toluenium carboranes are capable of protonating a mesityl ring to a high degree.[43, 73, 74] The toluenium acid [**65**][$CHB_{11}Me_5Br_6$] was prepared from the trityl salt via the triethylsilyl carborane (Scheme 5.6). Would this an arenium species convert **29b** into $\mathbf{62}^+$? Indeed, treatment of **29b** with 1 equivalent of [**65**][$CHB_{11}Me_5Br_6$] afforded [**62**][$CHB_{11}Me_5Br_6$] as the single product (Scheme 5.7). It was isolated as a yellow powder in high yield and characterized by a second X-ray crystallographic analysis, NMR spectroscopy (^{1}H, ^{13}C, ^{29}Si, ^{11}B) and IR spectroscopy. GC–MS analysis of the reaction quenched with different nucleophiles supported the formation of neutral compounds that are consistent with $\mathbf{62}^+$ as the precursor.

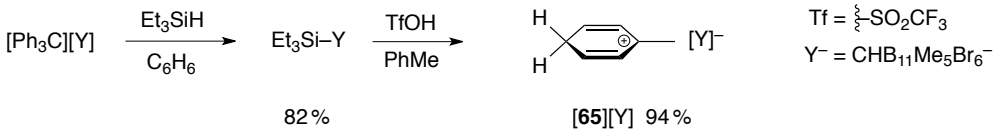

Scheme 5.6. Preparation of protonated toluene.

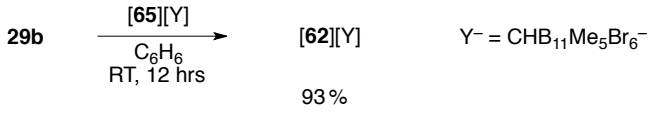

Scheme 5.7. Directed synthesis of allyl cation $\mathbf{62}^+$.

One- and two-dimensional NMR experiments in CD_2Cl_2 allowed a detailed characterization of $\mathbf{62}^+$ in solution (Table 5.2). Carbon atoms C19, C20 and C21 resonate at 225, 129 and 197 ppm, respectively. The deshielding is slightly less pronounced than in the comparable cation $\mathbf{60}^+$, a fact that might be a result of σ–π conjugation between the Si–C bond and the allyl π system. Carbon atom C18 resonates at 69 ppm, which is shifted downfield in comparison to the other saturated carbon atoms and is not in the range of usual sp^3 ^{13}C signals. This observation might again be attributed to a certain diene character of the C18–C21 system. Yet, to depict the silyl fragment as cationic $ArMe_2Si^+$ is not justified: the ^{29}Si NMR shift of $\mathbf{62}^+$ is found at $\delta = -4.2$ ppm, a value typically found for tetracoordinate, neutral silicon species.

Table 5.2. Experimental and calculated ^{13}C and ^{1}H NMR shifts of $\mathbf{62}^+$. Experimental shifts in CD_2Cl_2, CD_2Cl_2 = 54.0 ppm, $CHDCl_2$ = 5.32 ppm. Theoretical shifts calculated at the M06-L/DZ + (2df,pd)//M06-2X/DZ(2df,pd) level of theory; first column gas phase, second column in dichloromethane.

Position	$^{13}C_{expt}$	$^{13}C_{calcd}$	$^{13}C_{calcd}$	$^1H_{expt}$	$^1H_{calcd}$	$^1H_{calcd}$
C16	54.5	55.6	53.8	3.78	3.36	3.47
C17	40.6	42.1	41.5	3.11	2.76	2.74
C18	69.3	71.4	69.2	4.03	3.76	3.84
C19	225.2	210.2	208.6	–	–	–
C20	129.4	121.2	120.4	6.98	6.28	6.45
C21	196.8	193.0	189.7	–	–	–
C22	21.3	20.8	20.7	1.39	1.31	1.16
C23	34.6	31.6	31.2	2.78	2.41	2.33
C24	29.0	27.8	27.2	2.65	2.49	2.35

5.5 Isotope Labeling Study

Experiments with deuterated reactants or reagents were carried out to gain further insight into the mechanism that leads to $\mathbf{62}^+$. According to Scheme 5.4, deuterated silane **29b**-*d* in combination with $\mathbf{65}^+$ should give rise to the cation labeled only at C17. Conversely, treatment of **29b** with perdeuterated toluenium acid $[\mathbf{65}\text{-}d_9]^+$ would afford a product with deuterium at the C16 *exo* position but not at C17.

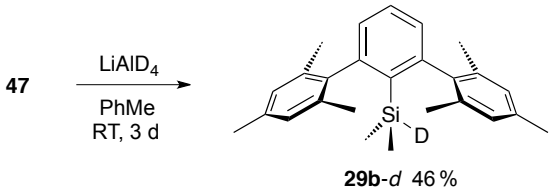

Scheme 5.8. Synthesis of the Si-deuterated silane **29b**-*d*.

Deuterated silane **29b**-*d* was prepared by the reduction of **47** with $LiAlD_4$ (Scheme 5.8). Reaction of **29b**-*d* under protic conditions yielded only the cation $\mathbf{62}^+$-*endo-d* with full deuteration of the C17 position (Scheme 5.9 a, Figure 5.3). The negatively polarized deuterium atom in **29b**-*d* did not seem to be involved in Brønsted acid–base chemistry and acted exclusively as a reducing agent towards Wheland intermediate $\mathbf{63}^+$.

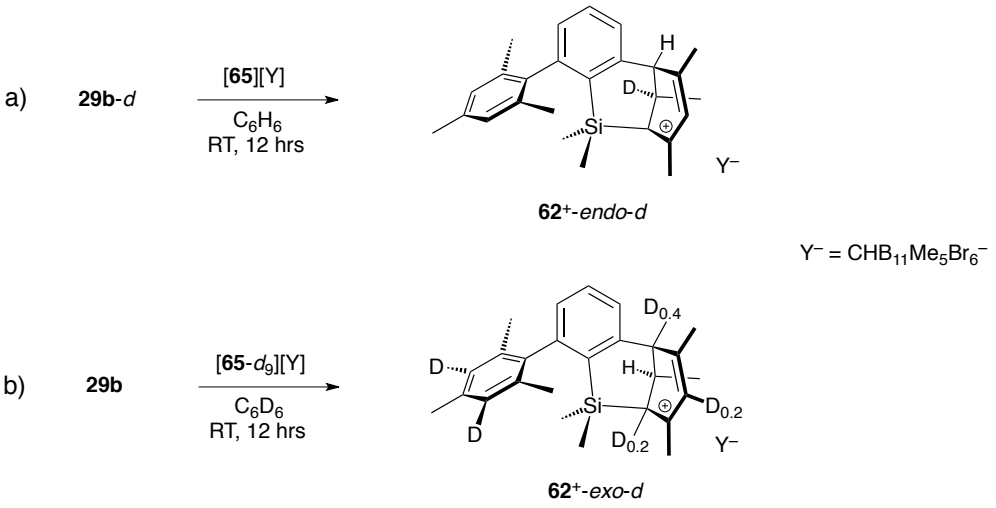

Scheme 5.9. Generation of deuterated allyl cations $\mathbf{62}^+$ using labeled starting materials.

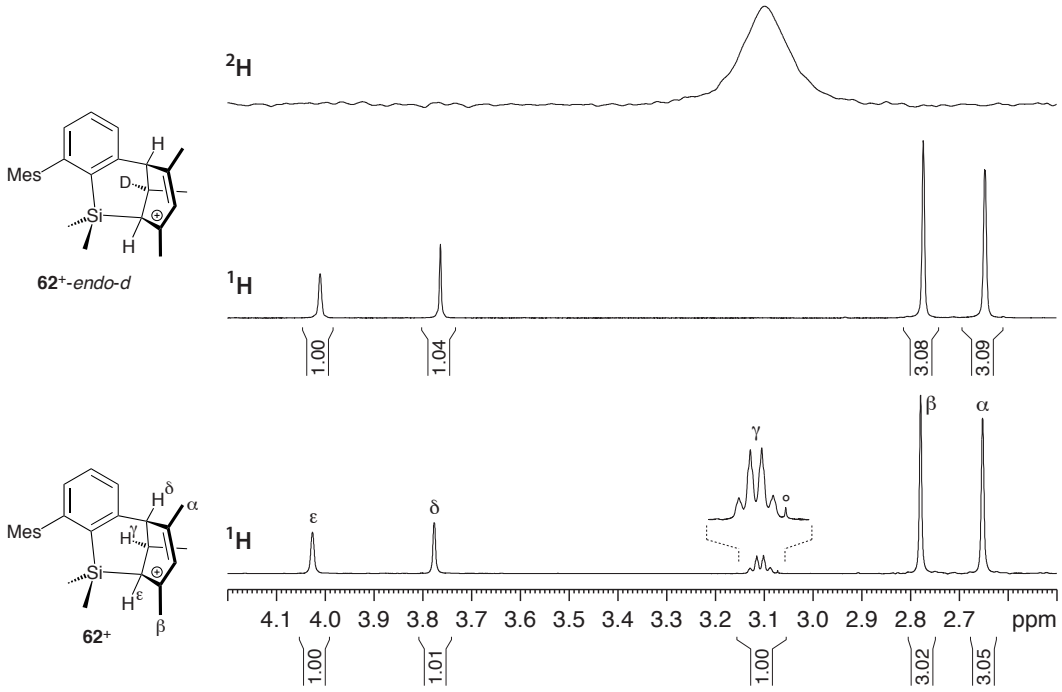

Figure 5.3. Detail of the ^{1}H NMR spectrum of [**62**][$CHB_{11}Me_5Br_6$] (lower spectrum) and the corresponding ^{1}H and ^{2}H NMR spectra of [**62**-*endo-d*][$CHB_{11}Me_5Br_6$] (upper spectra). The small peak marked with a circle stems from an impurity and is not part of the signal of H^{γ}. Conditions: 400 MHz (^{1}H), 300 K, 44 mg of [**62**][$CHB_{11}Me_5Br_6$] and 19 mg of [**62**-*endo-d*][$CHB_{11}Me_5Br_6$] in 0.6 mL CD_2Cl_2.

In the experiment with the labeled acid [**65**-d_9]$^+$, positions C16, C18, and C20 were partially deuterated, and the meta positions of the unchanged mesityl ring were fully deuterated (Scheme 5.9 b, Figure 5.4). The solvent C_6D_6 was used in this reaction because [**65**-d_9]$^+$ would have undergone fast H–D exchange in C_6H_6. The degree of deuteration was inferred from integration of the ^{1}H NMR spectra and from ^{2}H and ^{13}C NMR measurements.* Reversible protonation of the mesityl rings of **29b** lead to H–D scrambling and some washing in of H to the toluenium species. This scrambling accounts for the presence of some H in the *ipso* position of the cationic ring of **62**$^+$-*exo-d*. After the hydride transfer had taken place, H–D exchange continued on the unchanged mesityl ring, which is most likely due

*A reliable integration with errors of less than 5 % was achieved with the interval between two pulses d_1 = 15 s. The ^{2}H NMR spectra, being negatives of the ^{1}H NMR spectra, were used to confirm the position of deuteration. ^{13}C NMR spectra served the same purpose: carbon nuclei adjacent to ^{2}H exhibited $^1J_{C,D}$ coupling and an isotope shift.

to a slight excess of toluenium ions. The central ring was not deuterated under the reaction conditions, a finding that indicated its lower basicity. An orbital analysis supported this observation; the basic HOMO of $\mathbf{62}^+$ is expressed predominantly on the unchanged mesityl ring.

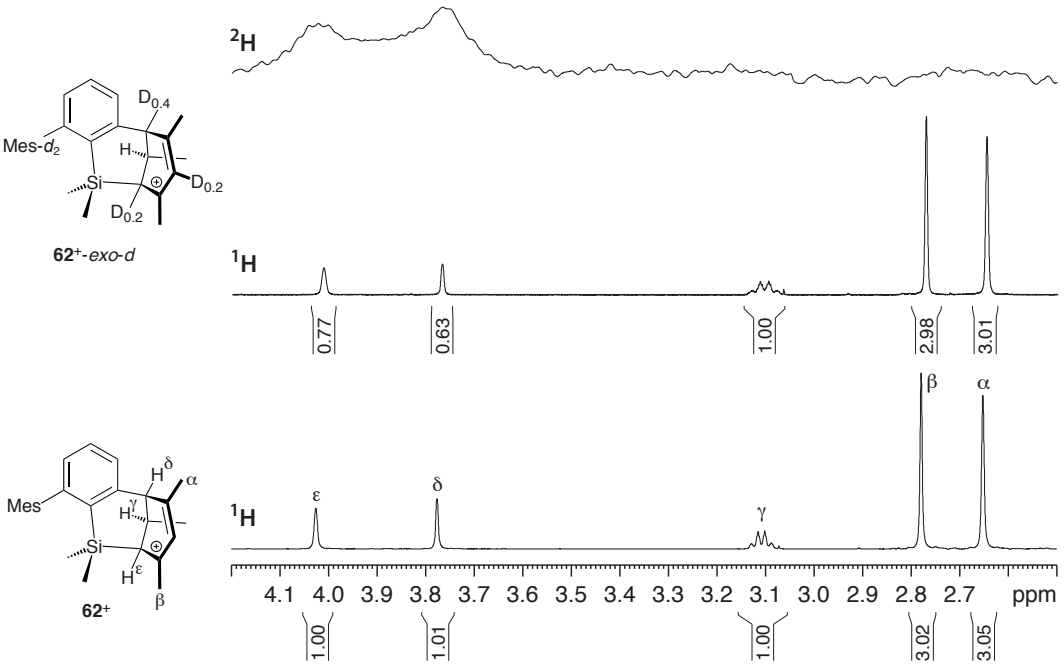

Figure 5.4. Detail of the ^{1}H NMR spectrum of [**62**][$CHB_{11}Me_5Br_6$] (lower spectrum) and the corresponding ^{1}H and ^{2}H NMR spectra of [**62**-*exo-d*][$CHB_{11}Me_5Br_6$] (upper spectra). Conditions: 400 MHz (^{1}H), 300 K, 44 mg of [**62**][$CHB_{11}Me_5Br_6$] and 10 mg of [**62**-*exo-d*][$CHB_{11}Me_5Br_6$] in 0.6 mL CD_2Cl_2.

5.6 Allyl Cation Versus Silylium Ion Character

The question arose as to whether $\mathbf{62}^+$ was best described as a silyl-stabilized allyl cation or a diene-coordinated silylium ion (Scheme 5.5). From a valence bond perspective the principal resonance structures of $\mathbf{62}^+$ to consider are $\mathbf{62a}^+$, $\mathbf{62b}^+$ and $\mathbf{62c}^+$. As pointed out above, the long-short-long-short pattern along Si-C18-C19-C20-C21 and the ^{13}C NMR signals of C18–C21 are in agreement with a certain silylium ion–diene character, $\mathbf{62c}^+$.

However, the observed structure deviates little from the hypothetical ideal allylic cation depicted by only **62a**$^+$ and **62b**$^+$. Silylium ions coordinated by π systems exhibit Si–C distances of more than 2.1 Åδ(29Si) $>$ 55 ppm;[30, 97, 153] neither is the case for **62**$^+$.

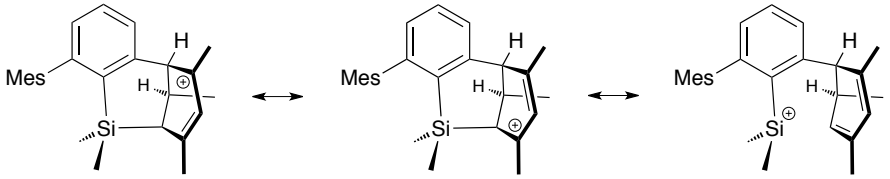

62a$^+$ **62b**$^+$ **62c**$^+$

Figure 5.5. Principal resonance structures of **62**$^+$.

A natural bond orbital (NBO) analysis of **62**$^+$ allowed a segmentation of the Si-C18-C19-C20-C21 fragment into Lewis forms with a *p* orbital cation acceptor on C19 interacting strongly with the Si–C18 σ bond and the C20–C21 π bond as donors. The analysis indicated significant delocalization of 4 electrons among three orbitals (σ, p and π), with occupancies of 1.67, 0.67 and 1.71 electrons, respectively. The effective polarization of the Si–C bond results in a percentage contribution of 23 from Si and 77 from C compared to a normal Si–C bond with around 30 from Si and 70 from C. The overall NBO picture of the cation is one in which resonance form **62b**$^+$ dominates but **62a**$^+$ and **62c**$^+$ are significant contributors of roughly equal importance.

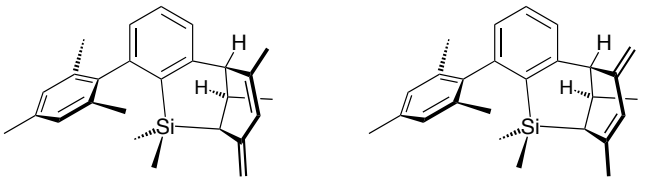

66a **66b**

The reactivity of **62**$^+$ further supports silyl-stabilized allyl cationic character. Treatment of the cation with nucleophiles of different hardness (CN^-, H_2O, F^-) afforded elimination products **66** formed by proton abstraction at C23 and C24, as evidenced by ^{1}H NMR spectroscopy and GC–MS; addition to the silicon nucleus was not observed. Cations with a higher silylium ion character, such as **27b**$^+$ or their donor adducts [**27b**(MeCN)]$^+$, give ad-

dition products R_3SiNu exclusively upon treatment with nucleophiles.[31, 153] In conclusion, although **62c**$^+$ has to be considered as a resonance structure to account for the observed bond lengths and the ^{13}C NMR spectrum, other data suggested its relevance is limited. The picture of a silyl-stabilized allyl cation is more apposite.

5.7 Experimental Part

5.7.1 General

For general reaction conditions and analytical instruments, see Sections 2.9.3 and 2.9.4.

Triflic acid and triflic acid-*d* were purchased from Acros and Aldrich, respectively, and used as received.

5.7.2 Protonated Toluene ([65][$CHB_{11}Me_5Br_6$])

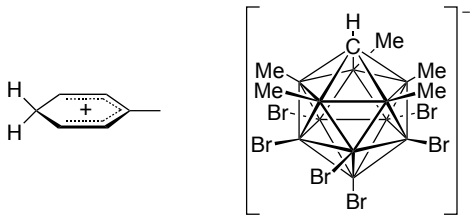

Chemical Formula: $[C_7H_9][C_6H_{16}B_{11}Br_6]$
Molecular Weight: 779.683 u

[toluenium][$CHB_{11}Me_5Br_6$] was prepared as described below by a modification of the literaure method.[74] [Et_3Si][$CHB_{11}Me_5Br_6$] was prepared according to literature procedures.[28, 35, 78, 154]

Since triflic acid can corrode metals and parts of a glovebox, the synthesis was carried out in a fumehood with carefully dried solvents and glassware. Traces of moisture lead to the formation of H_3O^+ salts.

[Et_3Si][$CHB_{11}Me_5Br_6$] (109.5 mg, 137 µmol) was dissolved in toluene (1 mL). A solution of TfOH (*ca.* 100 mg, 0.7 mmol) in toluene (1 mL) was added, and the mixture was stirred well for 20 min. A yellowish precipitate formed. The mixture was concentrated (*ca.* 70 % of the solvent removed) under reduced pressure, and hexane was added (5 mL) for a more complete precipitation. The supernatant was removed, and the residue was washed with hexane (2 × 3 mL) and dried in a vacuum overnight. The product was obtained as a yellowish powder (100.2 mg, 129 µmol, 94 %).

The deuterated compound [toluenium-d_9][$CHB_{11}Me_5Br_6$] was synthesized using

toluene-d_8 and triflic adid-d.

5.7.3 Allyl Cation ([62][$CHB_{11}Me_5Br_6$])

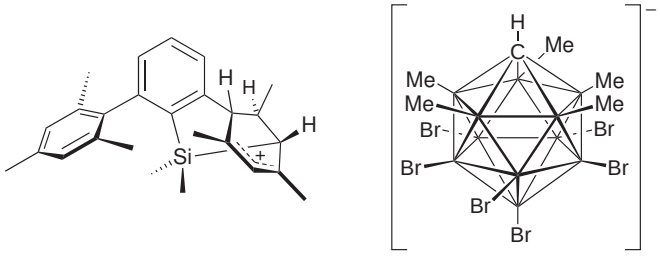

Chemical Formula: $[C_{26}H_{33}Si][C_6H_{16}B_{11}Br_6]$
Molecular Weight: 1060.162 u

General: The reaction was carried out in a glovebox with dry solvents.

2,6-Bis(2,4,6-trimethylphenyl)phenyldimethylsilane (16.8 mg, 45.1 μmol) and [toluenium][$CHB_{11}Me_5Br_6$] (35.3 mg, 45.2 μmol) were dissolved in benzene (1 mL). After a few minutes, a clear yellow-orange solution was obtained. It was stirred overnight at ambient temperature. Most of the solvent (*ca*. 0.8 mL) was removed under reduced pressure. The product was precipitated with hexane (3 mL), washed with hexane (2 × 2 mL), and dried in a vacuum. The allyl cation–carborane salt was obtained as a yellow powder (44.4 mg, 41.9 μmol, 93%). In the ^{1}H and ^{13}C NMR spectra, the presence of some hexane was observed; the signals did not disappear even after prolonged drying i.v. at room temperature. Drying at elevated temperatures lead to decomposition of the material.

Characterization

M.p.: (sealed capillary) Product forms a dark brown oil at 140–145 °C

IR (solution of 10 mg in 0.15 mL CH_2Cl_2, NaCl cell): 3049*w*, 3001*w*, 2958*m*, 2910*m*, 1570*s*, 1444*m*, 1417*m*, 1394*m*, 1353*w* 1316*s*, 1226*w*, 1187*w*, 1171*m*, 1149*w*, 1117*s*, 1054*w*, 980*m*, 966*s*, 925*m* 895*m*, 855*m*, 844*m*, 806*m*, 794*m*, 777*m*, 638*w*, 622*w*, 537*w*, 487*w*.

NMR: ^{1}H and ^{13}C NMR signals were assigned by HSQC and HMBC experiments.

^{1}H NMR (500 MHz, 44 mg in 0.6 mL CD_2Cl_2, $\delta(CHDCl_2)$ = 5.32 ppm): 7.57 (*dd*, ^{3}J = 7.7, ^{3}J = 7.7, 1 H, H^{β}), 7.35 (*dd*, ^{3}J = 7, ^{4}J = 1.0, 1 H, H^{γ}), 7.16 (*dd*, ^{3}J = 7, ^{4}J = 1.0, 1 H, H^{α}), 6.98 (*s*, 1 H, H^{κ}), 6.96 (*s*, 1 H, CH of mesityl ring), 6.91 (*s*, 1 H, CH of mesityl ring), 4.03 (broadened *s* (coupling to H^{ε} not resolved), 1 H, H^{η}), 3.78 (broadened *s* (coupling to H^{ε} not resolved), 1 H, H^{δ}), 3.11 (broadened *q* (couplings to H^{δ} and H^{η} not resolved), ^{3}J = 7.0, 1 H, H^{ε}), 2.78 (*s*, 3 H, H^{θ}), 2.65 (*s*, 3 H, H^{λ}), 2.32 (*s*, 3 H, *para*-CH_3 of mesityl ring), 2.06 (broad *s*, 1H, carborane CH), 1.88 (*s*, 3 H, *ortho*-CH_3 of mesityl ring), 1.79 (*s*, 3 H, *ortho*-CH_3 of mesityl ring), 1.39 (*d*, ^{3}J = 7.0, 3 H, H^{ζ}), 0.52 (*s*, 3 H, Si–CH_3), 0.19 (*s*, 15 H, carborane CH_3), −0.12 (*s*, 3 H, Si–CH_3).

^{13}C{^{1}H} NMR (126 MHz, 44 mg in 0.6 mL CD_2Cl_2, $\delta(CD_2Cl_2)$ = 54.0 ppm): 225.2 (C^{k}), 196.83 (C^{m}), 152.2 (C^{b}), 145.6 (C^{f}), 139.4 (*para*-C of mesityl ring), 137.6 (*ortho*-C of mesityl ring), 137.1 (*ortho*-C of mesityl ring), 137.0 (*ipso*-C of mesityl ring), 133.0 (C^{c}), 132.3 (C^{d}), 129.4 (C^{l}), 129.0 (*meta*-C of mesityl ring), 128.9 (*meta*-C of mesityl ring), 128.7 (C^{e}), 127.9 (C^{a}), 69.3 (C^{i}), 55.0 (broad, carborane CH), 54.5 (C^{g}), 40.6 (C^{h}), 34.6 (C^{o}), 29.0 (C^{p}), 21.5 (CH_3 of mesityl ring), 21.4 (CH_3 of mesityl ring), 21.3 ($CH_3$of mesityl ring), 21.3 (C^{n}), 2.6 (Si–CH_3), −1.1 (Si–CH_3), −1.5 (broad, carborane CH_3).

^{29}Si{^{1}H} NMR (99 MHz, 70 mg in 0.6 mL CD_2Cl_2, external $SiMe_4$ = 0 ppm): −4.2.

^{11}B NMR (96 MHz, 44 mg in 0.6 mL CD_2Cl_2, external $BF_3{\cdot}Et_2O$ = 0 ppm): −2.60, −9.39, −11.95.

allyl cation after drying i.v./RT overnight
1H NMR, 500 MHz, 300 K, 44 mg in 0.7 mL CD2Cl2
δ(CHDCl2) = 5.32 ppm

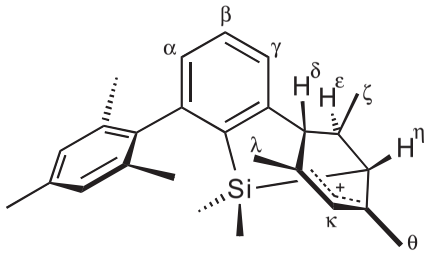

$CHB_{11}Me_5Br_6^-$

```
Current Data Parameters
NAME          sld_#0244a
EXPNO                  2
PROCNO                 1

F2 - Acquisition Parameters
Date_           20080620
Time              11.44
INSTRUM           spect
PROBHD   5 mm PABBI 1H/
PULPROG           zg30
TD               65536
SOLVENT          CD2Cl2
NS                  16
DS                   2
SWH           6009.615 Hz
FIDRES        0.091699 Hz
AQ            5.4526453 sec
RG                71.8
DW              83.200 usec
DE              20.00 usec
TE                300.0 K
D1          10.00000000 sec
TD0                  1

======== CHANNEL f1 ========
NUC1                1H
P1               7.40 usec
PL1              2.50 dB
SFO1        500.3017000 MHz

F2 - Processing parameters
SI                65536
SF          500.3000165 MHz
WDW                  no
SSB                   0
LB                 0.00 Hz
GB                    0
PC                 1.00
```

allyl cation after drying i.v./RT overnight
13C{1H} NMR, 125 MHz, 300 K, 44 mg in 0.7 mL CD2Cl2
δ(CD2Cl2) = 54.00 ppm

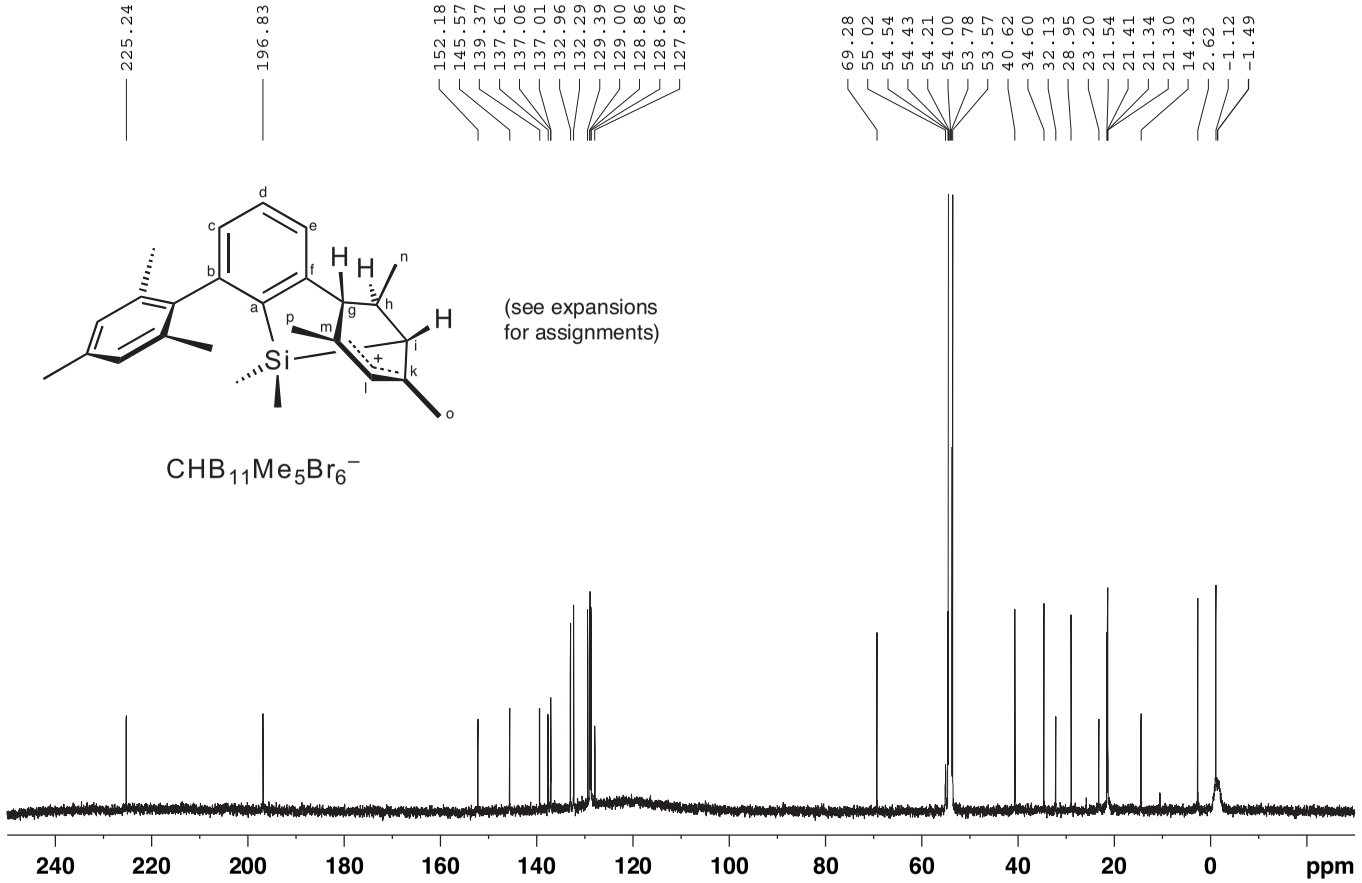

(see expansions for assignments)

$CHB_{11}Me_5Br_6^-$

```
Current Data Parameters
NAME          sld_#0244a
EXPNO                  3
PROCNO                 1

F2 - Acquisition Parameters
Date_           20080620
Time              11.56
INSTRUM           spect
PROBHD   5 mm PABBI 1H/
PULPROG          zgpg30
TD                65536
SOLVENT           CD2Cl2
NS                 3202
DS                    4
SWH           35714.285 Hz
FIDRES        0.544957 Hz
AQ            0.9175540 sec
RG                  114
DW             14.000 usec
DE              6.00 usec
TE                300.3 K
D1           2.00000000 sec
d11          0.03000000 sec
DELTA        1.89999998 sec
TD0                    1

======== CHANNEL f1 ========
NUC1                 13C
P1                13.07 usec
PL1               -2.20 dB
SFO1        125.8143731 MHz

======== CHANNEL f2 ========
CPDPRG2          waltz16
NUC2                 1H
PCPD2             75.00 usec
PL12              22.62 dB
PL13              25.62 dB
PL2                2.50 dB
SFO2        500.3020012 MHz

F2 - Processing parameters
SI                65536
SF          125.8004634 MHz
WDW                  EM
SSB                   0
LB                 2.00 Hz
GB                    0
PC                 1.40
```

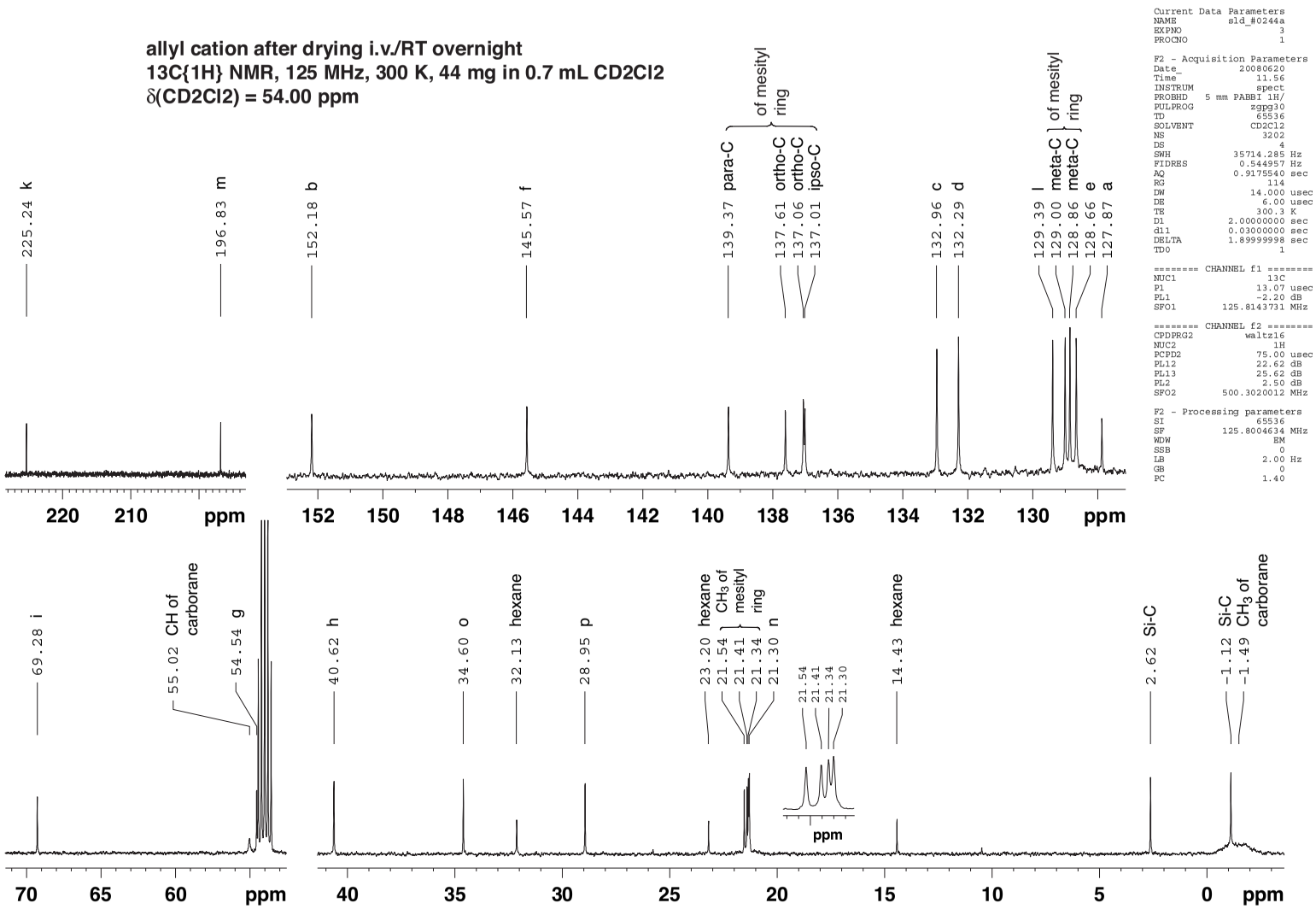


```
Current Data Parameters
NAME                 sld_#0244a
EXPNO                         3
PROCNO                        1

F2 - Acquisition Parameters
Date_               20080620
Time                   11.56
INSTRUM                spect
PROBHD    5 mm PABBI 1H/
PULPROG             zgpg30
TD                     65536
SOLVENT              CD2Cl2
NS                       3202
DS                          4
SWH                35714.285 Hz
FIDRES             0.544957 Hz
AQ                 0.9175540 sec
RG                        114
DW                   14.000 usec
DE                    6.00 usec
TE                    300.3 K
D1                2.00000000 sec
d11               0.03000000 sec
DELTA             1.89999998 sec
TD0                           1

======== CHANNEL f1 ========
NUC1                      13C
P1                    13.07 usec
PL1                   -2.20 dB
SFO1           125.8143731 MHz

======== CHANNEL f2 ========
CPDPRG2                waltz16
NUC2                       1H
PCPD2                 75.00 usec
PL12                  22.62 dB
PL13                  25.62 dB
PL2                    2.50 dB
SFO2           500.3020012 MHz

F2 - Processing parameters
SI                        65536
SF             125.8004634 MHz
WDW                          EM
SSB                           0
LB                         2.00 Hz
GB                            0
PC                         1.40
```

X-Ray Analysis

ORTEP representation (50 % thermal ellipsoids):

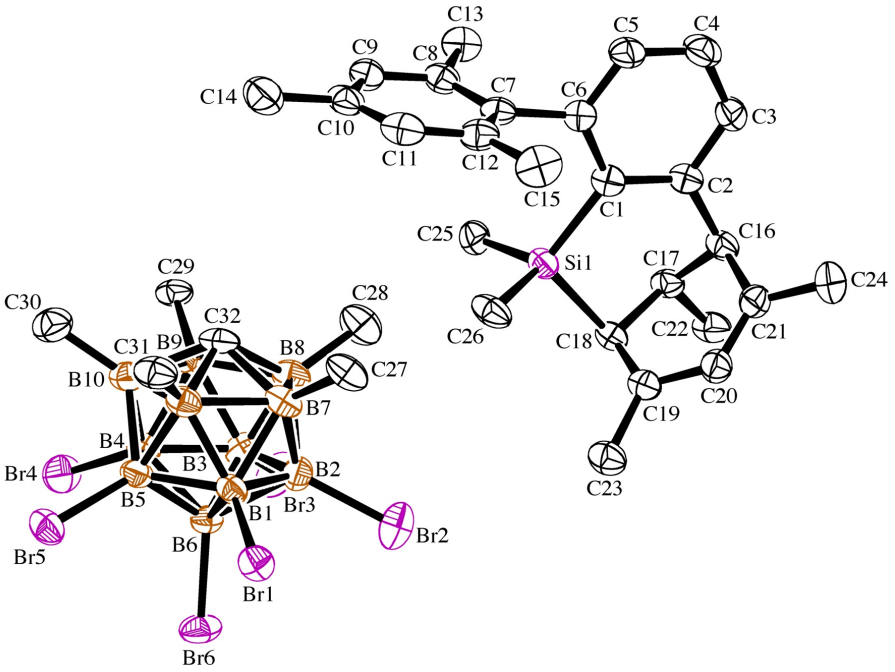

Packing diagram:

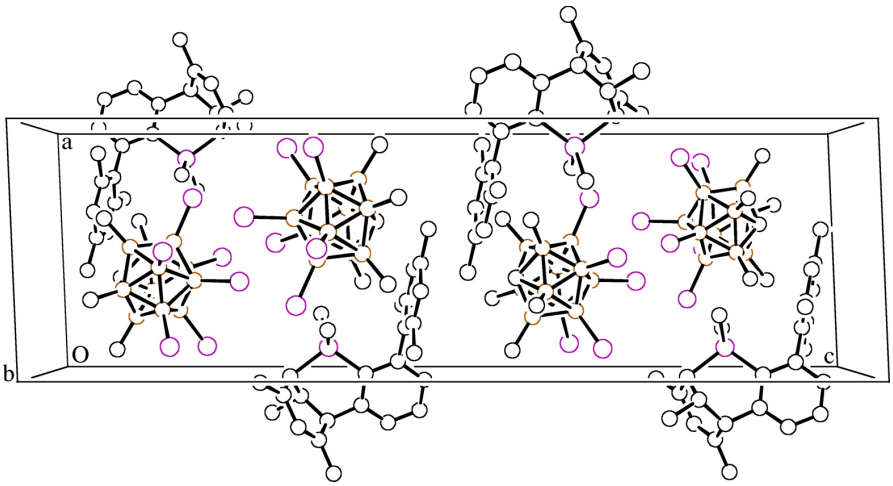

Table 5.3. Summary of the X-ray diffraction analysis of **62**$^{+}$.

Crystallized from	1,2-dichlorobenzene / hexane
Empirical formula	$C_{32}H_{49}B_{11}Br_6Si$
Formula weight [g mol^{-1}]	1060.15
Crystal color, habit	yellow, prism
Crystal dimensions [mm]	0.12 × 0.20 × 0.22
Temperature [K]	160(1)
Crystal system	monoclinic
Space group	$P2_1/c$ (#14)
Z	4
Reflections for cell determination	53116
2θ range for cell determination [°]	4 – 55
Unit cell parameters a [Å]	9.6689(4)
b [Å]	14.1286(5)
c [Å]	31.984(1)
α [°]	90
β [°]	92.431(1)
γ [°]	90
V [Å^3]	4365.3(3)
$F(000)$	2080
D_x [g cm^{-3}]	1.613
μ(Mo $K\alpha$) [mm^{-1}]	5.586
Scan type	ϕ and ω
2θ(max) [°]	55
Transmission factors (min; max)	0.339; 0.537
Total reflections measured	47991
Symmetry independent reflections	10010
R_{int}	0.095
Reflections with $I > 2\sigma(I)$	6550
Reflections used in refinement	10010
Parameters refined	469
Final $R(F)$ [$I > 2\sigma(I)$ reflections]	0.0458
$wR(F^2)$ (all data)	0.1022
Weights: $w = [\sigma^2(F_o^2) + (0.0432P)^2 + 1.4777P]^{-1}$ where $P = (F_o^2 + 2F_c^2)/3$	
Goodness of fit	1.027
Secondary extinction coefficient	0.0039(2)
Final Δ_{max}/σ	0.001
$\Delta\rho$ (max; min) [e Å^{-3}]	0.61; –0.72
$\sigma(d(C-C))$ [Å]	0.005 – 0.006

5.7.4 2,6-Bis(2,4,6-trimethylphenyl)phenyldimethylsilyl Triflate (47)

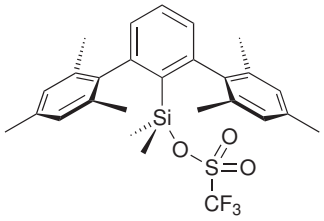

Chemical Formula: $C_{27}H_{31}F_3O_3SSi$
Molecular Weight: 520.679 u

General: The reaction was carried out in the hood under argon. All glassware was dried at 150 °C overnight. Since triflic acid corrodes metal needles, only Pasteur pipets were used for the transfer of liquids.

A solution of triflic acid (91.2 mg, 0.608 mmol) in dry benzene (1 mL) was added to a solution of 2,6-Bis(2,4,6-trimethylphenyl)phenyldimethylsilane (215 mg, 0.577 mmol) in dry benzene (3 mL). The mixture turned orange immediately, and hydrogend gas evolved. The mixture was stirred for 3 hrs at room temperature. Benzene and excess triflic acid were removed under reduced pressure. The remaining solid was dried in a vacuum overnight. The silyl triflate was obtained as a moisture-sensitive off-white powder (293 mg, 0.563 mmol, 98 %). For further reactions and the preparation of IR and NMR samples, the compound was tranferred into a glovebox.

Characterization

M.p.: (sealed capillary) 126.5–128 °C

IR (solution of 6 mg in 0.1 mL benzene, NaCl cell): 2965*w*, 2918*m*, 2859*w*, 1611*w*, 1558*w*, 1446*m*, 1392*s*, 1261*m*, 1244*s*, 1209*s*, 1154*s*, 1125*w*, 1086*w*, 948*s*, 855*s*, 817*s*, 801*s*, 776*w*, 748*w*, 733*w*, 626*s*, 517*w*.

^{1}H NMR (500 MHz, 52 mg in 0.6 mL C_6D_6, $\delta(C_6HD_5)$ = 7.15): 7.48 (*t*, $^3J = 7.6$, 1 H, H–C(4')), 7.48 (*s*, 4 H, H–C(3", 5", 3"', 5"')), 7.11 (*d*, $^3J = 7.6$, 2 H, H–C(3', 5')), 2.48 (*s*, 6 H, H_3C–C(4", 4"')), 2.32 (*s*, 12 H, H_3C–C(2", 6", 2"', 6"')), 0.28 (*s*, 6 H, H_3C–Si).

^{13}C{^{1}H} NMR (126 MHz, 52 mg in 0.6 mL C_6D_6, $\delta(C_6D_6)$ = 128.0)): 150.2 (quat. C),

139.7 (quat. C), 137.7 (quat. C), 136.2 (quat. C), 132.3 (CH), 129.5 (CH), 129.0 (CH), 128.7 (quat. C), 119.0 (*q*, $^{1}J_{C,F} = 317$, CF_3), 21.1 (CH_3, CH_3–C(4", 4"'), 20.9 (CH_3, CH_3–C(2", 6", 2"', 6"'), 2.0 (CH_3, Si–C).

$^{19}F\{^{1}H\}$ NMR (282.4 MHz, 52 mg in 0.6 mL C_6D_6, external CCl_3F = 0 ppm): −76.98.

$^{29}Si\{^{1}H\}$ NMR (59.9 MHz, 52 mg in 0.6 mL C_6D_6, external $SiMe_4$= 0 ppm): 28.3.

5.7.5 2,6-Bis(2,4,6-trimethylphenyl)phenyldeuterodimethylsilane (29b-*d*)

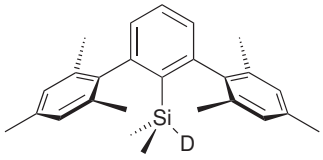

Chemical Formula: $C_{26}H_{31}DSi$
Molecular Weight: 373.624 u

Silyl triflate (161 mg, 0.309 mmol) was dissolved in dry toluene (3 mL). $LiAlD_4$ (18.5 mg, 0.441 mmol) was added, and the mixture was stirred for three days at room temperature. Toluene was removed under reduced pressure. The residue was extracted with hexane (3 × *ca.* 3 mL). The combined hexane layers were washed with water, then brine, and water again. The organic phase was dried with $MgSO_4$, filtered, and evaporated to dryness. Preparative thin-layer chromatography of the crude product (20 × 20 cm, 1 mm SiO_2, eluent cyclohexane–toluene 10:1, band at R_f 0.65) afforded the deuterated silane as a white powder (53 mg, 0.142 mmol, 46%).

Characterization

M.p.: 117.5–119 °C

IR (KBr): 2975*s*, 2952*s*, 2916*s*, 2855*m*, 2732*w*, 1944*w*, 1877*w*, 1811*w*, 1735*w*, 1611*m*, 1550*s*, 1483*m*, 1444*s*, 1377*m*, 1244*s*, 1174*m*, 1119*s*, 1085*m*, 1049*m*1032*m*, 855*s*, 838*s*, 828*s*, 808*s*, 791*s*, 739*s*, 693*w*, 664*s*, 602*w*, 577*s*, 525*m*, 502*w*.

^{1}H NMR (500 MHz, 22 mg in 0.6 mL C_6D_6, $\delta(C_6HD_5)$ = 7.15): 7.24 (*t*, $^{3}J = 7.6$, 1 H,

H–C(4')), 6.91 (*d*, $^{3}J = 7.6$, 2 H, H–C(3', 5')), 6.85 (*s*, 4 H, H–C(3", 5", 3"', 5"')), 2.19 (*s*, 6 H, H_3C–C(4", 4"')), 2.08 (*s*, 12 H, H_3C–C(2", 6", 2"', 6"')), −0.16 (*s*, 6 H, H_3C–Si).

$^{13}C\{^{1}H\}$ NMR (126 MHz, 22 mg in 0.6 mL C_6D_6, $\delta(C_6D_6) = 128.0$)): 149.5 (quat. C), 140.7 (quat. C), 136.7 (quat. C), 136.1 (quat. C), 134.5 (quat. C), 130.3 (CH), 128.4 (CH), 128.4 (CH), 21.2 (CH_3, CH_3–C(2", 6", 2"', 6"')), 21.1 (CH_3, CH_3–C(4", 4"')), −2.5 (CH_3, Si–C).

$^{29}Si\{^{1}H\}$ NMR (99.4 MHz, 22 mg in 0.6 mL C_6D_6, external $SiMe_4$ = 0 ppm): −23.4 (*t*, $^{1}J_{Si,D} = 29.5$).

MS (EI): 373 (10, $M^{\cdot+}$), 358 (100, $[M - CH_3]^{+}$), 179 (14), 59 (60).

Chapter 6

Silylium-Mediated Generation of Aryl Cations

6.1 Summary

The silylium-like species $[Et_3Si(X)]^+$ (**68**$^+$, X = PhF or Et_3SiH) and terphenylsilyl cation **27a**$^+$ abstract fluoride from fluorobenzene at slightly elevated or even ambient temperature. C–F activation by **68**$^+$ afforded phenylated carboranes 7- and 12-Ph–$CHB_{11}Cl_{11}$, the first of which was characterized by X-ray crystallography. These compounds were shown to act as phenylating reagents towards a series of nitrogen, oxygen and phosphorus nucleophiles. Computational and kinetic studies on the C–F activation of fluoroarenes by **27a**$^+$ indicated a transition state with some phenyl cation character, but also a certain assistance by π_{aryl} electron density. Based on the silylium-mediated fluoride transfer, a Friedel–Crafts arylation protocol was developed in which the generation of an incipient aryl cation is followed by intramolecular arene–arene coupling.

$[Et_3Si(X)]^+$

X = PhF or Et_3SiH

68$^+$

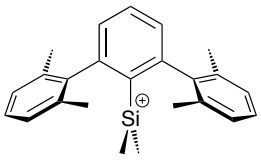

27a$^+$

6.2 Introduction

Silicon and fluorine are an unequal pair, and yet they form the strongest couple of all elements. The unmatched Si–F bond dissociation energy of 662 kJ mol^{-1} offers the possibility to abstract fluoride from almost every fluorine-containing species given a suitable silyl Lewis acid.[16, 155] In particular, fluoride abstraction from any organic molecule by a silylium ion R_3Si^+ is a thermodynamically favored process.[1] The differences in Si–F and C–F bond strengths have made it possible to use silicon-based Lewis acids in C–F activation to afford unusual carbocationic intermediates that were structurally characterized by X-ray crystallography.[156] Moreover, silylium-mediated conversion of fluorocarbons R_3CF to hydrocarbons R_3CH in the presence of a reducing agent has been accomplished (see Section 1.4.4, p. 48). Fluoride abstraction from organic precursors, however, has up to the present been restricted to aliphatic substrates, leaving the activation of C_{aryl}–F bonds a fundamental challenge. In view of the involved bond dissociation energies, the low reactivity of fluoroarenes is most likely of kinetic, not thermodynamic origin.[1, 157]

The high activation energy associated with the heterolytic Ph–X bond cleavage (X = leaving group), analogous to the first step in classical S_N1 reactions, is intrinsically tied to the instability of the phenyl cation.[158] In its ground state, $C_6H_5^+$ (**67**$^+$) possesses the unfavored electronic configuration $(\pi)^6(sp^2)^0$ (**67a**$^+$) with all bonding *p* orbitals filled and a lower-lying orbital remaining vacant.[159] The singlet cation **67a**$^+$ has been calculated to be about equally stable as $C_2H_3^+$, 111 kJ mol^{-1} less stable than CH_3^+ and 60 kJ mol^{-1} more stable than $C_2H_5^+$, in reasonable agreement with experimental hydride affinities in the gas phase (Figure 6.1).[124]

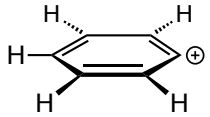

67$^+$

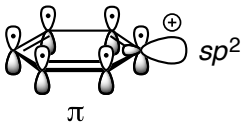

67a$^+$ singlet

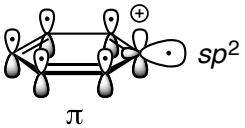

67b$^+$ triplet

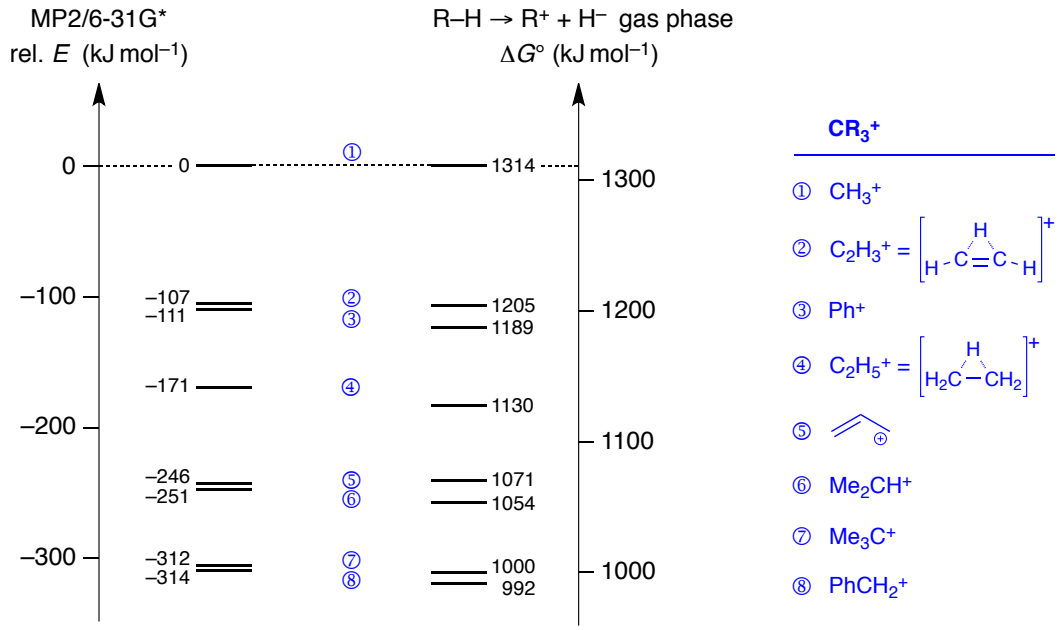

Figure 6.1. Calculated relative stabilities of carbocations (MP2/6-31G*, CH_3^+ = 0 kJ mol^{-1}) and free energies for the heterolytic dissociation $R_3C–H \rightarrow R_3C^+ + H^-$ in the gas phase.[124]

S_N1-like processes involving Ar–X substrates in solution are rare and have only been accomplished with extreme leaving groups or highly activated aryl moieties. A classical way of producing incipient aryl cations is the thermal or photoinduced decomposition of arenediazonium salts (Scheme 6.1 a). These species have been known since Sandmeyer's reports in the 1880s,[160, 161] and later Zollinger carried out pioneering studies on the mechanistic details of their reactions with nucleophiles.[162, 163] Aryl cations have also been obtained from tritiated precursors via β^- decay and subsequent loss of helium, a methodology that made it possible to work in environments of low nucleophilicity and in particular in the absence of a counterion. (Scheme 6.1 b).[164, 165] Evidence for the solvolytic generation of aryl cationic intermediates was offered by Sonoda and coworkers in 1985.[166–168] Their strategy was based on the cation-stabilizing effect exerted by electron-donating substituents on the aryl ring (Scheme 6.1 c). It is important to keep in mind that the substitution reactions discussed in this paragraph probably proceed via a loose S_N2_{Ar} path or radical intermediates rather than a purely dissociative cationic mechanism.[169, 170]

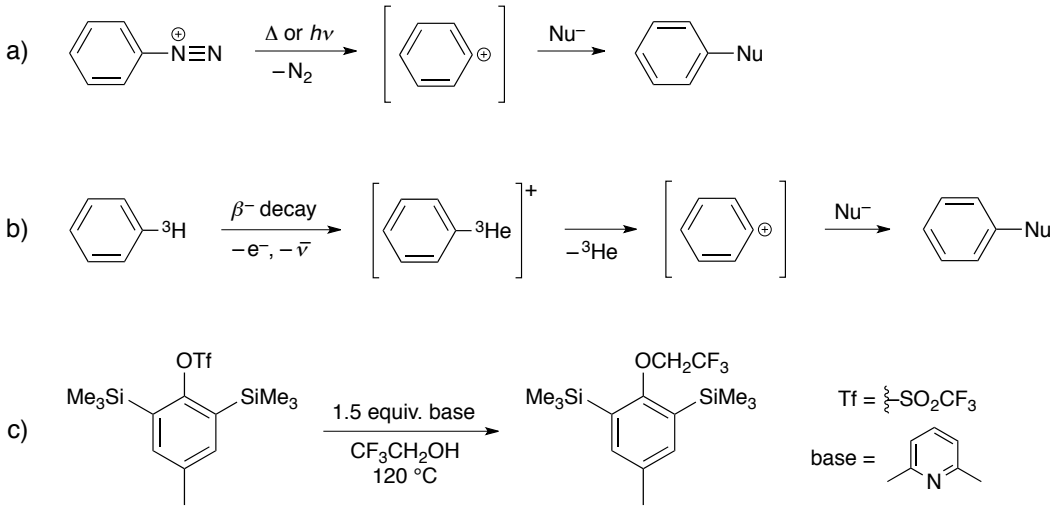

Scheme 6.1. Generation of aryl cations by a) decomposition of arenediazonium ions, b) β^- decay of tritium-substituted arenes and c) solvolysis of activated arenes.

Recent investigations into photochemically generated $RC_6H_4^+$ intermediates by the group of Albini have shed light on the reactivity and synthetic utility of aryl cations in the $(\pi)^5(sp^2)^1$ triplet state.[171–174] Halogenated cation precursors were demonstrated to undergo efficient coupling with arenes to give highly substituted biaryls (Scheme 6.2). However, the methodology required electron-rich starting materials, and the arene that acted as the nucleophile had to be used in excess. In addition, the aryl cations had to be formed in solvents of high polarity and selectively reacted with π nucleophiles, factors entailing a limited scope of the reaction.

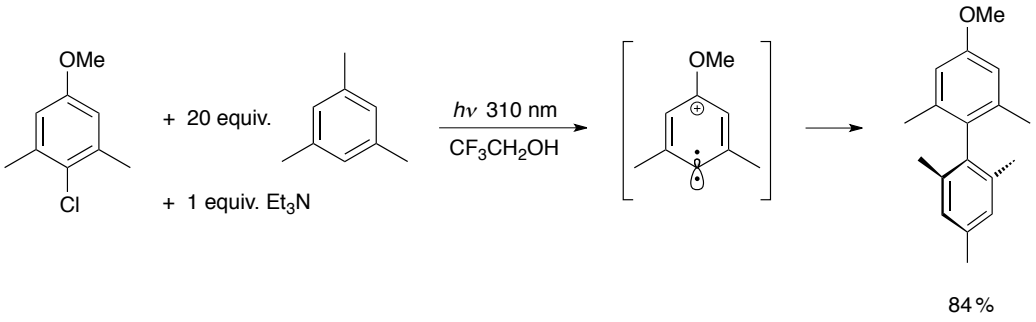

Scheme 6.2. Preparation of a biaryl by photoinduced Ar–Cl bond cleavage and trapping of the putative triplet aryl cation by an arene.[?]

6.3 Isolation of Phenyl Carboranes from the C–F Activation of Fluorobenzene

The statement that fluorobenzene is only inert, but not stable towards silylium ions provokes the question: How much heat—and for how long—does it take to overcome the activation barrier to fluoride transfer? A first answer to this issue came from a study of the reactivity of Et_3Si–carborane species in fluorobenzene.*

Heating a fluorobenzene solution of $[Et_3Si(X)][CHB_{11}Cl_{11}]$ ([**68**][$CHB_{11}Cl_{11}$], X = PhF or Et_3SiH)[175] to 80 °C for several hours, followed by the addition of hexane, afforded a crystalline colorless solid consisting of two Ph–$CHB_{11}Cl_{11}$ isomers, as inferred from ^{1}H, ^{13}C and ^{11}B NMR spectra (Scheme 6.3). X-ray-crystallographic analysis of one of the products and NMR studies of samples partially enriched in each isomer made it possible to identify them as 7- and 12-Ph–$CHB_{11}Cl_{11}$ (**69a,b**). Full characterization was achieved by MS, IR, and 2D NMR experiments (Table 6.1). The detective work it took to disentangle the spectroscopic data is described in the experimental part. In the reaction mixture, additional small amounts of 2- and 4-fluorobiphenyl were detected by GC–MS, which probably stem from attack of the incipient phenyl cation by fluorobenzene rather than the carborane.

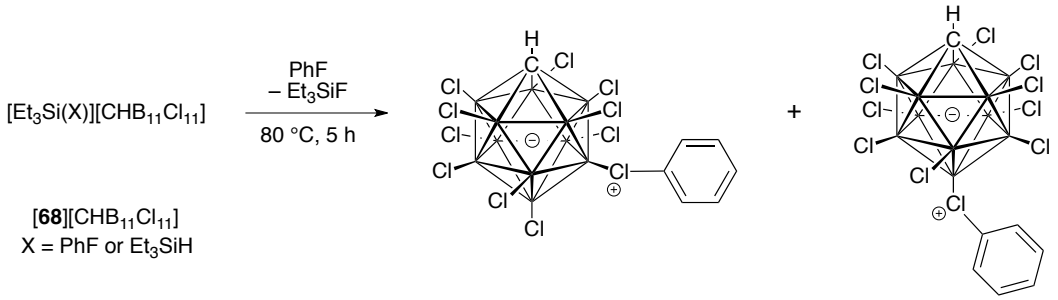

Scheme 6.3. Formation of phenyl carboranes **69** from the activation of fluorobenzene by **68**$^{+}$.

*The observation that $[Et_3Si(X)][CHB_{11}Cl_{11}]$ reacts with fluorobenzene and the elucidation of the crystal structure of 7-Ph-$CHB_{11}Cl_{11}$ are results from Dr. Christos Douvris and Dr. Nathanael P. Fackler from the group of Prof. Christopher A. Reed. Full characterization of the phenyl carboranes as well as subsequent reactivity studies were pursued at the University of Zurich in a collaboration with Prof. Reed. Fluoroarene activation by the (dixylylphenyl)dimethylsilylium ion was discovered independently at the University of Zurich.

Table 6.1. ^{1}H and ^{13}C{^{1}H} NMR data of **69**. 500 MHz (^{1}, 300 K, CD_2Cl_2 solution, C*H*DCl_2 = 5.32 ppm, *C*D_2Cl_2 = 54.0 ppm. Aromatic ^{1}H signals are multiplets, br = broad signal

	69a		**69b**	
	^{1}H	^{13}C	^{1}H	^{13}C
carborane CH	3.49 br	48.6 br	3.65 br	48.6 br
C_{ipso}	–	127.2	–	127.5
C_{ortho}	7.87–7.83	132.1	7.82–7.79	132.2
C_{meta}	7.72–7.67	133.3	7.67–7.63	133.1
C_{para}	7.83–7.78	135.1	7.79–7.75	134.9

The C–F activation hinges upon the use of the extremely weakly coordinating $CHB_{11}Cl_{11}^{-}$ counterion. Silylium-like species Et_3Si–Y with more nucleophilic carboranes (Y = $CHB_{11}H_5Cl_6^{-}$ and $CHB_{11}H_5Cl_6^{-}$)[75, 78] did not abstract fluoride from fluorobenzene under the conditions given in Scheme 6.3. The enhanced silyl Lewis acidity provided by the $CHB_{11}Cl_{11}^{-}$ anion seems to be crucial in terms of reaction kinetics.

A colorless single crystal of the composition **69a** · C_6H_5F was obtained from fluorobenzene–hexane at room temperature. X-ray crystallography revealed that the phenyl ring is bound to one of the lower-belt chlorine atoms of the carborane anion (Figure 6.2).

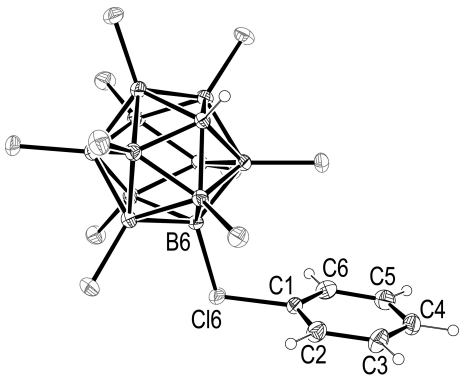

Figure 6.2. X-ray crystal structure of **69a** in **69a** · 0.5 C_6H_5F (30 % displacement ellipsoids, solvent molecule omitted for clarity.

The distances Cl6–C1 and B6–Cl6 are 1.7987(15) Å and 1.854(17) Å, respectively, and the B6-Cl6-C1 angle is 109.65(7)° (Table 6.2). These values can be compared to standard covalent C_{aryl}–Cl 1.74 Å,[176] and carborane B–Cl 1.77 Å distances as well as angles recently observed in dicoordinated chloronium species like Me_2Cl^+/Et_2Cl^+ and $(Me_3Si)_2Cl^+$ (central angles ranging from 102°/106° to 119°), respectively.[177, 178] The structural features in **69a** are thus consistent with mainly covalent B6–Cl6 and Cl6–C1 interactions and a pronounced chloronium ion character. The phenyl ring shows a slightly opened C2-C1-C6 angle but no significant distortions.

Table 6.2. Selected distances (Å) and angles (°) for the X-ray structure of **69a** and the calculated (B98/TZVP) structure **69a**-*syn*.

Parameter	Expt.	Cald.	Parameter	Expt.	Calcd.
B6–Cl6	1.854(2)	1.884	C6–C1	1.375(2)	1.388
Cl6–C1	1.799(2)	1.798	B6-Cl6-C1	109.65(7)	112.18
C1–C2	1.372(2)	1.388	Cl6-C1-C2	117.3(1)	117.28
C2–C3	1.386(2)	1.398	Cl6-C1-C6	116.8(1)	117.28
C3–C4	1.387(3)	1.398	C2-C1-C6	125.9(2)	125.25
C4–C5	1.382(2)	1.398	$\Sigma\angle$(C1)	360.0(1)	359.82
C5–C6	1.390(2)	1.398			

Calculations on **69** at the (B98/TZVP) level of theory were in agreement with the experimental findings and indicated a small energy difference between the two regioisomers. The two lowest-energy conformers of **69a** are of C_s symmetry, differing in the orientation of the phenyl moiety with respect to the carborane CH apex (**69a**-*syn*, **69a**-*anti*, Figure 6.3). The **69a**-*syn* conformer, corresponding to the structure found in the crystal, is only ΔE_{ZPE} = 2.45 kJ mol^{-1} (ΔH = 0.11 kJ mol^{-1}) higher in energy than **69a**-*anti*. On the basis of this small difference, it seems likely that packing forces determine the geometry that is adopted in the crystal. There is a good agreement between the observed and calculated structure, in particular with regard to the distances and angles around Cl6 (Table 6.2). For **69b**, two low-energy conformers of C_s symmetry were found that differ in the conformation of the phenyl ring with respect to the lower-belt chlorine atoms (**69b**-staggered, **69b**-eclipsed). The stag-

gered geometry is slightly higher in energy (ΔE_{ZPE} = 3.06 kJ mol^{-1}, ΔH = 0.60 kJ mol^{-1}) than the eclipsed form, but again the difference is small. The regioisomers **69a** and **69b** are close in energy, with **69a**-*anti* being ΔE_{ZPE} = 8.44 kJ mol^{-1} (ΔH = 8.45 kJ mol^{-1}) less stable than **69b**-eclipsed.

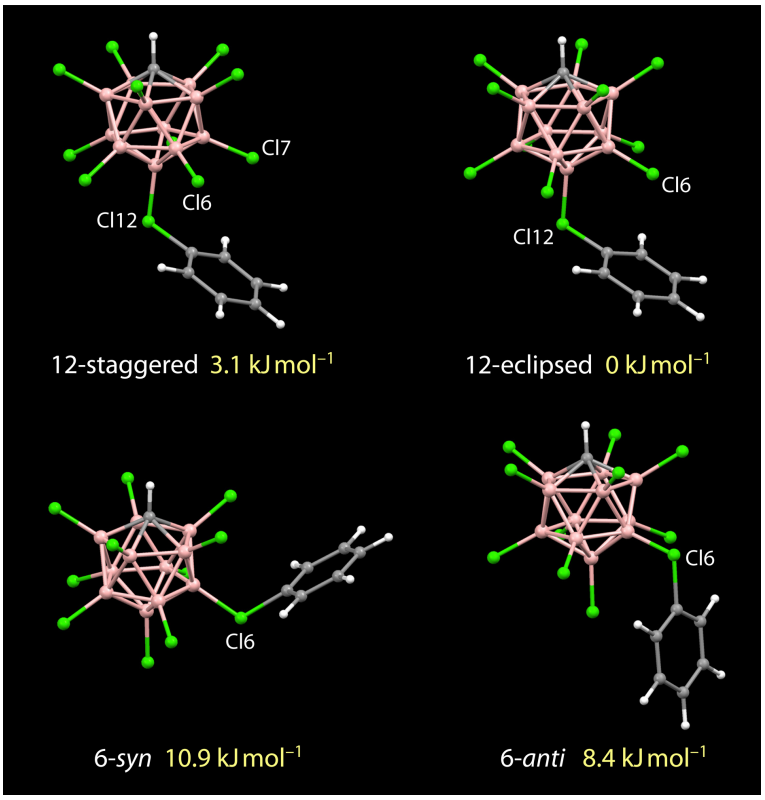

Figure 6.3. Calculated structures (B98/TZVP) of **69**.

6.4 Reactivity of the Phenyl Carboranes

Reactivity studies showed that the Ph–$CHB_{11}Cl_{11}$ isomers are inert in solution, but can act as phenylating agents towards nucleophiles. NMR spectra of CD_2Cl_2 and $CDCl_3$ solutions with varying ratios of **69** remained unchanged over more than two weeks suggesting neither isomerization nor dissociation into ions at room temperature. These findings are consistent with a reactivity which is lower than that of alkyl carboranes and comparable to that of

the diphenylchloronium ion.[77, 179] The decreased electrophilicity as compared to CH_3–carborane species can be rationalized in terms of a less favorable trajectory of attack and the stronger C–Cl bond in **69**.

The reactivity of **69** towards nucleophiles was tested by treating 1 mg of the isomer mixture with a 2–3-fold excess of a nucleophile in 1 mL of toluene (Scheme 6.4, Table 6.3). The mixtures were heated to 50 °C for one hour and analyzed by mass or NMR spectroscopy. When no nucleophile was added, no reaction took place under the same conditions, as evidenced by ^{1}H and ^{11}B NMR spectroscopy of a toluene-d_8 solution of **69**.

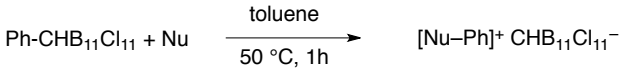

Scheme 6.4. Phenylation of nucleophiles by **69**.

With nitrogen nucleophiles, clean phenylation was observed for triethylamine, pyridine, and 4,4'-bipyridyl; furthermore, free $CHB_{11}Cl_{11}^{-}$ was detected as the only anionic species (analysis by positive and negative ESI MS). On the other hand, no reaction occurred with 2,2'-bipyridyl.

Table 6.3. Attempted phenylation of N, P and O nucleophiles by **69**.

Nucleophile	Expected Product	Expected *m/z*	Observed *m/z*
Et_3N	$[Et_3N–Ph]^+$	178.16	178.2
	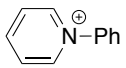	156.08	156.2
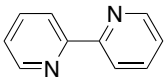	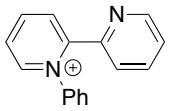	233.11	233.2
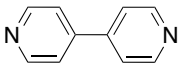	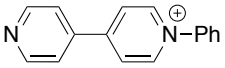	233.11	157.2 (st. mat.)
PPh_3	$[Ph_3P–Ph]^+$	339.13	339.1
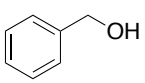	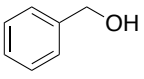	184.09	182.1 (3 isomers)

Thus triethylamine, although usually considered a slow nucleophile, seems to be reactive enough to attack **69** under the conditions chosen. In the pyridine series, the two compounds with unhindered nitrogen atoms are also reactive enough. However, in the case of 2,2'-bipyridyl, the nucleophilicity of the nitrogen atoms is significantly reduced, probably due to steric factors.

Triphenylphosphine was phenylated cleanly at the phosphorus atom. Both $[PPh_4]^+$ and $CHB_{11}Cl_{11}^-$ were detected by ESI MS. In addition, the reaction was repeated in an NMR spectrometer, where the formation of $[PPh_4]^+$ was confirmed based on its increasing ^{31}P NMR signal.

The situation became more puzzling with oxygen nucleophiles. H_2O, EtOH, BuOH, and $PhCH_2OH$ were tested as nucleophiles. Only with $PhCH_2OH$, signals of a neutral product could be detected by GC–MS. However, instead of m/z 184.1 for the expected product $PhCH_2OPh$, three signals associated with m/z 182.1 appeared in the gas chromatogram. According to an MS database search, the mass spectra matched best with those for *ortho*-, *meta*- and *para*-benzyltoluene.

The following reaction sequence can account for the formation of benzyltoluene isomers (Scheme 6.5): First the hydroxy group attacks the *ipso* carbon atom of **69** and is phenylated. The intermediate formed is an oxonium ion that carries a Brønsted-acidic hydrogen atom, but is also Lewis-acidic at the benzylic carbon atom. In principle, there is a second equivalent of $PhCH_2OH$ in the reaction mixture that could attack now, but it is not

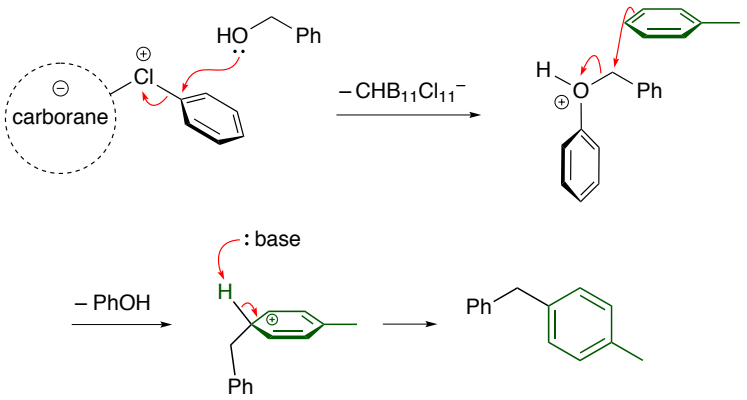

Scheme 6.5. Putative mechanism of formation of the benzyltoluene products.

likely that another molecule of it is in close proximity to the oxonium ion just after the phenylation step. Thus it is the relative reactivity of the solvent toluene towards the two electrophilic sites, $H^{\delta+}$ and $C^{\delta+}$, that determines the outcome of the reaction. It appears that attack at the carbon atom is the favored path. Deprotonation of the Wheland intermediate by either phenol that has just formed or another molecule of toluene then affords benzyltoluene. The final proton sink of the reaction is the additional equivalent of $PhCH_2OH$. In the proposed reaction mechanism, one equivalent of phenol is formed, and one should be able to detect it by the GC–MS. However, no corresponding peak was observed. A possible explanation for this is the fact that phenol is quite volatile (it sublimates at room temperature and atmospheric pressure) and is knonw to be difficult to observe by gas chromatography.

If the mechanism shown in Scheme 6.5 is the favored path for the reaction of **69** with alcohols RCH_2OH, one would expect RCH_2-tolyl isomers, phenol, protonated alcohol, and $CHB_{11}Cl_{11}^-$ as the products (Scheme 6.6). Of these molecules, at least the liberated carborane should be detectable. Indeed, $CHB_{11}Cl_{11}^-$ was the only anionic species detectable when the reactions with H_2O, EtOH, BuOH and $PhCH_2OH$ were analyzed by negative ESI MS.

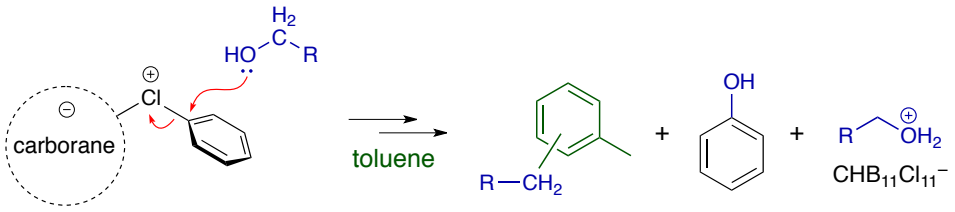

Scheme 6.6. Proposed general reactivity of **69** towards alcohols in toluene.

Different mechanisms can be discussed for the above phenylation reactions. In principle, one could imagine an S_N1-like process in which dissociation of **69** into ions is followed by attack of Ph^+ by the nucleophile (Scheme 6.7). However, the observation that $CHB_{11}Cl_{11}^-$ is only liberated in the presence of a nucleophile far better than toluene is not consistent with a unimolecular rate-limiting step. Two S_N2-like alternatives appear more reasonable: In the interchange mechanism, direct substitution of the carborane by the nucleophile takes place (6.7 b), and in the associative process, formation of a Meisenheimer

intermediate precedes the displacement of the carborane (6.7 c). A fourth possibility would be initial attack of the chlorine atom by the nucleophile to afford a λ^3-chlorane, which rearranges to give free anion and the phenylated nucleophile (6.7 d). Also this mechanism seems unlikely because migration of the boron cage would also be expected to some extent, but carboranes other than $CHB_{11}Cl_{11}^-$ were not observed.[180] Processes b) and c) thus represent plausible mechanistic scenarios, however, the experimental data do not allow a conclusion as to which of it is at work.

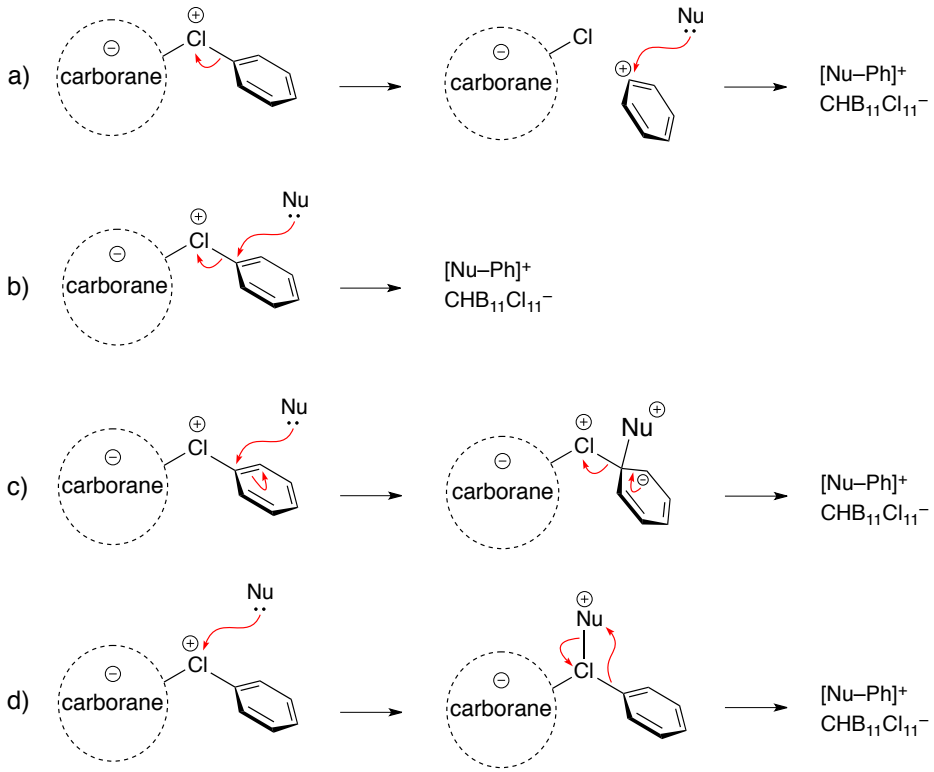

Scheme 6.7. Possible mechanisms for the phenylation of nucleophiles by **69**: a) dissociative, b) interchange, c) associative via Meisenheimer intermediate, d) associative via λ^3-chlorane intermediate.

6.5 Fluoroarene Activation by a Terphenylsilylium Ion

An extreme fluorophilicity was found for silylium carborane [**27a**][$CHB_{11}Cl_{11}$]. Fluoride transfer from fluorobenzene to silicon takes place within hours at room temperature to give silanes **70** and **71** (Scheme 6.8). Several unidentified minor by-products were observed as well, probably because equimolar amounts of highly reactive, Brønsted-acidic Wheland intermediates are formed. Addition of the sterically hindered base P(*o*-tol)$_3$ as a proton sponge leads to much cleaner reactions that afford **70** and **71** 27 % and 30 % yield based on ^{1}H NMR integrals. Pure samples of these compounds were obtained by preparative HPLC and fully characterized (see experimental part). As opposed to the fluorobenzene activation by [**68**][$CHB_{11}Cl_{11}$], only the xylyl rings or solvent molecules are phenylated in the case of [**27a**][$CHB_{11}Cl_{11}$]; the carborane anion remains unchanged, and the phosphine base is isolated only as [HP(*o*-tol)$_3$]$^+$ but not [PhP(*o*-tol)$_3$]$^+$.

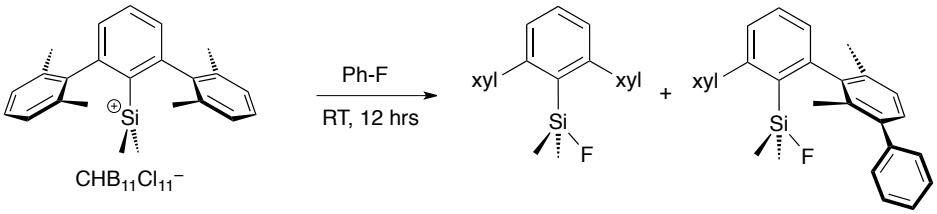

Scheme 6.8. C-F acitvation of fluorobenzene by **27a**$^+$.

The reactions of **68**$^+$ and **27a**$^+$ were carried out in an environment of exceptional low nucleophilicity, where one could imagine that they exhibit higher S_N1 character than previously studied systems. To address this important question regarding the dissociative nature of silylium-mediated C_{aryl}-F activations, the decay of **27a**$^+$ in different fluoroarene solvents was monitored by ^{1}H NMR spectroscopy at 300 K (Figure 6.4). In fluorobenzene, the disappearance of the cation followed pseudo first-order kinetics with a half-life of $t_{1/2}$ = 88 min (Figure 6.5). $t_{1/2}$ is independent of the amount of phosphine added (0–12 equivalents) and the carborane counterion ($CHB_{11}Cl_{11}^-$, $CHB_{11}H_5Br_6^-$). In 4-fluorotoluene, [**27a**][$CHB_{11}Cl_{11}$] decayed with $t_{1/2}$ = 52 min. In 1,4-difluorobenzene, no reaction took

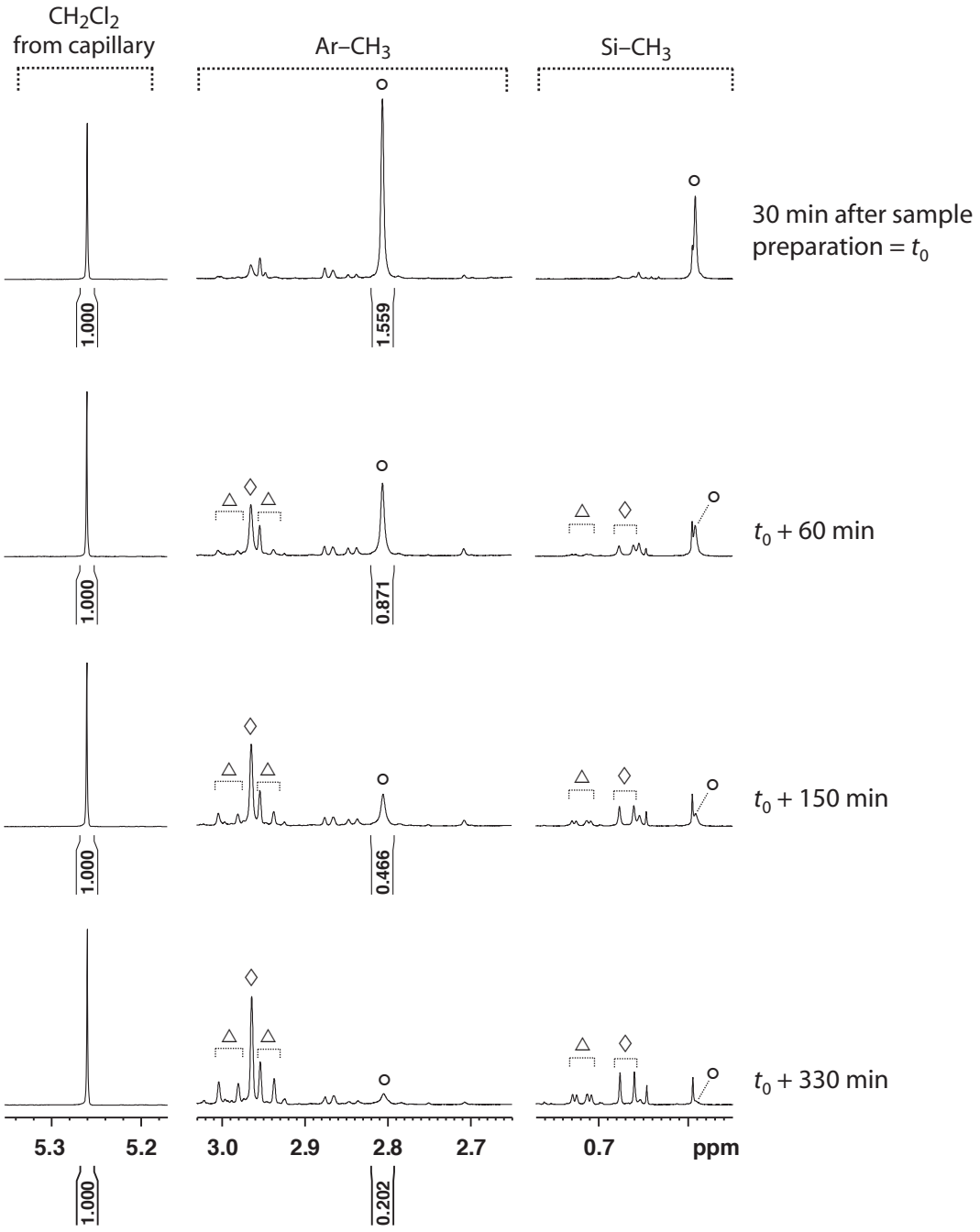

Figure 6.4. Fluoride abstraction from fluorobenzene by cation **27a**$^+$, as monitored by ^{1}H NMR spectroscopy. Conditions: 500 MHz, 315 K, 4.5 mg cation + 3.8 mg P(*o*-tol)$_3$ in 0.6 mL fluorobenzene, addition of a capillary with C_6D_6 + CH_2Cl_2 for locking/shimming and integration, C_6HD_5 = 7.16 ppm. ○ = cation, ◊ = **70**, △ = **71**.

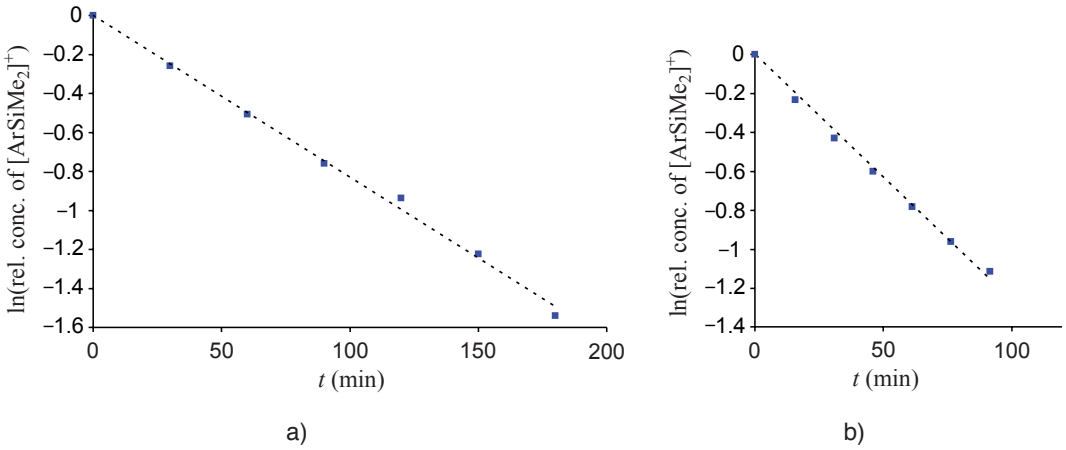

Figure 6.5. Decay of **27a**$^+$ in a) fluorobenzene and b) 4-fluorotoluene. The linearity of ln([**27a**$^+$]$_{rel}$) vs *t* indicates pseudo-first order kinetics.

place; the concentration of cation remained constant over 10 h. The reactivities 4-MeC_6H_4F > C_6H_5F > 4-FC_6H_4F suggest that fluoride abstraction proceeds via a transition state that is lowered by electron-donating substituents, *i.e.*, in which the inital fluoroarene possesses at least some aryl cationic character.[181]

In the calculated transition state for **27a**$^+$ + PhF → **71**, fluoride transfer to silicon is accompanied by nucleophilic attack on C_{ipso} by the xylyl π system (Figure 6.6). While the

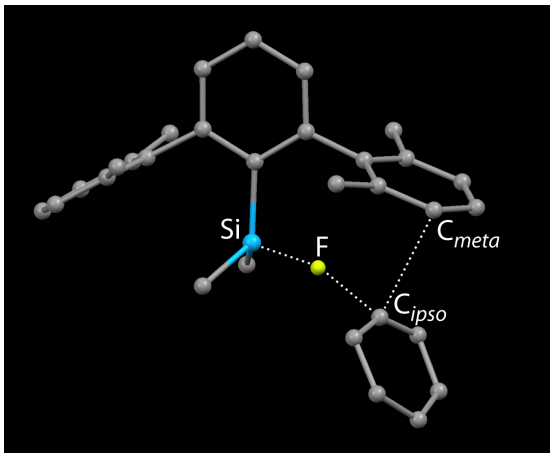

Figure 6.6. Calculated transition state (B98/DZ(2df,pd9)) for the reaction **27a**$^+$ + C_6H_5F → **71**. Distances: Si–F 1.680 Å, F–C_{ipso} 2.189 Å, C_{ipso}–C_{meta} 2.849 Å.

C_6H_5 moiety shows angle distortions typical of aryl cationic species (C_{ortho}-C_{ipso}-C_{ortho} 139°),[159] it can not be regarded as a free phenyl cation.

Computational analysis of this reaction process at the MP2/DZ(2df,pd)//B98/DZ(2df,pd) level of theory predicted ΔH_{calc} = 85.77 kJ mol^{-1} (100.17 kJ mol^{-1}, B98/DZ(2df,pd)), which matches well with the experimental values, ΔH_{exptl} = 82 kJ mol^{-1} and ΔS_{exptl} = −24 J mol^{-1} K^{-1}, determined with an Eyring plot (Figure). These numbers reflect the strong C_{aryl}–F bond that has to be broken and are in line with a reaction in which two or more molecules combine to form a transition state.

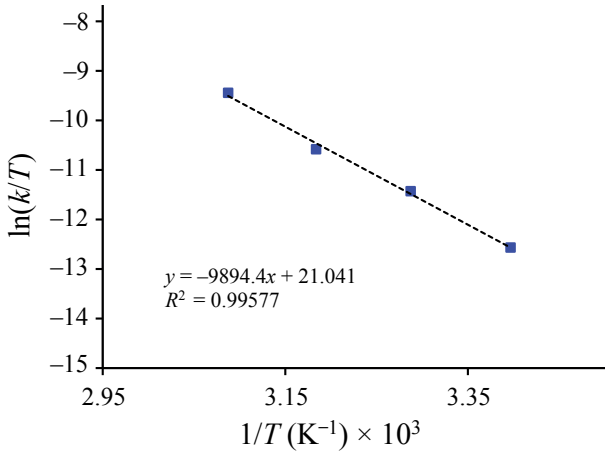

Figure 6.7. Eyring diagram for the reaction **27a** + C_6H_5F → **70**+ **71**.

At first sight it was not evident why terphenylsilyl cations of the type **27**$^+$ should show a higher electrophilicity than silylium-like species such as **68**$^+$. In view of the observed shielding of the ^{29}Si nucleus and the solid-state structure of **27a**$^+$, one would expect an even lower reactivity. The exceptional behavior of **27a**$^+$ can be understood in terms of the Curtin–Hammett principle.[182, 183] As could be concluded from NMR studies (Sections 3.4 and 2.7), the cation exhibits a dynamic equilibrium among four degenerate C_1 conformers with intramolecular π stabilization as well as solvent- and possibly anion-coordinated forms. The small energy barrier of <60 kJ mol^{-1} for all interconverion processes makes conformations of higher energy easily accessible, and it is likely that in a form other than the C_1 ground state the reactivity of **27a**$^+$ is significantly increased (Scheme 6.9). As soon

as the $SiMe_2$ fragment leaves its resting state, it becomes highly electron-deficient because of diminished π electron donation and the electron-withdrawing effect of the central benzene ring. This interpretation is also in line with the computational results (Section 2.3) that suggest a much more deshielded silicon nucleus in conformations deviating from the preferred geometry. Attack of the formal Si^+ by fluorobenzene is now associated with a decreased activation barrier and proceeds faster than with trialkylsilylium-like cations.

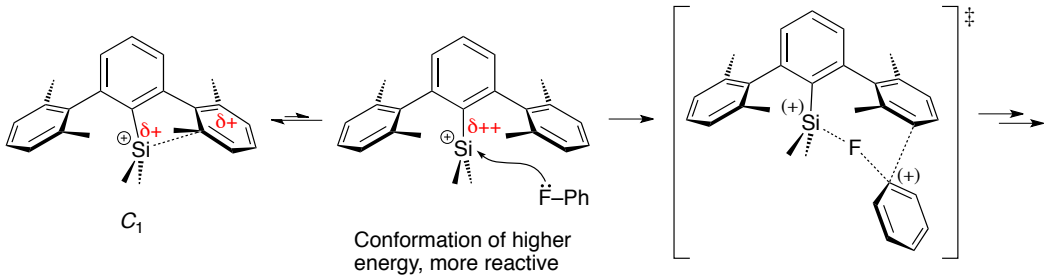

Scheme 6.9. Facilitated fluorobenzene activation by **27a**$^+$ in a conformation of higher reactivity.

6.6 Development of a Friedel–Crafts Arylation Protocol

The generation of incipient Ph^+ by **68**$^+$ and **27a**$^+$ paved the way for an application of aryl cations as synthetic intermediates. Carbocations play a crucial role in Friedel–Crafts reactions, in which they act as electrophiles towards aryl π systems. This kind of C–C bond formation has a long history and is well-established in the case of alkylation and acylation reactions.[184] An extension to analogous arene–arene couplings has not been accomplished because of the difficulty to prepare aryl cations in media of low nucleophilicity.[185]

Based on the observed phenylation of **27a**$^+$ to give **71**, the development of a Friedel–Crafts *arylation* protocol was envisioned. The strategy was to start from a fluorophenyl-substituted arene, from which a silyl cation would abstract fluoride in a first step (Scheme 6.10). The formal phenyl cation is then attacked by the arene π system, leading to a Wheland intermediate, and subsequent deprotonation by a base affords the cyclized product.

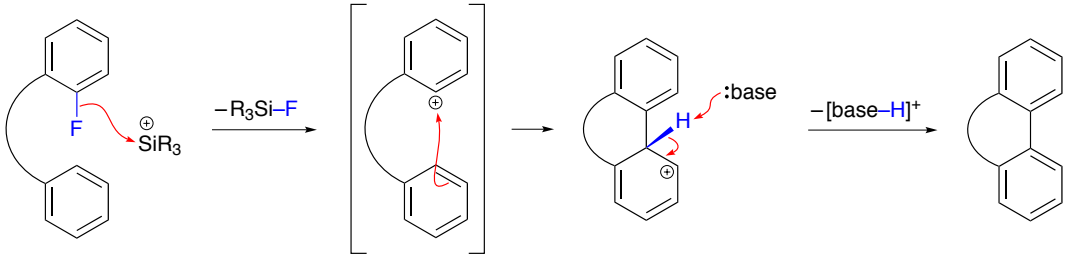

Scheme 6.10. Intramolecular Friedel–Crafts arylation initiated by silylium-mediated fluoride abstraction.

1-(2-Fluorophenyl)naphthalene (**72**) was chosen as a model substrate for the Friedel–Crafts arylation. It is synthetically readily accessible from 2-fluorophenylboronic acid and 1-bromonaphthalene,[186] and the expected product, fluoranthene (**73**), is commercially available, thus facilitating reaction control and identification by GC–MS and ^{1}H NMR spectrocopy.

A main challenge of the project was to find a silyl cation/Brønsted base pair that would bring about the desired cyclization but not form an inactive Lewis acid–Lewis base adduct. The combination of $i\mathrm{Pr_3Si^+}$ with P(*o*-tol)$_3$ turned out to fulfill this requirement. Both the formal $\mathrm{Si^+}$ and the phosphorus atom are shielded by relatively bulky substituents so that a direct interaction is thwarted; on the other hand, the silyl Lewis acidity towards fluorine and reaction with the small proton were not suppressed.

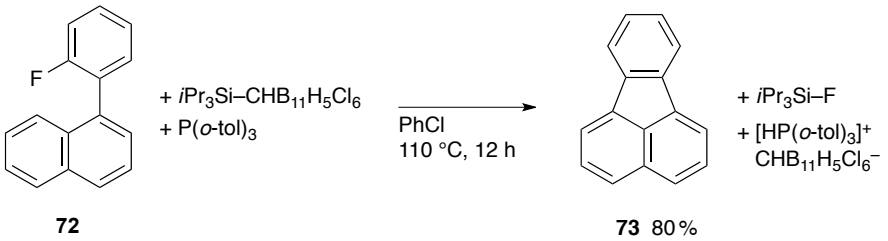

Scheme 6.11. Formation of fluoranthene by fluoride abstraction and intramolecular ring closure.

Heating a mixture of **72**, $\mathrm{Et_3Si–CHB_{11}H_5Cl_6}$ and P(*o*tol)$_3$ in chlorobenzene to 110 °C for 12 hours afforded **73** as the single organic product (Scheme 6.11). It was isolated in 80 % yield after thin-layer chromatography. Moreover, 92 % of the carborane anion could be re-

covered as [Cs][$CHB_{11}H_5Cl_6$] in the work-up. This was an important part of the procedure since the anion represents the most expensive component of the reaction. An unexpected issue was the difficult separation of the product from the phosphine base. P(*o*-tol)$_3$ exhibits an R_f value similar to that of **73**, which caused a slightly reduced yield. Attempts to remove the base in the course of the work-up were not successful, even when 1 M aqueous HCl was used in the extraction. Without addition of the phosphine to the reaction, a black mixture containing several unidentified by-products was obtained, probably due to the presence of highly acidic protonated arenes that caused polymerization.

The preparation of **73** from its fluoro precursor was a proof of principle that silyl Lewis acids can effect an unusual type of Friedel–Crafts chemistry. Further substrates, silyl cations and bases will have to be screened to probe the scope of the procedure. They will most likely allow for milder reaction conditions and an easier isolation of the cyclized product.

6.7 Experimental Part

6.7.1 General

For general reaction conditions and analytical instruments, see Sections 2.9.3 and 2.9.4.

6.7.2 Synthesis of Ph-$CHB_{11}Cl_{11}$ (69)

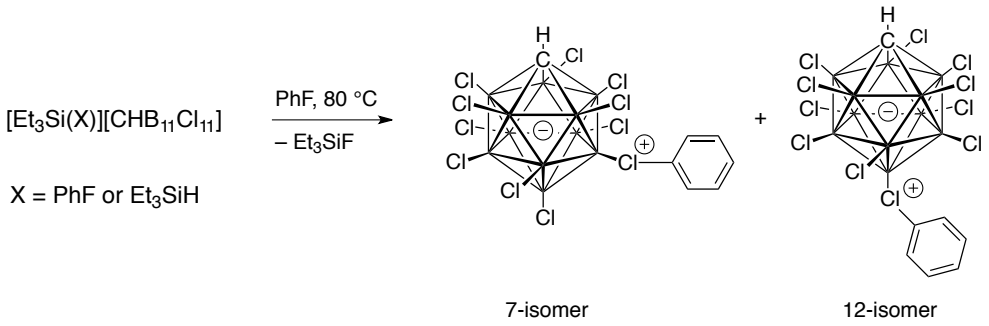

In a glovebox, $[Ph_3C][CHB_{11}Cl_{11}]$ (56.4 mg, 73.7 µmol), fluorobenzene (1.0 mL), and Et_3SiH (10 drops) were placed in a 4 mL glass vial. The vial was closed with a PTFE-lined screw cap and further sealed with PTFE tape and parafilm. It was taken out of the box and heated to 80 °C in an oil bath for 5 hrs. The vial was taken back into the glovebox, and the reaction mixture was transferred to a bigger vial. The reaction mixture was treated with hexane (5 mL) and put into the glovebox freezer overnight (−20 °C). A slightly ocherish crystalline precipitate was obtained. The supernatant was removed with a Pasteur pipet, and the residue was washed with pentane (2 × 2 mL) and dried in a vacuum. ^{1}H NMR analysis of this product showed that it still contained some fluorobenzene. The material was dissolved in CH_2Cl_2 (3 mL), and the solution was evaporated to dryness under reduced pressure. This process was repeated twice, and the residue was dried in a vacuum overnight. A mixture of 7-Ph-$CHB_{11}Cl_{11}$ and 12-Ph-$CHB_{11}Cl_{11}$, now free from fluorobenzene, was obtained in a ratio of 1.3 : 1 as a slightly ocherish powder (35.1 mg, 58.6 µmol, 80 %). Spectra of the mixture are displayed in Figures 6.8–6.10.

Characterization

^{1}H NMR (500 MHz, CD_2Cl_2): 7-Isomer: 7.87–7-83 (m, 2 H, H_{ortho}), 7.83–7.78 (m, 1 H, H_{para}), 7.72–7-67 (m, 2 H, H_{meta}), 3.49 (broad s, 1H, carborane H); 12-Isomer: 7.82–7-79 (m, 2 H, H_{ortho}), 7.79–7.75 (m, 1 H, H_{para}), 7.67–7.63 (m, 2 H, H_{meta}), 3.65 (broad s, 1H, carborane H).

^{13}C{^{1}H} NMR (125 MHz, CD_2Cl_2): 7-Isomer: 135.1 (C_{para}), 133.3 (C_{meta}), 132.1 (C_{ortho}), 127.2 (C_{ipso}), 48.6 (broad, carborane C); 12-Isomer: 134.9 (C_{para}), 133.1 (C_{meta}), 132.2 (C_{ortho}), 127.5 (C_{ipso}), 48.6 (broad, carborane C).

^{11}B NMR (128 MHz, CD_2Cl_2):

7-Isomer: -2.9, -8.2 to -14.4 (overlapping signals); 12-Isomer: -4.8, -11.0, -12.2.

IR (ATR): (isomer mixture) 3098w, 3015s, 1485m, 1468m, 1454m 1327w, 1297w, 1273w, 1119s, 1007s, 975s, 956s, 891m, 763s, 738s, 688m, 668s, 661s, 580m, 531s, 519s, 488s, 466s.

MS (EI): (isomer mixture) 598.8 (86, $M^{\cdot+}$), 112.0 (11, $PhCl^{\cdot+}$), 77.0 (100, Ph^{+}).

HRMS–EI (isomer mixture): $M^{\cdot+}$ calculated for $C_7H_6{}^{10}B_6{}^{11}B_5Cl_{11}$: 589.8285; found: 589.8280.

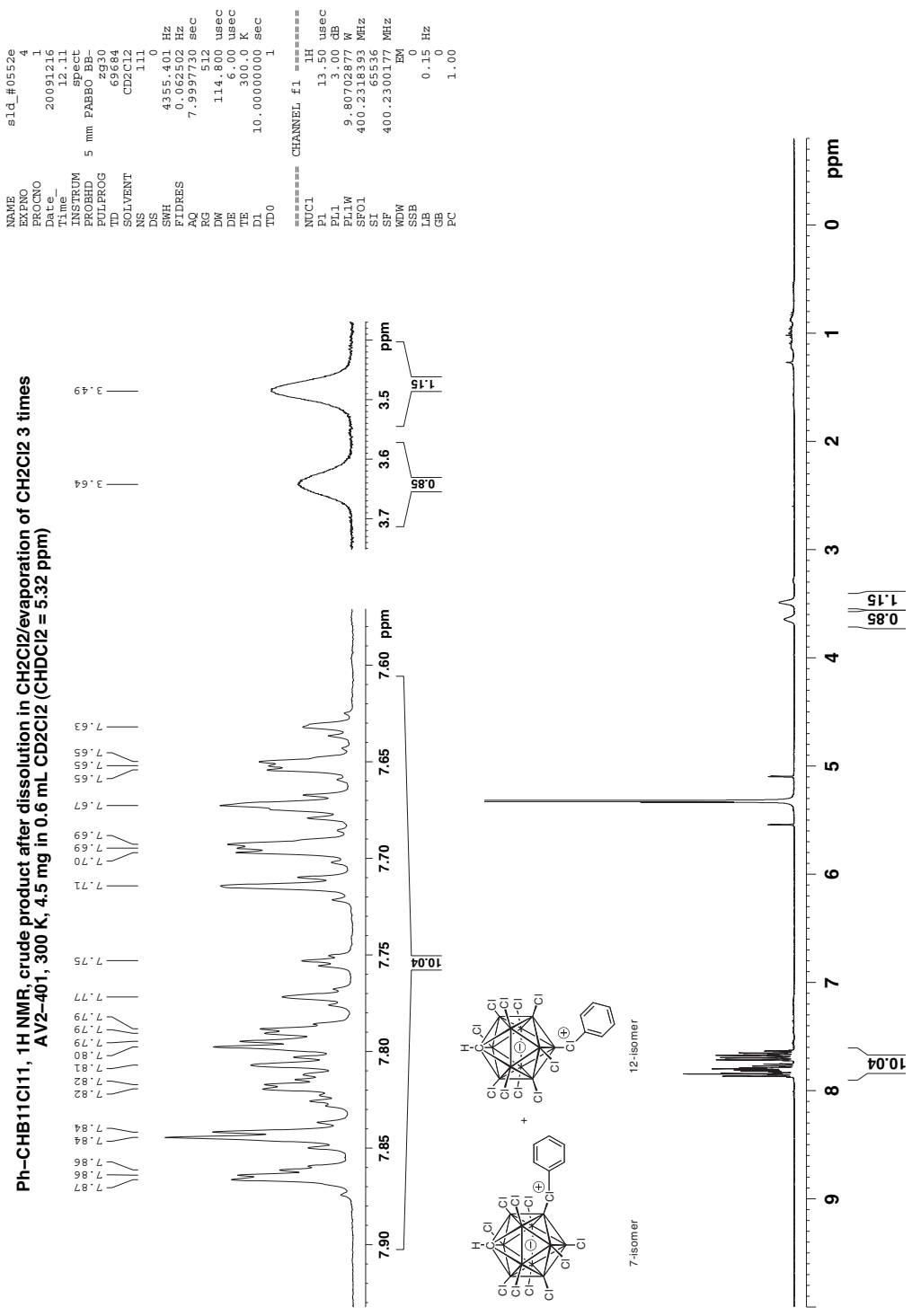

Figure 6.8. ^{1}H NMR spectrum of 7-Ph-$CHB_{11}Cl_{11}$ (major) and 12-Ph-$CHB_{11}Cl_{11}$ (minor). Conditions: 400 MHz, 300 K, 4.8 mg in 0.6 mL CD_2Cl_2 (solvent residual peak set to 5.32 ppm).

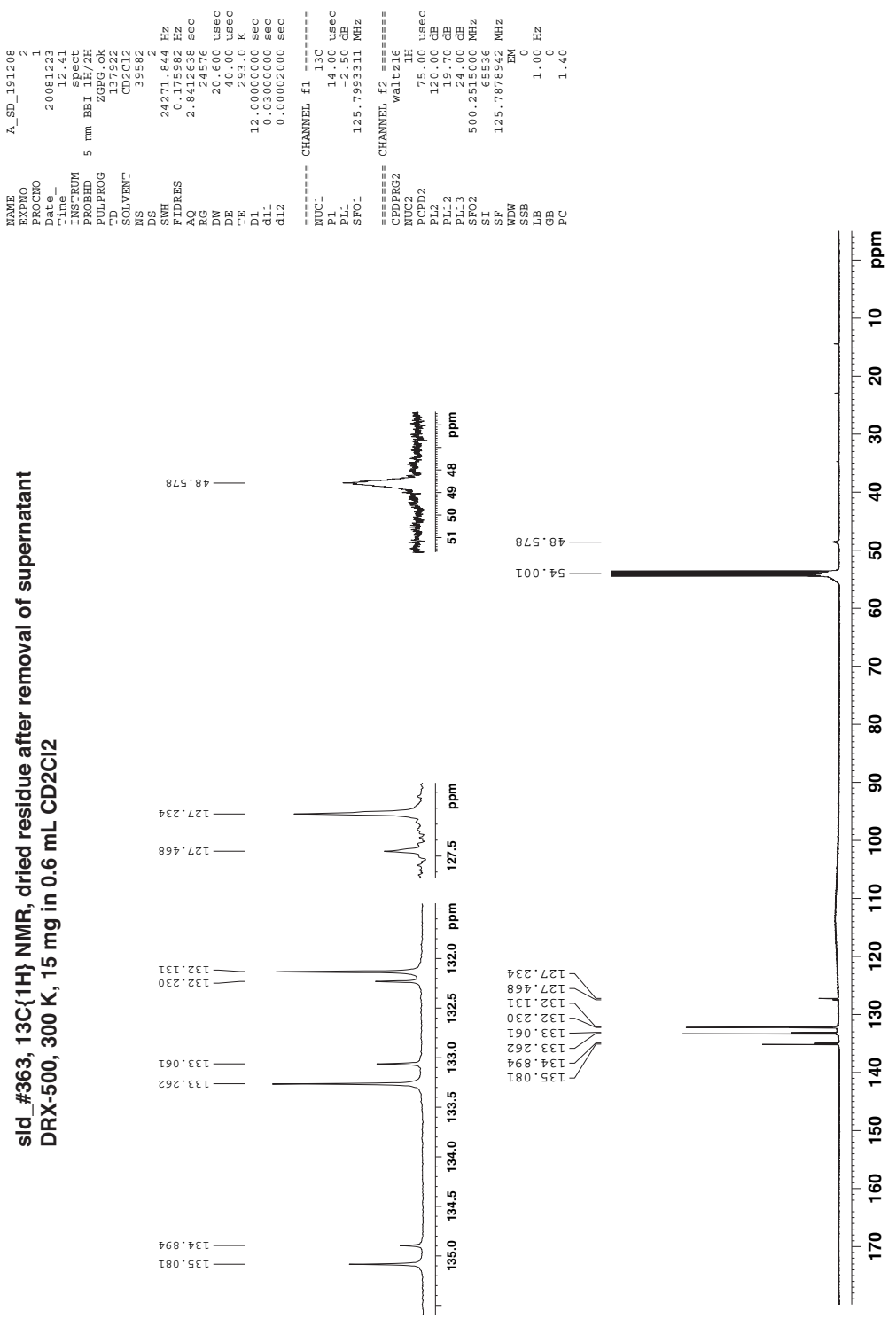

Figure 6.9. $^{13}C\{^{1}H\}$ NMR spectrum of 7-Ph-$CHB_{11}Cl_{11}$ (major) and 12-Ph-$CHB_{11}Cl_{11}$ (minor). Conditions: 125 MHz, 300 K, 15 mg in 0.6 mL CD_2Cl_2 (solvent peak set to 54.00 ppm).

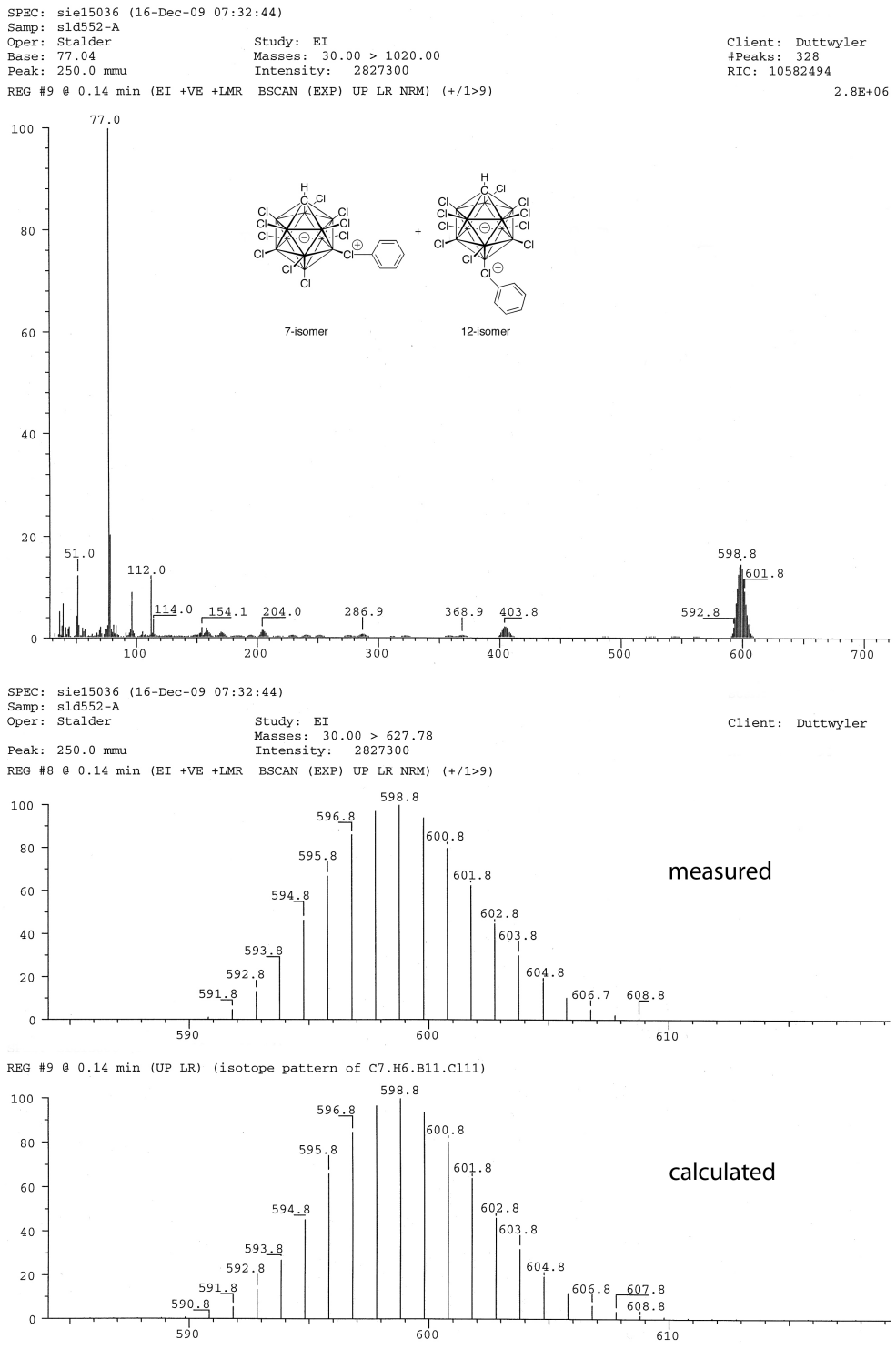

Figure 6.10. Mass spectrum (EI) of 7-Ph-$CHB_{11}Cl_{11}$ (major) and 12-Ph-$CHB_{11}Cl_{11}$ (minor). Top: Mass range *m/z* 30–700; bottom: measured and calculated isotope patterns for $M^{\cdot+}$.

X-ray Crystallography

Colorless prisms of the 7-isomer suitable for X-ray diffraction were obtained from fluorobenzene–hexane (summary of analysis in Table 6.4). There are one C_6H_5-$CHB_{11}Cl_{11}$ and half a molecule of disordered fluorobenzene present in the asymmetric unit of the unit cell (Figure 6.11), with the fluorobenzene being located at the inversion center. The H/F disordered site occupancy ratios are 87 %/13 %, 84 %/16 %, and 79 %/21 % for the half molecule of fluorobenzene.

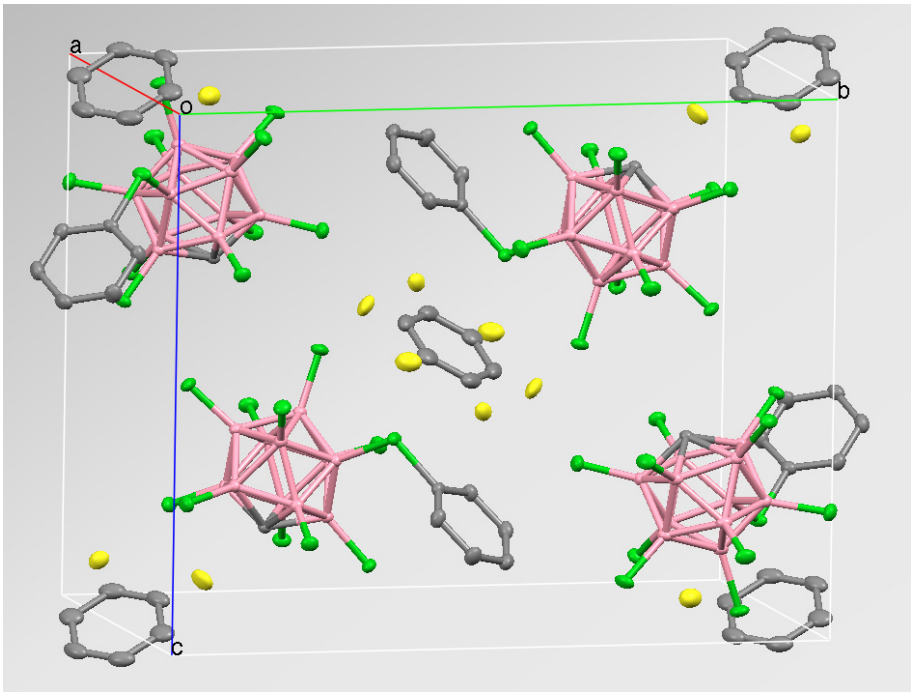

Figure 6.11. Unit cell in the crystal structure of Ph-$CHB_{11}Cl_{11}$·0.5 C_6H_5 F (50 % displacement ellipsoids).

Table 6.4. Summary of the X-ray diffraction analysis for 7-Ph-$CHB_{11}Cl_{11}$.

Temperature	100(2) K	
Wavelength	0.71073 Å	
Crystal system	Monoclinic	
Space group	P2(1)/c	
Unit cell dimensions	a = 8.9924(2) Å	$\alpha = 90°$
	b = 18.8302(5) Å	$\beta = 94.4850(4)°$
	c = 14.6665(4) Å	$\gamma = 90°$
Volume	2475.85(11) $Å^3$	
Z	4	
Density (calculated)	1.736 g/cm^3	
Absorption coefficient	1.240 mm^{-1}	
F(000)	1260	
Crystal size	0.20 x 0.19 x 0.12 mm^3	
Theta range for data collection	1.76 to 30.03°.	
Index ranges	-12<=h<=12, -26<=k<=26, -20<=l<=20	
Reflections collected	38102	
Independent reflections	7248 [R(int) = 0.0342]	
Completeness to theta = 30.03∞	100.0 %	
Absorption correction	Semi-empirical from equivalents	
Max. and min. transmission	0.8614 and 0.7851	
Refinement method	Full-matrix least-squares on F^2	
Data / restraints / parameters	7248 / 55 / 322	
Goodness-of-fit on F^2	1.034	
Final R indices [I>2sigma(I)]	R1 = 0.0287, wR2 = 0.0665	
R indices (all data)	R1 = 0.0371, wR2 = 0.0708	

6.7.3 Partial Separation and Identification of the Isomers

On the basis of the ^{1}H and $^{13}C\{^{1}H\}$ NMR spectra of the product mixure, it was assumed that two isomers of Ph-$CHB_{11}Cl_{11}$ had formed. The ^{1}H NMR spectrum contains two carborane C–H resonances as well as signals in the range of 7.9– 7.6 ppm, and the $13C\{^{1}H\}$ NMR spectrum consists of two sets of four signals in the region 135–127 ppm as well as a broad carborane C resonance (Figures 6.8 and 6.9). The spectra give no indication of the presence of a third isomer.

Samples enriched in each of the isomers were obtained from the solvent system dichloromethane–pentane 1:3. 18 mg of a crude sample of the reaction was suspended in 3 mL of this solvent mixture, and the supernatant was separated and evaporated to dryness. ^{1}H and ^{11}B NMR spectra of the undissolved residue and the dried supernatant indicate different ratios of the two isomers, with no measurable equilibration at room temperature over two weeks in dichloromethane-d_2 solution (Figures 6.12 and 6.13).

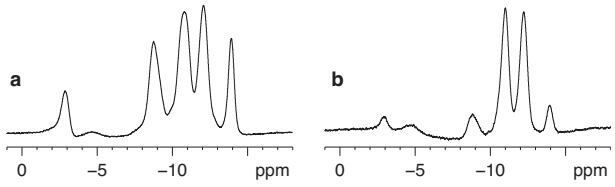

Figure 6.12. ^{11}B NMR spectra of the two fractions of Ph-$CHB_{11}Cl_{11}$ obtained from dichloromethane–pentane 1:3 (128 MHz, CD_2Cl_2); **a** = residue, **b** = dried supernatant.

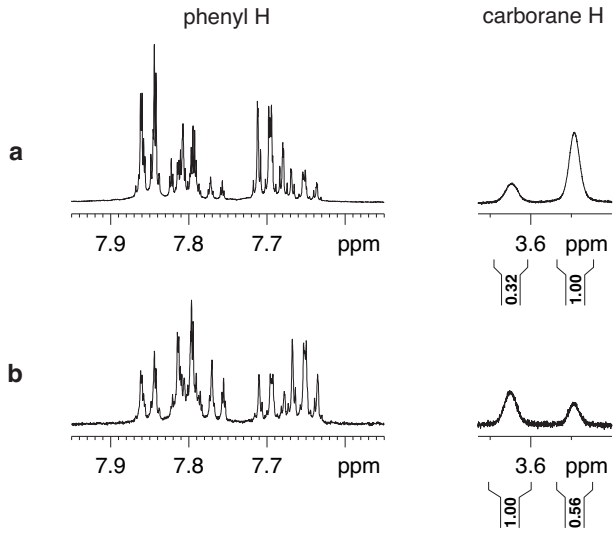

Figure 6.13. ^{1}H NMR spectra of the two fractions of Ph-$CHB_{11}Cl_{11}$ obtained from dichloromethane–pentane 1:3 (500 MHz, CD_2Cl_2); **a** = residue, **b** = dried supernatant.

A clarification on the nature of the dominant isomer in each fraction came from the respective ^{11}B NMR spectra. In the spectrum of the suspension residue, the complicated signals are in agreement with a desymmetrized carborane cage, or, in other words, the presence of mainly the 2- or 7-isomer. Conversely, the spectrum of the dried supernatant looks simpler, and one can imagine that in the absence of the peaks of the other isomer, a spectrum consistent with that of the 12-isomer would result. Difference spectra were plotted to test this hypothesis. The subtraction (**a** – **b**) should afford the signals of only the dominant isomer of the residue, while (**b** – **a**) was expected to reveal the peaks of only the dominant isomer in the supernatant.[†]

The difference spectra show a complicated pattern for the residue and signals qualitatively comparable to those of the free anion $CHB_{11}Cl_{11}^{-}$ for the other fraction (Figure 6.14). Only the 12-isomer, in which the phenyl ring is bound to the apical chlorine atom, can exhibit a spectrum with three peaks as observed for the dominant isomer in the supernatant (-4.8 ppm, -11.0 ppm, -12.2 ppm). In this case, the sets of boron atoms B2–6/B7–11 and B12 each give rise to one signal. On the basis of the crystal structure of the

[†]In practice, the second spectrum is subtracted from the first one in such a way that a reasonable baseline in the difference spectrum is obtained. That is, "(**a** – **b**)" = (**a** – $\frac{\mathbf{b}}{x}$).

7-isomer and the NMR data, it appears likely that the two compounds formed by the reaction of $[Et_3Si(X)][CHB_{11}Cl_{11}]$ with fluorobenzene are the 7- and the 12-isomer (Scheme 2, major/minor inferred from ^{1}H and ^{11}B NMR integrals of the crude product). This conclusion is also in agreement with the general observation that the halogen substituents attached to B7–11 and B12 are the most nucleophilic sites in chlorinated and brominated carboranes.

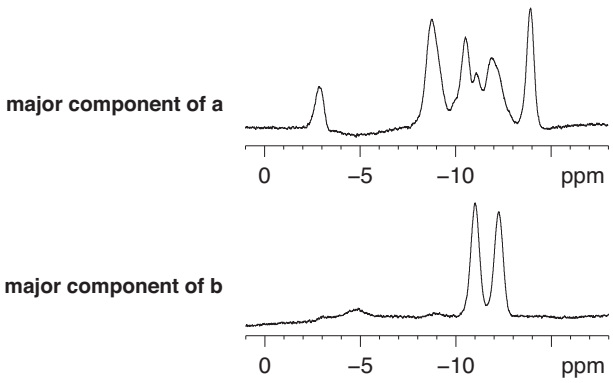

Figure 6.14. ^{11}B NMR spectra of the two isomers of Ph–$CHB_{11}Cl_{11}$, obtained by mutual subtraction of the spectra displayed in Figure 6.13 (128 MHz, CD_2Cl_2). **a** = 7-isomer, **b** = 12-isomer.

Difference plots were then generated from the ^{1}H NMR data shown in Figure 6.13. Based on the coupling patterns and integrals, all signals of the obtained spectra could be interpreted (Figure 6.15). For the 7-isomer, the *ortho*, *para*, and *meta* resonances appear at 7.85, 7.81, and 7.69 ppm, respectively. The respective shifts of the 12-isomer are 7.81, 7.77, and 7.65 ppm. Although the spectra are of higher order, approximate coupling constants $^{3}J \approx 7$–8 Hz and $^{4}J \approx 1$ Hz can be inferred.

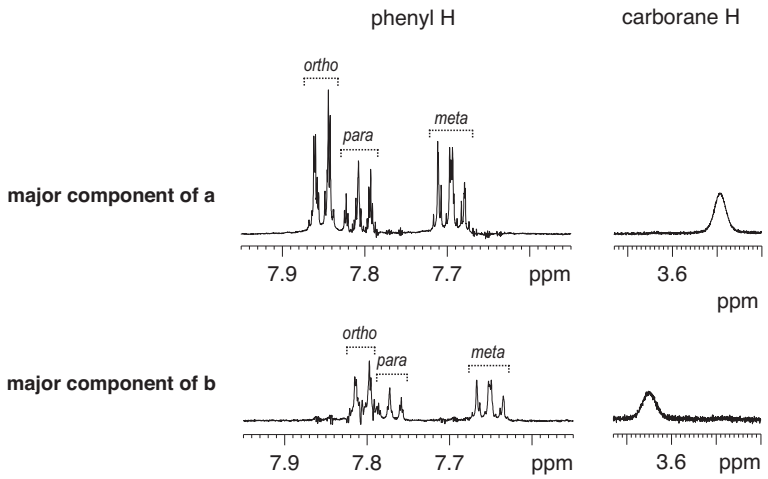

Figure 6.15. ^{1}H NMR spectra of the two isomers of Ph–$CHB_{11}Cl_{11}$, obtained by mutual subtraction of the spectra displayed in Figure 6.13 (500 MHz, CD_2Cl_2). **a** = 7-isomer, **b** = 12-isomer.

Two-dimensional ^{1}H/^{13}C NMR measurements are in full agreement with the conclusions drawn from the difference spectra and allowed for an assignment of all ^{13}C signals. An HSQC experiment revealed direct C–H couplings, and an HMBC spectrum further confirmed C–H and C–C connectivities including the quaternary C_{ipso} atoms (Figures 6.16 and 6.17).

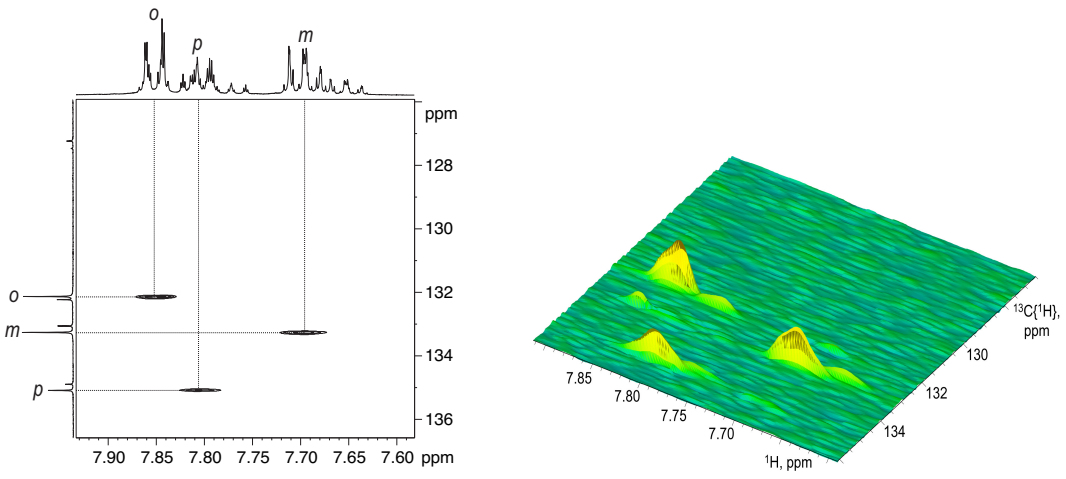

Figure 6.16. ^{1}H/^{13}C HSQC spectrum of the suspension residue (500 MHz for ^{1}H, CD_2Cl_2). In the contour plot (left), only $^{1}J_{C,H}$ crosspeaks of the dominant 7-isomer are displayed.

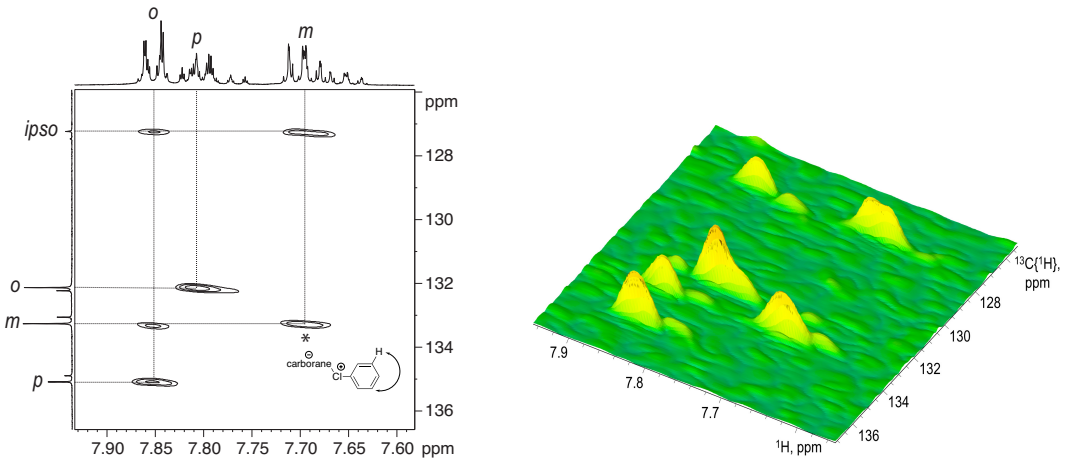

Figure 6.17. $^{1}H/^{13}C$ HMBC spectrum of the suspension residue (500 MHz for ^{1}H, CD_2Cl_2). In the contour plot (left), only $^{2}J_{C,H}$ and $^{3}J_{C,H}$ crosspeaks of the dominant 7-isomer are displayed. The cross-peak marked with an asterisk stems from H_{meta}–C_{meta} coupling.

IR spectra of a mixture of the isomers as a solid and in solution are consistent with the conclusions drawn from the NMR experiments. In a comparison of the solid-state spectra of [Cs][$CHB_{11}Cl_{11}$] and Ph-$CHB_{11}Cl_{11}$, the B–Cl vibrations in the product exhibit a more complicated pattern than in the cesium salt (Figure 6.18). This finding can be explained by a reduced symmetry of the anion cage in Ph-$CHB_{11}Cl_{11}$ because of a relatively strong Ph–Cl(carborane) interaction. The IR spectra of the mixture in the solid state and in dichloromethane or 1,2-dichloroethane solution are similar, giving no evidence for an isomerization process or dissociation into ions upon dissolution.

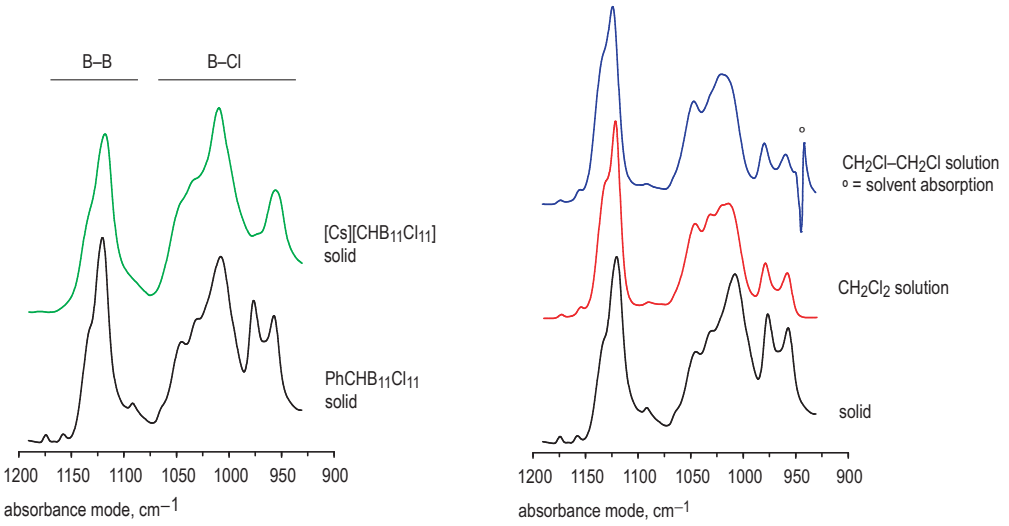

Figure 6.18. IR spectra. Left: solid-state spectra of $[Cs][CHB_{11}Cl_{11}]$ (top) and Ph-$CHB_{11}Cl_{11}$ (isomer mixture, bottom). Right: Spectra of Ph-$CHB_{11}Cl_{11}$ (isomer mixture); solid state (bottom), CH_2Cl_2 solution (12 mg in 0.5 mL, middle), 1,2-dichloroethane solution (12 mg in 0.5 mL, top).

6.7.4 Reaction of 27a$^+$ with Fluorobenzene

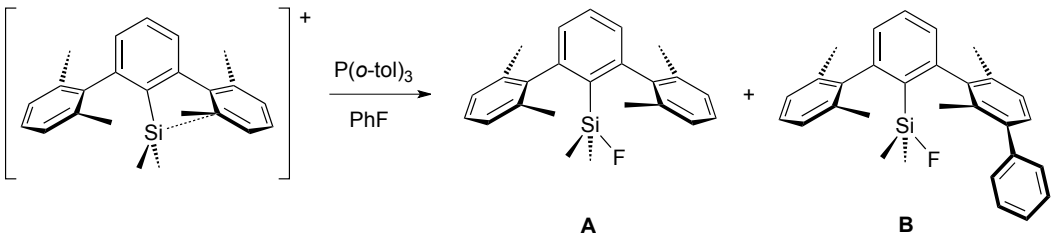

This reaction was carried out in a glovebox. [Cation][$CB_{11}H_6Cl_6$] (61.2 mg, 88.3 μmol) and P(*o*-tol)$_3$ (51.5 mg, 169 μmol) were placed in a 4 mL glass vial with a stir bar. Fluorobenzene (*ca*. 1.5 mL) was added, and the mixture was stirred for 18 hrs at RT. A clear yellow solution was obtained. ^{1}H NMR spectroscopy of the solution (0.6 mL of the neat reaction mixture in a 5 mm tube + a C_6D_6 capillary for locking and shimming) indicated yields of 27% and 30% for fluorosilanes **A** and **B**, respectively. (The same integration was obtained after evaporation of the solvent and redissolution in $CDCl_3$ and also with the counteranions $[CB_{11}H_6Br_6]^-$ and $[CHB_{11}Cl_{11}]^-$.) The reaction mixture was worked

up in a fumehood. It was extracted four times with EtOAc (5 mL)/H_2O (5 mL), and the organic layers were dried over $MgSO_4$ and evaporated to dryness. Preparative thin-layer chromatography (SiO_2, 20×20 cm, 2mm) afforded 15.7 mg of a mixture of **70** and **71** as concluded from NMR and mass spectra. For a more thorough analysis, part of the mixture was subjected to preparative HPLC (Waters Spherisorb S5 CN 20×250 mm Semi-Prep Column, eluent hexanes-CH_2Cl_2, flow 12 mL/min) to afford the separated fluorosilanes.

Characterization of Fluorosilane A

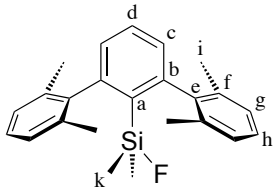

Detailed assignments of the NMR signals were made on the basis of $^1H/^{13}C$ HSQC and HMBC experiments.

^1H NMR (125 MHz, 1.6 mg in 0.6 mL $CDCl_3$): 7.51 (t, $^3J = 7.6$, 1 H, H^d), 7.16 (t, $^3J = 7.5$, 1 H, H^h), 7.08 (d, $^J = 7.5$, 4 H, H^g), 7.02 (d, $3J = 7.6$, 2 H, H^c), 2.03 (s, 6 H, H^i), -0.32 (d, $^3J = 8.2$, 6 H, H^k).

$^{13}C\{^1H\}$ NMR (75 MHz, 1.6 mg in 0.6 mL $CDCl_3$): 148.4 (C^b), 142.8 (C^e), 136.4 (C^f), 132.7 (d, $^2J = 13$, C^a), 130.7 (C^d), 128.4 (C^c), 127.4 (C^h), 127.1 (C^g), 21.0 (C^i), 0.6 (d, $^2J_{C,F} = 16$, C^k).

$^{29}Si\{^1H\}$ NMR (100 MHz, 1.6 mg in 0.6 mL $CDCl_3$): 20.1 (d, $^1J_{Si,F} = 279$).

IR (ATR): 3017w, 2958w, 2920w, 2858w, 1573w, 1558w, 1461m, 1444m, 1405w, 1378w, 1255m, 1174w, 1128w, 1075w, 1053w, 869s, 836s, 809m, 789s, 768s, 748m, 660w.

MS (EI): 362.1 (86, $M^{\cdot+}$), 347.1 (97, $[M - CH_3]^+$), 327.1 (22), 285.1 (100, $[M - SiMe_2F]^+$), 270 (16), 253 (18), 77 (21, $[SiMe_2F]^+$).

HRMS–EI: $M^{\cdot+}$ calculated for $C_{24}H_{27}FSi$: 362.1862; found: 362.1866.

Characterization of Fluorosilane B

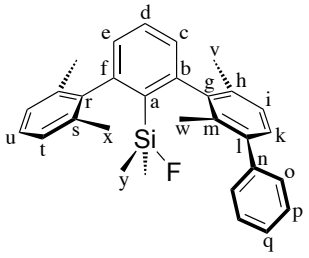

Detailed assignments of the NMR signals were made on the basis of ^{1}H/^{13}C HSQC and HMBC experiments. Rotation about the r–f and b–g axes is slow, rotation about the l–n axis is fast on the NMR time scale. Therefore, six ^{13}C ring resonances (r, s, s', t, t', u,) are observed for the xylyl ring; its CH_3 ^{13}C nuclei absorb isochronically (x, x'). In the ^{1}H NMR spectrum, the peaks of the CH_3 groups are distinguishable (x, x'), but the *meta*-CH signals overlap (t, t'). The phenyl ring gives rise to four ^{13}C (n, o, p, q) and three ^{1}H (o, p, q) signals. The CH_3 groups at Si are diastereotopic and afford two peaks in the ^{13}C and ^{1}H NMR spectrum (y, y').

^{1}H NMR (500 MHz, 2.1 mg in 0.6 mL CD_2Cl_2): 7.59–7.55 (m, 1 H, H^{d}); 7.42–7.38 (m, 2 H, H^{p}), 7.35–7.30 (m, 1 H, H^{q}), 7.33–7.30 (m, 2 H, H^{o}), 7.18–7.14 (m, 1 H, H^{u}), 7.17–7.12 (m, 2 H, H^{i}, H^{k}), 7.10–7.06 (m, 2 H, H$^{t,t'}$), 7.05–7.02 (m, 1 H, H^{e}), 2.07 (s, 3 H, H^{v}), 2.04, 2.02 (2 s, 2 × 3 H, H$^{x,x'}$), 1.90 (s, 3 H, H^{w}), −0.27, −0.28 (2 d, $^{3}J = 7.9$, 2 × 3 H, H$^{y,y'}$).

^{13}C{^{1}H} NMR (75 MHz, 2.1 mg in 0.6 mL CD_2Cl_2): 149.4 (C^{f}), 149.1 (C^{b}), 143.9 (C^{g}), 143.6 (C^{r}), 143.2 (C^{n}), 140.5 (C^{l}), 137.0, 137.0 (C$^{s,s'}$), 136.2 (C^{h}), 134.4 (C^{m}), 133.3 (d, $^{2}J_{C,F} = 13$, C^{a}), 131.4 (C^{d}), 129.9 (C^{o}), 129.4 (C^{k}), 129.1 (C^{c}), 129.1 (C^{e}), 128.6 (C^{p}), 127.8 (C^{u}), 127.6, 127.6 (C$^{t,t'}$), 127.4 (C^{i}), 127.1 (C^{q}), 21.5 (C^{v}), 21.3, 21.3 (C$^{x,x'}$), 19.4 (C^{w}), 1.1, 1.0 (2 d, $^{2}J_{C,F} = 16$, C^{y},$^{y'}$).

^{29}Si{^{1}H} NMR (99.4 MHz, 1.6 mg in 0.6 mL $CDCl_3$): 20.0 (d, $^{1}J_{Si,F} = 279$).

IR (ATR): 3022w, 2956w, 2921w, 1577w, 1558w, 1472m, 1445m, 1404, 1377w, 1254w, 1121w, 1073w, 1052w, 869s, 836s, 810m, 789s, 767s, 750m, 702s, 661m.

MS (EI): 438.1 (100, M$^{\cdot+}$), 423.1 (62, [M − CH_3]$^{+}$), 361.1 (66, [M − $SiMe_2F$]$^{+}$), 346.1

(13), 330 (6), 77 (16, $[SiMe_2F]^+$).

HRMS–EI: $M^{\cdot+}$ calculated for $C_{24}H_{27}FSi$: 438.2179; found: 438.2174.

6.7.5 Kinetics of the Fluoride Abstraction from Fluoroarenes

Sample preparation: In a glovebox, *ca.* 5 mg of [**27a**][carborane] (carborane = $CB_{11}H_6Br_6^-$ or $CHB_{11}Cl_{11}^-$) and 0–12 equiv. of P(*o*-tol)$_3$ were dissolved in 0.6 mL of neat fluoroarene. The solution was transferred to a 5 mm Young NMR tube or a conventional 5 mm NMR tube that was flame-sealed. For locking/shimming and integration, a capillary inside the 5 mm tube was used, containing C_6D_6 and a small amount of CH_2Cl_2. CH_2Cl_2 gives rise to a singlet in a region where no other resonances appear.

Kinetic measurements: Fluoride abstraction was followed after sample preparation by monitoring the disappereance of **27a** by ^{1}H NMR spectroscopy at 315 K. ^{1}H NMR spectra were taken every 30 min over 12 hrs. For fluorobenzene, 12 hrs corresponded to *ca.* 8 $t_{1/2}$. ^{11}B NMR spectroscopy confirmed the presence of unchanged carborane anions after the measurements. When P(*o*-tol)$_3$ was used as an additional base, the ^{31}P NMR spectra contained only signals of P(*o*-tol)$_3$ and $[H–P(o\text{-tol})_3]^+$; phenylated P(*o*-tol)$_3$ was not observed.

Data analysis: In all experiments with fluorobenzene and 4-fluorotoluene, an exponential decrease of the cation concentration was observed, irrespective of the counteranion and the amount of P(*o*-tol)$_3$ used. Data points of the first seven spectra (*ca.* 2 $t_{1/2}$) were evaluated assuming pseudo-first order kinetics with $v = k'[\text{cation}][\text{solvent}] \approx k[\text{cation}]$. The data were not consistent with pseudo-second order kinetics with the phosphine being involved. Values for k and $t_{1/2}$ were obtained by linear regression from plots of $\ln([\text{cation}]_{\text{rel}})$ against t and the relation $t_{1/2} = \ln(2)/k$ (pages 203–208). In the case of 1,4-difluorobenzene, the concentration of the cation remained constant over 600 min under the reaction conditions (page 209).

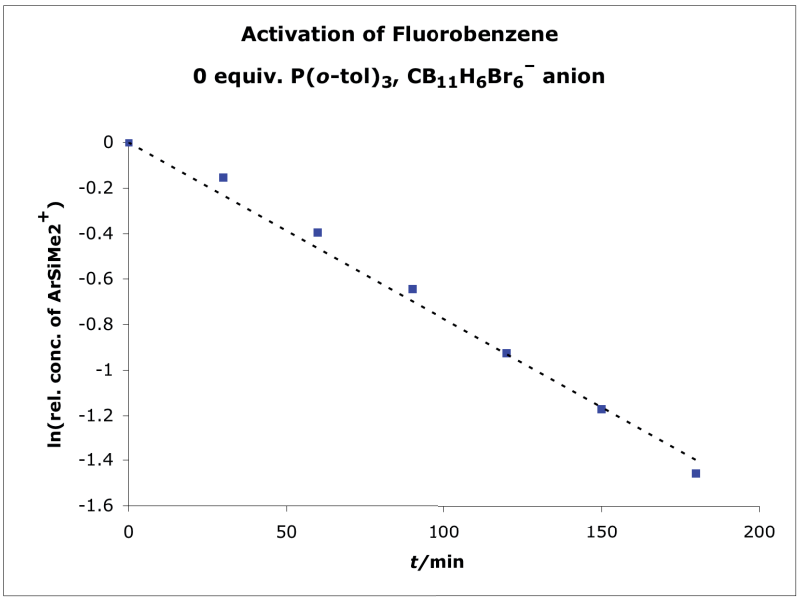

t (min)	Rel. conc. of $ArSiMe_2^+$	ln(Rel. conc. of $ArSiMe_2^+$)
0	1	0
30	0.85645933	-0.154948446
60	0.673046252	-0.395941227
90	0.524720893	-0.64488879
120	0.39553429	-0.927517794
150	0.309409888	-1.173088382
180	0.232854864	-1.457339919

$$k = 7.8 \cdot 10^{-3}\ \mathrm{M}^{-1}\ \mathrm{min}^{-1}$$

$$t_{1/2} = 89\ \mathrm{min}$$

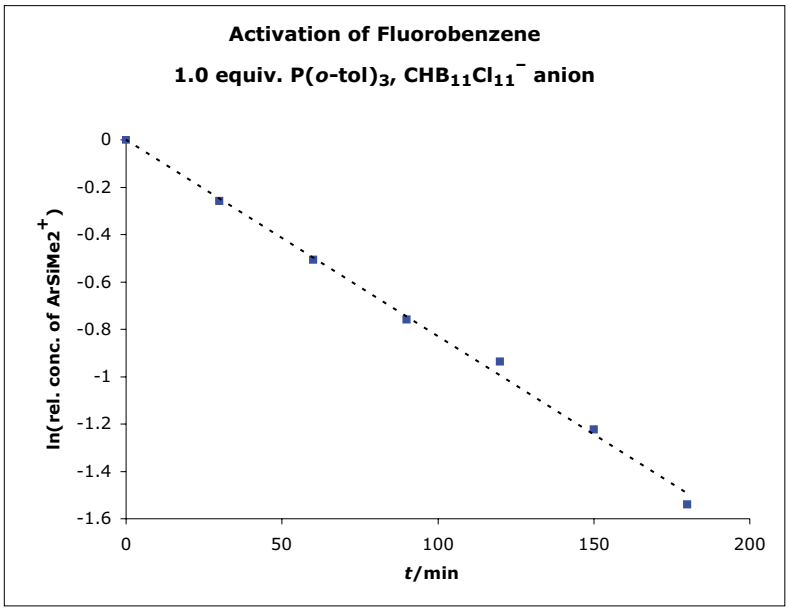

t (min)	Rel. conc. of $ArSiMe_2^+$	ln(Rel. conc. of $ArSiMe_2^+$)
0	1	0
30	0.772268409	-0.25842311
60	0.602731591	-0.506283303
90	0.46763658	-0.760063824
120	0.392220903	-0.935930071
150	0.294239905	-1.223359841
180	0.214370546	-1.540049236

$$k = 8.3 \cdot 10^{-3}\ \text{M}^{-1}\ \text{min}^{-1}$$
$$t_{1/2} = 83\ \text{min}$$

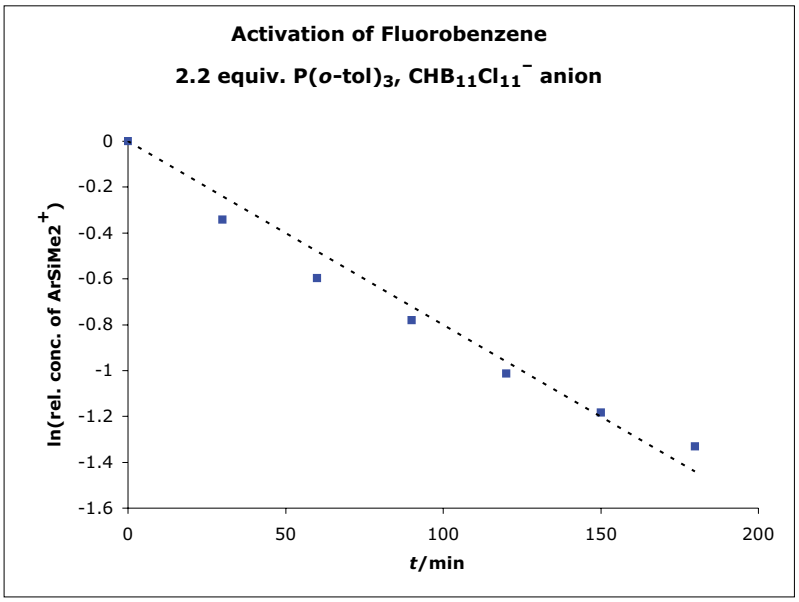

t (min)	Rel. conc. of $ArSiMe_2^+$	ln(Rel. conc. of $ArSiMe_2^+$)
0	1	0
30	0.710182768	-0.342232923
60	0.549608355	-0.598549336
90	0.458224543	-0.780395946
120	0.362532637	-1.014640775
150	0.305796345	-1.184835939
180	0.26383812	-1.332419545

$$k = 8.0 \cdot 10^{-3}\ \text{M}^{-1}\ \text{min}^{-1}$$
$$t_{1/2} = 87\ \text{min}$$

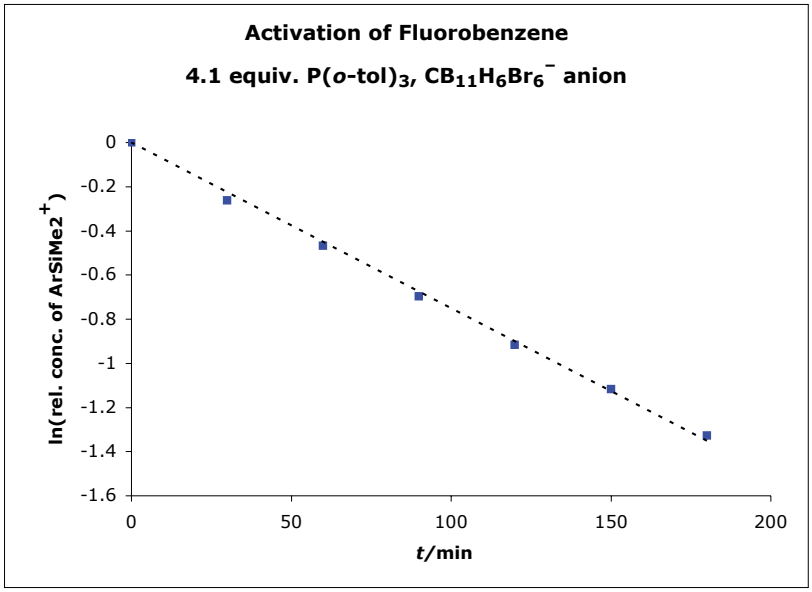

t (min)	Rel. conc. of $ArSiMe_2^+$	ln(Rel. conc. of $ArSiMe_2^+$)
0	1	0
30	0.76932416	-0.262242864
60	0.626871712	-0.467013366
90	0.49777418	-0.697608758
120	0.399433428	-0.917708167
150	0.32699312	-1.117816147
180	0.265074868	-1.32774297

$$k = 7.5 \cdot 10^{-3}\ \text{M}^{-1}\ \text{min}^{-1}$$
$$t_{1/2} = 93\ \text{min}$$

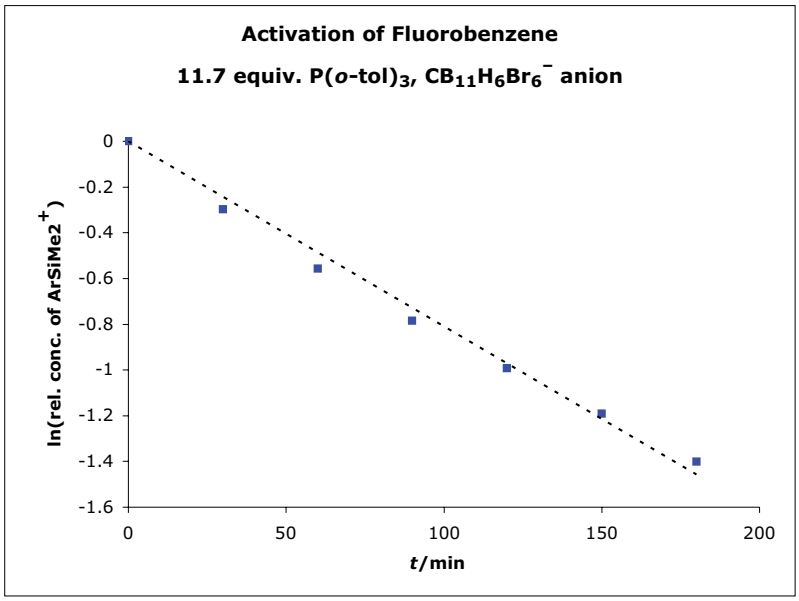

t (min)	Rel. conc. of $ArSiMe_2^+$	ln(Rel. conc. of $ArSiMe_2^+$)
0	1	0
30	0.742073171	-0.298307428
60	0.573109756	-0.556678034
90	0.455670732	-0.78598481
120	0.370853659	-0.991947746
150	0.30347561	-1.192454035
180	0.246341463	-1.401036643

$$k = 8.1 \cdot 10^{-3}\ \text{M}^{-1}\ \text{min}^{-1}$$
$$t_{1/2} = 86\ \text{min}$$

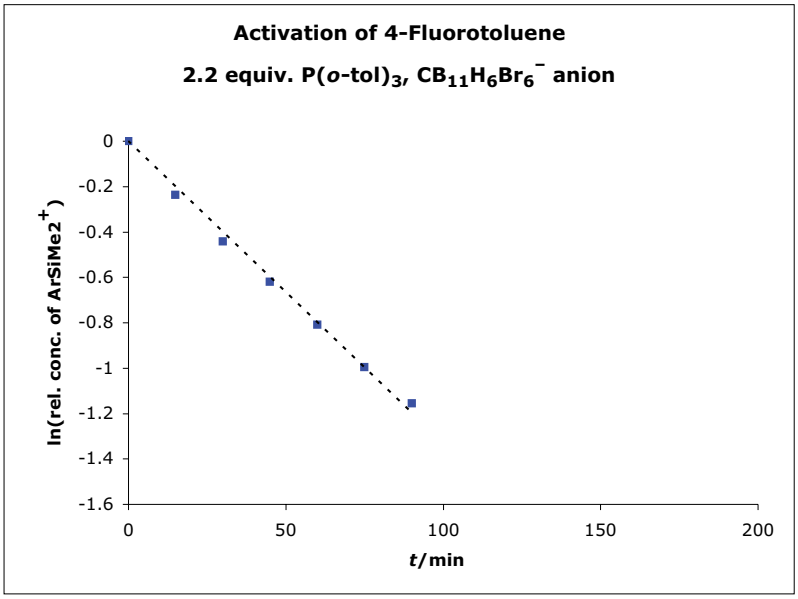

t (min)	Rel. conc. of $ArSiMe_2^+$	ln(Rel. conc. of $ArSiMe_2^+$)
0	1	0
15	0.788300836	-0.237875491
30	0.642525534	-0.442348722
45	0.537604457	-0.6206322
60	0.444753946	-0.81023408
75	0.369545032	-0.995482672
90	0.314763231	-1.15593457

$$k = 13.3 \cdot 10^{-3}\ \text{M}^{-1}\ \text{min}^{-1}$$
$$t_{1/2} = 52\ \text{min}$$

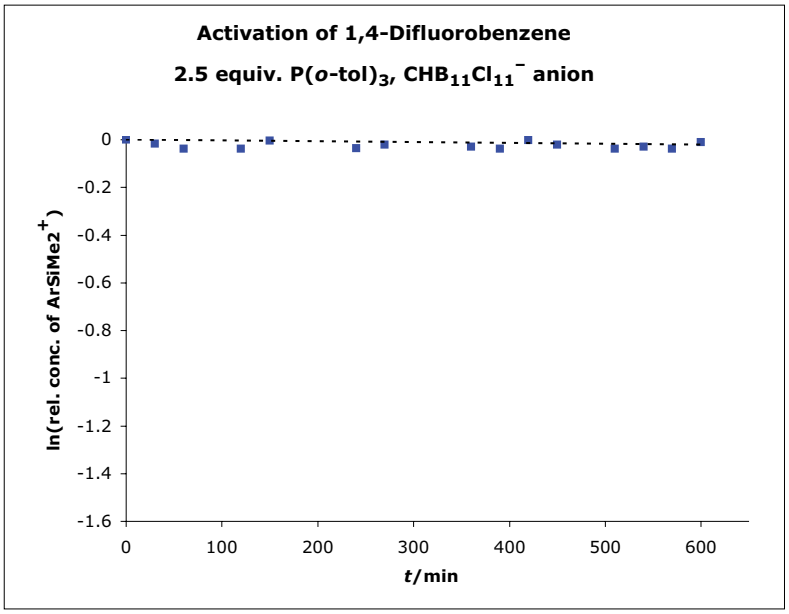

t (min)	Rel. conc. of $ArSiMe_2^+$	ln(Rel. conc. of $ArSiMe_2^+$)
0	1	0
30	0.983377078	-0.016762633
60	0.962379703	-0.038346205
90	1.006124234	0.006105558
120	0.962379703	-0.038346205
150	0.994750656	-0.00526317
180	1.006124234	0.006105558
210	1.023622047	0.023347364
240	0.965004374	-0.035622645
270	0.979877515	-0.0203277
300	1.023622047	0.023347364
330	1.006124234	0.006105558
360	0.971128609	-0.029296369
390	0.962379703	-0.038346205
420	0.997375328	-0.002628122
450	0.979877515	-0.0203277
480	1.032370954	0.031858054
510	0.962379703	-0.038346205
540	0.971128609	-0.029296369
570	0.962379703	-0.038346205
600	0.988626422	-0.011438752

Activation Parameters of the Fluoride Abstraction

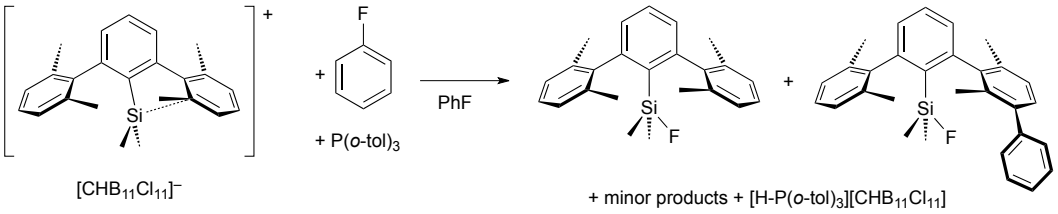

The reaction was monitored by ^{1}H NMR spectroscopy at four temperatures over the range 295–325 K; the disappearance of the cation was observed using the integrals of its CH_3 groups. For each temperature, the reaction was followed over 4–6 $t_{1/2}$, and data points of the first 1.5 $t_{1/2}$ were evaluated in order to determine the rate constant k. Effective reaction temperatures inside the NMR instrument were measured by the ethylene glycol method.[‡]

The activation parameters were derived from a plot of $\ln(\frac{k}{T})$ versus $\frac{1}{T}$ assuming the Eyring relation

$$\ln(\frac{k}{T}) = \frac{-\Delta H^{\ddagger}}{R}\frac{1}{T} + \ln(\frac{k_B}{h}) + \frac{\Delta S^{\ddagger}}{R}.$$

In such a diagram,

$$\text{slope} = \frac{-\Delta H^{\ddagger}}{R} \Rightarrow \Delta H^{\ddagger}$$

$$y \text{ intercept} = \ln(\frac{k_B}{h}) + \frac{\Delta S^{\ddagger}}{R} \Rightarrow \Delta S^{\ddagger}$$

$\Delta G^{\ddagger}$ results from $\Delta G^{\ddagger} = \Delta H^{\ddagger} - T\Delta S^{\ddagger}$.

[‡]Bruker reference sample containing 80 % ethylene glycol/20 % DMSO-d_6; S. Braun, H.-O. Kalinowski, S. Berger, *150 and More Basic NMR Experiments*, Wiley-VCH, Weinheim 1998.

T	k ($M^{-1}min^{-1}$)	$t_{1/2}$ (min)	$\frac{1}{T}$ (K^{-1})	$\ln(\frac{k}{T})$
294.4	$1.03 \cdot 10^{-3}$	675	$3.397 \cdot 10^{-3}$	-12.57
304.2	$3.31 \cdot 10^{-3}$	210	$3.287 \cdot 10^{-3}$	-11.43
314.1	$7.97 \cdot 10^{-3}$	87	$3.184 \cdot 10^{-3}$	-10.58
323.9	$25.7 \cdot 10^{-3}$	27	$3.087 \cdot 10^{-3}$	-9.44

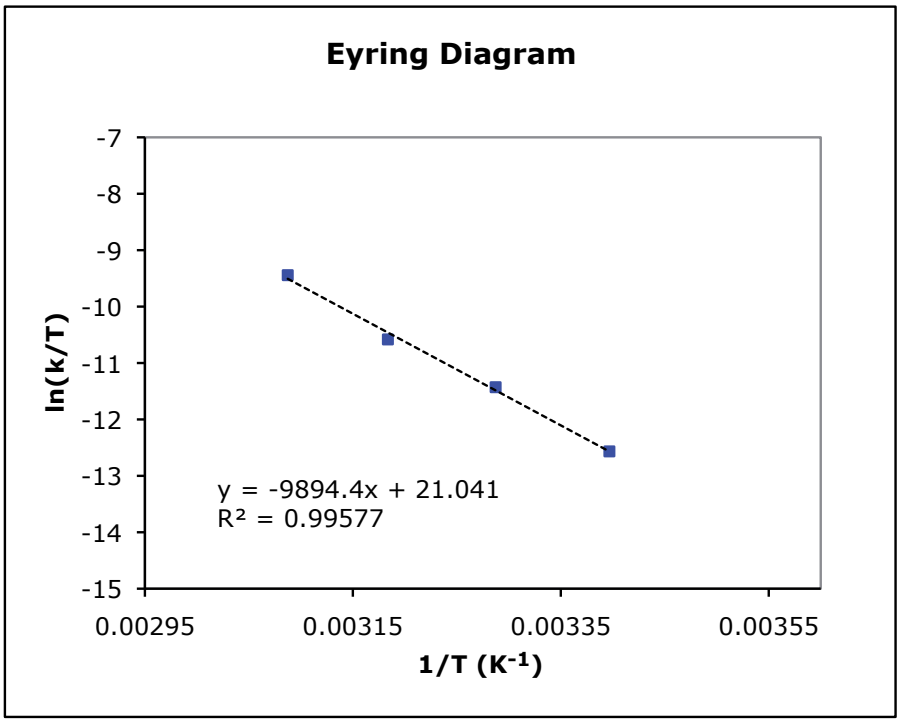

From this plot:

$$\Delta H^{\ddagger} \approx 82 \text{ kJ mol}^{-1}$$

$$\Delta S^{\ddagger} \approx -24 \text{ J mol}^{-1} \text{ K}^{-1}$$

$$\Delta G^{\ddagger} \approx 90 \text{ kJ mol}^{-1}$$

6.7.6 Computational Methodology

6.7.6.1 General

All calculations have been carried out using the GAMESS[1] and GAUSSIAN[2] software packages, employing both density functional theory as well as conventional second order Møller-Plesset perturbation theory (MP2).[3] The B98,[4] and B97-D[5] density functionals were used, together with Dunning's DZ(2df,pd) basis set[6] for determination of structure and properties. An ultrafine grid was employed for all computations. For each optimized geometry, the Hessian (matrix of second derivative) was calculated to determine local minima (positive definite) or nth-order saddle points (n negative eigenvalues), as well as for thermodynamic properties. Visualization and analysis of structural and property results were obtained using QMView[7] and WebMO.[8]

[1]M. Schmidt, K. K. Baldridge, J. A. Boatz, S. Elbert, M. Gordon, J. H. Jenson, S. Koeski, N. Matsunaga, K. A. Nguyen, S. J. Su, T. L. Windus, M. Dupuis, and J. A. Montgomery, *J. Comp. Chem.*, 1993, **14**, 1347.

[2]Gaussian 09, Revision E, M. J. Frisch, G. W. Trucks, H. B. Schlegel, G. E. Scuseria, M. A. Robb, J. R. Cheeseman, G. Scalmani, V. Barone, B. Mennucci, G. A. Petersson, H. Nakatsuji, M. Caricato, X. Li, H. P. Hratchian, A. F. Izmaylov, J. Bloino, G. Zheng, J. L. Sonnenberg, M. Hada, M. Ehara, K. Toyota, R. Fukuda, J. Hasegawa, M. Ishida, T. Nakajima, Y. Honda, O. Kitao, H. Nakai, T. Vreven, J. A. Montgomery, Jr., J. E. Peralta, F. Ogliaro, M. Bearpark, J. J. Heyd, E. Brothers, K. N. Kudin, V. N. Staroverov, R. Kobayashi, J. Normand, K. Raghavachari, A. Rendell, J. C. Burant, S. S. Iyengar, J. Tomasi, M. Cossi, N. Rega, J. M. Millam, M. Klene, J. E. Knox, J. B. Cross, V. Bakken, C. Adamo, J. Jaramillo, R. Gomperts, R. E. Stratmann, O. Yazyev, A. J. Austin, R. Cammi, C. Pomelli, J. W. Ochterski, R. L. Martin, K. Morokuma, V. G. Zakrzewski, G. A. Voth, P. Salvador, J. J. Dannenberg, S. Dapprich, A. D. Daniels, Ö. Farkas, J. B. Foresman, J. V. Ortiz, J. Cioslowski, and D. J. Fox, Gaussian, Inc., Wallingford CT, 2009.

[3]C. Møller and M. S. Plesset, *Phys. Rev.*, 1934, **46**, 618.

[4]Becke, A. D. *J. Chem. Phys.* **1998**, *108*, 9624-9631.

[5] Grimme, S. *J. Comput. Chem.* **2006**, *27*, 1787-1799.

[6] T. H. Dunning, *J. Chem. Phys.* **1989**, *90*, 1007.

[7]Baldridge, K.K.; Greenberg, J. *J. Mol. Graph.*, **1995**, *13*, 63.

[8]http://www.webmo.net.

6.7.6.2 Phenyl-Carborane Data

B97-D/DZV(2d,p)

Isomers (C_s)	Energy	Relative Energy	
phen_12b_carborane (eclipsed)	-5606.2187970920	0.0 (0.0)	0.172279
phen_12_carborane (staggered)	-5606.2172766732	0.95 (3.9748)	0.171971
phen_7b_carborane (anti)	-5606.2158772812	1.83 (7.6567)	0.171987
phen_7_carborane (syn)	-5606.2141102187	2.94 (12.301)	0.171752

B98/DZ(2df,pd)

Isomers (C_s)	Energy	FF	Energy + ZPE	Enthalpy
phen_12b_carborane (eclipsed)	-5605.6717177	PD	-5605.501070	-5605.470164
phen_12_carborane (staggered)	-5605.6705761	-17	-5605.499906	-5605.469937
phen_7b_carborane (anti)	-5605.6684253	PD	-5605.497856	-5605.466944
phen_7_carborane (syn)	-5605.6674302	-16.5	-5605.496923	-5605.466904

B98/DZ(2df,pd) Relative Energies in kcal/mol (kJ/mol)

Isomers (C_s)	Energy	Energy + ZPE	Enthapy
phen_12b_carborane (eclipsed)	0.0 (0.0)	0.0 (0.0)	0.0 (0.0)
phen_12_carborane (staggered)	0.7164 (3.0)	0.7304 (3.056)	0.14245 (0.60)
phen_7b_carborane (anti)	2.0660 (8.64)	2.0168 (8.438)	2.0206 (8.45)
phen_7_carborane (syn)	2.6905 (11.26)	2.6023 (10.888)	2.0457 (8.56)

6.7.7 Fluoranthene by Friedel–Crafts Arylation

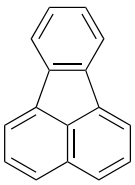

Chemical Formula: $C_{16}H_{10}$
Molecular Weight: 202.251

In a glovebox, 1-(2-fluorophenyl)naphthalene (10.3 mg, 46.3 μmol) and P(*o*-tol)$_3$ (36.5 mg, 120 μmol) were dissolved in PhCl (0.8 ml) in a 4 mL glass vial. *i*Pr$_3$Si–CHB$_{11}$H$_5$Cl$_6$ (47.2 mg, 93.6 μmol) was added, and the vial was closed with a PTFE-lined screw cap and

additionally sealed with Parafilm. It was transferred to a fume hood. The reaction mixture was heated to 110 °C for 12 h. A slightly yellow solution with a small amount of a colorless precipitate was obtained. PhCl was removed under reduced pressure at RT. To the residue, H_2O (1 mL) and CsCl (*ca*. 60 mg) were added. The mixture was three times extracted with 2 mL of a 1:1 mixture of hexanes/EtOAc ([Cs][$CHB_{11}H_5Cl_6$] dissolved in the organic layer). The organic layers were dried over $MgSO_4$ and concentrated using a rotary evaporator. Addition of *ca*. 3 mL of a mixture of hexanes/CH_2Cl_2 afforded [Cs][$CHB_{11}H_5Cl_6$] as a colorless precipitate which was seperated by filtration through a small glass frit G4 and washed with hexane (92 % of the carborane recovered). The filtrate was concentrated, and the crude product was purified by thin-layer chromatography (SiO_2, 2 mm, 20 × 20 cm, hexanes/CH_2Cl_2 50:1). Fluoranthene gave a strongly fluorescing band at R_f 0.23–0.35. It was obtained as a colorless solid whose GC–MS and ^{1}H NMR data were consistent with those of a purchased sample (yield 7.5 mg, 80 %).

References

[1] Blanksby, S. J.; Ellison, G. B. *Acc. Chem. Res.* **2000**, *36*, 255–263.

[2] Michalczyk, M. J.; West, R.; Michl, J. *Organometallics* **1985**, *4*, 826–829.

[3] Related phenyl(*m*-carboranyl)halonium ions afford borylation and phenylation products: Gusel'nikov, L. E.; Nametkin, N. S. *Chem. Rev.* **1979**, *79*, 529–577.

[4] West, R.; Fink, M. J.; Michl, J. *Science* **1981**, *214*, 1343–1344.

[5] Fink, M. J.; Michalczyk, M. H.; Haller, K. J.; West, R.; Michl, J. *Organometallics* **1984**, *3*, 793–800.

[6] Kira, M.; Maruyama, T.; Kabuto, C.; Ebata, K.; Sakurai, H. *Angew. Chem. Int. Ed.* **1994**, *33*, 1489–1491.

[7] Kinjo, R.; Ichinohe, M.; Sekiguchi, A.; Takagi, N.; Sumimoto, M.; Nagase, S. *J. Am. Chem. Soc.* **2007**, *129*, 7766–7767.

[8] Ishida, S.; Iwamoto, T; Kabuto, C.; Kira, M. *Nature* **2003**, *421*, 725–727.

[9] Baldridge, K. K.; Uzan, O.; Martin, M. L. *Organometallics* **2000**, *19*, 1477–1487.

[10] Moteki, M.; Maeda, S.; Ohno, K. *Organometallics* **2009**, *28*, 2218–2224.

[11] Sekiguchi, A.; Yatabe, T.; Kabuto, C.; Sakurai, H. *J. Am. Chem. Soc.* **1993**, *115*, 5853–5854.

[12] Abersfelder, K.; White, A. J. P.; Rzepa, H. S.; Scheschkewitz, D. *Science* **2010**, *327*, 564–566.

[13] Sekiguchi, A.; Kinjo, R.; Ichinohe, M. *Science* **2004**, *305*, 1755–1757.

[14] Sasamori, T.; Hironaka, K.; Sugiyama, Y.; Takagi, N.; Nagase, S.; Hosoi, Y.; Furukawa, Y.; Tokitoh, N. *J. Am. Chem. Soc.* **2008**, *130*, 13856–13857.

[15] Power, P. P. *Chem. Commun.* **2003**, 2091–2101.

[16] Walsh, R. *Bond Dissociation Energies in Organosilicon Compounds.* In *ABCR Catalogue*, Gelest Inc., Tullytown, Pa (USA), 2000, 187–194.

[17] Chauhan, M.; Chuit, C.; Corriu, R. J. P.; Mehdi, A.; Reyé, C. *Organometallics* **1996**, *15*, 4326–4333.

[18] Corriu, R. J. P.; Kpoton, A.; Poirier, M.; Royo, G.; Corey, J. Y. *J. Organomet. Chem.* **1984**, *277*, C25–C30.

[19] Kost, D.; Kingston, V.; Gostevskii, B.; Ellern, A.; Stalke, D.; Walfort, B.; Kalikhman, I. *Organometallics* **2002**, *21*, 2293–2305.

[20] Kira, M; Ishida, S.; Iwamoto, T.; Kabuto, C. *J. Am. Chem. Soc.* **1999**, *121*, 9722–9723.

[21] Jutzi, P.; Kanne, D.; Krüger, C. *Angew. Chem. Int. Ed.* **1986**, *25*, 164–164.

[22] Xiong, Y.; Yao, S.; Driess, M. *J. Am. Chem. Soc.* **2009**, *131*, 7562–7563.

[23] Powell, W. H. *Pure Appl. Chem.* **1993**, *65*, 1357–1455.

[24] Lambert, J. B.; Zhao, Y.; Zhang, S. M. *J. Phys. Org. Chem.* **2001**, *14*, 370–379.

[25] Müller, T. *Adv. Organomet. Chem.* **2005**, *53*, 155–215.

[26] Hollenstein, S.; Laube, T. *J. Am. Chem. Soc.* **1993**, *115*, 7240–7245.

[27] Kato, T.; Reed, C. A. *Angew. Chem. Int. Ed.* **2004**, *43*, 2908–2911.

[28] Xie, Z.; Bau, R.; Benesi, A.; Reed, C. A. *Organometallics* **1995**, *14*, 3933–3941.

[29] Küppers, T.; Bernhardt, E.; Eujen, R.; Willner, H.; Lehmann, C. W. *Angew. Chem. Int. Ed.* **2007**, *46*, 6346–6349.

[30] Lambert, J. B.; Zhang, S.; Ciro, S. M. *Organometallics* **1993**, *13*, 2430–2443.

[31] Reed, C. A. *Acc. Chem. Res.* **1998**, *31*, 325–332.

[32] Kim, K.-C.; Reed, C. A.; Elliot, D. W.; Mueller, L. J.; Tham, F.; Lin, L.; Lambert, J. B. *Science* **2002**, *297*, 825–827.

[33] Müller, T. *Organometallics* **1998**, *17*, 278–280.

[34] Olsson, L.; Ottosson, C.-H.; Cremer, D. *J. Am. Chem. Soc.* **1995**, *117*, 7460–7479.

[35] Xie, Z.; Manning, J.; Reed, R. W.; Mathur, R.; Boyd, P. D. W.; Benesi, A.; Reed, C. A. *J. Am. Chem. Soc.* **1996**, *118*, 2922–2928.

[36] Lambert, J. B.; Zhao, Y. *Angew. Chem. Int. Ed.* **1997**, *36*, 400–401.

[37] Lambert, J. B.; Zhao, Y.; Wu, H.; Tse, W. C.; Kuhlmann, B. *J. Am. Chem. Soc.* **1999**, *121*, 5001–5008.

[38] Lambert, J. B.; Lin, L. *J. Org. Chem.* **2001**, *66*, 8537–8539.

[39] Bartlett, P. D.; Condon, F. E.; Schneider, A. *J. Am. Chem. Soc.* **1944**, *66*, 1531–1539.

[40] Corey, J. J.; West, R. *J. Am. Chem. Soc.* **1963**, *85*, 2430–2433.

[41] Carey, F. A.; Hsu, C.-L. *J. Organomet. Chem.* **1969**, *19*, 29–41.

[42] Krossing, I.; Raabe, I. *Angew. Chem. Int. Ed.* **2004**, *43*, 2066–2090.

[43] Reed, C. A.; Fackler, N. L. P.; Kim, K.-C.; Stasko, D.; Evans, D. R. *J. Am. Chem. Soc.* **1999**, *121*, 6314–6315.

[44] Reed, C. A. *Acc. Chem. Res.* **1998**, *31*, 133–139.

[45] Körbe, S.; Schreiber, P. J.; Michl, J. *Chem. Rev.* **2006**, *106*, 5208–5249.

[46] Reed, C. A. *Acc. Chem. Res.* **2009**, *43*, 121–128.

[47] Avelar, A.; Reed, C. A. *Angew. Chem. Int. Ed.* **2009**, *48*, 3491–3493.

[48] Kessler, M.; Knapp, C.; Sagawe, V.; Scherer, H.; Uzun, R. *Inorg. Chem.* **2010**, *49*, 5223–5230.

[49] Ivanov, S. V.; Miller, S. M.; Anderson, O. P.; Sointsev, K. A.; Strauss, S. H. *J. Am. Chem. Soc.* **2003**, *125*, 4694–4695.

[50] Geis, V.; Guttsche, K.; Knapp, C.; Scherer, H.; Uzun, R. *Dalton Trans.* **2009**, 2687–2694.

[51] Lambert, J. B.; Zhang, S. *J. Chem. Soc., Chem. Commun.* **1993**, 383–384.

[52] Lambert, J. B.; Zhang, S.; Stern, C. L.; Huffman, J. C. *Science* **1993**, *260*, 1917–1918.

[53] Reed, C. A.; Xie, Z.; Bau, R.; Benesi, A. *Science* **1993**, *262*, 402–404.

[54] Pauling, L. *Science* **1994**, *263*, 983.

[55] Olah, G. A.; Rasul, G.; Li, X.; Buchholz, H. A.; Sandford, G.; Surya Prakash, G. K. *Science* **1994**, *263*, 983–984.

[56] Lambert, J. B.; Zhang, S. *Science* **1994**, *263*, 984–985.

[57] Reed, C. A.; Xie, Z. *Science* **1994**, *263*, 985–986.

[58] Xie, Z.; Liston, D. J.; Jelínek, T.; Mitro, V.; Bau, R.; Reed, C. A. *J. Chem. Soc., Chem. Commun.* **1993**, 384–386.

[59] Hoffmann, S. P.; Kato, T.; Tham, F. S.; Reed, C. A. *Chem. Commun.* **2006**, 767–769.

[60] Douvris, C.; Nagaraja, C. M.; Chen, C.-H.; Foxman, B. M.; Ozerov, O. V. *J. Am. Chem. Soc.* **2010**, *132*, 4946–4953.

[61] Entries 1 and 2: Küppers, T.; Bernhardt, E.; Eujen, R.; Willner, H.; Lehmann, C. W. *Angew. Chem. Int. Ed.* **2007**, *46*, 6346–6349; entries 3, 7 and 11: Kessler, M.; Knapp, C.; Sagawe, V.; Scherer, H.; Uzun, R. *Inorg. Chem.* **2010**, *49*, 5223–5230;

entries 4 and 5: Xie, Z.; Bau, R.; Benesi, A.; Reed, C. A. *Organometallics* **1995**, *14*, 3933–3941; entry 6: Hoffmann, S. P.; Kato, T.; Tham, F. S.; Reed, C. A. *Chem. Commun.* **2006**, 767–769; entries 8–10 and 12: Xie, Z.; Manning, J.; Reed, R. W.; Mathur, R.; Boyd, P. D. W.; Benesi, A.; Reed, C. A. *J. Am. Chem. Soc.* **1996**, *118*, 2922–2928.

[62] Stoyanov, E. S.; Kim, K.-C.; Reed, C. A. *J. Am. Chem. Soc.* **2006**, *128*, 8500–8508.

[63] Entries 1–4: Lambert, J. B.; Zhang, S.; Ciro, S. M. *Organometallics* **1993**, *13*, 2430–2443; entries 5 and 6: Own measurements at the University of Zurich; entry 7: Kessler, M.; Knapp, C.; Sagawe, V.; Scherer, H.; Uzun, R. *Inorg. Chem.* **2010**, *49*, 5223–5230.

[64] Müller, T. *Angew. Chem. Int. Ed. Engl.* **2001**, *40*, 3033–3036.

[65] Panisch, R.; Bolte, M.; Müller, T. *J. Am. Chem. Soc.* **2006**, *128*, 9676–9682.

[66] Sekuguchi, A.; Muratami, A.; Fukuya, N.; Kabe, Y. *Chem. Lett.* **2004**, *33*, 530–531.

[67] Lickiss, P. D.; Masangane, P. C.; Sohal, W. In *Organosilicon Chemistry V*, Auner, N.,; Weis, J. (Eds.), Wiley-VCH: New York, 2003, p. 45.

[68] Khalimon, A. Y.; Lin, Z. H.; Simionescu, R.; Vyboishchikov, S. F.; Nikonov, G. I. *Angew. Chem. Int. Ed.* **2007**, *46*, 4530–4533.

[69] Lee, V. Y.; Sekiguchi, A. *Acc. Chem. Res.* **2007**, *40*, 410–419.

[70] Inoue, S.; Ichinohe, M.; Yamaguchi, T.; Sekiguchi, A. *Organometallics* **2008**, *27*, 6056Ð-6058.

[71] Ichinohe, M.; Igarashi, T.; Sanuki, K.; Sekiguchi, A. *J. Am. Chem. Soc.* **2005**, *127*, 9978–9979.

[72] Sekiguchi, A.; Matsuno, T.; Ichinohe, M. *J. Am. Chem. Soc.* **2000**, *122*, 11250–11251.

[73] Reed, C. A. *Chem. Commun.* **2005**, 1669–1677.

[74] Reed, C. A.; Kim, K.-C.; Stoyanov, E. S.; Stasko D.; Tham, F. S.; Mueller, L. J. *J. Am. Chem. Soc.* **2003**, *125*, 1796–1804.

[75] Juhasz, M.; Hoffmann, S.; Stoyanov, E. S.; Kim, K.-C.; Reed, C. A. *Angew. Chem. Int. Ed.* **2004**, *43*, 5352–5355.

[76] Stoyanov, E. S.; Hoffmann, S. P.; Juhasz, M.; Reed, C. A. *J. Am. Chem. Soc.* **2006**, *128*, 3160–3161.

[77] Kato T.; Stoyanov, E. S.; Geier, J.; Grützmacher, H.; Reed, C. A. *J. Am. Chem. Soc.* **2004**, *126*, 12451–12457.

[78] Stasko, D.; Reed, C. A. *J. Am. Chem. Soc.* **2002**, *124*, 1148–1149.

[79] Zhang, Y.; Reed, C. A. *Dalton Trans.* **2008**, 4392–4394.

[80] Douvris, C.; Reed, C. A. *Organometallics* **2008**, *27*, 807–810.

[81] Kato, T.; Tham, F. S.; Boyd, P. D. W.; Reed, C. A. *Heteroatom Chem.* **2006**, *17*, 209–216.

[82] Basuli, F.; Aneetha, H.; Huffman, J. C.; Mindiola, D. J. *J. Am. Chem. Soc.* **2005**, *127*, 17992–17993.

[83] Pons, V.; Heinekey, D. M. *J. Am. Chem. Soc.* **2003**, *125*, 8428–8429.

[84] Gelabert, R.; Moreno, M.; Lluch, J. M.; Lledós, A.; Pons, V.; Heinekey, D. M. *J. Am. Chem. Soc.* **2004**, *126*, 8813–8822.

[85] Matthews, S. L.; Pons, V.; Heinekey, D. M. *J. Am. Chem. Soc.* **2005**, *127*, 850–851.

[86] Vogt, M.; Pons, V., Heinekey, D. M. *Organometallics* **2005**, *24*, 1832–1836.

[87] Egbert, J. D.; Bullock, R. M.; Heinekey, D. M. *Organometallics* **2007**, *26*, 2291–2295.

[88] Johannsen, M.; Jørgensen, K. A.; Helmchen, G. *J. Am. Chem. Soc.* **1998**, *120*, 7637–7638.

[89] Hara, K.; Akiyama, R.; Sawamura, M. *Org. Lett.* **2005**, *7*, 5621–5623.

[90] Klare, H. F. T.; Bergander, K.; Oestreich, M. *Angew. Chem. Int. Ed.* **2009**, *48*, 9077–9079.

[91] Zhang, Y.; Huynh, K.; Manners, I.; Reed, C. A. *Chem. Commun.* **2008**, 494–496.

[92] Sennett, M. S.; Hagnauer, G. L.; Singler, R. E. *Macromolecules* **1986**, *19*, 959–964.

[93] Zhang, Y.; Chen, E. Y.-X. *J. Organomet. Chem.* **2010**, *695*, 1464–1471.

[94] Scott, V. J.; Çelenligil-Çetin, R.; Ozerov, O. V. *J. Am. Chem. Soc.* **2005**, *127*, 2852–2853.

[95] Douvris, C.; Ozerov, O. V. *Science* **2008**, *321*, 1188–1190.

[96] Steinberger, H.-U.; Müller, T.; Auner, N.; Maerker, C.; Schleyer, P. v. R. *Angew. Chem. Int. Ed.* **1997**, *36*, 626–628.

[97] Müller, T.; Bauch, C.; Ostermeier, M.; Bolte, M.; Auner, N. *J. Am. Chem. Soc.* **2003**, *125*, 2158–2168.

[98] Clyburne, J. A. C.; McMullen, N. *Coord. Chem. Rev.* **2000**, *210*, 73–99.

[99] Twamley, P. P.; Haubrich, S. *Adv. Organomet. Chem.* **1999**, *44*, 1–65.

[100] Chen, C.-T.; Siegel, J. S. *J. Am. Chem. Soc.* **1994**, *116*, 5959–5960.

[101] All calculations presented in this thesis were carried out by Prof. Kim K. Baldridge, Organic Chemistry Institute of the University of Zurich.
The conformational analyses were carried out using the Gaussian98 [a] and GAMESS [b] software packages. The computations employ a variety of levels of theory for comparative purposes. Wavefunction-based methods considered include Hartree-Fock, second order Moller-Plesset perturbation theory (MP2) [c], and hybrid density functional theory (HDFT) using the B3LYP functional. The B3LYP functional uses the Becke's 3 parameter functional [d] in combination with non-local correlation provided by the Lee-Yang-Parr expression [e, f] with both local and

nonlocal terms, B3LYP. Dunning's double-ζ polarized sets, denoted DZ(2df,pd) and DZ+(2df,pd), were employed.[g] Full geometry optimizations were performed and uniquely characterized via second derivatives (Hessian) analysis to determine the number of imaginary frequencies. From the fully optimized structures, single point NMR computations were performed, using the CSGT method,[h] and calibrated with respect to TMS. Visualization and analysis was carried out using QMView.[i]
[a] Frisch, M. J.; Trucks, G. W.; Schlegel, H. B.; Scuseria, G. E.; Robb, M. A.; Cheeseman, J. R.; Zakrzewski, V. G.; Montgomery, J. A. J.; Stratmann, R. E.; Burant, J. C.; Dapprich, S.; Millam, J. M.; Daniels, A. D.; Kudin, K. N.; Strain, M. C.; Farkas, O.; Tomasi, J.; Barone, V.; Cossi, M.; Cammi, R.; Mennucci, B.; Pomelli, C.; Adamo, C.; Clifford, S.; Ochterski, J.; Petersson, G. A.; Ayala, P. Y.; Cui, Q.; Morokuma, K.; Malick, D. K.; Rabuck, A. D.; Raghavachari, K.; Foresman, J. B.; Cioslowski, J.; Ortiz, J. V.; Stefanov, B. B.; Liu, G.; Liashenko, A.; Piskorz, P.; Komaromi, I.; Gomperts, R.; Martin, R. L.; Fox, D. J.; Keith, T.; Al-Laham, M. A.; Peng, C. Y.; Nanayakkara, A.; Gonzalez, C.; Challacombe, M.; Gill, P. M. W.; Johnson, B.; Chen, W.; Wong, M. W.; Andres, J. L.; Gonzalez, C.; Head-Gordon, M.; Replogle, E. S.; Pople, J. A. *Gaussian98*, Revision A6, Pittburgh PA, 1998; [b] Schmidt, M. W.; Baldridge, K. K.; Boatz, J. A.; Elbert, S. T.; Gordon, M. S.; Jensen, J. H.; Koseki, S.; Matsunaga, N.; Nguyen, K. A.; Su, S.; Windus, T. L.; Elbert, S. T. *J. Comp. Chem.* **1993**, *14*, 1347; [c] Møller, C.; Plesset, M. S. *Phys. Rev.* **1934**, *46*, 618–622; [d] Becke, A. D. *J. Chem. Phys.* **1993**, *98*, 5648–5652; [e] Lee, C.; Yang, W.; Parr, R. G. *Phys. Rev. B* **1988**, *37*, 785; [f] Miehlich, B.; Savin, A.; Stoll, H.; Preuss, H. *Chem. Phys. Lett.* **1989**, *157*, 200; [g] Dunning, T. H. *J. Chem. Phys.* **1989**, *90*, 1007; [h] Keith, T. A.; Bader, R. F. W. *Chem. Phys. Lett.* **1993**, *210*, 223–231; [i] Baldridge, K. K.; Greenberg, J. P. *J. Mol. Graphics* **1995**, *13*, 63.

[102] Du, C.-J. F.; Hart H.; Ng, K.-K. D. *J. Org. Chem.* **1986**, *51*, 3162–3165.

[103] Saednya, A.; Hart, H. *Synthesis* **1996**, 1455–1458.

[104] Gutowsky, H. S.; Holm, C. H. *J. Chem. Phys.* **1956**, *25*, 1228–1234.

[105] Chen, C.-T.;Chadha, R.; Siegel, J. S. *Tetrahedron Lett.* **1995**, *36*, 8403–8406.

[106] Evans, D. A.; MacMillan, D. W. C.; Campos, K. R. *J. Am. Chem. Soc.* **1997**, *119*, 10859–10860.

[107] Evand, D. A.; Burgey, C. S.; Para, N. A.; Vojkovsy, T.; Tregay, S. W. *J. Am. Chem. Soc.* **1998**, *120*, 5824–5825.

[108] Gao, Y.; Lane-Bell, P.; Vederas, J. C. *J. Org. Chem.* **1998**, *63*, 2133–2143.

[109] Evans, D. A.; Rovis, T.; Kozlowski, M. C.; Tedrow, J. S. *J. Am. Chem. Soc.* **1999**, *121*, 1994–1995.

[110] Evans, D. A.; Masse, C. E.; Wu, J. *Org. Lett.* **2003**, *4*, 3375–3378.

[111] Hubig, S. M.; Kochi, J. K. *J. Org. Chem.* **2000**, *65*, 6807–6818.

[112] Panisch, R.; Bolte, M.; Müller, T. *Organometallics* **2007**, *26*, 3524–3529.

[113] Meyer, R.; Werner, K.; Müller, T. *Chem.—Eur. J.* **2002**, *8*, 1163–1172.

[114] Furukawa, S.; Kobayashi, J.; Kawashima, T. *J. Am. Chem. Soc.* **2009**, *131*, 14192.

[115] Cozzi, F.; Annunziata, R.; Benaglia, M.; Baldridge, K. K.; Aguirre, G.; Estrada, J.; Sritana-Anant, Y.; Siegel, J. S. *Phys. Chem. Chem. Phys.* **2008**, *10*, 2686–2694.

[116] Cozzi, F.; Ponzini, F.; Annunziata, R.; Cinquini, M.; Siegel, J. S. *Angew. Chem. Int. Ed.* **1995**, *34*, 1019–1020.

[117] Cozzi, F.; Cinquini, M.; Annunziata, R.; Siegel, J. S. *J. Am. Chem. Soc.* **1993**, *115*, 5330–5331.

[118] Hammett, L. P. *Physical Organic Chemistry*, McGraw-Hill: New York, London, 1940, p 188.

[119] Smith, M. B.; March, J. *March's Advanced Organic Chemsitry*, John Wiley and Sons: New York, 2001, p 241.

[120] Prakash, G. K. S.; Schleyer, P. v. R. *Carbonium Ions*, Wiley: New York, 1968, chapter 18.

[121] Prakash, G. K. S.; Schleyer, P. v. R. *Stable Carbocation Chemistry*, Wiley: New York, 1997, chapter 14.

[122] Olah, G. A.; Prakash, G. K. S. *Carbocation Chemistry*, Wiley: New York, 2004, chapter 8.

[123] Aue, D. H. In *Divalent Carbocations*, Stang, P. J., Rappoport, Z., Eds., Wiley: Chichester, 1997, chapter 3.

[124] Apeloig, Y.; Müller, T. In *Divalent Carbocations*, Stang, P. J., Rappoport, Z., Eds., Wiley: Chichester, 1997, chapter 2.

[125] Olah, G. A. *Science* **1970**, *168*, 1298–1311.

[126] Deno, N. .; Richey, H. G., Jr.; Friedman, N.; Hodge, J. D.; Houser, J. J.; Pittman, C. U., Jr. *J. Am. Chem. Soc.* **1963**, *85*, 2991–2995.

[127] Olah, G. A.; Comisarow, M. B. *J. Am. Chem. Soc.* **1964**, *86*, 5682–5683.

[128] Bollinger, J. M.; Olah, G. A. *J. Am. Chem. Soc.* **1968**, *90*, 682–6086.

[129] Schleyer, P. v. R.; Su, T. M.; Saunders, M.; Rosenfeld, J. *J. Am. Chem. Soc.* **1969**, *91*, 5174–5176.

[130] Pittman, C. U. *J. Chem. Soc. D* **1969**, 122-123.

[131] Generation and IR characterization of the parent allyl cation in a matrix of SbF_5: Buzek, P.; Schleyer, P. v. R.; Vančik, H.; Mihalic, Z.; Gauss, J. *Angew. Chem. Int. Ed.* **1994**, *33*, 448–451.

[132] To the best of the writer's knowledge, the three structures discussed in the introduction of this chapter are the only reports on crystal structures of allyl cations that are not stabilized by additional π systems or heteroatoms.

[133] Maier, G.; Emrich, R.; Malsch, K.-D.; Schneider, K.-A.; Nixdorf, M.; Irngartinger, H. *Chem. Ber.* **1985**, *118*, 2798–2810.

[134] Olah, G. A.; Staral, J. S.; Spear, R. J.; Liang, G. *J. Am. Chem. Soc.* **1975**, *97*, 5489–5497.

[135] Lambert, J. B.; Lin, L.; Rassolov, V. *Angew. Chem. Int. Ed.* **2002**, *41*, 1429–1431.

[136] Otto, M.; Scheschkewitz, D.; Kato, T.; Midland, M. M.; Lambert, J. B.; Bertrand, G. *Angew. Chem. Int. Ed.* **2002**, *41*, 2275–2276.

[137] Müller, T. *Angew. Chem. Int. Ed.* **2002**, *41*, 2276–2278.

[138] Jones, J. N.; Cowley, A. H.; Macdonald, C. L. B. *Chem. Commun.* **2002**, 1520–1521.

[139] Lambert, J. B. *Angew. Chem. Int. Ed.* **2002**, *41*, 2278.

[140] Ogawa, K.; Minegishi, S.; Komatsu, K.; Kitagawa, T. *J. Org. Chem.* **2008**, *73*, 5248–5254.

[141] Structural, orbital and property calculations were carried out using the Gaussian03 [al and GAMESS [b] software packages.
[a] Gaussian03, Truhlar/Zhao module, Minnesota Supercomputer Center; [b] Schmidt, M. W.; Baldridge, K. K.; Boatz, J. A.; Elbert, S. T.; Gordon, M. S.; Jensen, J. H.; Koseki, S.; Matsunaga, N.; Nguyen, K. A.; Su, S.; Windus, T. L.; Dupuis, M.; Montgomery, J. A., Jr. *J. Comput. Chem.* **1993**, *14*, 1347–1363.

[142] Lambert, J. B.; Zhao, Y.; Emblidge, R. W.; Salvador, L. A.; Liu, X.; So, J.-H.; Chelius, E. C. *Acc. Chem. Res.* **1999**, *32*, 183–190.

[143] Lambert, J. B. *Tetrahedron* **1990**, *46*, 2677–2689.

[144] Labmert, J. B.; Lin, L.; Keinan, S. *Org. Biomol. Chem.* **2003**, *1*, 2559–2565.

[145] Lambert, J. B.; Liu, C.; Kouliev, T. *J. Phys. Org. Chem.* **2002**, *15*, 667–671.

[146] Klaer, A.; Saak, W.; Haase, D; Müller, T. *J. Am. Chem. Soc.* **2008**, *130*, 14956–14957.

[147] Müller, T.; Juhasz, M.; Reed, C. A. *Angew. Chem. Int. Ed.* **2004**, *43*, 1543–1546.

[148] Sugawara, M.; Yoshida, J. *J. Org. Chem.* **2000**, *65*, 3135–3142.

[149] Hassall, K. S.; White, J. M. *Org. Lett.* **2004**, *6*, 1737–1739.

[150] Lambert, J. B.; Zhao, Y. *J. Am. Chem. Soc.* **1996**, *118*, 7868–7868.

[151] Schormann, M.; Garratt, S.; Hughes, D. L.; Green, J. C.; Bochmann, M. *J. Am. Chem. Soc.* **2002**, *124*, 11266–11267.

[152] Howells, R. D.; Mc Cown, J. D. *Chem. Rev.* **1977**, *77*, 69–92.

[153] Duttwyler, S.; Do, Q.-Q.; Linden, A.; Baldridge, K. K.; Siegel, J. S. *Angew. Chem. Int. Ed.* **2008**, *47*, 1719–1722.

[154] Jelínek, T.; Baldwin, P.; Scheidt, W. R.; Reed, C. A. *Inorg. Chem.* **1993**, *32*, 1982–1990.

[155] Becerra, R; Walsh, R. In *The Chemistry of Organic Silicon Compounds, Vol. 2*, Patai, S.; Rappoport, Z. (Eds.), John Wiley and Sons: Chichester, 1998, chap. 4, p. 170.

[156] Douvris, C.; Stoyanov, E. S.; Tham, F. S.; Reed, C. A. *Chem. Commun.* **2007**, 1145–1147.

[157] C_{aryl}–F activation in the gas phase using transition metal monocations has been reported: a) Cornehl, H. H.; Hornung, G.; Schwarz, H. *J. Am. Chem. Soc.* **1996**, *118*, 9960–9965; b) Bajanson, A.; Taylor, J. W. *Organometallics* **1989**, *8*, 2020–2024. C_{aryl}–F activation using transition metals, mainly via oxidative addition: a) Young, R. H., Jr.; Grushin, V. V. *Organometallics* **1999**, *18*, 294–296; b) Aizenberg, M.; Milstein, D. *Science* **1994**, *265*, 359–361. Reviews: a) Braun, T.; Perutz, R. N. In *Comprehensive Organometallic Chemistry III, Vol 1*, Crabtree, R. H.; Mingos, M. P. (Eds.), Elsevier: Oxford, 2007, p. 725–758; b) Torrens, H. *Coord. Chem. Rev.* **2005**, *249*, 1957–1985.

[158] Stang, P. J. In *Divalent Carbocations*, Stang, P. J., Rappoport, Z., Eds., Wiley: Chichester, 1997, p 451.

[159] Calculations: a) Laali, K. K.; Rasul, G.; Prakash, G. K. S.; Olah, G. A. *J. Org. Chem.* **2002**, *67*, 2913–2918; b) Aschi, M.; Harvey, J. N. *J. Chem. Soc., Perkin Trans. 2* **1999**, 1059–1062; c) Hrusák, J.; Schröder, D.; Iwata, S. *J. Chem. Phys.* **1997**, *106*, 7541–7549; d) Nicolaides, A.; Smith, D. M.; Jensen, F.; Radom, L. *J. Am. Chem. Soc.* **1997**, *119*, 8083–8088; e) Harvey, J. N.; Aschi, M.; Schwarz, H.; Koch, W. *Theor. Chem. Acc.* **1988**, *99*, 95–99.

[160] Sandmeyer, T. *Ber. Dtsch. Chem. Ges.* **1884**, *17*, 1633–1635.

[161] Hodgson, H. H. *Chem. Rev.* **1947**, *40*, 251–277.

[162] Zollinger, H. *Diazo Chemistry I*, VCH: New York, 1995.

[163] Zollinger, H. *Acc. Chem. Res.* **1973**, *6*, 335–341.

[164] Angelini, G.; Fornarini, S.; Speranza, M. *J. Am. Chem. Soc.* **1982**, *104*, 4773–4780.

[165] Speranza, M. *Chem. Rev.* **1993**, *93*, 2933–2980.

[166] Himeshima, Y.; Kobayashi H.; Sonoda, T. *J. Am. Chem. Soc.* **1985**, *107*, 5286–5288.

[167] Apeloig, Y.; Arad, D. *J. Am. Chem. Soc.* **1985**, *107*, 5285–5286.

[168] Dichiarante, V.; Salvaneschi, A.; Protti, S.; Dondi, D.; Fagnoni, M.; Albini, A. *J. Am. Chem. Soc.* **2007**, *129*, 15919–15926.

[169] Wu, Z.; Glaser, R. *J. Am. Chem. Soc.* **2004**, *126*, 10632–10639.

[170] Cuccovia, I. M.; da Silva, M. A.; Ferraz, H. M. C.; Pliego, J. R., Jr.; Riveros, J. M.; Chaimovich, H. *J. Chem. Soc., Perkin Trans. 2* **2000**, 1896–1907.

[171] Fagnoni, M.; Albini, A. *Acc. Chem. Res.* **2005**, *38*, 713–721.

[172] Dichiarante, V.; Fagnoni, M.; Albini, A. *J. Org. Chem.* **2010**, *75*, 1271–1276.

[173] Lazzaroni, S; Dondi, D.; Fagnoni, M.; Albini, A. *J. Org. Chem.* **2010**, *75*, 315–323.

[174] Milanesi, S.; Fagnoni, M.; Albini, A. *J. Org. Chem.* **2005**, *70*, 603–610.

[175] $[Et_3Si(X)][CHB_{11}Cl_{11}]$ was freshly prepared from $[Ph_3C][CHB_{11}Cl_{11}]$ and an excess of triethylsilane in fluorobenzene. Under these conditions, Et_3Si^+ probably exists as a solvent- or Et_3SiH-coordinated cation ($\delta(^{29}Si)$ = 87 ppm in fluorobenzene). See also: Hoffmann, S. P.; Kato, T.; Tham, F. S.; Reed, C. A. *Chem. Commun.* **2006**, 767–769.

[176] Estop, E.; Alvarez-Larena, A.; Belaaraj, A.; olans, X.; Labrador, M. *Acta Cryst.* **1997**, *C53*, 1932–1935.

[177] Stoyanov, E. S.; Stoyanova, I. V.; Tham, F. S.; Reed, C. A. *J. Am. Chem. Soc.* **2010**, *132*, 4062–4063.

[178] Lehmann, M; Schulz, A.; Villinger, A. *Angew. Chem. Int. Ed.* **2009**, *48*, 7444-7447.

[179] Olah, G. A.; Sakakibara, T.; Asensio, G. *J. Org. Chem.* **1978**, *43*, 463–468.

[180] Grushin, V. V. *Acc. Chem. Res.* **1992**, *25*, 529–536.

[181] Relative energies of 4-$RC_6H_4^+$ singlet cations have been calculated to be R = H, 0 kJ mol^{-1}; R = CH_3, -2.8 kJ mol^{-1}; R = F, $+8.9$ kJ mol^{-1}: Aschi, M.; Harvey, J. N. *J. Chem. Soc., Perkin Trans. 2* **1999**, 1059–1062.

[182] Curtin, D. Y. *Rec. Chem. Prog.* **1954**, *15*, 111-128.

[183] Seeman, J. I. *Chem. Rev.* **1983**, *83*, 83–134.

[184] Olah, G. A. *Friedel–Crafts Chemistry*, John Wiley and Sons: New York, 1973.

[185] Reports on cationic arylations where products were detected by gas chromatography: Kamigata, N.; Kobayashi, M.; Minato, H. *Bull. Chem. Soc. Jpn.* **1972**, *45*, 2047–2050; Abramovitch, R. A.; Saha, J. G *Can. J. Chem.* **1965**, *43*, 3269–3278.

[186] 1-(2-Fluorophenyl)naphthalene was prepared by Roman Maag, Siegel group, Organic Chemistry Institute, University of Zurich.

Curriculum Vitae

Education

August 2005–present	**University of Zurich** PhD thesis on the synthesis and study of sterically enshrouded silanes and silicon- and carbon-based cations derived from them. Advisor: Prof. Jay S. Siegel
October 2007–January 2008	**University of Riverside, California, USA** Special training in the synthesis of carborane anions. Advisor: Prof. Christopher A. Reed
October 2000–June 2005	**University of Zurich** Undergraduate studies and diploma thesis. Advisor: Prof. Jay S. Siegel
August 1994–January 1999	**Kantonsschule Stadelhofen, Zurich** Matura type B (Latin).

Work Experience

August 2005–present	**University of Zurich** PhD student in the group of Prof. Jay S. Siegel. Teaching experience as a laboratory advisor for highschool students, lecture assistant, and assistant in practical courses.
October 2007–January 2008	**University of Riverside, California, USA** Research associate; investigations into highly reactive cationic intermediates such as the phenyl cation. Advisor: Prof. Christopher A. Reed

Achievements and Honors

October 2001	Alfred Werner scholarship from the Alfred-Werner-Stifung
October 2002	Alfred Werner scholarship from the Alfred-Werner-Stifung
June 2005	"Auszeichnung der Diplomarbeit" from the University of Zurich
June 2005	"Auszeichung für hervorragende Leistungen während des Studiums" from the University of Zurich
April 2007	Poster prize at the Dorothy Crowfoot Hodgkin Symposium in Zurich

Publications, Presentations and Posters

Publications

"Synthesis of 2,6-Diarylphenyldimethylsilyl Cations: Polar-π Distribution of Cationic Character"
S. Duttwyler, Q. Do, A. Linden, K. K. Baldridge, J. S. Siegel, *Angew. Chem. Int. Ed.* **2008**, *47*, 1719–1722.

"Synthesis and Crystal Structure of a Silyl-Stabilized Allyl Cation Formed by Disruption of an Arene by a Protonation–Hydrosilylation Sequence"
S. Duttwyler, Y. Zhang, A. Linden, C. A. Reed, K. K. Baldridge, J. S. Siegel, *Angew. Chem. Int. Ed.* **2009**, *48*, 3787–3790.

„Intramolecular Halogen Stabilization of Silylium Ions Directs Gearing Dynamics"
P. Romanato, S. Duttwyler, A. Linden, K. K. Baldridge, J. S. Siegel, *J. Am. Chem. Soc.* **2010**, *132*, 7828–7829.

"C–F Activation of Fluorobenzene by Silylium Carboranes: Evidence for Incipient Phenyl Cation Reactivity"
S. Duttwyler, C. Douvris, N. L. P. Fackler, F. S. Tham, C. A. Reed, K. K. Baldridge, J. S. Siegel, *Angew. Chem. Int. Ed.* **2010**, *in press*.

"Through- Space Interactions in Enshrouded *meta*-Terphenylsilanes"
S. Duttwyler, P. Romanato, A. Linden, K. K. Baldridge, J. S. Siegel, *manuscript in preparation*.

"A Hammett Relationship for Silylium Ions Stabilized by π Systems"
S. Duttwyler, A. Linden, K. K. Baldridge, J. S. Siegel, *manuscript in preparation*.

Presentations

Presentation at the Fall Meeting of the Swiss Chemical Society in September 2008
Presentation for the Rotary Club Forch (Kanton of Zurich) in March 2009

Posters

Posters presented in the course of the following events:

- Meetings of the Swiss Chemical Society (May 2006, October 2006, September 2007, September 2008, September 2009)
- Dorothy Crowfoot Hodgkin Symposium, Zurich (October 2006, April 2007, July 2008, November 2009)
- EuCheMS Chemistry Conference, Turin, Italy, September 2008
- Gordon Research Conference on Physical Organic Chemistry, Holderness NH, USA, June 2009
- Buergenstock Conference on Stereochemistry, Brunnen, Switzerland, May 2010